Author:
Campbell, Jennie S

Title:
Investigating novel players in inflammatory cell migration to sites of tissue damage in vivo

Investigating novel players in inflammatory cell migration to sites of tissue damage *in vivo*

Jennie Samantha Campbell

A dissertation submitted to the University of Bristol in accordance with the requirements for award of the degree of Doctor of Philosophy in the Faculty of Life Sciences.

School of Cellular and Molecular Medicine

Submission September 2019

Word count: 31,806

Abstract

The use of model organisms is vital for the improvement of our understanding of dynamic immunological processes. Previous work in the developing *Drosophila* embryo has demonstrated that epithelial wounding by laser ablation induces the rapid production of hydrogen peroxide (H_2O_2). This early damage signal activates the tyrosine kinase Src42a within the embryonic hemocytes – the innate immune cells of the organism. Src42a subsequently phosphorylates the tissue damage receptor Draper on its intracellular immunoreceptor tyrosine activation motif (ITAM) domain. This recruits a second kinase – Shark – and results in the activation of hemocytes and their subsequent migration to the damage site.

As kinase activation is key to the tissue damage response of these inflammatory cells, we reasoned that other hemocyte-specific proteins may also be phosphorylated following H_2O_2 signalling. Therefore, a phosphoproteomics screen was conducted in order to uncover novel H_2O_2/Src42a regulated phosphoproteins. Using this approach, we discovered a hemocyte wound recruitment defect in embryos lacking the PTP type phosphatase Pez. This was shown to be cell-autonomous; and time-lapse imaging revealed a lack of directionality within *Pez* mutant hemocytes in the presence of an epithelial wound. We also uncovered dynamic localisation of Pez *in vivo* and it's colocalization with Draper during the engulfment of apoptotic debris. Finally, we demonstrated that the loss of Draper and Src42a leads to the mislocalisation of Pez.

To investigate whether this signalling pathway is evolutionarily conserved, tail fin clipping of 3 dpf *Danio rerio* larvae was utilised. Excitingly, Draper orthologue (MEGF10) morphants showed a reduction in both neutrophil and macrophage numbers recruited to the wound margin. This observation was further confirmed by the generation transient CRISPant larvae. Finally, we demonstrated that the Pez orthologue – named PTPN21 – also plays a role in inflammation in the zebrafish following gene disruption by CRISPR.

Acknowledgements

I first wish to acknowledge the support and encouragement from my supervisor Prof. Will Wood throughout my time as a PhD student. Thank you for being such an enthusiastic and positive mentor. I am also extremely grateful for the experience I gained at the QMRI at the University of Edinburgh during my final year. I wish to thank Dr Yi Feng for the exciting opportunity expand my work into zebrafish and for her additional guidance.

I also wish to thank the members of the Wood lab for their friendship and support during my PhD. Particular thanks go to Dr Kate Comber whose patience and endless help in all manner of things was invaluable throughout my time in Bristol. Many thanks also to Dr Fred Rodrigues - especially for supervising me during my first year. Thanks also go to Dr Andrew Davidson - particularly for the last-minute help over the finishing line with edits, suggestions and words of encouragement. Further thanks also go to the newer lab members in Edinburgh the for making my time away from home so enjoyable. Thanks also go to the Feng lab for their technical help in planning and conducting my zebrafish experiments, as well as confirming I had correctly identified male and female fish!

I thank all my friends for their endless laughter over the past 4 years. Particularly Alice, who is the most positive and encouraging person I know and has always been there on the other end of the phone. Special thanks also to Siobhan, for introducing me to iced coffee, always being ready for a tea and a Boost and for reading through various drafts. Finally, to Dani, Richard and Victoria who I started this crazy journey with – thank you for all the fun adventures.

I am enormously grateful to my best friend and partner Adam for keeping me sane and feeding me whilst writing my thesis! Thank you for your constant love and support, especially following my move to Edinburgh.

Last but not least I thank my family – especially my parents Robert and Hazel. Thank you for always believing in, supporting and encouraging me. I love you both.

This work was funded by the Wellcome Trust as part of the PhD program in Dynamic Cell Biology at the University of Bristol. The Wood lab is funded by the Wellcome Trust.

Signed declaration

I declare that the work in this dissertation was carried out in accordance with the requirements of the University's *Regulations and Code of Practice for Research Degree Programmes* and that it has not been submitted for any other academic award. Except where indicated by specific reference in the text, the work is the candidate's own work. Work done in collaboration with, or with the assistance of, others, is indicated as such. Any views expressed in the dissertation are those of the author.

SIGNED:..... DATE:.....

Contents

List of tables

List of figures

Chapter 1: Introduction

Chapter 2: Materials and methods

Chapter 3: A phosphoproteomic screen uncovers novel regulators of hemocyte biology

Chapter 4: Investigating the role of the PTP type phosphatase Pez in hemocyte wound recruitment

Chapter 5: Investigating Draper and Pez orthologues in neutrophil and macrophage recruitment to tail fin wounds in Danio rerio

Chapter 6: Final discussion

List of appendices

List of supplementary movies

Abbreviations

AGM	Aorta-gonad-mesonephros
Arp2/3	Actin-related protein 2/3
ATP	Adenosine triphosphate
BDSC	Bloomington Drosophila Stock Center
BSA	Bovine serum albumin
Ca^{2+}	Calcium
CCP	Complement control protein
CHT	Caudal hematopoietic tissue
CK2	Casein-kinase-II
CNS	Central nervous system
CO_2	Carbon dioxide
COMO	Control morpholino
CRISPR	Clustered regularly interspaced short palindromic repeat
Crq	Croquemort
D	Aspartic acid
Dia	Diaphanous
DNA	Deoxyribonucleic acid
Dpf	Days post fertilisation
Dpi	Days post injury
Drpr	Draper
DUOX	Dual oxidase
E	Glutamic acid
EGF	Epidermal growth factor
(e)GFP	(Enhanced) green fluorescent protein
EMARDD	Myopathy, areflexia, respiratory distress and dysphagia
Ena	Enabled
Ex.x	Embryonic day x.x
F	Phenylalanine
F-actin	Filamentous actin
FACs	Fluorescent activated cell sorting

FERM	Band 4.1, ezrin, radixin and moesin domain
Fwd	Forward
G-6-P	Glucose-6-phosphate
gRNA	Guide ribonucleic acid
H	Histidine
H_2O_2	Hydrogen peroxide
Hpf	Hours post fertilisation
HSCs	Hematopoietic stem cells
ICD	Intracellular domain
Ig	Immunoglobulin
IL	Interleukin
ITAM	Immunoreceptor tyrosine activation motif
JNK	c-Jun N-terminal kinase
K	Lysine
KIF1C	Kinesin family member 1C
LC-MS	Liquid chromatography mass spectrometry
Leu	Leucine
mCh	mCherry
MEGF10	Multiple EGF-like domains 10
Met/M	Methionine
MO1	Morpholino 1
Mpx	Myeloid-specific peroxidase
mRNA	Messenger ribonucleic acid
Msn	Misshapen
N	Asparagine
NA	Numerical aperture
NADPH	Nicotinamide adenine dinucleotide phosphate
NETs	Neutrophil extracellular traps
NLS	Nuclear localisation sequence
P	Proline
PAM	Proto-spacer adjacent motif
(P)BAP	(Polybromo-containing) Brahma-associated proteins
PBS	Phosphate buffered saline

PBST	Phosphate buffered saline containing 0.1% Triton-X
PCR	Polymerase chain reaction
PD	Phosphatase dead
PDGF	Platelet derived growth factor
PGM	Phosphoglucomutase
PS	Phosphatidylserine
PTP	Protein tyrosine phosphatase
PTPN14	Protein tyrosine phosphatase non-receptor type 14
PTPN21	Protein tyrosine phosphatase non-receptor type 21
PVFs	PDGF/VEGF-related factors
PVR	PVF receptor
R	Arginine
Rev	Reverse
RFP	Red fluorescent protein
RNA(i)	Ribonucleic acid (interference)
ROS	Reactive oxygen species
Rpm	Rotations per minute
RT	Room temperature
RT-PCR	Reverse transcription polymerase chain reaction
S2 cells	Schneider 2 cells
Ser/S	Serine
sfGFP	Super folded green fluorescent protein
SFK	Src Family Kinase
SIMU	Six microns under
SLS	Scientific Laboratory Supplies
Srp	Serpent
Syk	Spleen tyrosine kinase
Tg	Transgenic
TGF	Transforming growth factor
Thr/T	Threonine
TM	Transmembrane
TMT	Tandem Mass Tag
TNF	Tumour necrosis factor

tracrRNA	Trans-activating CRISPR RNA
Tx	Triton
Tyr/Y	Tyrosine
UAS	Upstream activation sequence
V	Valine
VEGF	Vascular endothelial growth factor
W	Tryptophan
w	White
WT	Wild type
Yrk	Yes-related kinase

Chapter 1: Introduction

1.1 The innate immune system

Immune systems not only offer host organisms protection from invading pathogens, but also play vital roles in maintaining tissue homeostasis and integrity. The immune system of vertebrates is comprised of two arms – the innate and adaptive systems. Following tissue damage or pathogenic insult, the innate immune system is immediately activated to provide a rapid, generalised response. In comparison, activation of the adaptive immune response is delayed and not only generates a pathogen-specific response, but also builds an immunological memory to confer resistance to subsequent infections. Adaptive immunity is found exclusively in vertebrates; whilst plants, invertebrates and primitive organisms solely harbour innate immune systems.

The innate immune system protects hosts through both humoral and cellular responses. Immune cells are known as leukocytes, of which there are 5 main innate types: neutrophils, eosinophils, basophils, macrophages and dendritic cells. Cross talk between these innate leukocytes, as well as with the adaptive immune system (where present) mediate appropriate immune responses. For the purpose of this work, introduction shall be restricted to two relevant cell types – macrophages and neutrophils. These cell types are derived from the same myeloid progenitor and are recruited to sites of damage and infection.

1.1.1 The complex origins of macrophages

Macrophages – literally named 'big eaters' – are the professional phagocytes of the innate immune system and were first observed performing this function by Mechnikov in the early 1880s. In the circulatory system, macrophages are found as monocytic precursors awaiting activation. Specialised macrophages are also found in a variety of tissues - such as the Kupffer cells in the liver, or microglia in the brain.

All blood cells are generated through the process of hematopoeisis, which begins early in mouse embryogenesis at embryonic day 7 (E7.0)[1], and by week 3-4 of human gestation. This generates both red blood cell precursors as well as myeloid progenitors[2] from the primitive ectoderm. By E10.5 yolk sac macrophages are seen distributed evenly throughout the developing mouse[3] - where they likely play roles in tissue and structural remodelling[4,5], as well as facilitating vascularisation[6]. However the ability of embryonic macrophage to respond to tissue damage does not develop until E14.5[7].

This first wave of embryonic hematopoeisis is followed by a definitive wave, which generates hematopoietic stem cells (HSCs) from the ventral wall of the dorsal aorta in a region termed the aorta-gonad-mesonephros (AGM)[8]. These cells, along with those derived from the yolk sac, seed the liver during days 11-13 of mouse gestation - and week 5 in humans - to give rise to the main site of subsequent hematopoeisis during foetal development. This ultimately leads to the generation of mature red blood cells, lymphoid cells of the adaptive immune system and innate myeloid cells – including circulating monocytes[9,10]. Finally, the bone marrow is colonised prior to birth to provide the site of further hematopoeisis throughout the animal's life[8]. The loss of macrophages in the mouse embryo leads to slowed growth and death of the young animal perinatally[11,12] - indicating the importance of embryonic macrophages during development.

Whilst the macrophage of the brain, the microglia, have been shown to be solely derived from the earliest wave of embryonic macrophage[13], other tissue resident macrophages show different origins. For example, the Langerhans cells of the skin are derived from both the yolk sac and embryonic liver[14,15], whilst alveolar macrophage can be solely mapped back to foetal liver-derived monocytes[16]. Although all macrophages play key roles in tissue development and homeostasis[17] and immune responses,

their different origins and subsequent tissue specificity have been shown to govern their activation[18,19].

1.1.2 Neutrophils – origins and functions

Neutrophils are the most abundant leukocyte found in most mammals and play vital roles in pathogen clearance. Unlike macrophages, which arise early in human gestation, the first neutrophils are not specified until the bone marrow wave of hematopoeisis[20]. Following this, mature neutrophils can be found within human embryonic blood at 14-16 weeks of human gestation[21]. After birth, neutrophil counts rapidly rise during the first 2-3 days[22]. As neutrophils are remarkably short lived, the bone marrow proliferative pool is required to replenish neutrophil numbers throughout life[23]. In the latter stages of neutrophil differentiation the nucleus adopts the characteristic lobed structure[24,25], whilst cytoplasmic granules are generated in precursor cells through the process of granulopoiesis[23].

Primary neutrophil granules contain myeloperoxidase[26] which can be released into the extracellular space or fused with intracellular phagosomes following degranulation. When combined with hydrogen peroxide (H_2O_2), myeloperoxidase generates potent toxic agents which attack the surface components of microorganisms[27]. Mature neutrophils also contain secondary and tertiary granules which enclose a variety of further effector proteins. These include defensins[28], lactoferrin[29], and lysozyme[30] which all act as antimicrobial peptides; as well as three metalloproteases that are important for extracellular matrix degradation to permit neutrophil extravasation and migration[31]. The diverse contents of these granules are crucial for both the activation and response of neutrophils. As well as undergoing degranulation, neutrophils also form neutrophil extracellular traps (NETs) in response to pathogens. These structures are forcefully ejected from cells in a process named NETosis, and consist of DNA, histones and granule contents. This occurs downstream of neutrophil activation and is mediated in part by reactive oxygen species (ROS) and NADPH-oxidase complex[32,33], as well as cell-

cycle proteins[34]. Although dispensable during development[35], loss of functional neutrophils leads to persistent bacterial infections during early life and results in a dramatically reduced lifespan[36].

1.1.3 Acute and chronic inflammation, and the roles of macrophages and neutrophils

Acute inflammation is initiated following signalling in response to pathogen detection, as well as direct tissue damage. It is characterised by the recruitment of neutrophils, macrophages and adaptive lymphocytes in sequential order.

Following the production of a variety of damage signals including reactive oxygen species (ROS), interleukin (IL)-1ß, and tumour necrosis factor (TNF)-α, adhesion molecules are upregulated on inflamed endothelial cells[37,38]. These are able to capture circulating neutrophils that have been primed by further cytokines such as IL-8, to result in diapedesis and chemotaxis[39]. Once at the damage site, neutrophils work to eliminate infectious agents using NETosis, degranulation and phagocytosis, and also begin to clear necrotic wound debris. Despite preforming these seemingly crucial functions, wounds are able to close in the absence of neutrophils[40,41].

Macrophages are recruited at around 2 days post injury predominantly as monocytic precursors from the blood[42] and, following maturation into pro-inflammatory macrophages, further function in the clearance of debris, as well as spent apoptotic neutrophils[43]. In the latter stages of inflammation, wound associated macrophages transition to perform a more pro-regenerative role through the secretion of a variety of factors including transforming growth factor (TGF)-α and TGF-ß, as well as PDGF and VEGF[44]. This function of macrophages is crucial in the repair of the damaged tissue, and macrophage depletion causes significant delays in healing[45]. Following the appropriate coordinated response at damage sites infection is eliminated, the tissue heals and inflammation resolves.

However, in a variety of pathological conditions prolonged or chronic inflammation actively contributes to disease.

In chronic wounds such as diabetic ulcers and pressure ulcers, the inflammatory cascade is altered, and the initiation of healing is delayed or blocked. Elevated neutrophil numbers have been implicated in the pathology of chronic wounds[46], where their excessive activity contributes to persistent tissue damage via destruction of the cellular matrix[44]. Elevated numbers of pro-inflammatory macrophage are also present at chronic wounds[47] and suppress the secretion of pro-repair factors[48]. Ultimately, inflammatory signalling is propagated by the lack of healing in chronic wounds. Improving our understanding of immune cell activation will not only inform wound care but may also provide insight into the aberrant activation of the immune system in further conditions such as autoimmunity and cancer.

1.2 Using *Drosophila melanogaster* to study inflammatory cell biology

The fruit fly *Drosophila melanogaster* is one of the most intensively studied model organisms and was first proposed for biological research use at the turn of the 19th century by Charles W. Woodworth. Following the seminal work on heredity by Thomas Hunt Morgan which established the field of genetics, 8 Nobel prizes have been awarded for discoveries made in the fruit fly. *Drosophila* were first shown to be amenable to genetic transformation in 1987. Furthermore, during embryogenesis the organism remains static and is optically translucent which permits *in vivo* imaging. This, combined with their short generation time, high fecundity and the availability of the entire genome sequence[49] make fruit flies fantastic model organisms for tractable biological research.

1.2.1 The *Drosophila* immune system – hemocytes and their origins

As an invertebrate, *Drosophila*'s immune system is relatively simple, and they lack adaptive cell counterparts. The innate immune cells of the organism are referred to as hemocytes and perform several key functions analogous to vertebrate macrophages – namely they are the professional phagocytes of the fly.

Like their mammalian counterparts, hemocytes arise early in embryogenesis. Approximately five hours after egg laying, at embryonic stage 10, hemocytes are identifiable as a subpopulation of the head mesoderm[50]. This first wave of hematopoeisis gives rise to two types of hemocytes at this stage – plasmatocytes, which make up 95% of the population that disperse throughout the organism, and crystal cells, which are lower in abundance and remain restricted to the head region[51]. As such, the functional embryonic plasmatocytes of interest shall be referred to as (embryonic) hemocytes throughout.

The GATA transcription factor Serpent (Srp) is essential for the specification of hemocytes as well as the development of the gut[52], and plays a similar role to vertebrate GATA transcription factors which also specifies both blood cell lineages - erythrocytes and leukocytes - and promotes their survival[53–55]. The loss of hemocytes following hemocyte-specific *srp* mutation is recessive lethal during embryogenesis[52] - indicating their importance in fly development, and drawing parallels to the role of mammalian macrophages. Moreover hemocytes of embryonic origin persist into adulthood where they have been identified following metamorphosis[56].

From their origin in the head of the developing fly, hemocytes disperse along prepatterned routes that are governed by the expression of PDGF/VEGF-related factors (PVFs) which bind to and activate their cognate PVR receptors expressed on hemocytes[57,58]. Hemocytes

stereotypically follow the directional cues of PVF2 and PVF3 both ventrally and dorsally following invasive migration through the germ band[59], whilst PVF1 promotes hemocyte survival. At stage 13 in embryonic development the ventral and dorsal populations meet, resulting in their occupation of the entire ventral midline. At this time, the PVF directional cues begin to diminish[57] and as the embryo transitions into stage 14 contact repulsion becomes the main driving force governing hemocyte migration. This physical repulsion of cells away from each other following contact is mediated by both microtubules[60] and integrin[61] and results in the lateral migration of cells out from the ventral midline. Once this process is complete, hemocytes are fully dispersed to occupy the entirety of the developing organism (Figure 1.2.1).

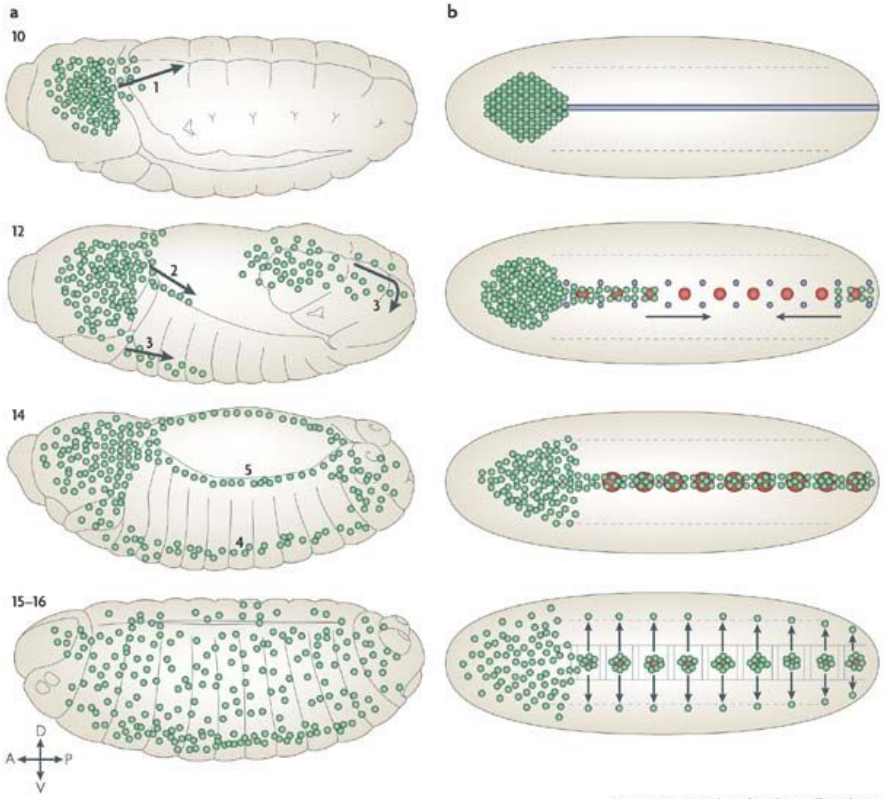

Figure 1.2.1: Dispersal of embryonic hemocytes follows pre-patterned routes.

Image from[51] showing a) lateral view and b) ventral view of *Drosophila melanogaster* embryonic stages 10-16. Hemocytes (green) are born in the head of the organism at stage 10. They undergo invasive migration of the germband and begin to migrate down the ventral midline at stage 12. At stage 14, hemocytes occupy the entire ventral midline and the PVF cues (blue PVF3, red PVF2) diminish. This drives the hemocytes to migrate laterally, so that they occupy the entirety of the developing fly at the end of embryogenesis (stage 16).

1.2.2 Hemocyte motility

The dynamic motility of hemocytes is crucial for their functions in embryogenesis and beyond. In the embryo, they harbour a sheet-like lamellipod which extends out from the cell body as the cells patrol the developing organism[57] (Supplementary movie 1). This highly dynamic structure can be up to 20 μm in length[62]. Hemocytes also extend exploratory filopodia of short lifespan which can be independent of, or integrated into, the lamellipod. The generation of these complex cellular protrusions directly relies on the underlying dynamic cytoskeleton that is formed of both actin and microtubules.

Actin monomers are globular proteins of approximately 42 kDa that are found in all eukaryotic cells. These undergo polymerisation to generate polarised filamentous actin (F-actin). A number of different regulators mediate the way in which F-actin is organised and thus directly contribute to cellular structures. The Arp2/3 complex generates the branched actin network that is responsible for lamellipod formation[63], and has previously been localised to the leading edge of hemocyte lamellipodia[64]. The upstream activator of the Arp2/3 complex, named SCAR/WAVE[65] in *Drosophila*, is both necessary and sufficient to induce hemocyte lamellipod formation[64,66]. The role of SCAR/WAVE in generating this dynamic structure is crucial for almost all aspects of hemocyte behaviours as *Scar* mutant cells show defective developmental dispersal, dramatic reduction in patrolling motility and reduced recruitment to sites of tissue damage.

The hemocyte actin cytoskeleton is also modulated by the bundling activities of the protein Fascin (encoded by *singed* in *Drosophila)*[67]. Fascin contains both an N- and C-terminal actin binding domain which mediate its ability to crosslink and bundle F-actin[68]. In hemocytes, Fascin localises along actin filaments within the lamellipod where it directly contributes to both the architecture and polarisation of the structure, as well as overall dynamics. Like the loss of branched actin, the absence of bundled

actin mediated by *Singed* has dramatic consequences for hemocytes - rending them unable to disperse or effectively migrate towards damage signals[67].

Enabled (Ena)[64,69] and, to a lesser extent, the formin Diaphanous (Dia)[70] are further regulators of hemocyte F-actin dynamics through modulation of actin bundles. Like the Arp2/3 complex, Ena localises to the lamellipod edge, where it caps fascin bundled F-actin[70]. Dia is instead found on a distinct subset of lamellipodial actin bundles and is thought to mediate the generation of probing filopods. Bundled actin in the form of filopodia are seen in the absence of SCAR and the Arp2/3 complex[66], indicating distinct regulatory mechanisms behind the generation of these structures. However, cell protrusions generated by Ena bundled actin directly contribute to lamellipodial shape. These bundles play crucial roles in hemocyte migration, as increased actin organisation driven by Ena overexpression results in an increase in migration speed both under basal conditions, as well as during chemotaxis[69,70]. Conversely, Dia is indispensable for the basal motility of hemocytes[64] – indicating Ena is the principal regulator of functional actin bundle organisation during migration (Figure 1.2.2).

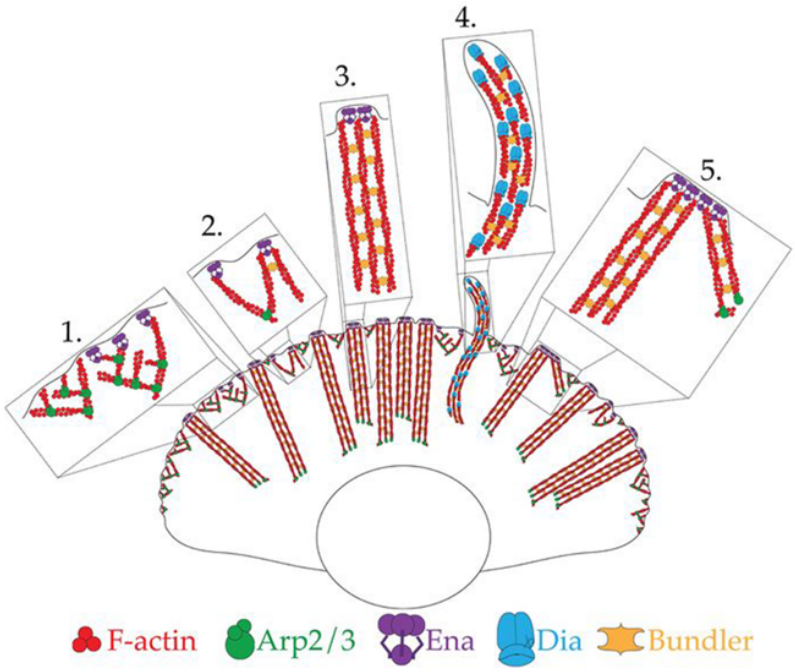

Figure 1.2.2: Regulation of actin within embryonic hemocytes

Figure from Davidson et al, 2019[64] to illustrate how actin is organised within hemocytes. F-actin can be arranged as a mesh network – mediated by the Arp2/3 complex (1), as filamentous bundles (3), or as a combination of these (2). Both of these structures can be capped by the bundling protein Ena at the edge of the lamellipod (2/3). The formin Dia can also form actin bundles which underly exploratory filopodia (4). Bundled actin can also contribute to the arrangement of actin in the lamellipod (5).

As well as bundled and branched actin, hemocytes also contain microtubule networks[60]. Like filamentous actin, microtubules are polarised polymers that are formed from tubulin dimers which also contribute to the maintenance of cellular structure. In the hemocyte cell body, microtubules form a stable basket-weave structure. In contrast, the lamellipodial microtubule network is highly dynamic and undergoes growth towards the cell periphery as well as collapse. Microtubule arms are found in the majority of hemocytes at stage 15 and orient in the direction of migration[60]. The maintenance and stability of this structure is dependent upon both the microtubule stabilising protein Orbit[71] and the beta integrin myospheroid[61]. Disruption of the microtubule cytoskeleton results in defective dispersal of hemocytes in the latter stages due to a loss of contact repulsion[60,61].

Although hemocytes contain two distinct cytoskeletal networks comprised of F-actin and microtubules, the loss of either is catastrophic for motility. The correct organisation and polarisation of the entire cytoskeleton is therefore intricately linked to the function of these cells.

1.2.3 Phagocytosis by hemocytes

During the developmental dispersal of hemocytes, they perform the vital task of clearing apoptotic debris that is generated as part of normal embryogenesis[50]. Evidence of these phagocytic events are seen as dense vacuoles within the cell's main body via visualisation by electron microscopy, as well as fluorescent negative areas in fluorescent microscopy following transgene expression[72,73]. Both this clearance function of hemocytes[52], as well as developmentally controlled apoptosis, are crucial to organism viability[74]. Therefore, a high degree of redundancy underlies hemocyte engulfment and they express multiple receptors which are known to mediate engulfment.

The best characterised signal for phagocytosis expressed on apoptotic cells is phosphatidylserine (PS)[75]. This is recognised by the tissue damage receptor Draper in *Drosophila* – which is expressed by both hemocytes and phagocytic glia found in the central nervous system - and is the orthologue *C. elegans* Ced-1, which also recognises PS[76-78]. In cultured *Drosophila* S2 cells – which are 'hemocyte-derived'[79] yet display limited basal phagocytic ability - the recognition of PS by ectopically expressed *Draper* is sufficient to drive robust phagocytosis[80]. Draper signalling in these cells occurs following exclusion of bulky headed phosphatases following ligand engagement and receptor clustering, to permit intracellular phosphorylation of Draper by the Src Family Kinase (SFK) Src42a[80]. This leads to downstream signalling through Shark, a second kinase, which promotes actin cytoskeletal rearrangement and phagocytic cup formation. This cascade is also operational during glial phagocytosis[81,82] where the loss of components of the Draper signalling axis result in the failure of glia to clear neuronal debris.

Conversely, the loss of Draper in hemocytes is, in fact, dispensable for phagocytosis[83] and instead leads to increased vacuolation which is indicative of defects in corpse processing[73]. Whilst the complete degradation of the contents of CED-1 mediated phagosomes in *C. elegans* takes approximately 60-80 mins[84], hemocyte phagocytic vacuoles seem remarkably long-lived (unpublished observations from the lab) and the timeline of their maturation, as well as how their contents is ultimately utilised, is not known.

A further receptor, six microns under (SIMU), acts upstream of Draper[83] in phagocytosis. Although the loss of SIMU leads to an increased numbers of uncleared corpses[85], double *Draper;SIMU* mutant hemocytes remain phagocytic. Hemocytes also express Croquemort, the orthologue of the mammalian scavenger receptor CD36[86–88]. Like SIMU, Croquemort plays a predominant role in corpse uptake *in vivo* during embryonic development, as mutant hemocytes show decreased efficiency in their clearance[87]. Remarkably, the transfection of mammalian cells (COS-7) with *croquemort* is able to promote phagocytic ability - demonstrating the function of this CD36 orthologue in corpse uptake is robustly conserved[88]. It has recently been shown that the presence of excessive developmental debris following the reduction in phagocytic ability of hemocytes is detrimental to their behaviours, as it leads to defects in basal migration and inflammatory responses[85]. This indicates that the timely clearance of developmental apoptosis is required for a fully functioning immune system.

Whilst the appropriate clearance of apoptotic debris undoubtedly contributes to orderly development, the engulfment of cell corpses is also important for hemocyte maturation as it leads to the upregulation of both Croquemort[87] and Draper[72] to reinforce their inflammatory identity. This is explored further below.

1.2.4 The hemocyte response to tissue damage

The rapid recruitment of hemocytes to wounds generated by epithelial laser ablation was first shown in 2005[89] in a process which involves their active polarisation and lamellipod-mediated migration. This model has thus been subsequently used to dissect the complex signalling involved in inflammatory cell recruitment to tissue damage. Although hemocytes are dispensable for embryonic wound closure, they play a vital role in debris clearance and pathogen engulfment[89].

The method of epithelial laser ablation in the developing *Drosophila* embryo leads to the generation of a circular lesion[90] following the necrotic death of the targeted cells – as identified by the absence of cleaved caspase staining[72]. The earliest signal released following ablation is the liberation of intracellular calcium[91], which is also observed following epidermal wounding in *C. elegans*[92] as well as damaged cells *in vitro*[93–95]. This emanates out as a wave through the embryonic epithelium from the damage site, propagated by innexin positive gap junctions[91,96]. Calcium levels remain high in the epithelium for approximately 15 minutes post-injury and dissipate before wound closure.

Subsequently, the enzyme dual oxidase (DUOX) is activated in the injured epithelium following the binding of calcium to the regulatory EF hand domain[91,97]. This rapidly produces hydrogen peroxide (H_2O_2) from superoxide[98], with levels peaking approximately 3 minutes after wounding. The loss of any component in this initial signalling cascade within the epithelium – including the maturation factor NIP which is required for correct folding and sub cellular localisation of DUOX[99] – results in a dramatic reduction in the number of hemocytes recruited to the damage site[91,100].

The emitted H_2O_2 inflammatory signal diffuses through the extracellular space and across cell membranes[101]. In hemocytes this oxidises a critical redox sensitive cysteine in the Src family kinase member Src42a[73,102]. This

is crucial to wound recruitment, as hemocyte-specific loss of Src42a reduces inflammation by 50% - directly analogous to the loss of the upstream signalling components in the epithelium[91]. Following activation, Src42a phosphorylates the receptor Draper on its intracellular immunoreceptor tyrosine activation motif (ITAM) domain - which conforms to a consensus YXXI/L-X_{6-12}-YXXL sequence[73,82]. This phosphorylation event is required for subsequent inflammatory signalling mediated by the recruitment of the downstream kinase, Shark[73]. Ultimately, this signalling axis activates directional migration of the hemocytes to the wound site (Figure 1.2.5), however further components downstream of Shark remain to be elucidated.

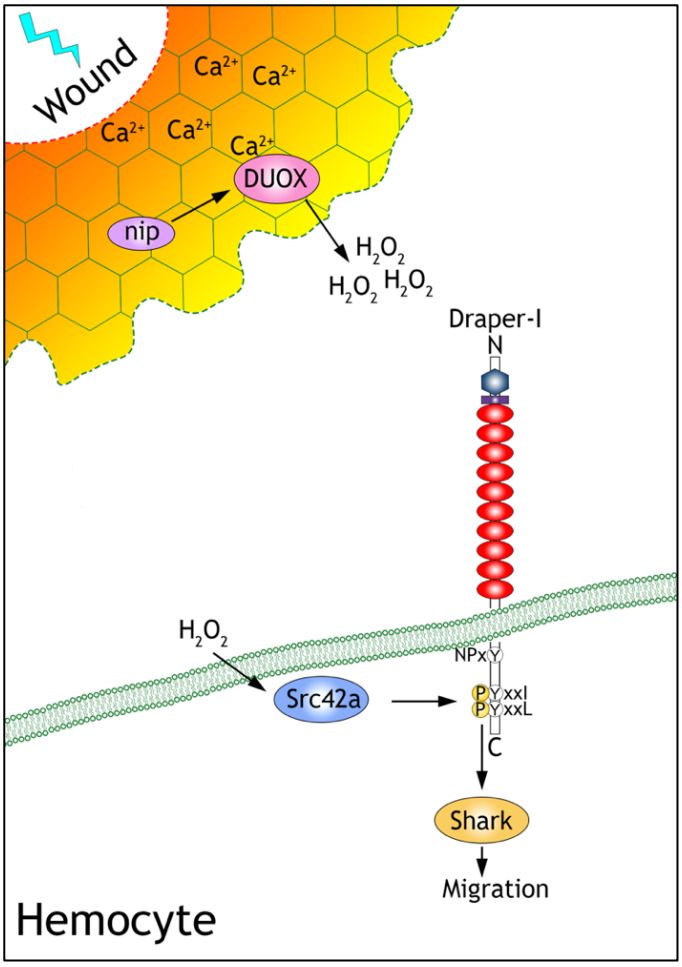

Figure 1.2.4: Damage signalling in hemocytes

Figure adapted from Evans et al, 2015[73]. Wounding by laser ablation leads to the release of intracellular calcium (Ca^{2+}), which activates DUOX. DUOX produces hydrogen peroxide (H_2O_2). Inside embryonic hemocytes, this oxidises and activates Src42a which phosphorylates the tissue damage receptor Draper on its intracellular ITAM domain. This recruits a second kinase Shark to facilitate chemotaxis.

1.2.5 How successive signals shape fly inflammation

In the absence of developmental apoptosis[74], hemocytes develop and disperse normally but lack the ability to respond to wounds - despite the presence of the H_2O_2 signal[72,100]. It was elegantly shown that the engulfment of apoptotic corpses during hemocyte dispersal is necessary to trigger the downstream signalling required to generate their inflammatory identity. Upon engulfment, hemocyte calcium levels dramatically rise[72] similar to observations following phagocytosis both *in vitro* and in *C. elegans*[103]. This then activates the c-Jun N-terminal kinase (JNK) signalling pathway and leads to the upregulation of Draper which fully restores hemocyte responsiveness to wounds. Presumably, a similar pathway leads to the upregulation of Croquemort downstream of corpse engulfment[87]. However the elevation of Draper levels appears to be of strictest importance in shaping the hemocyte inflammatory identity, as overexpression of *Draper* in the apoptotic-null background is sufficient to rescue both hemocyte wound recruitment and pathogen engulfment[72]. This is therefore considered a mechanism of innate immune cell priming whereby corpse engulfment functionalises hemocytes through Draper upregulation.

1.2.6 Insights from beyond the embryo

Embryonic hemocytes persist into adulthood and are accompanied by cells of larval origin following a second wave of hematopoeisis in the larval lymph gland. As in the embryo, the majority (95%) of larval hemocytes are also plasmatocytes[56]. Recent work in the pupal wing demonstrated the hemocyte inflammatory response to laser ablation wounds persists throughout the fly life cycle[104]. As a larger area with more responding cells, pupae were used to model wound recruitment *in silico*. This work suggests a yet unknown secondary chemotactic signal, which diffuses slower than H_2O_2, is involved in hemocyte wound responses. Crucially this is not ATP, which, although involved in mammalian leukocyte activation following damage[105,106], is dispensable for hemocyte wound recruitment[100] and further does not fit the diffusion model[104].

Additionally, this work uncovered a stage of hemocyte desensitisation following wounding – whereby period of 3 hours is required in order for hemocytes to respond to a subsequent signal. It is possible that this is due to a delay in turnover of previously activated components of the signalling pathway to return hemocytes to their basal state. The upregulation of Draper levels described previously via transcription and translation has been shown to take 90 minutes to prime these cells to allow for response to stimulus[72]. Perhaps this, coupled with the clearance of the excessive debris generated by ablation – which renders hemocytes less responsive to tissue damage[85] – might mediate desensitisation.

1.3 *Danio rerio* as a vertebrate model

The freshwater fish *Danio rerio* (zebrafish) is native to South Asia and, like *Drosophila*, is particularly amenable for scientific use as they are both cost-effective and easy to maintain. Moreover, female zebrafish can spawn in the order of hundreds of eggs every 2-3 days[107]. Embryonic development occurs rapidly at 28.5°C, and all major organ precursors can be identified as early as 36 hours post fertilisation (hpf)[108]. Crucially, the early zebrafish larva is translucent and thus amenable to *in vivo* imaging. Documented use of zebrafish in research can be traced back as early as 1934[109] – while true pioneering work using zebrafish was published over 50 years later, following the generation of some of the earliest homozygous mutant vertebrates[110]. Since then, zebrafish have become vital to our understanding of many pathological conditions including cancer[111], neuropsychiatric disorders[112], diabetes[113–115] and liver disease[116].

1.3.1 Development of the zebrafish immune system

During the rapid development of the zebrafish embryo, hematopoiesis begins at 12 hours post fertilisation (hpf) where myeloid progenitors arise from the anterior lateral plate mesoderm[117]. This primitive wave of hematopoiesis is followed by a second wave at which, as in mammals, generates HSCs from the wall of the dorsal aorta[118]. These cells differentiate in the yolk sac, before migrating to a region of the tail named

the caudal hematopoietic tissue (CHT) between 24-30 hpf. The subsequent role of the CHT in hematopoeisis is analogous to that of the mammalian foetal liver[119].

Zebrafish macrophages have been identified as early as 15 hpf arising from the yolk sac of the developing embryo by the markers *draculin* and *L-plastin*[118]. These cells were demonstrated to be functional at 26-30 hpf, when they are seen to engulf erythroblasts from the blood and migrate to sites of infection[118]. Although the neutrophil marker myeloid-specific peroxidase (Mpx – the orthologue of mammalian myeloperoxidase) is expressed as early as 18-20 hpf[120], mature neutrophils are not identifiable until 48 hpf by electron microscopy of their electron-dense cytoplasmic granules[121,122]. These neutrophils in 2 day old fish were found to be functional following recruitment to tailfin wounds, and at 3 dpf neutrophils exist throughout the embryo – with a large population found in the CHT[120,121].

As a vertebrate, zebrafish also harbour an adaptive immune system – with fish B cells expressing immunoglobulin (Ig) proteins and T cells harbouring T cell receptor equivalents[123]. The fish thymus begins to develop after the innate immune system has been specified, alongside macrophage and neutrophil functionality, at 48 hpf[122]. Although T cell progenitors are seen invading the rudimentary thymus at 68 hpf[124], T cells are not seen in circulation until 3 weeks post fertilisation[125] – with their humoral responses not developing for a further 1-3 weeks. Furthermore, although VDJ rearrangement of zebrafish B cell Igμ has been detected as early as 4 dpf[126], Igμ expression is not seen until 10 dpf in the pancreas during the early stages of lymphopoiesis. Like T cells, others suggest B cells are not present until the fish reach 3 weeks of age[127]. Therefore, like *Drosophila*, the early zebrafish larva provides an innate immune specific model for the study of inflammation.

1.3.2 H_2O_2 damage signalling in zebrafish

In 2006, tail fin transection of larval zebrafish was introduced as a model for the study of innate inflammation[128], and has directly informed and corroborated studies in the fly. As in *Drosophila* epithelial wounding, a wave of calcium is rapidly produced from intracellular stores and persists for up to 5 minutes post transection[129]. This early signal is not only important in zebrafish inflammation, but further initiates the regeneration of the amputated tissue - which takes around 3 days[130].

Following the initial calcium wave, H_2O_2 produced by DUOX in epithelial cells is also released from the wound margin - with levels peaking at 20 minutes post injury[131]. This acts as a permissive signal for leukocyte recruitment, and *duox* knockdown in embryos causes a dramatic reduction in inflammation[132]. In neutrophils, the H_2O_2 signal oxidises and activates the SFK Lyn[102] – the orthologue of *Drosophila* Src42a[73] - to permit chemotaxis. Although zebrafish macrophage also express Lyn, their H_2O_2-mediated wound recruitment is not reliant on this kinase. Instead, a further SFK - Yes-related kinase (Yrk) - is involved in the transduction of the inflammatory signal[133] to promote macrophage recruitment. Currently, the signalling downstream of activated SFKs in zebrafish leukocytes remains to be elucidated.

This highlights the importance of H_2O_2-SFK damage signalling two distinct model organisms. Together, they offer an exciting and powerful model to investigate inflammatory cell recruitment to tissue damage whereby novel genes can rapidly be tested in *Drosophila* before being validated in a vertebrate system.

1.3.3 The roles of zebrafish neutrophils and macrophages at the wound site

As in mammals, neutrophils are the first cells to arrive at larval tail fin wounds, accompanied by macrophages previously resident in the fin fold. In the first 6 hours post fin amputation, neutrophils act to clear cellular

debris at the wound margin[134]. Although similar to the role of hemocytes at wounds in *Drosophila,* the phagocytic capability of neutrophils is dramatically reduced in comparison - as whilst hemocytes can contain an abundance of vacuoles[73] and disperse following debris uptake at the wound site[104], zebrafish neutrophils engulf a limited amount of detritus before undergoing apoptosis[134]. However more recent reports identify both neutrophil survival following injury in the fish and their subsequent reverse migration[135–137].

Zebrafish macrophage numbers at the wound site peak later at 48 hpi, due to reduced migration speed in comparison to the early responding neutrophils[134,138,139]. Once at the damage site, macrophages also begin to clear cellular debris - including neutrophil corpses. There is seemingly no recruitment interplay between neutrophils and macrophages following wounding in the fish, as each cell type retains the ability to respond to wounds in the absence of the other[134]. However, the loss of either population differentially affects the subsequent repair of the tissue. In the absence of macrophages, wound debris accumulates, and the subsequent regeneration of the tail is both delayed and defective. Conversely, the loss of neutrophils enhances fin regrowth[134]. This indicates differential functions of zebrafish leukocytes at wounds following H_2O_2 mediated recruitment.

As well as fundamental roles in neutrophil and macrophage recruitment, the loss of both H_2O_2 and SFK activity throughout the damaged tissue leads to the stalling of tailfin regeneration[133,140]. Thus, advances in our understanding of H_2O_2/Src42a signalling may be of wider importance in the field of repair.

1.4 Similarities to mammalian signalling

1.4.1 Hydrogen peroxide signalling

In vitro, H_2O_2 has been shown to promote chemotaxis of mouse peritoneal neutrophils[141]. Rat macrophages also respond to H_2O_2 *in vitro*, and undergo

cell spreading[142]. As seen in both *Drosophila* and zebrafish epithelial wounds, H_2O_2 production has also been identified at the site of dermal wounds in the mouse[143]. This has been shown to directly promote repair and regeneration – analogous to the role of H_2O_2 in the promotion of fin regeneration in the fish. Specifically, persistent wound-site H_2O_2 in the murine model is required for angiogenesis via VEGF expression. Thus, H_2O_2 constitutes a relevant inflammatory signal that can be easily studied in both *Drosophila* and zebrafish.

1.4.2 Src Family kinase (SFK) signalling

A variety of SFKs are important for mammalian immune responses. In macrophage, three predominant SFKs are expressed – Hck, Fgr and Lyn[144]. Mutations in both the *Hck* and *Fgr* genes dramatically impair mouse survival following *Listeria* infection[145], whilst triple mutant *hck, fgr, lyn* macrophages display extremely limited phosphorylation of downstream targets. Finally, gain-of-function mutation of Hck results in augmented inflammation *in vivo*, as well as increased macrophage phagocytosis[146]. Although SFK and subsequent Syk activity were shown to be dispensable for neutrophil chemotaxis *in vitro*[147], *hck, fgr* double knockout mice show reduced neutrophil recruitment to inflammatory sites in the liver[148]. This shows direct parallels to the role of Src42a, Lyn and Yrk activation in *Drosophila* and zebrafish inflammatory cell responses[73,102,129].

1.4.3 Immunoreceptor tyrosine activation motif (ITAM) signalling

Mammalian ITAM signalling has been most extensively studied in the adaptive immune system. ITAM motifs are found in the cytoplasmic domains of subunits of the B cell receptor (which activates B cells[149]), as well as in the CD3 complex[150], which associates with the T cell receptor to promote T cell activation. Functional ITAM domains are also found in the innate immune system – for example in the protein DAP12, which is important in natural-killer cell activation[151].

As described for Draper[73,80,82], both ligand-dependent and independent signalling occurs through mammalian ITAMs[152]. Following SFK phosphorylation, spleen tyrosine kinase (Syk) or Zap70 kinases are recruited to ITAMs[153] analogous to Shark recruitment to phosphorylated Draper in *Drosophila*[73,82]. Ultimately, SFK-ITAM-Syk signalling in mammalian leukocytes controls cell proliferation, survival and differentiation[152]. Thus, expanding our understanding of how the Draper ITAM signalling axis in *Drosophila* operates will provide direct insight to mammalian leukocyte signalling.

1.5 Genetic tools in model organisms

1.5.1 The GAL4/UAS system

A key genetic tool employed by model organism researchers is the Gal4/UAS system. The yeast *GAL4* gene encodes a positive transcriptional regulator[154] which binds to an Upstream Activating Sequences (UAS) in the yeast genome. This bipartite system was exploited by Fische*r et al*[155] who demonstrated its use for transgene expression in *Drosophila*. It has subsequently incorporated into zebrafish research[156]. When integrated into the genome and placed downstream of a known gene promoter, GAL4 can induce the expression of a subsequently encoded protein preceded by a UAS site. This allows for tissue-specific expression of both fluorophores and fluorescently tagged proteins for visualisation by microscopy. Gal/UAS can also be used for tissue-specific gene knock-down by RNAi.

1.5.2 RNAi knockdown in *Drosophila*

RNA interference (RNAi) induces gene silencing following the introduction of exogenous double stranded RNA into host cells. This is processed and cleaved to form the RNA-induced silencer (RISC) complex which is loaded with a single strand of RNA. This sequence targets the complex to complementary RNA within the cell and leads to its degradation following enzyme cleavage[157]. RNAi has been exploited for the degradation of target mRNAs for biological research following the generation of complementary RNA sequences that enter the RNAi pathway[158,159]. This results in the

decreased translation of the target protein. Several commercial libraries of transgenic UAS-RNAi are available for protein knockdown in *Drosophila*. The off-target effects of RNAi mediated gene silencing in the fly is reported to occur in 15-40% UAS-RNAi lines[160,161]. Thus, whilst tissue specific, RNAi knockdown must be used in conjunction with mutants for analysis.

1.5.3 Morpholino knockdown in zebrafish

Morpholinos are synthesised DNA derivatives which bind to mRNAs to block translation and splicing[162,163]. Following injection into developing zebrafish embryos they are able to deplete target protein expression[164]. Prior to the availability of direct gene editing, morpholinos were extensively used in zebrafish studies to elucidate protein function. However, once mutants were generated it became clear that morpholino phenotypes were both different and more severe in comparison[165,166]. Morpholino experiments must therefore be adequately controlled and compared to genetic mutants for validity[166].

1.5.4 CRISPR-Cas9 gene editing

The CRISPR-Cas system confers prokaryotes resistance to invading plasmids, viruses and phages[167]. The Cas enzyme associates with clustered regularly interspaced short palindromic repeat (CRISPR) guide RNA sequences (crRNA) encoded by the CRISPR locus to cleave complementary coded DNA at a proto-spacer adjacent motif (PAM) site (NGG). By generating a double stranded DNA break, bacteria and archaea are able to degrade foreign nucleic acids to prevent transmission. Three types of CRISPR-Cas systems have been identified[168] with differing complexity – particularly within the Cas protein, which is often functional as a multimer. The second family of systems (Type II) are relatively simple, with Cas9, a trans-activating crRNA (tracrRNA) and the targeting crRNA (guide RNA -gRNA) constituting a functional tripartite complex[169]. By generating gRNAs against genes of interest and injecting alongside Cas9

and tracrRNA it is possible to edit genes in living organisms for biological research purposes.

1.6 Thesis outline

By improving our understanding of damage signalling through exploitation of the genetic tools available for use in *Drosophila melanogaster* and *Danio rerio* we hope to identify novel, conserved regulators of inflammatory cell biology.

The aims of this project are to:

- Uncover novel players involved in embryonic hemocyte migration to epithelial wounds in *Drosophila* downstream of H_2O_2 and Src42a
- Determine whether novel regulators of inflammation in *Drosophila* are conserved in zebrafish

Chapter 2: Materials and Methods

2.1 Fly stocks

2.1.1 Macrophage drivers and fluorescent UAS-constructs

The following lines were used for the tissue specific expression of the subsequently listed UAS constructs in the hemocyte lineage. The fluorescent UAS constructs were either used to label hemocytes as a whole, or to allow for imaging of subcellular structures/proteins.

Driver lines				
Name	**Genotype**	**Expression**	**Supplier**	**Ref.**
serpent-Gal4	*;serpent-Gal4;*	Hemocytes	Gift from Paul Martin, University of Bristol	[170]
croquemort-Gal4	*croquemort-Gal4*	Hemocytes	Gift from Paul Martin, University of Bristol	[89]
serpent-Gal4.2	*w; {srp-Gal4.2}* & *w;; {srp-Gal4.2}*	Hemocytes	Generated in the lab by Kate Comber	unpublished
serpent-3xH2A-mCherry	*w; P{srp-H2A-3xmCh}* & *w;; P{srp-H2A-3xmCh}*	Hemocyte nuclei, weak expression in epithelium	Gift from Daria Siekhaus, IST Austria, Vienna	[171]

Table 2.1.1 a: Driver lines

Fluorescent UAS constructs			
Name	**Genotype**	**Supplier**	**Ref.**
UAS-GFP	*w; P{UAS-GFP}* *w;; P{UAS-GFP}*	Gift from Paul Martin, University of Bristol	[172]
UAS-eGFP	*w; P{UAS-2xeGFP}* *w;; P{UAS-2xeGFP}*	Bloomington Drosophila Stock Center	[173]
UAS-mCherry-CLIP	*w;; P{UAS-mCherry-CLIP170}*	Gift from Brian Stramer, KCL, London	[60]
UAS-drpr-GFP	*w; UAS-Drpr-I::GFP[attP16]* *w;; UAS-Drpr-I::GFP[VK27]*	Generated in the lab by Frederico Rodrigues	Unpublished
UAS-Pez-sfGFP	*w;; P{UAS-Pez-sfGFP[attP88]*	Generated for this project	Unpublished
UAS-Pez-mCherry	*w;; P{UAS-Pez-mCherry[attP88]*	Generated for this project	Unpublished

Table 2.1.1 b: Fluorescent UAS constructs

2.1.2 Mutants fly lines

Mutants used in this thesis are listed below. Where mutations were homozygous lethal, viable fly stocks were maintained over fluorescent balancer chromosomes to allow for the selection of homozygous embryos for experiments. The balancers used were either CyOdfd or CTG for the second chromosome, and TM3dfd, TM6bdfd or TTG for the third chromosome. The Bifocal mutant used in this study is viable, however the first chromosome balancer FTG was used to obtain the required stock also harbouring hemocyte-specific fluorescence. FTG/CTG/TTG chromosomes carry *twist-gal4, UAS-GFP* for ubiquitous GFP expression and CyOdfd/TM3dfd/TM6bdfd chromosomes carry *deformed-YFP* for YFP expression in the pattern of the *deformed* gene. Thus, these fluorescent balancers allow for the positive selection of mutant embryos.

Mutant lines			
Name	**Genotype**	**Supplier**	**Ref.**
White control	w^{1118}		
$CG10919^{MIMIC}$	y^1w^*; $Mi\{MIC\}CG10919^{MI13566}$	Bloomington Drosophila Stock Center (BDSC)	
$CG10919^{PBAC}$	w^{1118}; $PBac\{WH\}CG10919^{f00574}$	BDSC	
$Polybromo^{\Delta 86}$	$y^1w^{67}c^{23}$; $P\{EPgy2\}polybromo^{EY14080}$	BDSC	174
Phospho-glucomutase	y^1w^*;$P\{Mae-UAS.6.11\}Pgm1^{LA00593}$/*TM3*, Sb^1Ser^1	BDSC	
Pez^{CB}	w^{1118}; $P\{RS3\}Pez^{CB-5380-3}$/*Cyo*	Kyoto Stock Center	
Pez^2	*w*; Pez^2	Gift from Hugo Stocker, ETH Zürich, Zürich	175
Bifocal	y^1,$P\{SUPor-P\}Bif^{KG07899}$	BDSC	
$Mesh^{f04955}$	w^{1118};$PBac\{WH\}mesh^{f04955}$/*TM6B*,Tb^1	BDSC	

Misshapen^{172}	*w*; msn*^{172} *P{neoFRT}80B/TM6B*	BDSC	176
Draper$^{\Delta 5}$	*w;; drpr*$^{[\Delta 5]}$	Gift from Marc Freeman, OSHO, Portland	177
Src42a$^{[E1]}$	*w*^{1118}*; Src42A*^{E1}*/CyO*	BDSC	178

Table 2.1.2: Mutant lines

2.1.3 UAS constructs used for RNAi knockdown, rescue and overexpression experiments

The following UAS constructs were used to manipulate protein levels when combined with the appropriate Gal4 driver. UAS-RNAi constructs were used to induce hemocyte-specific knockdown of CG10919, Bifocal, Phosphoglucomutase, Misshapen, Pez, and Polybromo to probe for their cell-autonomous functions.

Further UAS constructs encoding Misshapen, Draper and full-length and truncated Pez proteins were also used for overexpression and rescue experiments in embryonic hemocytes.

UAS constructs for rescue/overexpression			
Name	**Genotype**	**Supplier**	**Ref.**
UAS-Pez	*w;; UAS-Pez[M{RFP.attP}]*	Gift from Hugo Stocker, ETH Zürich, Zürich	175
UAS-Pez$^{\Delta PD}$	*w;;UAS-Pez^{PDC1186A}[M{RFP.attP}]*	Gift from Hugo Stocker, ETH Zürich, Zürich	175
UAS-Pez$^{\Delta PTP}$	*w;;UAS-Pez^{PTP}[M{RFP.attP}]*	Gift from Hugo Stocker, ETH Zürich, Zürich	175
UAS-Pez$^{\Delta FERM}$	*w;;UAS-Pez^{FERM}[M{RFP.attP}]*	Gift from Hugo Stocker, ETH Zürich, Zürich	175
UAS-drpr-I	*w; UAS-Drpr-I*	Gift from Eric H. Baehrecke, UMass, Worcester	179
UAS-msn	*w*; P{UAS-msn.S}2*	BDSC	180

Table 2.1.3: UAS protein expression constructs

UAS constructs for RNAi			
Name	**Genotype**	**Supplier**	**Ref.**
KK RNAi control	*y,w[1118];P{attP,y[+],w[3`]}*	Vienna Drosophila Resource Center (VDRC)	
Trip control (luciferase RNAi)	*y1v1; P{TRiP.JF01355}attP2*	BDSC	[181]
CG10919/GD	*w^{1118}; P{GD13353}v23273*	VDRC	[182]
CG10919/KK	*w; P{KK107143}VIE-260B*	VDRC	[183]
SP7/KK	*w; P{KK111500}VIE-260B*	VDRC	[183]
Polybromo/KK	*w; P{KK101808}VIE-260B*	VDRC	[183]
PGM/GD	*w^{1118}; P{GD11561}v34954*	VDRC	[182]
PezTRiP861	*y1sc*v1; P{TRiP.HM500861}attP2*	BDSC	[184]
PezTRiP862	*y1sc*v1; P{TRiP.HM500862}attP2*	BDSC	[184]
Bifocal/KK	*w; P{KK105557}VIE-260B*	VDRC	
Mesh/KK	*w; P{KK101838}VIE-260B*	VDRC	
Misshapen RNAi TRiP	*P{TRiP.HMJ02084}*	BDSC	

2.2 Antibodies

The following antibodies were used in this research for immunofluorescent staining.

2.2.1 Primary antibodies

Antibody	Description	Epitope recognised	Supplier	Dilution	Ref.
Mouse anti-armadillo	N2 7A1 Monoclonal MIgG2a	Armadillo, *D. melanogaster*	Developmental Studies Hybridoma Bank	1:25	[185]
Chicken anti-GFP	Polyclonal IgY	GFP	Abcam Ab13970	1:500	
Mouse anti-mCherry	1C51 Monoclonal IgG2a	mCherry	Abcam Ab125096	1:500	
Mouse anti-singed	Sn 7C Polyclonal	Singed, *D. melanogaster*	Developmental Studies Hybridoma Bank	1:100	[186]
Rabbit anti-L-plastin	Polyclonal	L-plastin, *Danio rerio*	Gift from Yi Feng, QMRI, Edinburgh	1:500	[187]

Table 2.2.1: Primary antibodies

2.2.2 Secondary antibodies

Antibody	Description	Fluorescence	Supplier	Dilution
Goat anti-chicken	Polyclonal	Alexa Fluor® 488	Invitrogen A11039	1:200
Goat anti-mouse	Polyclonal	Alexa Fluor® 568	Invitrogen A21124	1:200
Goat anti-rabbit	Polyclonal	Alexa Fluor® 488	Invitrogen A11034	1:200
Goat anti-rabbit	Polyclonal	Alexa Fluor® 568	Invitrogen A11011	1:200

Table 2.2.2: Secondary antibodies

2.3 Fly work

2.3.1 Rearing conditions

Fly stocks not in immediate use were kept at 18°C in vials and flipped into new food approximately every 5 weeks. Food recipes are listed as in Appendix 1 – there was a change in food recipe following the lab relocation from the University of Bristol to the University of Edinburgh which did not affect viability.

2.3.2 Fly selection and crosses

To obtain flies of the correct age, sex and genotype flies were anaesthetised on CO_2 emitting pads (FlyStuff, SLS). Virgin females were selected dependent upon the presence of the meconium visible through the abdomen due to the lighter colour of newly eclosed flies.

To set up genetic crosses, virgin females and males of the required genotypes were placed in vials ensuring that the number of males did not outnumber the females. These vials were placed at 25°C, unless this lowered viability - in which case they were kept at room temperature (22°C) and flipped every 2-3 days to stimulate egg laying and prevent overcrowding of progeny. As with cross founders, once the cross progeny emerged, they were anaesthetised with CO_2 and selected by following phenotypic markers.

2.3.2 Embryo collection

Fly 'cages' (Figure 2.3.2) were made up using a custom-made, plastic, mesh-topped cylinder and a 55 mm petri dish containing apple juice agar (Appendix 2) spotted with yeast paste (Allinson Easy Bake Yeast mixed with distilled water) to stimulate laying. Newly eclosed flies were added to the cages and left to acclimatise for at least 24 hours before embryos were collected for experiments.

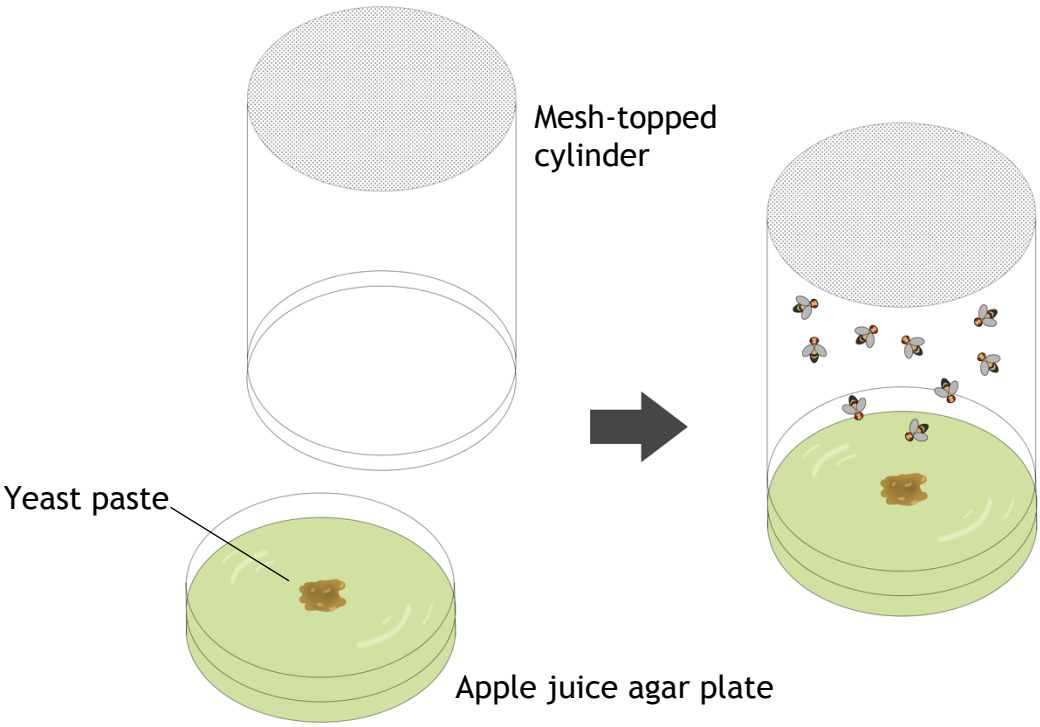

Figure 2.3.2: Fly cages for embryo collection

Custom-made, mesh top cylinders were fitted to apple juice agar plates to create a fly 'cage'. The apple juice plate spotted with yeast paste was changed every day for laying and collection of embryos.

For experiments, apple juice plates were changed between 4pm-6pm and cages were left at 22°C overnight for laying. The following morning, the plates were removed and washed with distilled water and agitated with a paintbrush to suspend embryos. The embryos were subsequently collected using a cell strainer (Fisherbrand 70 µm). Following this, cell strainers were submerged in bleach for 1 min and 20 seconds to dechorionate the embryos. To remove the bleach the embryos were washed in copious amounts of distilled water.

To select embryos of the appropriate stage and genotype, cell strainers containing dechorionated embryos were viewed down a Leica M165 FC Fluorescent benchtop microscope. This allowed for visualisation of the autofluorescent amnioscerosa for staging, as described in the Atlas of *Drosophila* development[188], as well as fluorescent balancers to negatively select against for genotyping.

2.4 Live imaging

2.4.1 Mounting embryos for live imaging

Following dechorination and embryo selection as described in 2.3.2, embryos were picked using a custom-made tungsten needle and placed on double sided scotch tape affixed to a glass microscope slide. The embryos were then orientated ventral side up using the needle and covered with a small drop Voltalef oil (VWR International). Two 1.5 size coverslips (Scientific Laboratory Supplies, SLS) were stuck down either side of the mounted embryos to make a 'bridge' to prevent crushing of the embryos before a 1 size coverslip (SLS) was placed over the top. The top coverslip was secured in place using nail polish spotted at each corner. Mounted embryos were left for a minimum of 5 minutes to allow for the nail polish to dry, and for the embryos to recover from the process.

2.4.2 Live imaging

The majority of this project was conducted on a spinning disc confocal microscope (Ultraview; PerkinElmer). For wounding and cell morphology studies, a Plan Apochromat x40 (NA 1.3) oil objective lens was used. However, for the study of fluorescent proteins at the subcellular level *in vivo* a Plan-Apochromat x63 (NA 1.4) oil objective lens was used. Further experiments were conducted on a Zeiss LSM880 Airy Scanning confocal using a Plan Apochromat x40 (NA 1.3) oil objective lens.

For basal migration and wound recruitment, Z-Stacks were collected to a depth of 10 µm at an interval of 0.5 µm. For basal migration and wound recruitment, images were acquired at 30 second intervals. To investigate

protein dynamics (Pez/Draper), Z stacks of 7 µm depth imaged every 0.5 µm were acquired every 15 seconds.

2.4.3 Wounding by laser ablation and analysis

A micropoint nitrogen ablation laser (Andor) was fitted to both a Leica DMI6000B Ultraview Vox spinning-disk system (Perkin Elmer) and a Zeiss LSM880 Airy Scanning confocal. This was used to reproducibly ablate the epithelium of the embryo on the ventral surface.

To calculate the wound perimeter, images were exported to FIJI and the Bright Field channel was used to visualise the wound edge. This was subsequently measured using the ellipse shape function. For consistency in the quantification of hemocytes recruited to the wound, hemocytes were counted provided their cell body touched the boundary line of the wound perimeter (Appendix 3.4.1). The number of hemocytes recruited to wounds was divided by the perimeter to take into account differing wound sizes.

2.4.4 Embryo injection

To assess the space occupied by the embryonic macrophages, 70kDa rhodamine-dextran (Molecular Probes/Invitrogen) was injected into the embryo underneath the epithelium. Embryos were mounted as described above (2.4.1), but Volatef oil and top coverslips were not added until after injection. Prior to injection, embryos were desiccated in a small box containing silica beads (Sigma-Aldrich) for 7 minutes to aid the injection process by creating space in the embryo. A FemtoJet/InjectMan injection system (Eppendorf) and Femototips size II were then used to inject into the head region of the embryo. The mounting process was then completed as described in 2.4.1.

2.4 Fixed samples

2.4.1 Embryo fixation

Following dechorionation (2.3.2), embryos were collected from a cell strainer using a paintbrush and transferred to a small glass vial containing a 1:1 ratio of 4% methanol-free paraformaldehyde (MP Biomedicals, diluted in

PBS) and heptane (Sigma-Aldrich). Where the genotype of interest did not occur at a high frequency following overnight laying, embryos were selected by the absence of fluorescent balancers as described above (2.3.2). Following selection with a Tungsten needle they were transferred individually into a glass vial containing fixative mixture. Vials were then placed on a rotator at (Stuart, SB3) at maximum speed (40 rpm) at room temperature for 20-30 minutes. The lower aqueous phase was then removed using a glass Pasteur pipette (VWR international) and replaced with an equal volume of 100% methanol. Embryos were then devitellinised by vigorous shaking of the glass vial – meaning they sank to the bottom of the lower methanol phase. The methanol containing devitellinised embryos was then removed using a glass Pasteur pipette and transferred to an Eppendorf. Embryos were then washed thrice with 100% methanol and stored at -20°C.

2.4.2 Immunostaining

Before staining, embryos were quickly washed thrice in PBS-Tx-BSA (0.3% Triton-X (Sigma-Aldrich), 0.5% BSA (Sigma-Aldrich)) and left on an orbital shaker (Stuart) for 20 minutes – this process was repeated 3 times. Primary antibodies diluted in PBS-Tx-BSA were then added following the removal of the last wash, and embryos were incubated at 4°C overnight. Once incubated, embryos were washed thrice with PBS-Tx-BSA for 10 minutes, interspersed with three quick washes each time. A blocking solution of 2% horse serum (Sigma-Aldrich) diluted in PBS-Tx-BSA was then added and Eppendorfs were left on a rotator for 30 minutes at room temperature. Following blocking, secondary antibodies were diluted in PBS-Tx-BSA were added and incubated at room temperature for 1 hour in the dark on a rotator. Again, to remove the antibody embryos were washed thrice with PBS-Tx-BSA for 10 minutes, interspersed with three quick washes. Once the last wash was removed, embryos were covered with Vectashield Mounting Medium (Vector Laboratories Inc.) and stored at 4°C until mounted.

2.4.1 Mounting fixed embryos

Stained embryos were transferred to a watch glass using a glass Pasteur pipette. Embryos of the correct genotype and stage were selected under a

fluorescent bench top microscope and transferred to a glass slide (as per 2.4.1 – microscope slide, double sided scotch tape, size 1.5 coverslip side bridges and size 1 coverslip top). A single embryo was selected using a P2/10 pipette (Pipetteman), this was then orientated by moving the top coverslip until the embryo rolled into the correct position. Once this was achieved, the top coverslip was fixed in place using nail polish. For hemocyte dispersal, embryos were mounted laterally, for protein expression embryos were mounted ventral side up to visualise macrophage.

2.4.1 Imaging of fixed samples

For macrophage dispersal, fixed embryos ranging from stage 11-15 were imaged using a Zeiss LSM880 confocal microscope with a 25x/NA 0.8 objective lens visualise the entire embryo. For a more detailed assessment of locus expression a 40x/NA 1.3 objective lens was used.

2.5 Zebrafish work

2.5.1 Rearing conditions

Adult zebrafish (*Danio rerio)* were kept and handled according to UK Home Office Regulations. Transgenic zebrafish used in this project were maintained under the Home Office license held by Dr Yi Feng at the QMRI, University of Edinburgh.

2.5.2 Breeding and embryo collection

Breeding tanks of adult zebrafish were set up the evening before embryos were required. Two female fish were placed in a breeding tank and were separated from a single male using a tank divider. The following morning, tank dividers were removed, and fish were allowed to mate. To collect eggs, the adult fish were transferred to a new tank, and the water from their breeding tank was run through a small sieve. The sieve was then washed through to remove tank debris, before the eggs were transferred to a 100mm Petridish (Thermo Scientific) by washing the sieve with embryo medium (see Appendix 3). Embryos were kept for up to 4 days post fertilisation at 28.5°C in an incubator with light cycle.

2.5.3 Transgenic zebrafish lines

The following transgenic fish were used for visualisation of neutrophils and macrophage within larvae.

Fluorescent lines			
Marker	**Strain/Genotype**	**Supplier**	**Ref.**
DsRed Neutrophils	*Tg{Lysc:DsRed2}*	Gifted use by Yi Feng, University of Edinburgh	[189]
Nuclear mScarlet Macrophage	*Tg{Mpeg:NLS-Scarlet}*	Gifted use by Yi Feng, University of Edinburgh	Unpublished

Table 2.5.2: Transgenic zebrafish

2.5.4 Microinjection morpholino into zebrafish embryos

Once eggs were collected following successful breeding (2.5.2), they were aligned along a microscope slide held in a Petridish lid. A PicoLiter Injector (Warner Instruments, PLI-90A) and custom-made borosilicate glass capillary needles (World Precision Instruments 1B100F-4) were used to inject the required amount of morpholino liquid into the yolk sac of 1-4 cell stage embryos. Prior to injection, morpholinos were heated to 65°C for 5 minutes.

Morpholinos used in this thesis to knockdown MEGF10 are documented below. To remain consistent with the publication which generated and validated these sequences, the names remain the same (thus MO2 is omitted).

	Morpholino sequences			
Name	**Sequence**	**Target**	**Amount**	**Ref.**
COMO	CCTCTTACCTCAGTTACAATTTATA	Control - human beta-globin intron	6ng	
MO1	ACACGCTGCACAAAGACACAAAGCT	MEGF10 - 3' splice acceptor of intron 4–exon 5	6ng	[190]
MO3	TATTTGCAGTGTTTGTCTCACCTGC	MEGF10 - 5' splice donor of exon 8-intron 8	12ng	[190]

Table 2.5.4: Morpholino sequences

Following injection, embryos were reared to 3 dpf at 28.5°C – when the fish become larvae following hatching[108]. Each day, dead embryos were removed, and the embryo medium replaced.

2.5.5 Validation of morpholino disruption

To validate splice disruption of MEGF10 following morpholino injection, RNA was extracted and cDNA synthesised according to the published protocol by Peterson and Freeman[191]. Briefly, 50 3 dpf larvae from both conditions (COMO and MO1) were culled with anaesthetic and placed into a 1.5 ml Eppendorf tube. The medium was removed and replaced with 250 µl Trizol (Invitrogen) and larvae were gently homogenised with a pestle. An additional 750 µl Trizol was added and the samples were incubated at room temperature (RT) for 5 minutes. Following this, 200 µl chloroform (Sigma-Aldrich) was added and tubes were repeatedly inverted to mix for 15 seconds. Samples were then incubated at RT for 2 minutes, before being spun at 12,000 g for 15 minutes at 4°C in an ultracentrifuge. Following this, the colourless upper phase (which contains RNA) was transferred to a new Eppendorf and 500 µl isopropanol (Sigma-Aldrich) was added to precipitate.

Samples were incubated at RT for 10 minutes before being centrifuged at 10,000g for 15 minutes at 4°C to form a gel-like pellet of RNA at the bottom of the tube. The supernatant was removed, and the pellet washed in 1 ml of 75% ethanol (Sigma-Aldrich) with gentle mixing by inversion. Following centrifugation at 7,500g for 15 minutes at 4°C the ethanol was removed, and the pellet allowed to air dry for 10 minutes. The RNA pellet was resuspended in 100 µl RNase free water (Sigma-Aldrich) following incubation for 10 minutes at 55°C with finger vortexing. RNA quality was checked using a nanodrop.

cDNA was synthesised using the SuperScript™ First-Strand Syntehesis System for RT-PCR (Invitrogen, Life Technologies). 1-2 µg of total RNA was transcribed according to protocol using supplied oligo(dT) primers. PCR was then performed (GoTaq Polymerase, anneal temp 58°C, 38 cycles) on the resulting cDNA of the MO1 locus using the following primers:

MO1 fwd: AATGCATCGACGCAAGTCTC
MO1 rev: ACACACACCACCGTTCTGAC

This would yield a fragment of 481 bp in the absence of morpholino, and a fragment of 379 bp following exon skipping by morpholino disruption as previously reported[190].

2.5.6 CRISPR-Cas9 gene editing of zebrafish embryos

To generate transient CRISPR mutant zebrafish embryos, guide RNA sequences containing BSiYi/MwoI sites, and thus PAM sites, were identified in both MEGF10 and PTPN21 DNA sequences as far upstream of the gene as possible. Synthesised RNA was obtained from Sigma-Aldrich/Merck. These are outlined in the following table as the complementary target DNA sequence with PAM site:

CRISPR guide sequences			
Name	**Target DNA sequence including PAM**	**Target**	**Restriction enzyme**
MEGF10 gRNA1	GCTACAGAACGGCCTATCGCagg	MEGF10 exon 3	BSiYI
MEGF10 gRNA2	TGTCAGTGTGAGCCGGGCTGggg	MEGF10 exon 4	BSiYI
PTPN21 gRNA1	GAATCAGGGCGCTGTGCCGGtgg	PTPN21 exon 12	BSiYI
PTPN21 gRNA2	GGTGGCATCATGTAGGGCTGcgg	PTPN21 exon 11	MwoI

Table 2.5.6: CRISPR target sequences

Embryos were injected into the cell at the single-cell stage with the following mixture:

- 1 µl tracrRNA (250ng/µl – Sigma-Aldrich)
- 1 µl gRNA1
- 1 µl gRNA2
- 0.3 µl NLS-Cas9 (NE BioLabs)
- 1.7 µl RNAse free water (Sigma-Aldrich)

For control injections, Cas9 was omitted and replaced with a further 0.3 µl RNAse free water.

2.5.7 Tailfin transection at 3dpf and fixation timepoints

3 dpf larvae were anaesthetised by the addition of a few drops of 0.02% buffered 3-aminobenzoic acid ethyl ester (Tricaine/MS-222) into the embryo medium and were left until paralysed. Using a non-sterile scalpel, the entire tailfin and a small portion of the trunk distal to the end of the vasculature was removed on a bench top microscope. The time was logged for each batch of amputated fish and amputation time was controlled to a maximum of 15 minutes. The embryo medium was then replaced, and dishes were returned to 28.5°C.

At 2 hours post injury (hpi), 6 hpi and 22 hpi larvae were culled using an abundance of Tricaine. They were subsequently collected into 1.5 ml Eppendorf tubes and the anaesthetic medium was replaced with 4% Paraformaldehyde containing 0.4% Triton-X diluted in PBS. Fish were then left to fix overnight at 4°C or at RT for 2 hours.

2.5.8 Staining of zebrafish embryos and imaging

Following fixation, fish were washed in PBS containing 0.1% Triton-X (PBST) thrice for 20 minutes on a benchtop orbital shaker. They were then blocked with 5% horse serum diluted in PBST at room temperature for 2 hours. Primary antibodies were diluted in 2-5% horse serum in PBST. Embryos were covered with 500 µl antibody mixture and left to shake on an orbital shaker overnight at 4°C. Following antibody incubation, fish were washed thoroughly in PBST (8-10x for 20 minutes). Secondary antibodies were diluted in PBST containing 2-5% horse serum. 500 µl of secondary mixture including 1 µl Dapi was used to cover samples and they were left at 4°C overnight covered on an orbital shaker. Finally, the secondary antibodies were removed, and stained fish were washed in PBST 8 times for 15 minutes each. They were then placed into Vectashield mounting medium.

Stained samples were batch mounted laterally in Vectashield onto microscope slides and squashed beneath a top coverslip to the height of bridging coverslips (SLS size 1). Coverslips were secured with nail polish. Samples were imaged using 25x objective lens (numerical aperture 0.8) on a Zeiss LSM880 confocal microscope. Z-stacks through the entire fish tail were acquired in 2 µm steps.

2.5.9 Quantification of wound recruitment

Images were exported to FIJI and neutrophils and macrophage recruited to the wound margin were quantified in a zone up to 150 µm proximal to wound margin.

2.6 Data collection and statistical testing

All data was logged using Microsoft Excel, and simple functions such as hemocytes/µm of wound perimeter were calculated here.

For statistical testing, data was imported into GraphPad Prism for analysis. To determine the appropriate statistical test for each experiment, distribution was tested for by normality tests included in the software. F-tests were also used to determine whether the standard deviation of separate data sets were comparable. The results of these tests were used to select the correct tests which are recorded at the bottom of each graph presented in this thesis. Significance is annotated by: * $p<0.05$, ** $p<0.01$, *** $p<0.005$, **** $p<0.001$. Graphs were generated and exported from Prism.

2.7 Image processing

Following analysis using FIJI, images were saved in TIFF format. Brightness and contrast were auto corrected for images to allow for best visualisation. Scale bars and image panels were generated in FIJI, before being exporting to Adobe Photoshop for figure building.

Chapter 3: A phosphoproteomic screen uncovers novel regulators of hemocyte biology

3.1 Introduction

3.1.1 Inflammation in *Drosophila* – key players and uncovering novel phosphotargets

The use of *Drosophila melanogaster* to study inflammatory cell biology provides an excellent platform – not only due to the genetic toolkit available to Drosophilists, but also the ability to exploit live imaging. The embryonic stage harbours a population of macrophage-like cells, termed hemocytes[50], which carry out a variety of functions including apoptotic cell clearance and pathogen engulfment. Hemocytes also sense and undergo chemotaxis towards sites of tissue damage, where they perform the important function of clearing both the necrotic and apoptotic debris generated[89].

Previous work has identified the signalling pathway responsible for recruiting *Drosophila* hemocytes to wounds. Upon laser ablation of the embryonic epithelium, an initial wave of calcium emanates out from the site of damage[73]. This calcium wave triggers the activation of the NADPH oxidase enzyme DUOX via its EF hands, leading to the rapid production of Hydrogen Peroxide (H_2O_2)[91]. The H_2O_2 inflammatory signal is essential in recruiting both hemocytes in *Drosophila* and leukocytes in zebrafish to sites of tissue damage[100,129,131]. Within *Drosophila* hemocytes, the H_2O_2 signal oxidises the tyrosine kinase Src42a, resulting in its activation. This subsequently leads to the phosphorylation of the cell death receptor Draper on its intracellular immunoreceptor tyrosine-based activation motif (ITAM) domain[82]. This phosphorylation event causes Shark kinase activation and subsequent hemocyte migration to the wound site. This entire cascade reflects the SFK-ITAM-Syk signalling pathway employed by the vertebrate adaptive immune system[192]. As the immune system is highly complex, we hypothesise that both H_2O_2 mediated oxidation and Src42a activation may target other intracellular proteins involved in the damage response of hemocytes.

To investigate this further, a phosphoproteomic assay was undertaken in the lab to uncover novel candidate hemocyte-specific proteins with altered phosphorylation states dependent upon H_2O_2 stimulation and/or Src42a activity (unpublished and conducted by Dr Fred Rodrigues, figure 3.1.2).

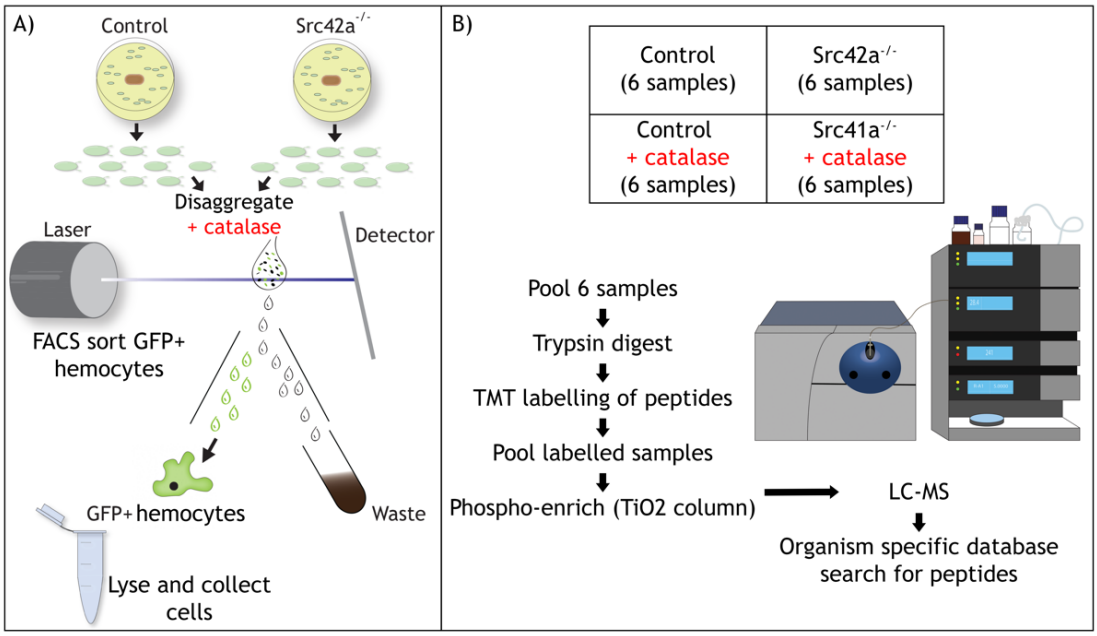

Figure 3.1.1: Schematic for phosphoproteomics assay to uncover novel H2O2/Src42a dependent phosphoproteins.

A) Processing of control (*srp-gal4,UAS-GFP*) embryos and Src42a mutant embryos (*Src42a[E1]; srp-gal4, UAS-GFP*). Embryos were selected at stage 15 and were disaggregated by crushing in the presence/absence of catalase. GFP+ hemocytes were subsequently sorted by FACs, collected, lysed and stored. B) In total 6 samples for each condition were collected. These were pooled and protein levels were normalised by μg protein. Samples were then digested with trypsin, and the resultant peptides were labelled with TMT depending on condition. All labelled samples were then pooled, and phospho-enriched by TiO2 column. Both the flow through and phosphoproteins were then sent for LC-MS and the resultant peptides detected were searched for in organism specific databases.

Briefly, both control and *Src42a*$^{[E1]}$ mutant embryos were selected at stage 15 and disaggregated by crushing. This disrupted the entire embryonic epithelium to engage global inflammatory signalling in place of a single ablation wound. Disaggregation was carried out in both the presence and absence of catalase - to quench the resultant H_2O_2 signalling -, and GFP positive hemocytes (via UAS-GFP driven under the control of *serpent-Gal4*) were collected by fluorescence activated cell sorting (FACs). Hemocytes were then lysed and each condition was digested with trypsin to obtain peptide fragments. Peptides were then tandem mass tag (TMT) labelled according to sample, before being pooled. Following phospho-enrichment the pooled sample was investigated by liquid chromatography-mass spectrometry (LC-MS). An organism-specific database search was then conducted to identify for the peptides isolated by this method.

In total, this approach detected 421 phosphopeptides that were depleted by more than 30% following the abolition of the H_2O_2-Src42a signalling pathway (Figure 3.1.2A) – with 25% of these (105) being reduced in all conditions tested. To analyse these results further, GO analysis was completed using the PANTHER v.14.0 system (http://www.pantherdb.org[193] – Figure 3.1.2 Bi-iii). Unexpectedly, this revealed a high abundance of proteins associated with metabolic processes (Bi). This, coupled with an abundance of proteins belonging to the nucleic acid binding class PC00171 (Biii), perhaps indicates the presence of false-positives within the data set - however proteins with more expected associations such as the biological processes localisation (GO:0051179) and adhesion (GO:0022610) were also identified in lower number. Finally, a high percentage of the proteins identified were associated with catalytic activity (GO:0003824) perhaps indicting further enzymes alongside of the kinase activity of Src42a are regulated downstream of H_2O_2 signalling in hemocytes.

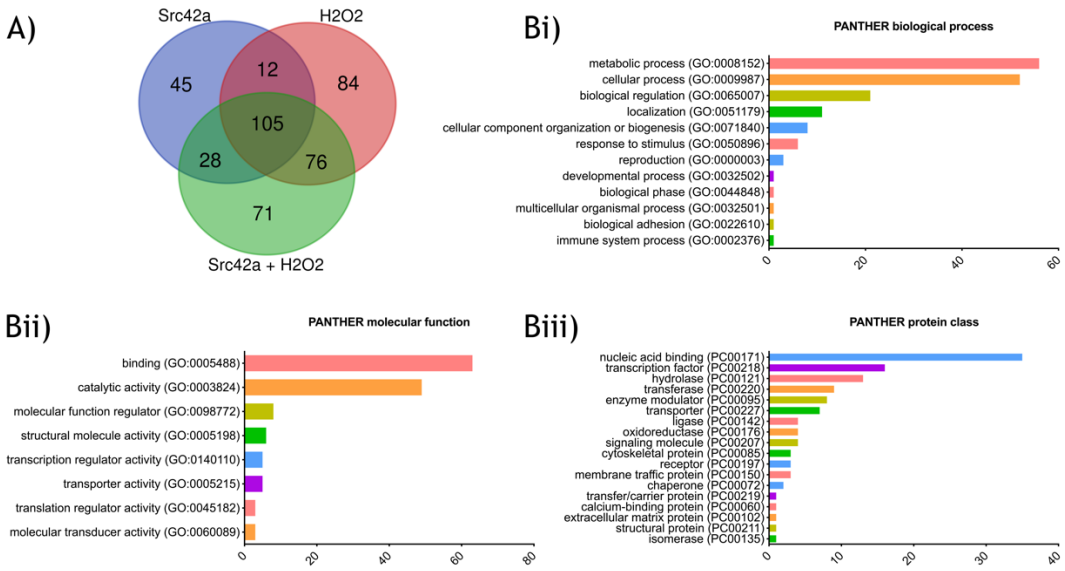

Figure 3.1.2: Analysis of proteomics hits with phosphorylation statuses dependent upon H_2O_2-Src42a damage signalling in hemocytes.

A) Venn diagram to illustrate the number of hemocyte-derived peptides with phosphorylation statuses increased in the presence of the labelled pathway constituent. 421 peptides were identified in total with decreased of 30% in level following the addition of catalase and/or Src42a mutation. Bi-iii) GO analysis performed using PANTHER for biological process, molecular function and protein class for the phosphoproteins dependent upon H_2O_2 and/or Src42a signalling for their phosphorylation.

Due to the diverse nature of the phosphoproteins identified by this approach, suitable candidates were selected for testing dependent upon the level of change recorded for the phosphopeptide detected. The hits with the greatest change were then compiled, and a literature search was completed to identify the most promising candidates. Those chosen are outlined in Table 3.1.1. By investigating these proteins, we hope to uncover novel players implicated in the wound response of *Drosophila* embryonic macrophages.

Protein identified	**Level in absence of Src42a**	**Level in absence of H_2O_2**	**Level in absence of Src42a+H_2O_2**	**Modification**
Bifocal	0.119 5.978	0.263 0.9	0.319 6.211	Multiple Ser P; Thr P
Phospho-glucomutase	0.302	0.263	0.319	Thr P
Polybromo	0.457	0.577	0.34	Ser P
Mesh	0.319	0.717	0.389	Thr P; Ser P
Misshapen	0.63	0.549	0.667	2x Ser P; Tyr P
Pez	0.46	0.272	1.007	2x Ser P
CG10919	2.258	17.19	17.514	Met oxidation

Table 3.1.1: Proteins of interest identified by phosphoproteomics.
The level of phosphoprotein present expressed as a function of the amount in control. Modifications detected listed as well as defect uncovered in this thesis. Levels are expressed as a function of the abundance in the WT control sample.

3.1.2 Existing literature on proteomics hits and rationale

To assess the suitability of the candidates outlined in Table 3.1.1 for investigation in an inflammatory cell context, we examined previous literature. Context and rationale are briefly explored for each protein below:

Bifocal

Bifocal was first identified in 1997 as a protein of 1063 amino acids in length which colocalises with F-actin and plays a key role in photoreceptor morphogenesis[194]. Antibody staining of developing embryos revealed Bifocal expression from the blastoderm stage through to stage 16 – where expression was seen strongest throughout the central nervous system (CNS). Over expression of Bifocal has been shown to impact on photoreceptor cell migration, which is thought to be due to a potential role in cytoskeletal regulation[195]. In 2005 Bifocal was shown to directly bind to F-actin with a specific binding region at the protein's N terminus[196]. Here, we have identified Bifocal expression in *serpent*-Gal4 expressing cells in the embryo, which may indicate a further role outside of the CNS. As actin remodelling is important for the function of hemocytes – for example the activation of the Arp2/3 complex by SCAR/WAVE is crucial to lamellipod formation and migration[66]. Therefore, it may be that Bifocal plays an actin dependent role in hemocyte responses following H_2O_2/Src42a dependent phosphorylation.

Phosphoglucomutase (PGM)

The enzyme phosphoglucomutase is essential for the conversion of glucose-1-phosphate to glucose-6-phosphate (G-6-P). If the cell requires energy, G-6-P enters the glycolytic pathway to provide ATP - otherwise G-6-P is used to generate biosynthetic intermediates. Whilst it is reasonable to assume that an enzyme with an intermediate phosphorylated state may be a 'red-herring' result following phosphoenrichment, the PGM phosphopeptide detected was the second most decreased in the absence of H_2O_2 and Src42a. This may therefore indicate an inflammation specific role in hemocytes. Excitingly, glycolysis has been shown to be important in both neutrophil and macrophage functions (reviewed in[197]).

Polybromo

Polybromo is a core component of the chromatin remodelling complex named Polybromo containing Brahma-associated proteins (PBAP)[198]. PBAP and BAP (which contains the protein OSA in place of Polybromo and BAP170) are found in distinct chromosome regions where they regulate gene expression. In the context of immune responses, the BAP complex is required for transcription of antimicrobial peptides following bacterial infection[199]. More recently, it was shown that Polybromo directly influences inflammation in the gut independently of the PBAP complex[200]. *Polybromo* mutant flies have hyper-inflamed guts which contributes to increased mortality rates following bacterial infection. It may be that Polybromo also contributes to the inflammatory activation of hemocytes.

Mesh

The transmembrane protein Mesh is 1431 amino acids long and contains several extracellular domains including a complement control protein (CCP) domain[201]. Mesh is thought to mediate cell-cell interactions at septate junctions and is strongly expressed in the developing gut of the embryo. As well as affecting gut morphology, the loss of Mesh reduces ROS production in the gut leading to an increase in bacterial load[202]. No role for Mesh is described outside of the gut, however a further CCP domain containing protein, SR-C, is known to act as a phagocytic receptor in hemocytes[203]. It may be that Mesh's CCP plays an additional functional role in hemocytes.

Misshapen

Misshapen is a serine/threonine kinase[176] and was selected from the results of the phosphoproteomics assay as many of the top hits – including those described above – were phosphorylated on serine or threonine residues, rather than tyrosines (which constitute Src42a target sites). As misshapen itself was phosphorylated on a tyrosine residue dependent upon H_2O_2 and Src42a we reasoned it may well provide a kinase link to our proteins of interest. In fact, Bifocal has already been identified as a downstream phospho-target of Misshapen in photoreceptor growth cone motility[195]. Misshapen expression is seen in the mesoderm during embryonic

development and is also weakly expressed in the CNS. As well as being involved in the control of cell shape in the eye, misshapen also modulates egg chamber size and shape through actin organisation[204].

Pez

Pez is a PTP type phosphatase which harbours an N-terminal FERM domain[175]. In *Drosophila*, Pez acts upstream of the transcriptional activator Yorkie to control intestinal stem cell proliferation. This function is dependent upon the FERM domain, and the catalytic activity of the protein is refuted[205]. The mammalian orthologue of Pez – named PTPN21 – has been implicated in Src family kinase signalling – where it has been shown to bind directly to Src and even augment signalling[206–208]. We therefore chose to investigate Pez based on its potential to interact with Src42a directly.

CG10919

No literature on CG10919 exists. According to FlyBase, the locus produces a protein of 187 amino acids long with no obvious functional domains. We selected this protein for investigation as it was the only modified protein that increased in all conditions.

3.1.3 Chapter aims

Having identified proteins with an altered phosphorylation status dependent upon H_2O_2 and Src42a in *serpent-Gal4* expressing cells we hypothesise that some may be novel regulators of hemocyte biology. The aims of this chapter are therefore to:

1. Determine whether the proteomics hits regulate basal hemocyte behaviours.
2. Determine whether the proteomics hits are involved in recruitment of hemocytes to wounds.

Results

3.2 Basal hemocyte behaviour in proteomics mutants

3.2.1 Mutant embryos display normal developmental dispersal patterns of embryonic hemocytes

To examine whether the proteins of interest have any effect on the basal migration of hemocytes, their developmental dispersal was investigated in comparison to control animals. Hemocytes differentiate from the mesoderm in the head of the developing fly and migrate out along prepatterned routes that are governed by the expression of PDGF/VEGF (PVF) ligands[57]. PVFs activate PVR receptors on hemocytes to drive their migration. Hemocytes migrate both ventrally along the ventral nerve cord and dorsally, so that by stage 14 in embryonic development they occupy the entirety of the ventral midline. Cytoskeleton dynamics underlying motility, as well as the β-integrin myospheroid, are also key for the complete and correct dispersal of hemocytes[60,61,66,186].

Following fixation and staining at stage 14 in embryonic development and lateral visualisation, we revealed no obvious defect in developmental dispersal in the mutants tested, as hemocytes were observed occupying the entirety of the ventral midline (Figure 3.2.2). This indicates that hemocytes are properly specified in the mutants tested, and that they are adequately positioned to respond to epithelial wounds. Mesh and Polybromo mutants are omitted as no data was collected.

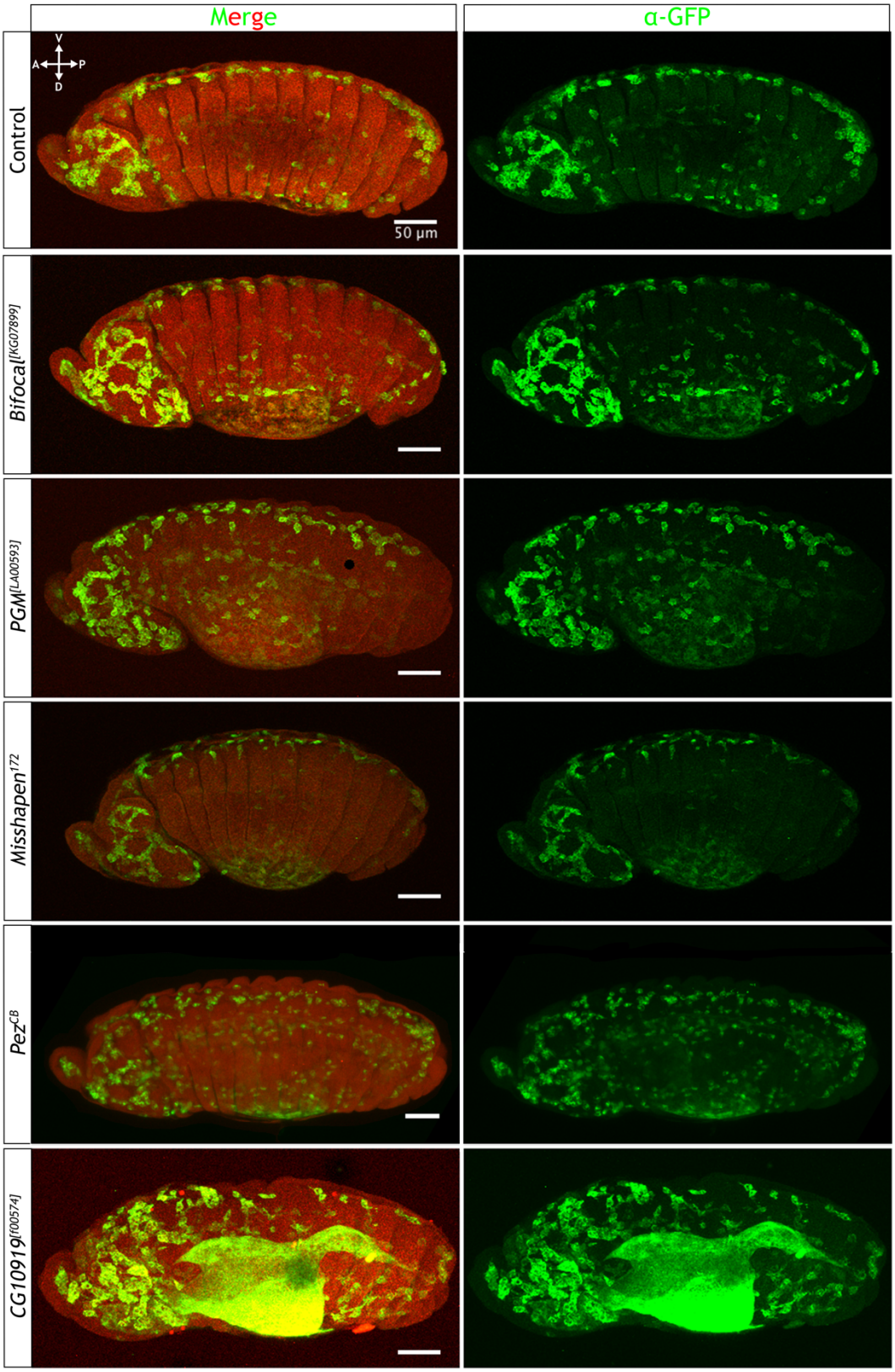

Figure 3.2.1: Normal hemocyte dispersal in mutant embryos.

Stage 14 proteomics mutants expressing *serpent-Gal4,UAS-GFP* were fixed and stained with α-GFP (488 secondary) and α-singed (561 secondary). Representative images show hemocytes have migrated to occupy the ventral midline and are comparable to control. Scale bars at 50μm.

3.2.2 Investigating basal hemocyte morphology in phosphoproteomic mutants

In order to investigate hemocyte function at stage 15, commercially available mutants were obtained and crossed to *;serpent-Gal4, UAS-GFP;* or *;;serpent-Gal4.2, UAS-2xeGFP* - dependent upon the which chromosome the mutation was located on. The *srp-Gal4(.2)* driver lines are highly specific for hemocytes[170]. We imaged mutant embryos at stage 15 and observed cell morphology. This revealed normal cell shape – with cells harbouring a sheet-like lamellipod extending out from the cell body - in all mutants except *misshapen*[172] (Figure 3.2.3A). Hemocytes in this mutant displayed a stellate appearance which we investigate further below.

A major function of hemocytes during embryogenesis is the engulfment of developmentally generated apoptotic debris. These engulfed apoptotic bodies appear as vacuoles contained within the cell body of hemocytes at stage 15 – which are completely absent if global apoptosis is blocked[72]. As well as being critical for normal development to proceed, corpse engulfment is required for the upregulation of Draper and the subsequent response of hemocytes not only to epithelial wounds, but to pathogenic insult[72]. Draper itself is also involved in efferocytosis[81,82,177], and can be seen accumulating at phagocytic cups *in vitro*[80] and *in vivo* (unpublished Wood lab data). Although dispensable in the process of engulfment, Draper plays a crucial role in the processing of engulfed corpses – which is independent of the intracellular ITAM motif[73]. This function of Draper is reflected as increased vacuolation of hemocytes is overserved in *Draper* mutant cells.

As vacuolation is therefore a readout of both the phagocytic and processing ability of these cells we sought to quantify the number of vacuoles across our mutants. To achieve this, vacuoles were manually counted across 10 μm Z-stacks in cells where the entire cell body could be identified. The total number of vacuoles counted was divided by the number of hemocytes analysed to obtain an average number of vacuoles per cell. As well as control embryos, we also quantified vacuolation in *Src42a*$^{[E1]}$ mutants. This approach revealed normal numbers of vacuoles across all mutants except *Src42a*$^{[E1]}$ –

which showed increased vacuolation – and *Misshapen*^{172} – which showed lower numbers of vacuoles when compared to control cells (Figure 3.2.3B).

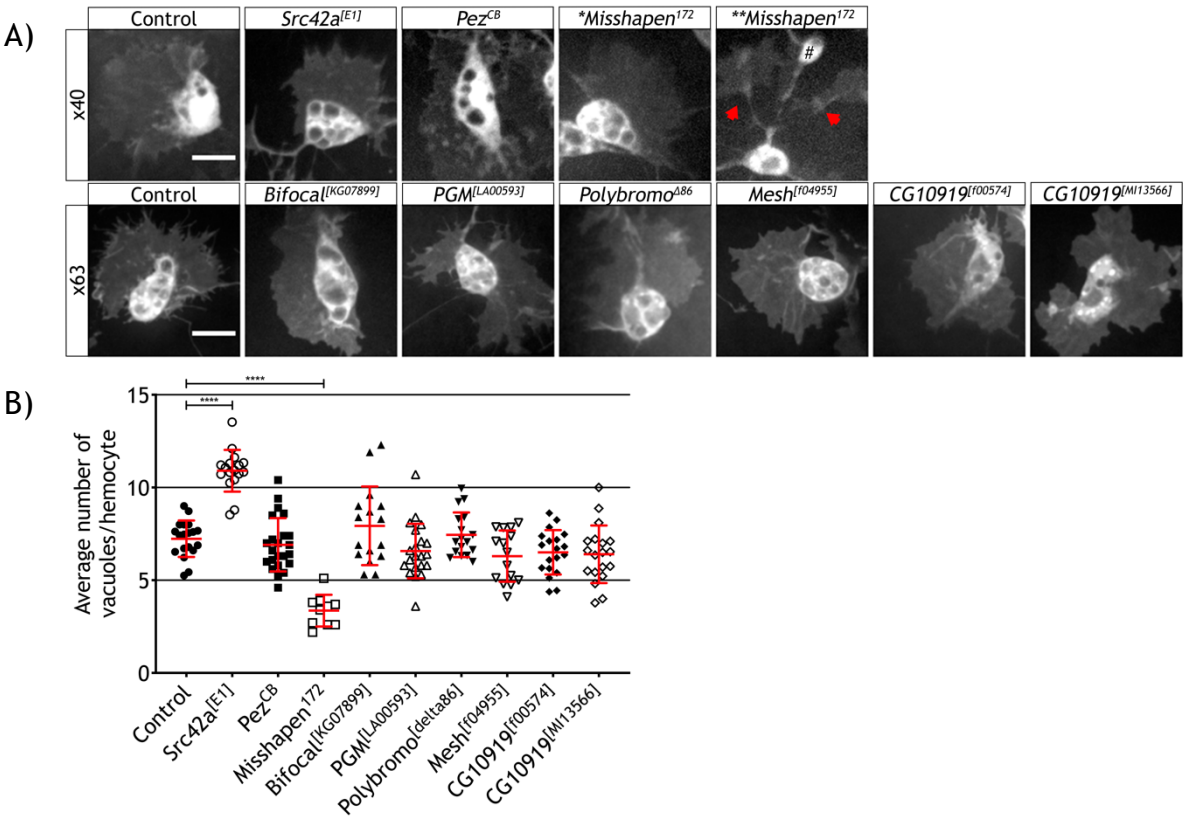

Figure 3.2.2: Investigating cell morphology in proteomics mutants.

A) Proteomics mutants expressing GFP under the control of *serpent-Gal4(.2)* were imaged at either x40 or x63. Scale bars at 10μm for both magnifications. This revealed normal cell morphology in all mutants except *Misshapen*^{172}. Although some cells were seen with 'fried egg' morphology (*) in this mutant, most hemocytes displayed stringy, stellate shapes (red arrows) with satellite cell bodies (denoted by hashtag in ** image). B) Quantification of vacuole numbers in mutants. Individual data points plotted along with mean and SD. Significance tested by Ordinary one-way ANOVA. Control n=19; *Src42a*$^{[E1]}$ n=17; *Bifocal*$^{[KG07899]}$ n=17; *PGM*$^{[LA00593]}$ n=21; *Polybromo*$^{[delta86]}$ n=18; *Mesh*$^{[f04955]}$ n=15; *Pez*^{CB} n=23; *CG10919*$^{[f00574]}$ n=19; *CG10919*$^{[MI13566]}$ n=19.

3.3 Misshapen controls hemocyte morphology

Due to the striking morphology of *misshapen*^{172} mutant hemocytes (Supplementary movie 2) we investigated whether spatial constriction might be driving this phenotype. The cavity through which hemocytes migrate at stage 15 is opened following the separation of the underlying ventral nerve cord from the epithelium above[50,209]. To investigate this space, we injected fluorescent dextran into both control and *msn*^{172} embryos – an approach used previously[61,209]. This revealed no obvious defect (Figure 3.3.1A), suggesting that the cells are under normal spatial constriction and that Misshapen may play a cell autonomous role in controlling hemocyte morphology.

To confirm this observation, we expressed a misshapen RNAi construct in hemocytes under the control of *serpent*-Gal4 and alongside UAS-GFP. Although the phenotype was less severe in these animals, we did identify satellite cell bodies which are never seen in control hemocytes (Figure 3.3.1B & C). Finally, although re-expression of UAS-Misshapen into *Misshapen* mutant hemocytes appeared to ameliorate the phenotype, using the parameters investigated this was not statistically significant. Taken together this demonstrates that *misshapen* is predominantly required cell autonomously in hemocytes to control morphology. Although the cells are not under spatial constriction, some contribution may come from the underlying CNS over which these cells migrate to worsen the phenotype in mutants compared to hemocyte-specific RNAi.

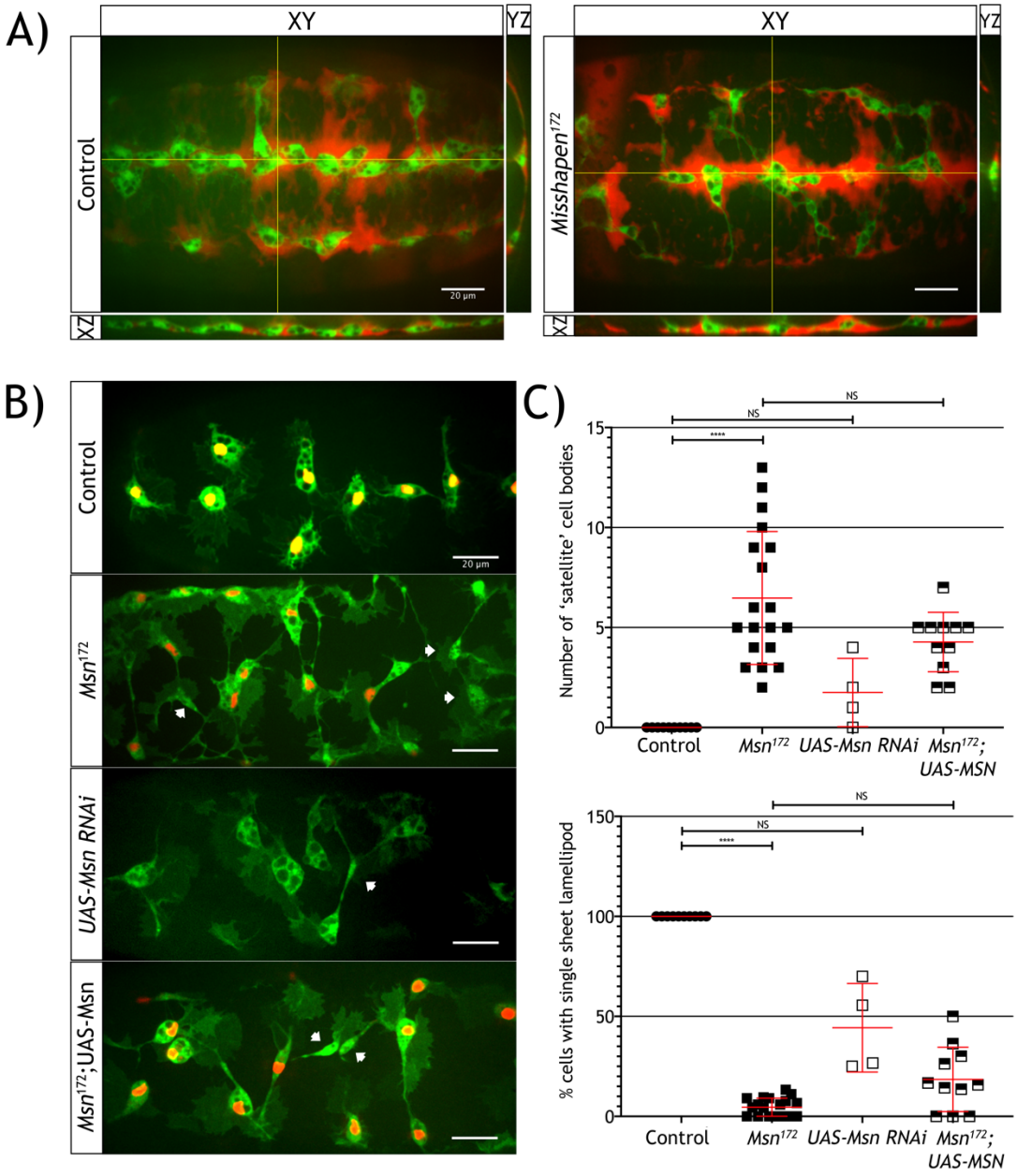
A)
XY
YZ
XZ
Control
Misshapen172
20 µm
B)
Control
Msn172
UAS-Msn RNAi
Msn172;UAS-Msn
20 µm
C)
Number of 'satellite' cell bodies
% cells with single sheet lamellipod
NS
****
Control
Msn172
UAS-Msn RNAi
Msn172; UAS-MSN

Figure 3.3.1: Hemocytes in *Misshapen* mutants are not spatially constrained.
A) Fluorescent dextran was injected into control and *Misshapen*^{172} mutant stage 15 embryos to investigate the cavity in which hemocytes reside. Z projections shown, as well as orthogonal views of the ventral surface. There appears to be no spatial constriction of hemocytes in *Misshapen* mutants. B) Hemocytes expressing cytosolic GFP, as well as nuclear mCherry (*serpent-H2A-3xmCherry)* were imaged at stage 15 in control and *misshapen* mutant embryos. This revealed that some cell bodies in *misshapen*^{172} mutants are not associated with nuclei (denoted with white arrows) – we term these satellite cell bodies. There are no cells in the representative mutant image that display normal cell morphology. *Misshapen*^{172} mutants expressing GFP and nuclear mCherry as well as a UAS-msn rescue construct display a less severe phenotype, however satellite cell bodies are still present (white arrows). UAS-MSN RNAi and GFP expressing hemocytes are also seen with unusual cell projections. All scale bars at 20μm. C) Quantification of satellite cell bodies and cell morphology. Expression of UAS-MSN is not sufficient to completely rescue the defect. Individual data points plotted as well as SD. Control n=10; mutant n=19, RNAi n= 4; UAS-MSN Rescue n=11. Significance tested by Kruskal-Wallis Multiple comparisons as control data is not normally distributed.

3.4 The involvement of the proteomics hits in hemocyte wound recruitment

In order to investigate the potential involvement of the proteins identified by the phosphoproteomics approach in driving inflammatory cell migration (Figure 3.1.1 and Table 3.1.1) we conducted a series of wound recruitment experiments using our laser ablation assay[73]. Stage 15 embryos for each mutant expressing hemocyte GFP as well as control (;*srp*-Gal4, UAS-GFP) and *Src42a*$^{[E1]}$ as a positive control were wounded on the ventral epithelium by laser ablation. Following a 1 hour recruitment period, wounded embryos were imaged over a 10 μm Z-stack – with images taken every 0.5 μm. To measure the wound perimeter, Bright-Field (BF) images were taken in which the wound outline can be seen (Appendix 4). The number of GFP+ hemocytes at the wound were then quantified, with hemocytes classified as 'at the wound' if their cell body touched the wound perimeter. Using this method, hemocyte numbers could be accurately and reproducibly counted at the wound site.

To control for differences in wound size, recruitment numbers were divided by the wound perimeter which is the source of the chemoattractant[104]. By normalising data to control levels, we could directly compare the effect of the proteomics mutants on hemocyte responses. We were able to validate this approach, as we observed a 50% decrease in hemocyte responses in *Src42a*$^{[E1]}$ mutants as described previously[73].

We observed a significant reduction in wound recruitment in mutants for Bifocal, Polybromo, Pez and CG10919 (Figure 3.4.1). As the CG10919 protein is completely unknown we validated this result with the use of a second mutant which gave an analogous phenotype.

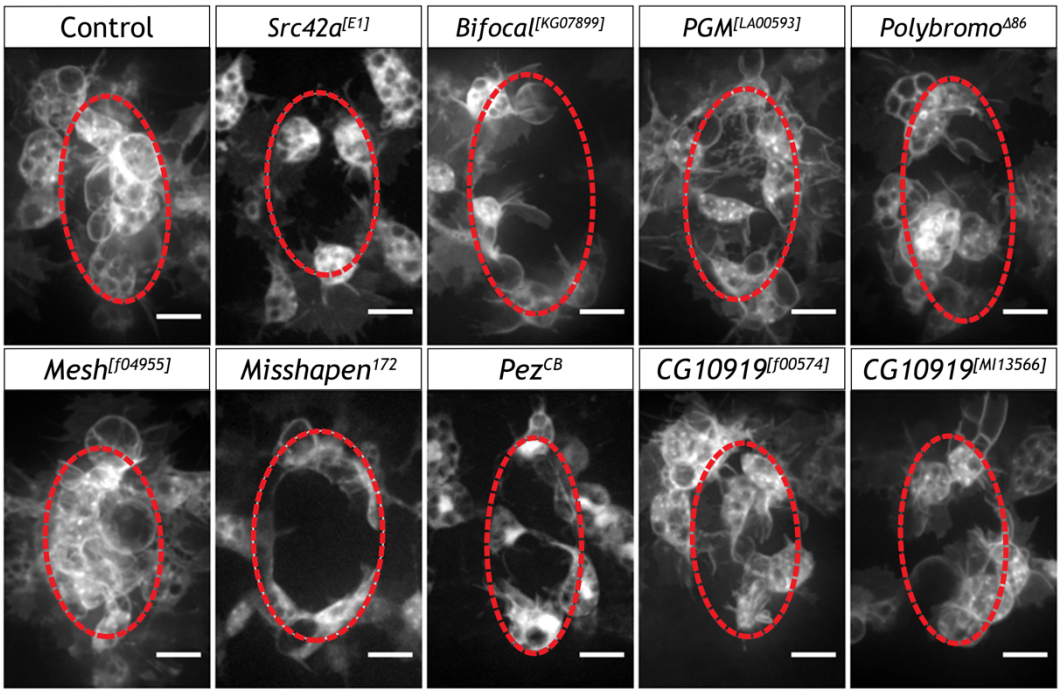
Control
Src42a[E1]
Bifocal[KG07899]
PGM[LA00593]
Polybromo[Δ86]
Mesh[f04955]
Misshapen172
PezCB
CG10919[f00574]
CG10919[MI13566]

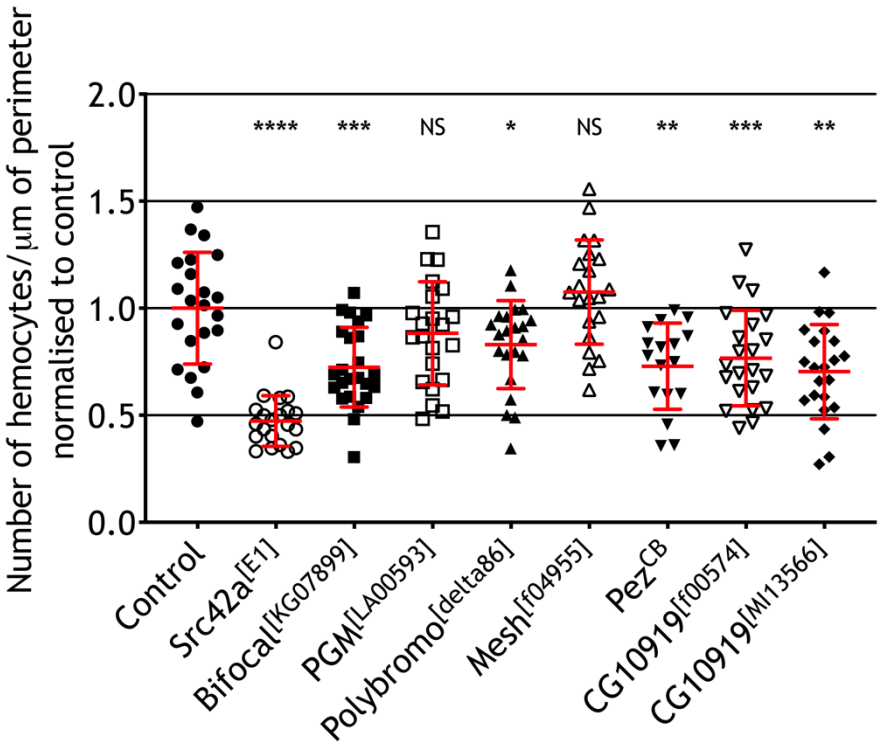
Number of hemocytes/μm of perimeter normalised to control
2.0
1.5
1.0
0.5
0.0
****
***
NS
*
NS
**
***
**
Control
Src42a[E1]
Bifocal[KG07899]
PGM[LA00593]
Polybromo[delta86]
Mesh[f04955]
PezCB
CG10919[f00574]
CG10919[MI13566]

Figure 3.4.1: Investigating wound recruitment in phosphoproteomics mutants.
A) Representative images taken 1 hour post ablation of control and mutant embryos. The wound margin was visualised by brightfield imaging and the perimeter is denoted by the red dotted lines. Scale bars at 10 μm. B) Quantification of hemocyte wound recruitment 1 hour post ablation. Number of hemocytes per μm of wound perimeter normalised to control for comparable visualisation. A decrease in inflammation is seen in *Src42a, Bifocal, Polybromo, Pez and CG10191* mutants was calculated One-Way ANOVA with multiple comparisons. Individual data points plotted with SD. Control n=22; *Src42a*$^{[E1]}$ n=21; *Bifocal*$^{[KG07899]}$ n=24; *PGM*$^{[LA00593]}$ n=22; *Polybromo*$^{[delta86]}$ n=22; *Mesh*$^{[f04955]}$ n=21; *Pez*^{CB} n=17; *CG10919*$^{[f00574]}$ n=22; *CG10919*$^{[MI13566]}$ n=22.

Due to the morphological defect seen in *msn*^{172} mutants, it proved difficult to accurately calculate the number of hemocytes at the wound margin (representative image in Figure 3.4.1). Therefore, we adapted the wound recruitment assay to include a fluorescent nuclear marker – H2A-3xmCherry under the direct control of the *serpent* promoter. As we often observed 'satellite cell bodies' in misshapen mutants, this allowed us to accurately quantify cell numbers at the wound edge by the presence of nuclei (Figure 3.4.2). This approach revealed a mild decrease in the number of hemocytes recruited at the one hour timepoint.

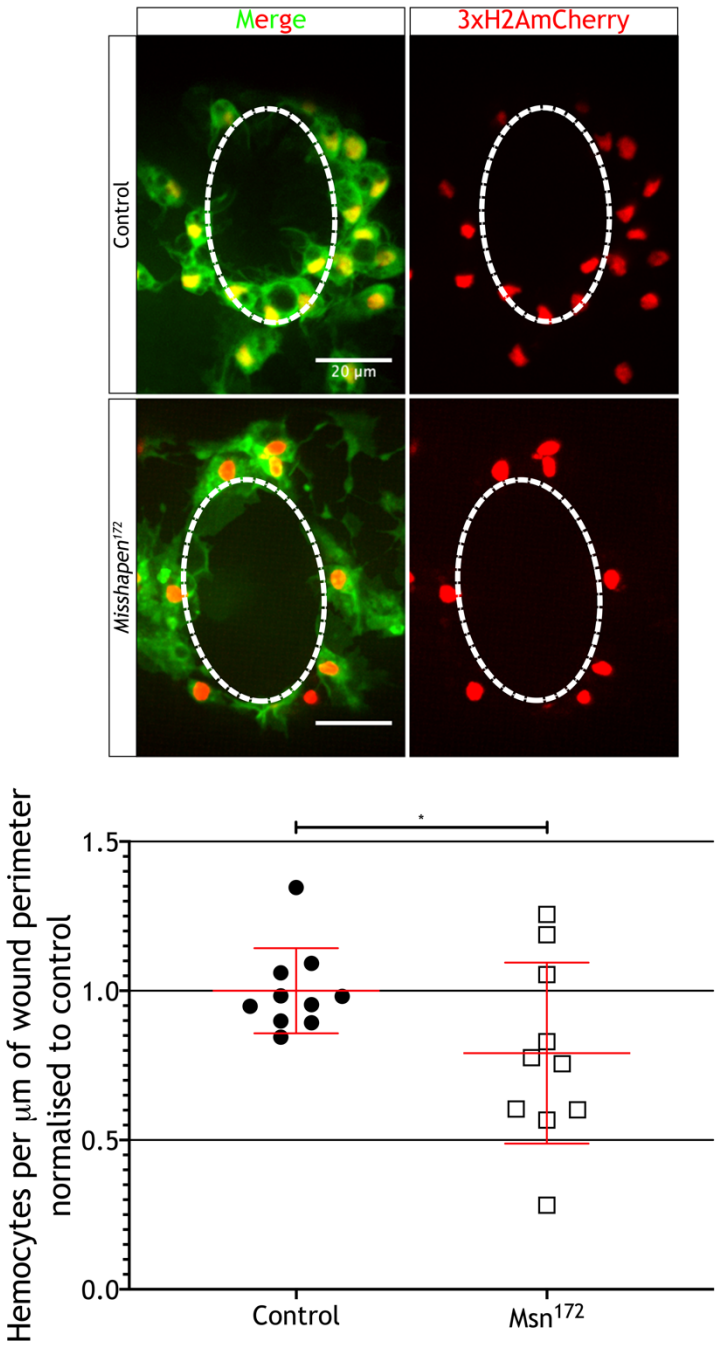

Figure 3.4.2: *Misshapen*^{172} mutants show a reduced number of hemocytes recruited to epithelial wounds.

A) Representative images of wounded embryos expressing cytosolic eGFP and nuclear mCherry (3xH2AmCherry) at the one hour timepoint. Scale bars at 20µm. B) Quantification of hemocytes recruited to epithelial wounds at the one hour timepoint in control and *Misshapen*^{172} *(Msn*^{172}*)* mutants. Individual data points plotted as well as mean and standard deviation. A significant decrease in recruitment was calculated by Welch's T-test due to differing SD. Control and *Msn*^{172} n=10.

As roles for our proteins of interest have not been described in hemocytes we sought to validate the wound recruitment phenotypes seen in the whole animal mutants. To achieve this, we crossed UAS-RNAi constructs directed against the proteins outlined in Table 3.1.1 to the fluorescent line *serpent-Gal4, UAS-GFP; croquemort-Gal4, UAS-GFP* and repeated the 1 hour wound recruitment assay.

Several different *Drosophila* RNAi libraries exist with preferred controls for each. The GD RNAi library was generated by the random P-element insertion of UAS-RNAi constructs into the *white*^{1118} mutant fly line. Whereas the newer KK library was generated by the targeted integration of transgenes into one of two landing sites. Thus, the control line for GD UAS constructs is *white*^{1118} whereas the control for the KK library is the host landing site strain. For the final library - TRiP – an RNAi construct directed against luciferase was used as a control. Unlike the other two libraries, the use of this line controls against the expression of a transgene in the hemocyte lineage. By comparing wound recruitment of hemocytes expressing UAS-LuciferaseRNAi to the controls for the other libraries, we demonstrate that the engagement of the RNAi machinery in hemocytes does not affect wound recruitment (Appendix 5).

As the CG10919 locus encodes a protein of unknown function, wound recruitment was also investigated following the knockdown of the protein Sp7 which is encoded approximately 11 bp downstream of CG10919. This approach was taken to confirm the phenotypes seen in CG10919 mutants used previously were not due to extensive gene disruption in this region – particularly as Sp7 has been previously implicated in septic wound responses[210].

By comparing RNAi experiments to their relevant controls, we observed a wound recruitment defect in hemocytes lacking CG10919, Bifocal and Pez (Figure 3.4.2) at one hour post ablation. This confirms the phenotypes identified in the mutants are cell autonomous. Further, the use of RNAi against Sp7 did not affect wound recruitment.

Conversely, the expression of RNAi directed against Polybromo did not affect hemocyte wound recruitment. This indicates the effect of Polybromo on wound recruitment may not be hemocyte-specific. Finally, we observed a wound recruitment phenotype in PGM RNAi expressing hemocytes which was not observed previously with the mutant. This discrepancy may either indicate that the PGM mutant produces functional protein or may be due to off-target effects of the RNAi construct used.

A)

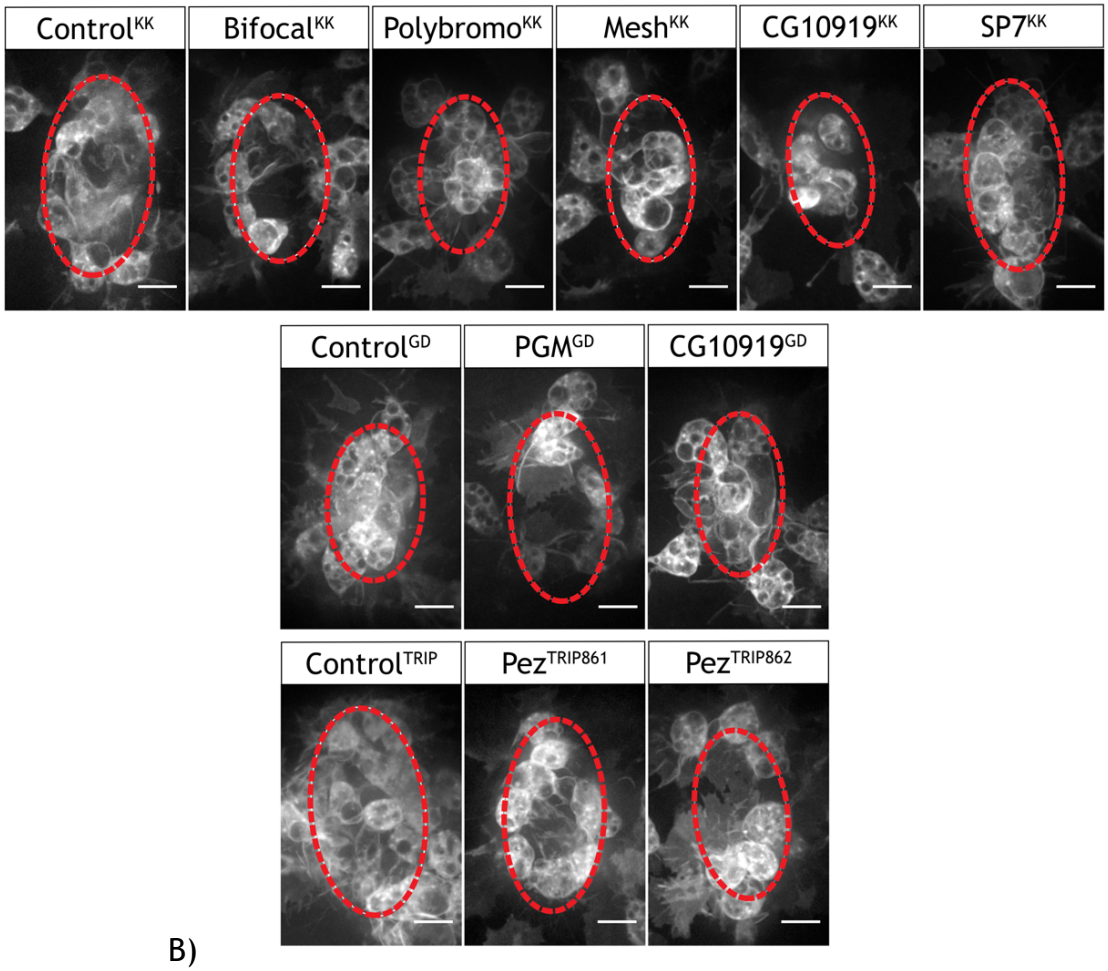
Control^KK
Bifocal^KK
Polybromo^KK
Mesh^KK
CG10919^KK
SP7^KK
Control^GD
PGM^GD
CG10919^GD
Control^TRIP
Pez^TRIP861
Pez^TRIP862

B)

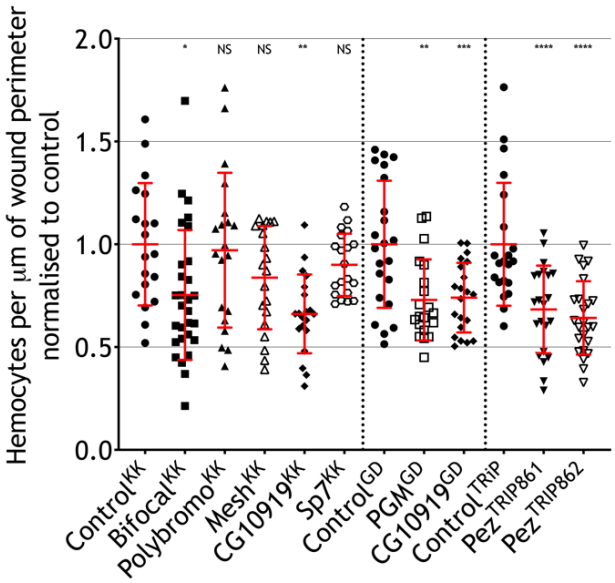
Hemocytes per μm of wound perimeter normalised to control
2.0
1.5
1.0
0.5
0.0
*
NS
NS
**
NS
**
***
****
****
Control^KK
Bifocal^KK
Polybromo^KK
Mesh^KK
CG10919^KK
Sp7^KK
Control^GD
PGM^GD
CG10919^GD
Control^TRiP
Pez^TRIP861
Pez^TRIP862

Figure 3.4.3: Hemocyte-specific RNAi expression reveals cell-autonomous roles in wounding for Bifocal, Pez and CG10919.

A) Representative images taken 1 hour post ablation in embryos expressing UAS-RNAi constructs under the control of *serpent-Gal4*. Wound outline denoted by the red dashed line as estimated using brightfield imaging. Scale bars at 10μm. B) Quantification of hemocyte wound recruitment at one hour. Calculated as a function of wound perimeter and normalised to relevant controls. Individual data points plotted as well as mean and standard deviation. Ordinary one-way ANOVAs performed on different RNAi libraries separately to determine significance. KK: Control n=19; Bifocal n=29; Polybromo n=20; Mesh n=20; CG10919 n=20; Sp7 n=20. GD: Control n=22; PGM n=20; CG10919 n=21. TRIP: Control n=21; Pez861 n=22; Pez862 n=24.

3.5.1 Validating expression of positive hits in embryonic hemocytes

Having identified robust, hemocyte-specific requirements for Bifocal, Pez and CG10919 in wound recruitment and a role for cell shape control by Misshapen, we finally sought to confirm their expression in hemocytes. To achieve this, mutant fly lines in which Gal4 had been inserted into the gene locus were used to drive the expression of UAS-GFP. As this resource was not available for CG10919, we instead endogenously tagged the protein with GFP using the MiMIC insertion mutant and replacing the disruption cassette with a cassette that includes eGFP by recombination-mediated cassette exchange (EGFP-FlAsH-StrepII-TEVcs-3xFlag {GFSTF})[211,212].

This approach revealed weak ubiquitous expression of the loci/proteins investigated. To confirm expression in hemocytes, embryos were co-stained with an antibody directed against singed – an actin bundling protein which is abundant in hemocytes[67,186] (Figure 3.5.1). Using this method, we saw strong overlap between GFP expression and singed using *Pez-Gal4 and Msn-Gal4*. There is also some evidence for Bifocal and CG10919 expression in hemocytes, although the GFP signal is weaker.

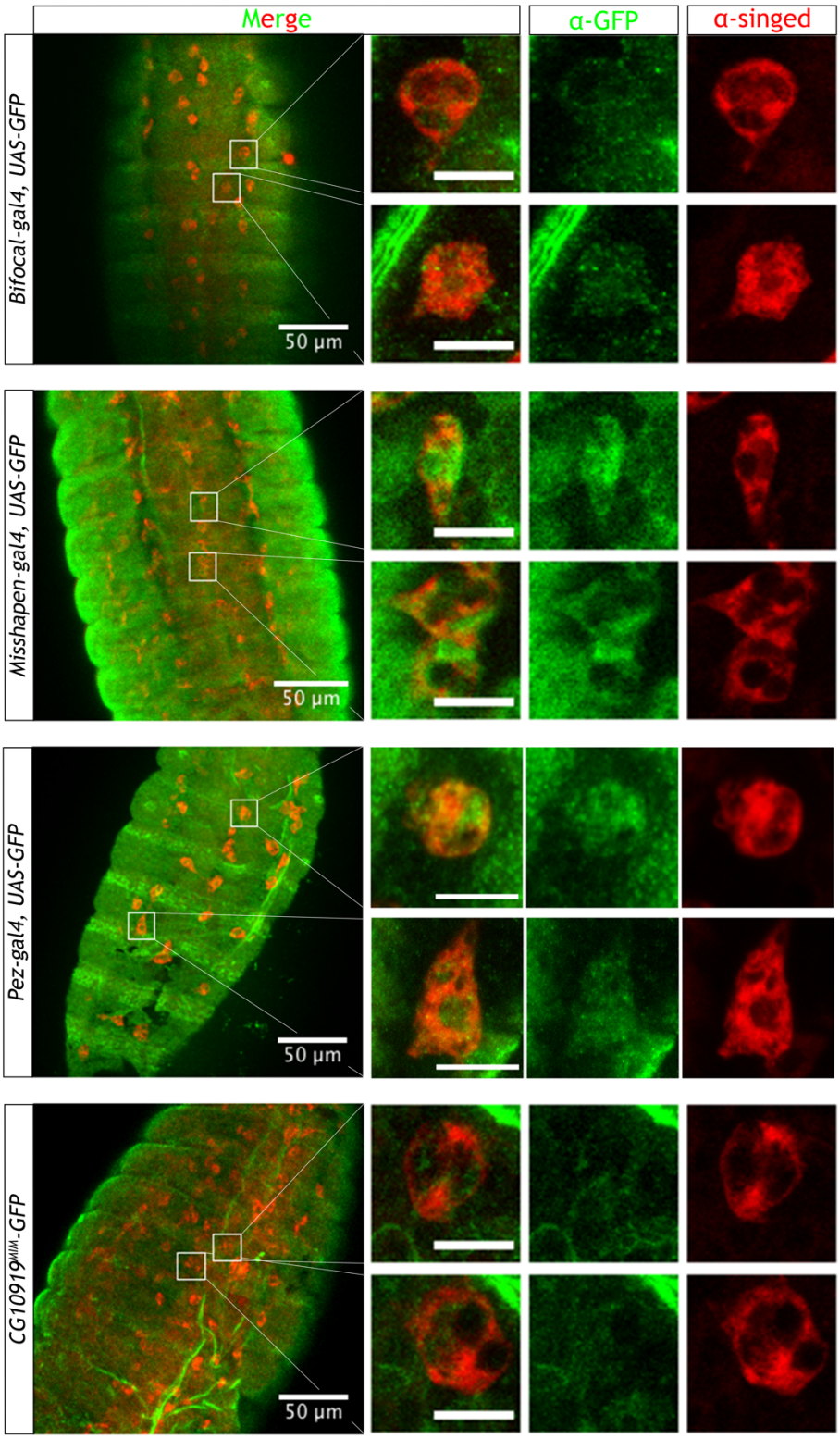

Figure 3.5.1: Staining reveals expression of Bifocal, Misshapen, Pez and CG10919 in hemocytes.

Stage 15 embryos were fixed and stained with α-GFP (secondary 488) and α-singed (secondary 561). Ventral overviews of embryos are shown with scale bar at 50µm, as well as higher magnification images of hemocytes (white boxes) with scale bars at 10µm.

3.5 Discussion

3.5.1 Rationale

The recruitment of *Drosophila* hemocytes to epithelial wounds is dependent upon H_2O_2 activation of the Src Family Kinase Src42a[73,100]. A single target of Src42a in this process is known – the tissue damage receptor Draper. Src42a phosphorylates Draper on its intracellular ITAM domain, which transduces the signal to a second kinase named Shark[73,82]. This cascade ultimately results in the migration of hemocytes towards the damage site. As kinase activation is crucial in this process, we reasoned that other proteins involved in this inflammatory response may well be phosphorylated dependent upon activated Src42a. Thus, a phosphoproteomics screen was conducted to identify novel phosphopeptides that are dependent upon H_2O_2/Src42a. Seven proteins of particular interest were identified by this approach and investigated for novel roles in hemocyte biology. Below is a summary table of these hits, their modifications and the subsequent defect identified:

Protein identified	Modification	Defect identified
Bifocal	Multiple Ser P; Thr P	Wound recruitment
Phosphoglucomutase	Thr P	Inconclusive
Polybromo	Ser P	Wound recruitment
Mesh	Thr P; Ser P	None
Misshapen	2x Ser P; Tyr P	Morphological
Pez	2x Ser P	Wound recruitment
CG10919	Met oxidation	Wound recruitment

Table 3.5.1: Summary of proteomics phenotypes

3.5.2 Validation of approach taken

In order to be able to FACs sort hemocytes from crushed animals, GFP was driven in the lineage using *serpent-Gal4,* which is highly expressed in hemocytes[170]. This approach successfully sorted between 376,000-465,000

single, live GFP+ cells from 1000-1120 embryos of each condition. As approximately 600 hemocytes are found in *Drosophila* embryos[170] these numbers constitute between 55%-77.5% recovery following sorting. However this is likely a mild over estimate as the hemocyte specific *serpent* promoter used is also weakly expressed in some areas of the fat body at stage 14[170]. We therefore expect some 'contamination' of our FACs sorted hemocyte protein sample. Clearly, some hits from our approach are false-positives as Mesh, which is strongly localised to the gut[201,202], and whose phosphorylation status was decreased by between 30% and 70% in the absence of Src42a and H_2O_2, did not give a hemocyte defect.

The results of the phosphoproteomic screen identified 653 phosphopeptides from a total of 522 proteins. Unfortunately, Draper's ITAM domain – which is phosphorylated by H_2O_2 activated Src42a[73] – was not identified by this approach as a positive control. However, the autophosphorylation of Src42a itself following activation was detected as a phosphopeptide. Further, both the Serpent and Singed proteins were also identified in cell extracts from the phosphoenrichment flow through. These results indicate the method was suitable to recover hemocyte specific proteins.

Rather than extracting proteins from laser-ablated embryos, the method of embryo disaggregation itself was taken to mimic wound conditions. It was reasoned that, following total epithelial (and indeed embryonic) disruption, H_2O_2 would be readily produced. Therefore, this method exposes all hemocytes to the signal, rather than just those in the vicinity of a wound. It would be possible to test for the presence of H_2O_2 by combining the crushed embryo lysate to potassium iodide and acetic acid. H_2O_2 would thus be confirmed by colour change to brown following iodine liberation. Ultimately, the use of crushing in place of a previously generated wound proved fruitful as we were able to identify novel regulators of hemocyte wound recruitment.

3.5.3 Misshapen in hemocyte shape control

Having set out to identify novel phosphotargets of Src42a, a tyrosine kinase, we instead identified a large number of serine/threonine phosphopeptides (approximately 90% of the proteomics results). Of the 48 proteins phosphorylated on tyrosines downstream of H_2O_2 and Src42a, we identified a serine/threonine kinase – Misshapen – which we hypothesised may have the capability to act downstream of Src42a and provide a kinase link. Although we identified a mild wound recruitment defect in *misshapen* mutant embryos, we further uncovered a more striking defect in hemocyte morphology.

By quantifying the presence of satellite cell bodies, as well as the presence of a single sheet lamellipod we were able to determine a significant change in cell morphology in mutant embryos. Although the expression of UAS-Msn in *Misshapen* mutant hemocytes mildly rescued the defect, this was not significant. Furthermore, whilst the specific expression of Msn RNAi in hemocytes lead to the generation of satellite cell bodies, quantified data was not statistically different from control. More data is therefore required to determine whether Misshapen plays a cell autonomous role in hemocyte shape change.

There have been several studies investigating the role of Misshapen in both the regulation of morphology and cell migration in *Drosophila*. Roles for Misshapen in cytoskeletal regulation have been demonstrated in both photoreceptor cells in the eye, as well as in border cells in the ovaries[176,213]. Furthermore, Misshapen is important for migration of distinct cell types – such as nuclear migration in the eye[214], growth cone motility[215], epithelial follicle cell migration[216] and border cell migration in the ovaries[217]. Unlike in border cells - where the depletion of Misshapen protein blocks migration via an increase in integrin[216] - hemocytes in *misshapen* mutants still retain their ability to migrate - as here we demonstrate they not only undergo normal developmental dispersal, but continue to migrate at embryonic stage 15. As we were unable to rescue the Misshapen morphology defect by the expression of Myospheriod (Integrin βPS) in hemocytes (data not shown) we

believe that Misshapen plays an integrin-independent role in hemocyte morphology.

We have identified multiple, aberrant protrusions in *Misshapen* mutant hemocytes, which is also seen in ovarian border cells lacking Misshapen[213]. The protrusive activity of *Misshapen* mutant hemocytes is so severe that often the cell is unable to undergo coordinated migration, and fragments of cell body begin migrating away from the main cell – what we have termed 'satellite' cell bodies. As well as integrins, current known proteins downstream of Misshapen include Bifocal[195], the small Rho GTPase cdc42[195] and moesin[213] – all of which have described roles for cytoskeletal organisation[194,218–221]. Here, we have shown normal hemocyte morphology in Bifocal mutants which excludes it as a regulator of hemocyte shape downstream of Misshapen.

Cdc42 is a known regulator of cell polarisation[222] and has also been shown to regulate hemocyte morphology. The expression of constitutively active Cdc42 in hemocytes leads to rounded cells that lack cell protrusions. Furthermore, these hemocytes have also been seen to contain two nuclei[62]. This is in direct contrast to *Misshapen* mutant hemocytes, in which we see a stellate morphology, multiple protrusions and the presence of cell bodies which completely lack nuclei. It is therefore possible that Misshapen regulates Cdc42 to control hemocyte morphology, particularly as Cdc42 mutation also results in cells with multiple leading edges[89]. It would therefore be interesting to determine whether the expression of constitutively active Cdc42 alters the morphological defect caused by the loss of Misshapen.

Finally, Moesin is a member of the Ezrin, Radixin and Moesin (ERM) protein family which can bind to both the plasma membrane and actin[223,224]. Although its role has not been defined in hemocytes, it is known to contribute to nurse cell shape in *Drosophila* ovaries[225]. As we see with Misshapen mutant hemocytes, Moesin nurse cell clones have abnormal cell protrusions which radiate from the periphery. Moreover, knockdown of moesin in melanoma

cells results in an increase in cell length[226] which is also reminiscent of the stellate Misshapen phenotype we present here. As moesin activation has been identified as a direct consequence of Misshapen phosphorylation in border cells in the regulation of cell protrusion[213] it would be interesting to determine if this also occurs in hemocytes to regulate cell shape.

3.5.4 A hemocyte specific role for CG10919, Pez and Bifocal in wound recruitment

As the only protein with upregulated post-translational modification (PTM) in all of the conditions investigated by proteomics, we chose to investigate the protein CG10919. Unlike the majority of proteins identified, the CG10919 peptide was oxidised rather than (de)phosphorylated. This oxidation occurred on the N-terminal methionine – a PTM which is known to both activate and inactivate proteins[227]. Here we show that the loss of CG10919 results in a robust reduction in hemocyte recruitment to wounds. As CG10919 encodes an unknown protein, with no orthologues and no identifiable functional domains we have no insight into how it may function in this process. We therefore chose not to continue investigating the role of CG10919 in hemocyte inflammation.

We have also identified a wound recruitment defect in *Bifocal* mutant embryos. Previously, Bifocal expression has been reported in the embryonic CNS[194]. However, here we show it is also expressed in hemocytes - as we have not only identified it following FACS sorting of *serpent* expressing hemocytes, but shown that expression of the locus overlaps with the actin bundling protein singed that is enriched in hemocytes[186]. Previous roles for Bifocal in the control of cell migration have been described[195,196,218], and here we show an additional role in chemotactic migration to wounds. Although Bifocal has been shown to regulate cytoskeletal dynamics in other cell types, we see no obvious hemocyte morphological defects under basal conditions and no effect on developmental dispersal. If Bifocal is involved in the control of hemocyte cytoskeletal networks following wounding, it may require the H_2O_2 stimulus and Src42a activity to exert this function as identified by our proteomics. To investigate this, wound recruitment in *Bifocal* mutants could

be live imaged to observe the manner in which hemocytes migrate to wounds in comparison to control. Additionally, the use of specific cytoskeletal probes – such as LifeAct-GFP (F-actin) and mCherry-Clip170 (microtubules) – would provide direct insight into the underlying structures controlling hemocyte shape. As there is no known orthologue of Bifocal, and BLAST sequence alignment does not identify any conserved functional domains, this hit from our screen does not constitute a promising candidate for continued study in this thesis.

Finally, we show that both the global and hemocyte-specific loss of the PTP type phosphatase Pez results in a reduction of hemocytes recruited to epithelial wounds. This constitutes a novel function of Pez in the fly, as previous work has shown a distinct function in the regulation of hippo signalling in the gut[175]. As we show no defect in basal migration, and no obvious morphological defect in *Pez* mutant hemocytes we believe we have uncovered a novel regulator specific to inflammation. As the orthologue of Pez has been shown to bind to Src family kinases in other organisms[206–208], Pez is the most promising candidate identified and is therefore explored and discussed further in Chapter 4.

3.5.5 Methods for assessing gene expression in *Drosophila* embryos

Due to the lack of specific antibodies for the CG10919, Misshapen, Pez and Bifocal proteins, two genetic methods were employed to assess whether the loci (and thus the proteins) were expressed at embryonic stage 15. For CG10919, recombination-mediated cassette exchange was used to endogenously tag the protein with GFP[210,211]. This could then be detected using anti-GFP antibodies following fixation and is thus a reflection of the protein level. This method revealed weak expression throughout the embryo at stage 15 and limited evidence of expression in hemocytes. As CG10919 was oxidised on its N terminal methionine following disaggregation to mimic wounding, and this PTM is known to alter protein levels[226], it may be interesting to probe for CG10919 after wounding to determine if levels increase or decrease.

As MiMIC lines were not obtained for Misshapen, Pez and Bifocal we instead used lines in which Gal4 was inserted into the loci to drive *UAS-GFP* expression. This method overexpresses GFP in the pattern of the endogenous locus expression as soon as transcription is activated in the gene region. Thus, unlike endogenous protein tagging, this is not reflective of protein levels. In future this may be improved by the generation of specific antibodies or by endogenous protein tagging.

3.5.6 Elevated levels of vacuoles in *Src42a* mutant embryos

As a positive control for our wounding experiments we included a mutant for Src42a. We identified a 50% reduction in hemocyte numbers recruited to sites of laser ablation[73] as previously described - which validates the screen presented here. Although previous work identified a mild morphological defect in *Src42a* mutant hemocytes – whereby the cell spread was decreased – the number of vacuoles they contain was not reported. Here we have shown a marked increase in vacuole number which phenocopies the loss of Draper[73]. Signalling downstream of Draper is therefore believed to be involved in the degradation of ingested corpses. As the ITAM of Draper – the site of Src42a phosphorylation following wounding – is not involved in vacuole processing, it is possible that Src42a phosphorylates Draper at other sites to mediate this process. Indeed, further Src42a phosphorylation sites upstream of the ITAM sequence have been identified in *Draper* transformed S2 cells[80], and phosphomimetic constructs of these sites could be used to investigate functionality and implicate the role of Src42a in perpetuating corpse degradation signalling.

3.5.7 Conclusion

Using a novel phosphoproteomic assay we have identified proteins involved in hemocyte wound recruitment, as well as a role for Misshapen in the regulation of hemocyte morphology. We also identify a potential role for Src42a in vacuole processing which has not been reported previously. As the main aim of this thesis is to identify novel regulators of inflammation, we identify Pez as the most promising candidate with a human orthologue.

Chapter 4: Investigating the role of the PTP type phosphatase Pez in hemocyte wound recruitment

4.1 Introduction

To build on the screen conducted in Chapter 3, the protein Pez was selected as the most promising novel regulator of inflammatory cell migration following epithelial wounding. This chapter therefore further investigates the role of Pez in hemocyte wound recruitment.

4.1.1 The PTP-type phosphatase Pez

Pez was first characterised by Edwards et al in 2001[228] following a screen to identify novel FERM-domain containing proteins in *Drosophila*. As well as an N terminal Band 4.1, ezrin, radixin, moesin (FERM) domain, Pez harbours a protein tyrosine phosphatase (PTP) domain at its C terminus. Both domains are connected by a central linker region (Figure 4.1.1).

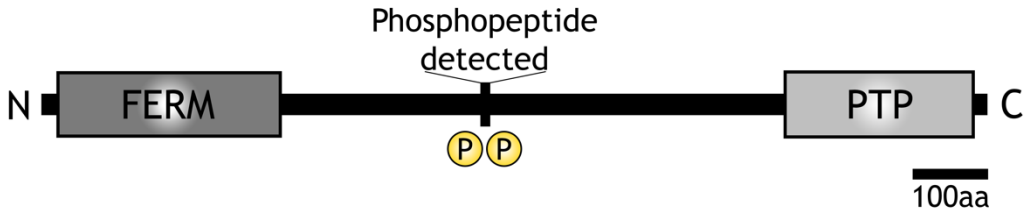

Figure 4.1.1: Domain organisation of *Drosophila* Pez.
Pez is 1252aa in length, with an N-terminal FERM domain, and C-terminal PTPase domain. The central linker region includes the phosphopeptide uncovered by phosphoproteomics. The two phospho-serines detected in this region were phosphorylated dependent upon both H_2O_2 and Src42a.

Drosophila Pez shares approximately 36% sequence identity with the human orthologue, tyrosine-protein phosphatase non-receptor type 21 (PTPN21) – with the FERM and PTP domains showing the greatest homology, and the central linker region showing wider divergence[228]. Despite this, both Pez and PTPN21 share key similarities in this deviating region, including 5 proline rich repeats and, crucially, a consensus site for the phosphopeptide detected by

the approach outlined in Chapter 3. This consensus phosphosite – YxS*xS*xPDL (where x is not a basic amino acid) – is also present in mouse PTPN21, where it has been shown to be phosphorylated in a range of tissues including the liver, brown fat and spleen[229]. The approach by Huttlin et al does not reveal information about the kinase(s) involved, however the sequence xSxx[D/E]x – where x cannot be basic – conforms to the casein kinase II (CK2) consensus sequence[230].

Whilst the phosphatase activity of Pez has been disputed[205], the FERM domain has been implicated in the proliferation of intestinal stem cell following tissue injury[175] via activation of the Hippo pathway. This negative regulation of Yorkie (known as YAP in mammals) is a conserved function of PTPN14, which is a further member of the mammalian FERM PTPase family alongside PTPN21[231–234]. Intriguingly, in the context of this study on cell migratory behaviours, PTPN14 has also been shown to regulate cell motility[235] *in vitro* by regulating the tyrosine phosphorylation levels of junctional proteins such as beta-catenin.

Human PTPN21 was initially identified alongside PTPN14 by Moller et al[206]. Interestingly, PTPN21 was shown not only to associate with the Src tyrosine kinase $pp60^{src}$ but to be phosphorylated by both v-Src and c-Src. This was corroborated by later studies in which PTPN21 was found to both bind to and activate Src, leading to augmented EGFR signalling[208]. Like PTPN14, PTPN21 has also been shown to impact cell migration[207] – a function which required both the PTP catalytic activity and FERM domain. This was due to the formation of a complex with PTPN21, focal adhesion kinase (FAK), actin and Src. The interaction between PTPN21 and Src was dependent upon residues 1-325, which lie within the FERM domain of the protein.

It is an intriguing possibility that the Src interacting properties of PTPN21 may be directly evolutionarily conserved between *Drosophila* Pez and Src42a, and this notion forms the basis of this study into the potential role of Pez in hemocyte wound recruitment.

4.1.2 Chapter aims

1) Characterise the nature of the wound recruitment defect seen in Pez mutants.
2) Elucidate which domain of Pez is required in this process.
3) Investigate the potential mechanism of Pez involvement in the H_2O_2/Src42a/Draper signalling axis.

Results

4.2 Pez mutant hemocytes are less readily recruited to sites of tissue damage

Previous work outlined in this thesis demonstrated a reduction in the number of hemocytes recruited to epithelial wounds at the one-hour timepoint in Pez mutant embryos (Chapter 3). In order to gain more information about the nature of this phenotype, wound recruitment was investigated by time-lapse imaging following epithelial laser ablation for 2 hours. This approach revealed a significant decrease in the number of hemocytes recruited to wounds in Pez^{CB} mutants in comparison to control at both the 40 and 60 minute timepoints (Figure 4.2.1A & B). This phenotype was not sustained over the 2 hour time course as the wounds began to close (Appendix 6). The phenotype seen at 40 and 60 minutes was corroborated using a second Pez mutation – Pez^{2} (a kind gift from Hugo Stocker) - in which a large portion of the Pez allele has been excised[175].

To investigate whether the loss of Pez contributes to abrogated wound closure, wound perimeter was investigated as a function of wound size at 10 minutes post ablation (Figure 4.2.1C). This revealed that wounds in Pez^{CB} mutants closed at a comparable rate to control over the entire 2 hour time course. A similar closure rate was also seen in Pez^{2} mutants over a 1hour time course. Thus, it can be concluded that the loss of Pez does not affect wound closure. Therefore, the hemocyte wound recruitment phenotype seen at 40 and 60 minutes is cell autonomous and is not due to wounds becoming larger, rather than smaller, over time.

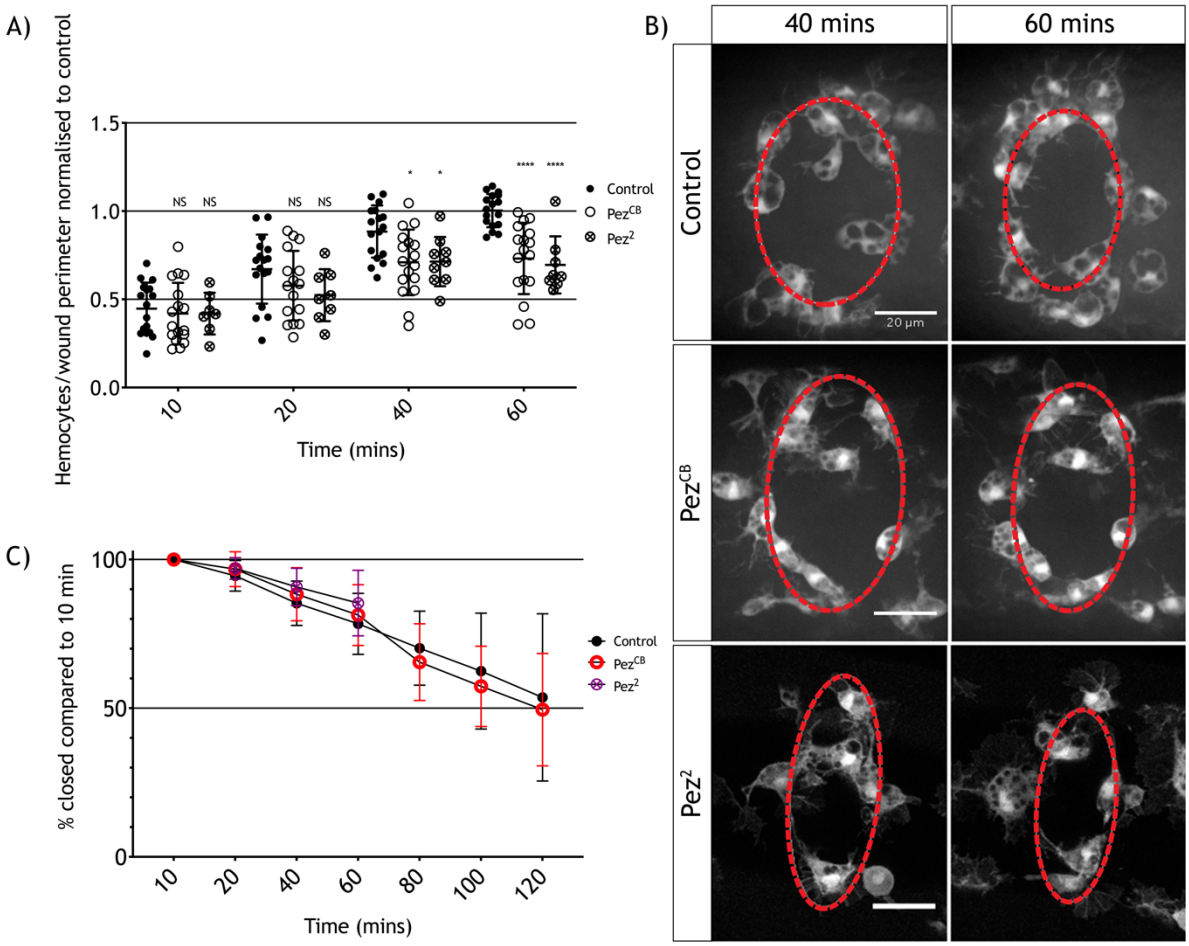

Figure 4.2.1: Global loss of Pez affects hemocyte wound recruitment at the 40 and 60minute timepoints, but wounds close normally.

A) Time-lapse data of laser generated epithelial wounds in Control, Pez^{CB} and Pez^{2} reveals a wound recruitment defect in Pez mutants at both the 40 and 60 minute timepoints. The number of hemocytes at the wound site was counted, divided by the wound perimeter and normalised to control levels at 1 hour for comparison. Individual data points plotted - as well as mean and standard deviation indicated for n=17 (Control), n=16 (Pez^{CB}) and n=10 (Pez^{2}) wounded embryos. Multiple t-tests used to confer significance using the Holm-Sidak method between Control and Pez^{CB} and Control and Pez^{2}. B) Representative stills taken from time-lapses at 40 and 60minutes. Wound perimeter is denoted by the dashed red line as visualised using bright-field. Hemocytes visualised using cytosolic eGFP. Scale bars: 20 µm. C) Analysis of wound perimeter as a function of wound size at 10minutes via brightfield imaging reveals epithelial wounds in Pez mutant embryos close at the same rate as control. Mean and standard deviation plotted for n=17 (Control), n=16 (Pez^{CB}) and n=10 (Pez^{2}) wounded embryos – includes n=5 (Control) and n=6 (Pez^{CB}) imaged to 120 min. There is no statistical difference between closure rates as confirmed by Multiple t-tests between Control and each Pez mutant respectively.

In order to determine whether a migratory defect is present in Pez mutant hemocytes following laser ablation, cells were first tracked at stage 15 in the absence of a wound. At this stage in embryonic development, hemocytes are fully dispersed and undergo random 'patrolling' behaviours.

Hemocytes in both Control and *Pez*^{CB} mutant embryos were tracked using the manual tracking function in FIJI over one hour, with images collected at 30 second intervals. Track statistics were extracted, and two key features were investigated – cell speed and the intrinsic directionality of the cell tracks. This latter analysis of migratory behaviour, also called the meandering index, describes the total track length as a function of the track displacement. Thus, a value of 1 indicates a cell is migrating in a true straight line. This approach revealed that Pez mutant hemocytes migrate at the same speed (Figure 4.2.2A) and in the same random manner (Figure 4.2.2B) as control. We therefore conclude that Pez is indispensable for normal hemocyte migration at stage 15.

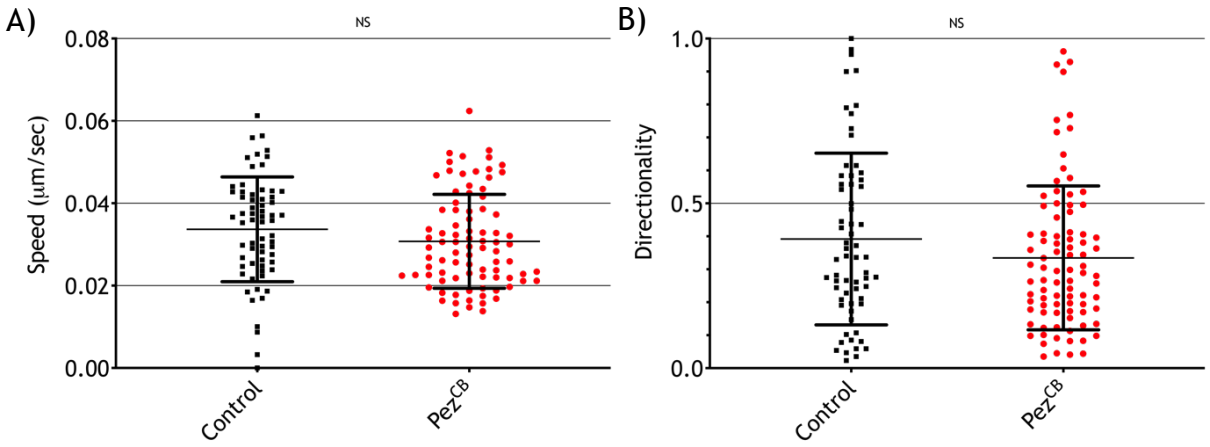

Figure 4.2.2: Tracking of embryonic hemocytes at stage 15 under basal conditions reveals no defect in *Pez^{CB}* mutants.

Hemocytes in 3 Control and 3 Pez^{CB} mutant embryos were tracked for 1 hour at stage 15 using the manual tracking plugin found within FIJI. A) Cell speeds of both Control and Pez mutant hemocytes are comparable - no statistical difference was determined by Mann-Whitney U Test as Pez^{CB} data is not normally distributed. N=3 embryos, n=65 cells (Control); N=3 embryos, n=86 cells (Pez^{CB}). Individual cell speeds plotted, with mean ± standard deviation. B) Directionality as measured by the meandering index of both control and Pez^{CB} mutant hemocytes. Mann-Whitney U test reveals no statistical difference between control and Pez^{CB} migratory behaviours. N=3 embryos, n=65 cells (Control); N=3 embryos, n=86 cells (Pez^{CB}). Individual directionality values plotted, with mean ± standard deviation.

As the loss of Pez does not affect the basal migratory behaviour of hemocytes at stage 15, cells were tracked in the presence of epithelial wounds in order to investigate an inflammation specific role for Pez in promoting cell migration. Tracking of cells, as described previously, over 2 hour time courses revealed that the reduction in the number of hemocytes present at wounds in Pez^{CB} mutants was not due to slower migrating speed, but due to a lack of directionality in cell tracks in responding cells (Figure 4.2.3A & B). Further to this, the wound arrival time of hemocytes in Pez^{CB} mutant embryos was around 5 minutes later than in control (Figure 4.2.3C). Hemocytes also spent less time at the wound (Figure 4.2.3D) and were also frequently observed leaving the wound site before the end of imaging (Figure 4.2.3E, ns but trend apparent). These results therefore demonstrate a defect in accurately sensing and migrating towards wounds in Pez^{CB} mutant hemocytes.

A)

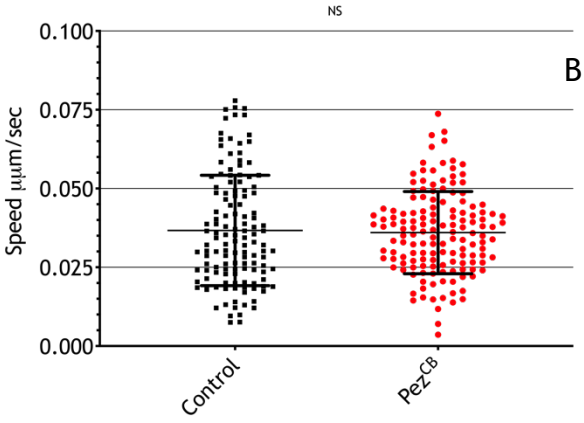
NS
Speed μm/sec
0.100
0.075
0.050
0.025
0.000
Control
Pez^CB

B)

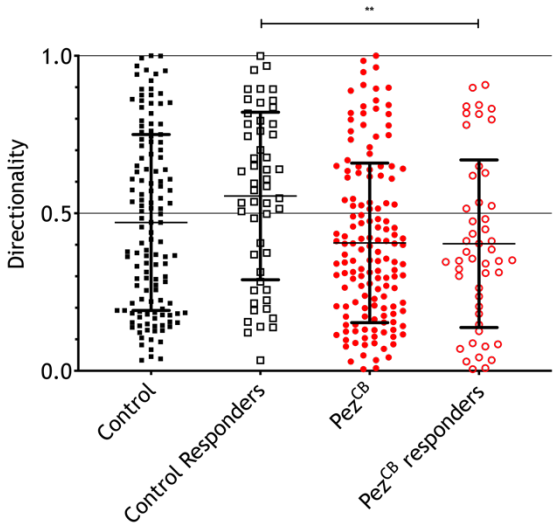
**
Directionality
1.0
0.5
0.0
Control
Control Responders
Pez^CB
Pez^CB responders

C)

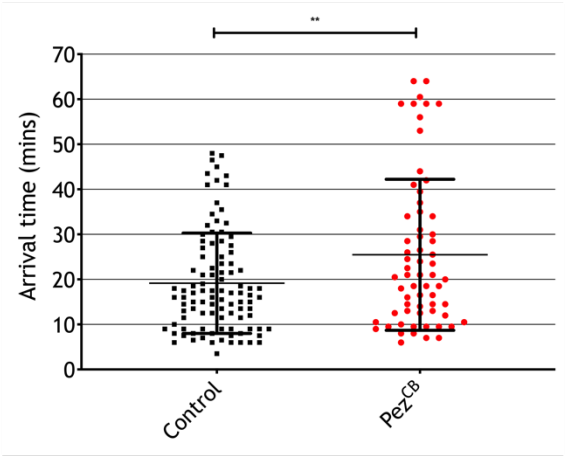
**
Arrival time (mins)
70
60
50
40
30
20
10
0
Control
Pez^CB

D)

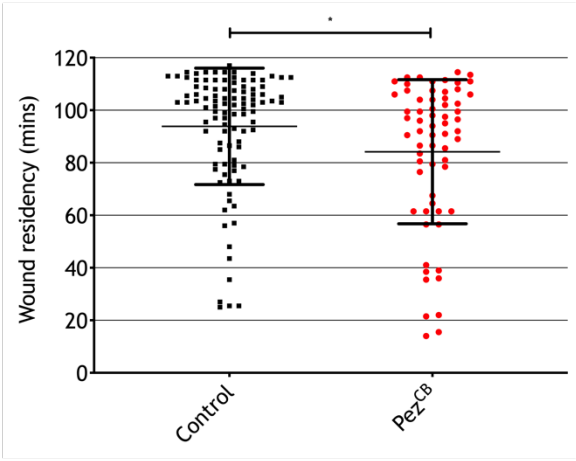
*
Wound residency (mins)
120
100
80
60
40
20
0
Control
Pez^CB

E)

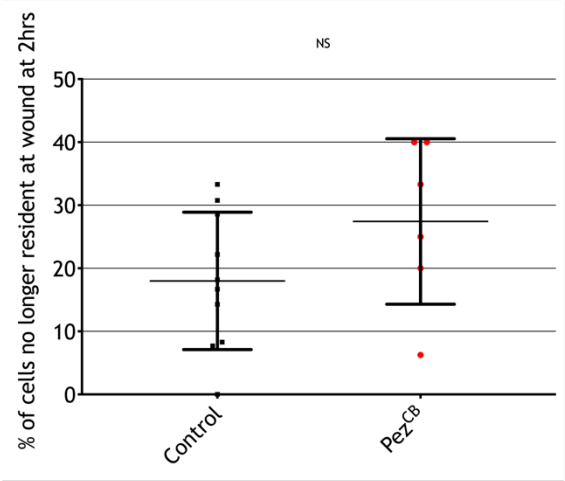
NS
% of cells no longer resident at wound at 2hrs
50
40
30
20
10
0
Control
Pez^CB

Figure 4.2.3: Manual tracking of hemocytes responding to laser generated epithelial wounds reveals a decrease in intrinsic directionality of *Pez^{CB}* mutants, a later wound arrival time and a reduction in time spent at the wound.

A) There is no difference in cell speed of *Pez^{CB}* (n=146 cells) mutants in the presence of an epithelial wound compared to Control (n=130 cells). Mann-Whitney U test. B) Responding hemocytes in Pez mutants migrate less directionally in the presence of a wound (Control n=53 responders, *Pez^{CB}* n=53 responders) – as characterised by the cells that reach the wound site by 2 hours post ablation. Mann-Whitney U test C) Pez mutant hemocytes reach the wound at later timepoints and D) have lower residency time at the wound site when compared to control. (Both Mann-Whitney U test). E) A trend is apparent for more cells leaving the wound site before wound closure in *Pez^{CB}* mutants however this is not significant by unpaired t-test.

4.3 Pez genetically interacts with the Src42a/Draper signalling axis in wound recruitment

As Pez was first identified as a potential player in hemocyte wound recruitment through a phosphoproteomic approach to identify novel components of the H_2O_2/Src42a/Draper signalling axis (Chapter 3), genetic interaction studies were employed to determine whether Pez lies within the same pathway. The basis for genetic interaction studies holds that if transheterozygotes of two genes of interest produce an analogous phenotype to homozygous mutants of either gene, then both proteins can be inferred to belong to the same pathway. This approach was successfully used when Draper was identified as the target receptor of H_2O_2 activated Src42a in hemocyte wound recruitment[73].

Firstly, heterozygous mutant embryos were investigated for hemocyte recruitment to ventral epithelial wounds at the one-hour time point. This revealed no significant difference between Control and either *Src42a*$^{[E1]}$/+ or *Pez*^{CB}/+. However, both transheterozygotes generated showed a significant reduction in the number of hemocytes recruited to epithelial wounds at the one-hour time point when compared to single Pez heterozygotes (Figure 4.3.1). These data indicate that Pez lies within the signalling axis of interest, however this approach is unable to provide temporal resolution related to the involvement of Pez in this wound recruitment pathway.

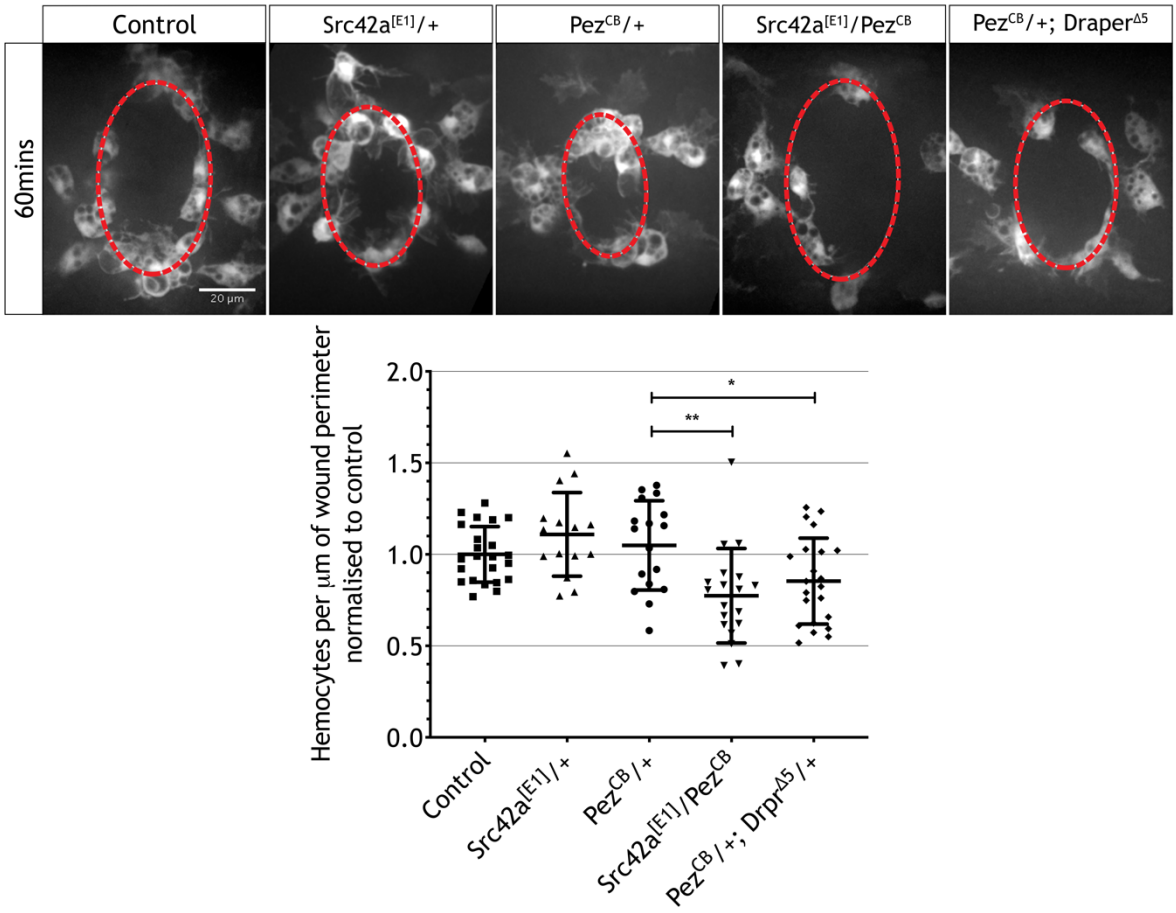

Figure 4.3.1: Pez interacts genetically with both Src42a and Draper in hemocyte wound recruitment.

Wound recruitment of hemocytes at the one-hour timepoint was investigated in heterozygous and transheterozygous embryos with representative images. Scale bar at 20μm. This approach revealed a wound recruitment phenotype in both Pez^{CB}/$Src42a^{[E1]}$ and Pez^{CB}/+;$Drpr^{\Delta5}$/+ in comparison to Pez^{CB}/+ - as tested by one way ANOVA with Sidak's multiple comparisons. Significance was only tested against Pez^{CB}/+ as this single test did not reveal significant differences between Pez^{CB}/+ and Control, and Pez^{CB}/+ and $Src42a^{[E1]}$/+. Control n=23; $Src42a^{[E1]}$/+ n= 15; Pez^{CB}/+ n=17; $Src42a^{[E1]}$/Pez^{CB} n=19; Pez^{CB}/+;$Drpr^{\Delta5}$/+ n=20.

4.4 The FERM domain of Pez is required for efficient hemocyte wound recruitment

In order to determine which domain of Pez is functional in the process of wound recruitment, truncated UAS-Pez constructs were used in rescue experiments. Four different transgenic fly lines constructs were obtained as a kind gift from Hugo Stocker[175]: full length Pez (UAS-Pez), Pez without the FERM domain (UAS-Pez$^{\Delta FERM}$), Pez lacking the entire phosphatase domain (UAS-Pez$^{\Delta PTP}$) and a form of Pez with the key catalytic cysteine of the phosphatase domain mutated to alanine (UAS-Pez$^{\Delta PD}$ – where PD denotes phosphatase dead) (as seen in Figure 4.4.1B). All of these constructs contain the phosphosite detected by the proteomics approach (outlined in Chapter 3 and illustrated in Figure 4.1.1).

UAS constructs were expressed alongside eGFP driven by *srp-Gal4.2* in the *Pez^{CB}* mutant background to investigate whether any were sufficient to rescue the wound recruitment defect. It should be noted that the *Pez^{CB}* locus contains a large 6.046 kb insertion (information publicly available on FlyBase) and it is unknown if any truncated Pez transcripts are generated in these mutant flies. As previously, hemocytes at the wound site were counted at the 1 hour timepoint following epithelial laser ablation. Using this approach, hemocyte numbers at the wound returned to numbers comparable to control when full length Pez (UAS-Pez) was re-expressed – indicating the integrity of this experiment (Figure 4.4.1A&C).

However, the overall result proved inconclusive as whilst Pez lacking the FERM domain (UAS-Pez$^{\Delta FERM}$) and Pez lacking catalytic activity (UAS-Pez$^{\Delta PD}$) were also able to rescue the defect, Pez without the phosphatase domain (UAS-Pez$^{\Delta PTP}$) did not. This result, with significance determined using one-way ANOVA, is a result of a single low data point in the UAS-Pez$^{\Delta PTP}$ data group that is not removed by outlier testing.

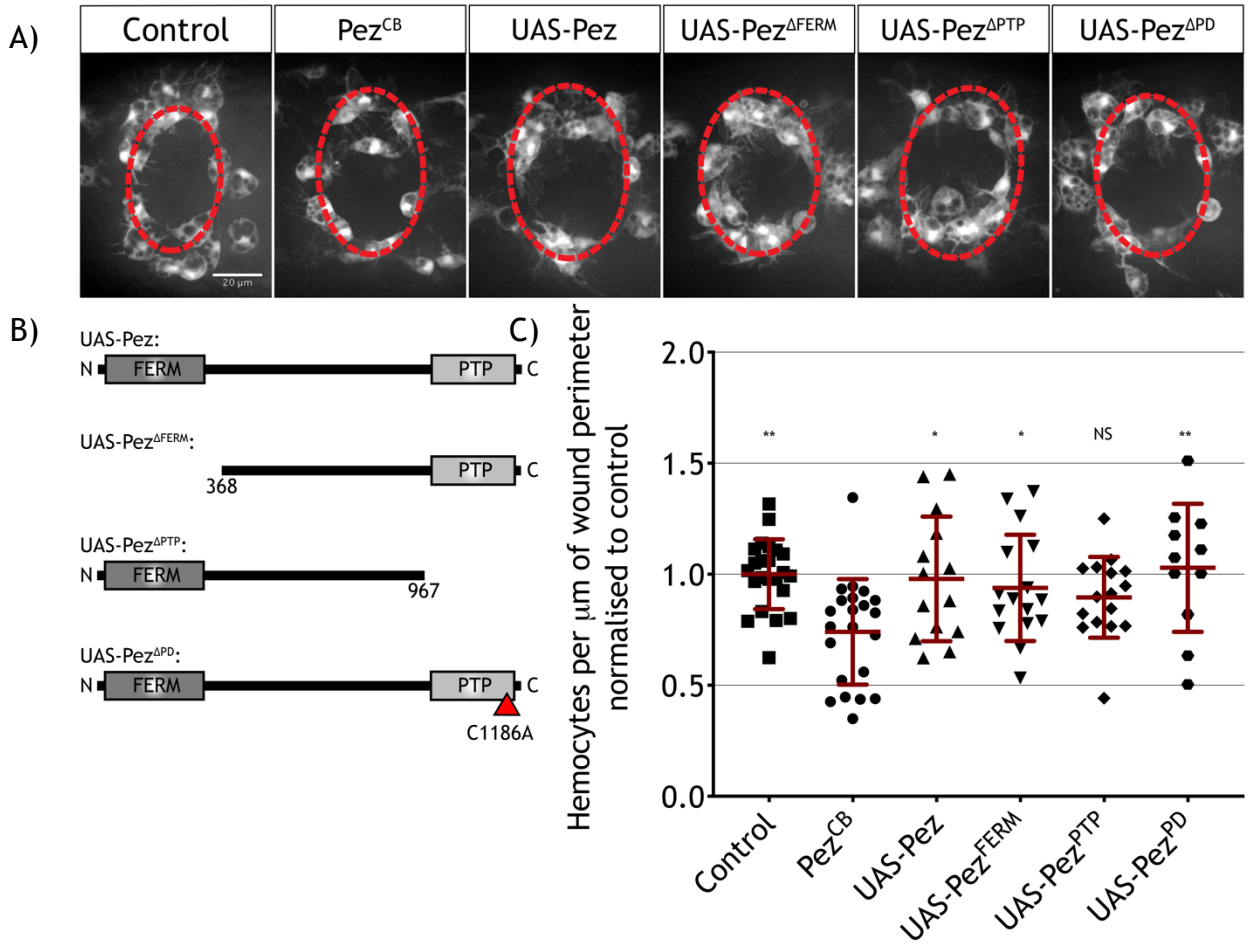

Figure 4.4.1: UAS-Pez rescue experiments in *Pez^{CB}* mutant background prove inconclusive.

A) Representative images taken from 1 hour post wounding of UAS rescue experiments. Full length, and 2 mutated UAS-Pez constructs (represented in B)) were able to rescue the wound recruitment defect seen at 1 hour in the Pez^{CB} mutant. Scale bar at 20μm. C) Individual data points plotted, as well as mean and standard deviation for each genotype tested. UAS-Pez$^{\Delta PTP}$ data is not statistically distinct from Pez^{CB} data. Statistical significance determined by one-way ANOVA with Dunnett's multiple comparisons. Control n=23 embryos; Pez^{CB} n=22, UAS-Pez rescue n=14; UAS-Pez$^{\Delta FERM}$ n=16; UAS-Pez$^{\Delta PTP}$ n=16 and UAS-Pez$^{\Delta PD}$ n=11.

As the rescue experiment was unable to provide information on the domain of Pez required in wound recruitment, it was repeated in the *Pez*^{2} excision allele background. Unlike the *Pez*^{CB} mutant, *Pez*^{2} has been published[175] and its effect on the gene is known. *Pez*^{2} was generated by excision of the P-element *P(GawB)NP4748* which is inserted into the Pez locus. This resulted in a loss of 3083 bp of coding sequence which causes a downstream frame shift (Figure 4.4.2 adapted from[175]). This background was therefore used for its genetic validity.

As seen with the *Pez*^{CB} background, full length UAS-Pez was able to rescue the 1 hour wound recruitment defect seen in *Pez*^{2} mutants (Figure 4.4.2A&C). Both the UAS-Pez$^{\Delta PTP}$ and the related catalytic mutant UAS-Pez$^{\Delta PD}$ are able to rescue the number of hemocytes recruited to the wound site. However, the defect seen in the excision background cannot be rescued by UAS-Pez$^{\Delta FERM}$. As these data groups are more distinct, and the mutant background is less likely to produce any viable Pez transcript, we believe this demonstrates a specific requirement for the FERM domain in wound recruitment. We therefore conclude that Pez may play a localisation-specific role during wounding as FERM domains are involved in localising proteins to the plasma membrane[223].

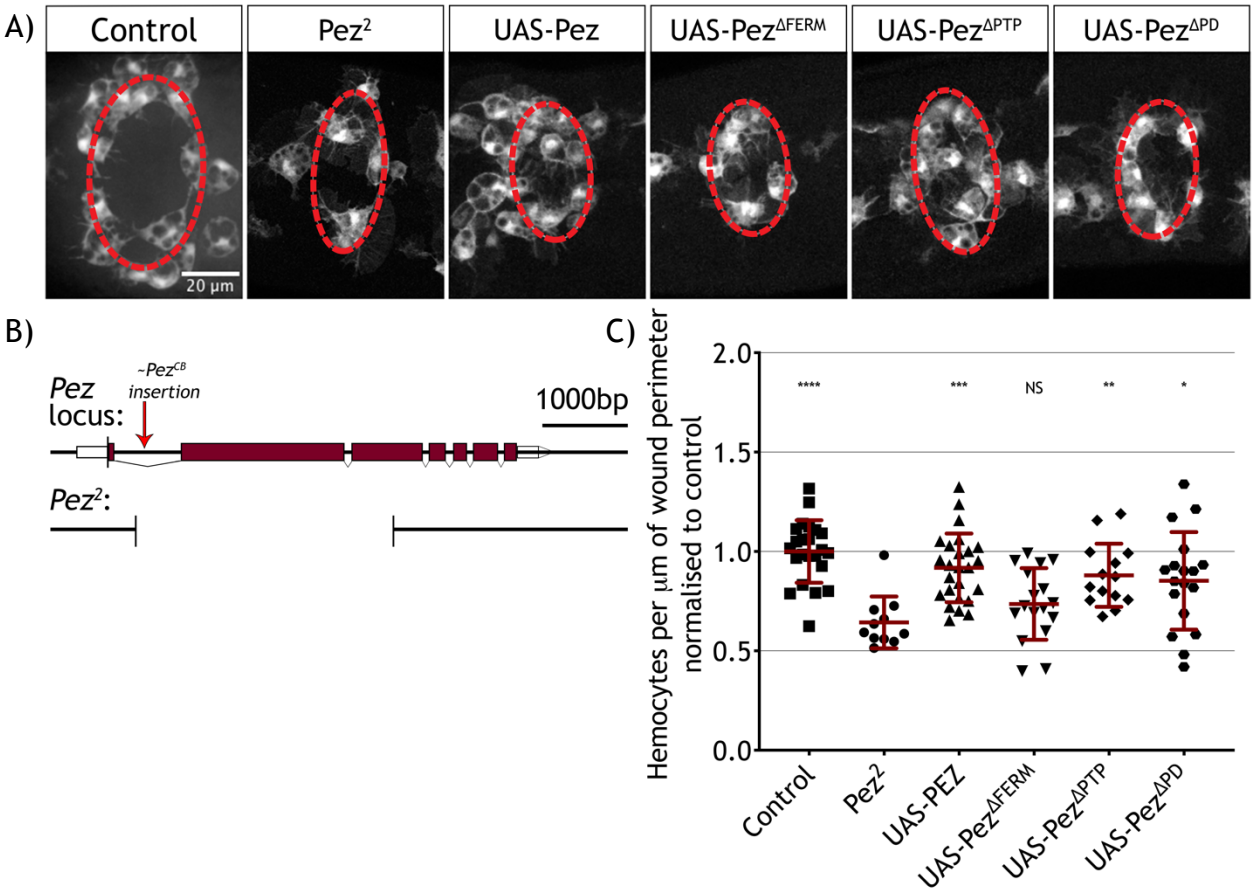

Figure 4.4.2: UAS-Pez rescue experiments in *Pez*^{2} mutant background reveal the FERM domain is required for efficient hemocyte wound recruitment.

A) Representative images taken from 1 hour post wounding of UAS rescue experiments. UAS-Pez, UAS-Pez$^{\Delta PTP}$ and UAS-Pez$^{\Delta PD}$ are sufficient to rescue the wound recruitment defect as quantified in C. B) Shows a representation of the extent of coding region excision in Pez^{2} mutants and the approximate location of the CB insertion. C) Quantification of wound recruitment. Individual data points plotted along with mean and SD. Statistical significance determined by one-way ANOVA with Dunnett's multiple comparisons. Control n=23 embryos; Pez^{2} n=13, UAS-Pez rescue n=26 UAS-Pez$^{\Delta FERM}$ n=17; UAS-Pez$^{\Delta PTP}$ n=14 and UAS-Pez$^{\Delta PD}$ n=18.

4.5 The use of fluorescent constructs reveals Pez localisation at sites of active Draper signalling

As we believe localisation of Pez via its FERM domain may be important in its hemocyte function, two fluorescent UAS-Pez constructs were generated – Pez-sfGFP and Pez-mCherry to visualise Pez dynamics *in vivo* (Figure 4.5.1, constructs in Appendix 7). Fluorophores were added to the C terminus of the Pez coding sequence, following a short GSSSSS linker sequence. This location was chosen as C-terminally GFP tagged genomic Pez was shown to be functional in the control of whole animal body size[175].

As well as investigating the basal localisation of Pez in hemocytes, we also wished to investigate its co-localisation alongside Draper. Thus, a third fluorescent construct was used – UAS-Draper-eGFP. This construct was generated previously in the lab (Dr Fred Rodrigues, unpublished Figure 4.5.1 with construct in Appendix 8), and C-terminally tagged Draper was selected over N-terminal GFP due to improved signal.

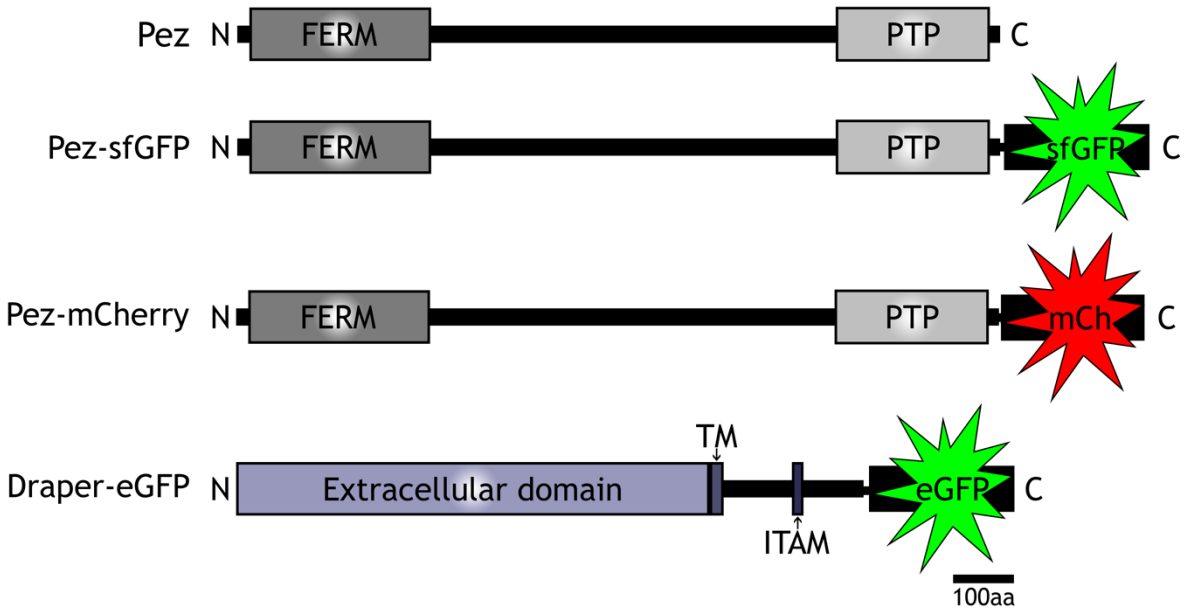

Figure 4.5.1: Representation of fluorescent constructs.

Pez was tagged C terminally with sfGFP and mCherry following a short linker region. Draper-eGFP was generated previously in the lab (unpublished). Draper is annotated to show the N-terminal extracellular domain, transmembrane domain (TM) and immunoreceptor tyrosine-based activation motif (ITAM) – the site of Src42a phosphorylation.

Initially, flies harbouring *UAS-Pez-sfGFP* were recombined with *srp-Gal4.2* to investigate Pez localisation in hemocytes under basal migratory behaviours at stage 15. To capture dynamics, 7 μm stacks of 15 slices were imaged at 15 second intervals by spinning disc microscopy. Unexpectedly, Pez-sfGFP is not only weakly diffuse through the cell cytosol, but also appears in puncta in both the cell body and lamellipodium (Figure 4.5.2A). These puncta - particularly those within the lamellipod - are highly dynamic (Supplementary movie 3), and flow inward towards the cell body. We therefore believe these are not merely inert protein aggregates.

To investigate Pez localisation in hemocytes during their developmental dispersal, stage 12 embryos were imaged over an extended period during this process. As hemocytes migrate out from their origin in the head region of the developing organism, they perform the important function of clearing apoptotic debris that is generated as part of normal development[236]. As well as being an integral part of the wound recruitment signalling cascade, the damage receptor Draper also mediates phagocytosis of apoptotic cells[78]. This ligand-dependent activation of Draper also involves Src42a and Shark, and thus is another example of active Draper signalling[82] with the apoptotic marker phosphatidylserine (PS) sufficient to activate the system *in vitro*[80].

In stage 12 embryos, Pez-sfGFP shows uniform expression throughout the cell cytosol (Figure 4.5.2B) and we attribute the lack of punctae to the lower expression of the *serpent-Gal4.2* promoter at this stage in development. As Pez-sfGFP expressing hemocytes encounter apoptotic debris, Pez-sfGFP is seen to accumulate at the cup (Figure 4.5.2B white arrow heads) which suggests the involvement of Pez in this second Draper-mediated hemocyte function.

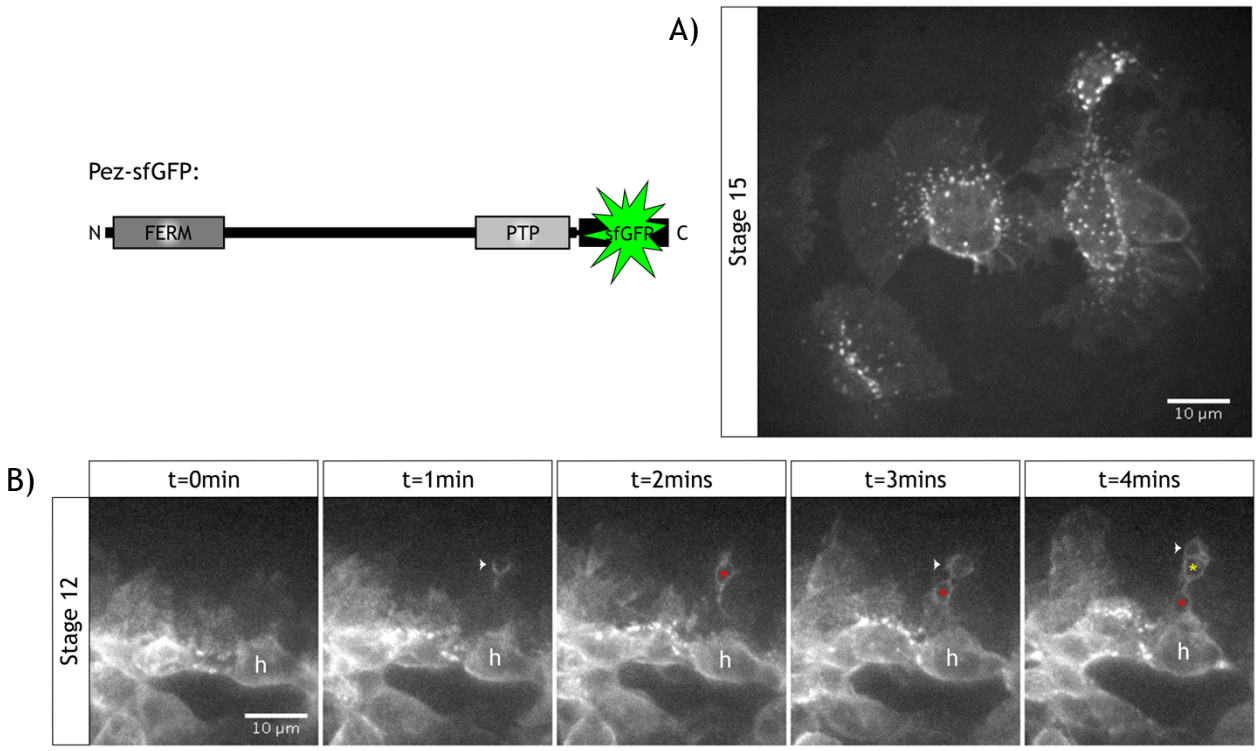

Figure 4.5.2: Localisation of Pez-sfGFP *in vivo*.
UAS-Pez-sfGFP was driven under the control of srp-gal4.2 in the hemocyte lineage. A) At stage 15 Pez-sfGFP shows punctate localisation throughout the cell body and cytosol. Scale bar 10µm. B) Earlier during development, at stage 12, Pez-sfGFP is seen diffuse throughout the cell. As hemocytes migrate out of the head, they encounter apoptotic debris which they phagocytose. The white arrow heads at both 1, 3 and 4mins indicate Pez localisation at phagocytic cups. This debris is fully engulfed, as indicated by the completed cups noted with the red and yellow Asterix respectively. The hemocyte cell body is denoted by h.

Due to the linear manner in which Pez-sfGFP puncta appeared to track back towards the cell body, we reasoned that they may be travelling along microtubules in active transport. To investigate this hypothesis, the localisation of Pez-sfGFP was investigated alongside the microtubule marker mCherry-Clip170 which is a fluorescent microtubule binding protein. This approach was unable to confirm whether Pez travels along microtubules, most likely due to the delay between the acquisition of the images in the two separate channels (Supplementary movie 4).

To investigate the basal localisation of Draper in hemocytes, *srp-gal4.2, UAS-Draper-eGFP* flies were imaged as described for Pez-sfGFP transgenic lines. At stage 15 this revealed a more diffuse cytosolic localisation in comparison to Pez-sfGFP (Figure 4.5.3), with some aggregation of Draper around intracellular vacuoles. These vacuoles are ingested cell corpses; thus, this localisation may be attributed to the role of Draper in corpse processing[237].

Investigating Draper-eGFP localisation at stage 12 during hemocyte dispersal also revealed the recruitment of Draper to phagocytic cups. This corroborates the *in vitro* finding of Draper localisation to both PS-coated beads and cell corpses to phagocytic cups generated by S2 cells[80].

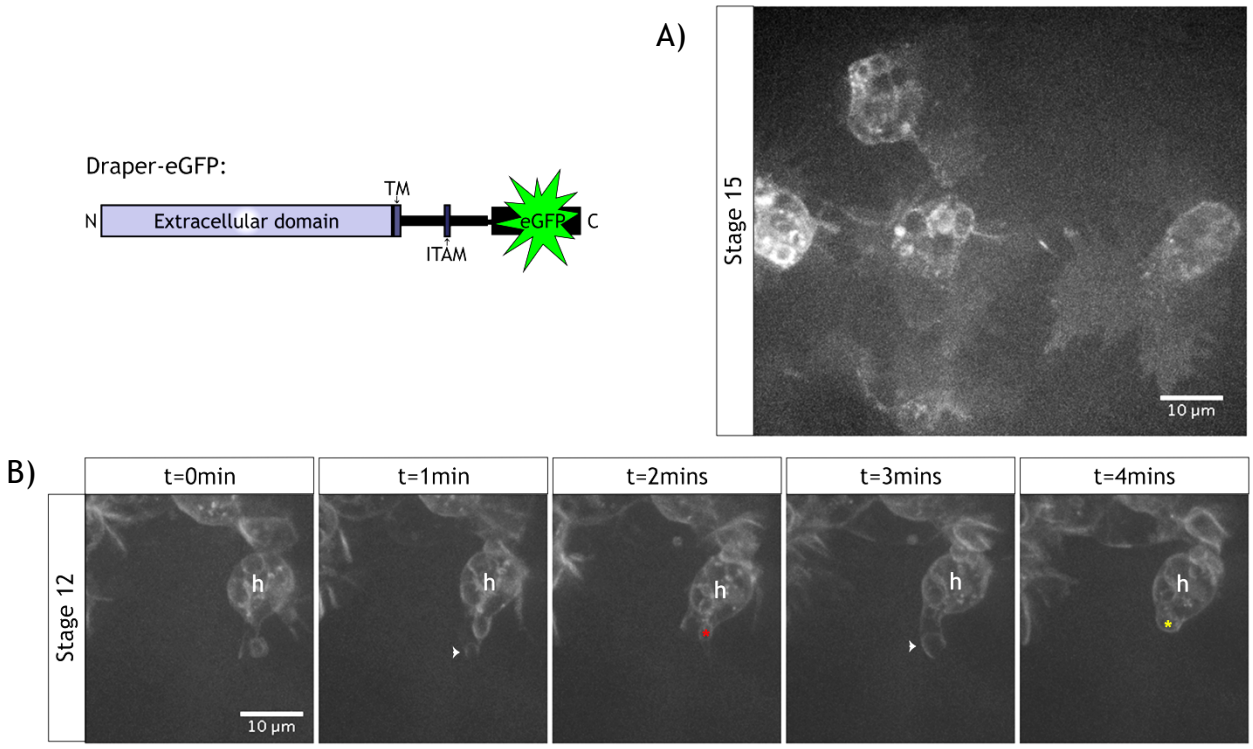

Figure 4.5.3: Localisation of Draper-eGFP in vivo.

UAS-Draper-eGFP was driven under the control of srp-gal4.2 in the hemocyte lineage. A) At stage 15 Draper-eGFP shows diffuse localisation throughout the cytosol, with some increased localisation around intracellular vacuoles. Scale bar 10µm. B) Earlier during development, at stage 12, Draper-eGFP is also seen diffuse throughout the cell. As hemocytes migrate out of the head, they encounter apoptotic debris which they phagocytose. The white arrow heads at both 1, and 3 mins indicate Draper localisation at phagocytic cups. This debris is fully engulfed, as indicated by the completed cups noted with the red and yellow Asterix respectively. The hemocyte cell body is denoted by h.

As both Pez and Draper were independently shown to localise to hemocyte phagocytic cups in vivo, we generated a fly line harbouring both UAS-Pez-mCherry and UAS-Draper-eGFP under the control of *serpent-Gal4.2*. Using these transgenic animals, we were able to colocalise Draper and Pez to phagocytic cups at stage 12 in embryonic development (Figure 4.5.4) by imaging at 15 second intervals over a 7 μm Z-stack imaged at 0.5 μm slices. Analysing the fluorescent intensity profile over a line manually drawn around the cup allowed Pez and Draper localisation to be visualised in arbitrary units (AU). This approach could not temporally resolve Draper and Pez cup localisation at its formation at this acquisition rate, but revealed that both proteins remain at the cup following completion as it is drawn back into the cell body.

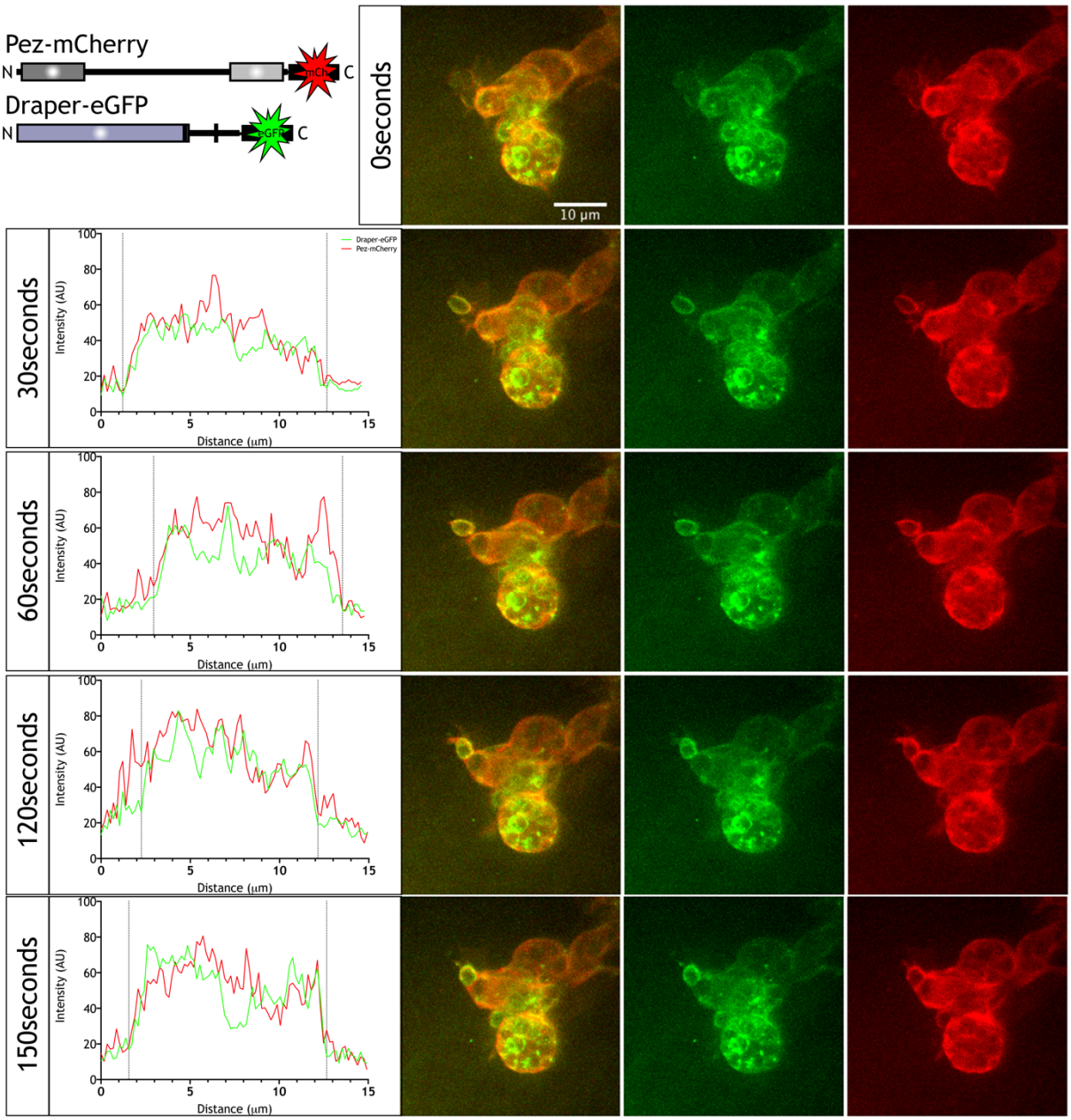

Figure 4.5.4: Draper-eGFP and Pez-mCherry colocalise at phagocytic cups.
Representative images of Draper-eGFP and Pez-mCherry during phagocytic cup generation and completion. Scale bar 10µm. To visualise fluorophore intensity, a 15 µm line was drawn around the cup, starting and finishing outside in the area of background to the LHS of the cup. The intensity data is plotted as arbitrary units over distance, with the dotted vertical lines representing the beginning and end of the line covering the cup.

4.6 Pez-sfGFP mislocalises in the absence of Draper and Src42a

To investigate whether Pez localisation is dependent on the Draper inflammatory signalling axis, Pez-sfGFP puncta in Draper$^{\Delta 5}$ and Src42a$^{[E1]}$ mutants were imaged. Due to the dynamic nature of the puncta, their numbers were quantified over a 5 minute interval (where images were taken every 15 seconds) and averaged. There was a significant increase in the number of puncta across the entire cell – as marked by the red outline (Figure 4.6.1A) – in *Draper* mutants in comparison to control (Figure 4.6.1B).

To investigate the subcellular localisation of Pez puncta across the different mutants, the percentage of puncta in the cell body was calculated. This revealed a significant increase in the number of puncta residing in the cell body in both *Draper$^{\Delta 5}$* and *Src42a$^{[E1]}$* mutants in comparison to control (Figure 4.6.1C). Pez-sfGFP can also be seen aggregating around intracellular vacuoles in *Draper$^{\Delta 5}$* mutants, with intermittent accumulation as seen by 'flashing' at this subcellular localisation (Supplementary movie 5). We therefore conclude that Pez-sfGFP is less dynamic throughout the lamellipodium in the absence of Draper and Src42a, and also that there may be some unresolved vacuole signalling that Pez participates in at intracellular vacuoles in the absence of Draper.

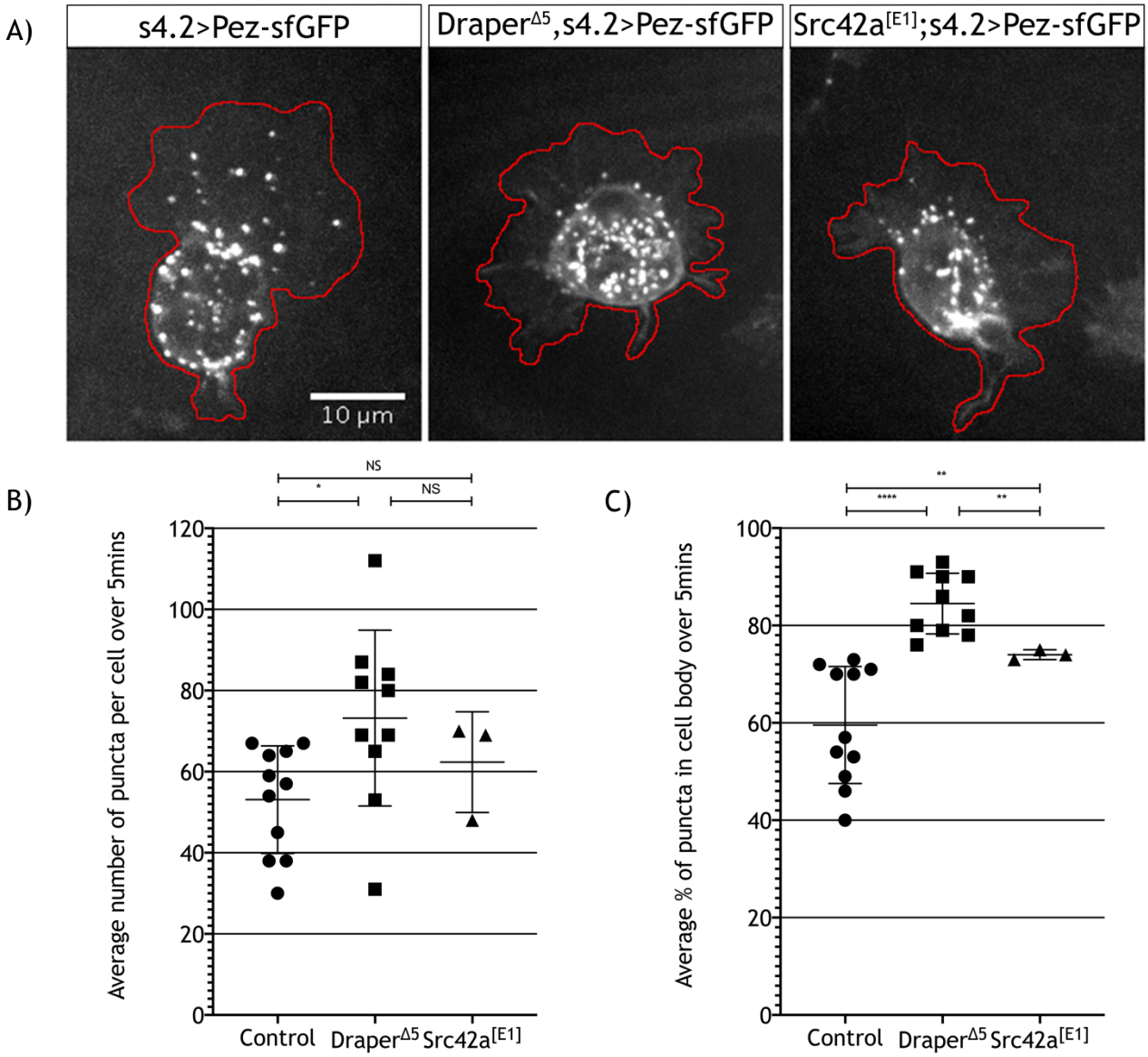

Figure 4.6.1: More Pez-sfGFP puncta are located within the cell body in Draper and Src42a mutant embryos.

A) Representative images of Pez-sfGFP puncta at stage 15 in control, Draper$^{\Delta5}$ and Src42a$^{[E1]}$ mutant embryos. Cell outlines in red include the cell body and lamellipodium. Scale bar 10µm. B) Quantification of puncta numbers as an average over 5mins of imaging at 15sec intervals. Individual data points plotted, with mean and SD. Whilst a trend is apparent for more puncta in Draper$^{\Delta5}$ mutants this is not significant as tested by One-Way ANOVA. C) The % of puncta located within the cell body as an average over 5minutes of imaging. Individual data points plotted along with mean and SD. There is a significant increase in the proportion of puncta in the cell bodies of Draper$^{\Delta5}$ and Src42a$^{[E1]}$ mutant embryos in comparison to control as tested by Brown-Forsythe and Welch ANOVA tests due to unequal SD. Control N=3 embryos, n=9 cells; Draper$^{\Delta5}$ N=5 embryos, n=10 cells; Src42a$^{[E1]}$ N=3 embryos, n=3 cells.

4.7 Pez-sfGFP puncta increase following wounding in a Draper dependent manner

To determine whether Pez localisation changes following wounding by laser ablation, Pez-sfGFP puncta were investigated over 5 minutes following tissue injury in control and mutant animals. Due to the increase in and mislocalisation of Pez-sfGFP puncta under basal conditions (Figure 4.6.1), both mean puncta number and % of puncta in the cell body were normalised to basal levels in each genotype investigated. This revealed an increase in the number of puncta per cell in control wounded embryos in comparison to basal levels. This was Draper dependent, as the same increase from basal levels is not seen in *Draper*$^{\Delta 5}$ mutants (Figure 4.7.1A and B).

Comparing the subcellular localisation of puncta - as measured by percentage puncta in the cell body - revealed a significant increase in the proportion of puncta found in hemocyte cell bodies in control cells in comparison to Draper mutants following wounding (Figure 4.7.1C). We speculate that Draper may therefore increase the internalisation of Pez-sfGFP from the cell periphery following wounding, perhaps through interaction with and internalisation of the activated receptor itself.

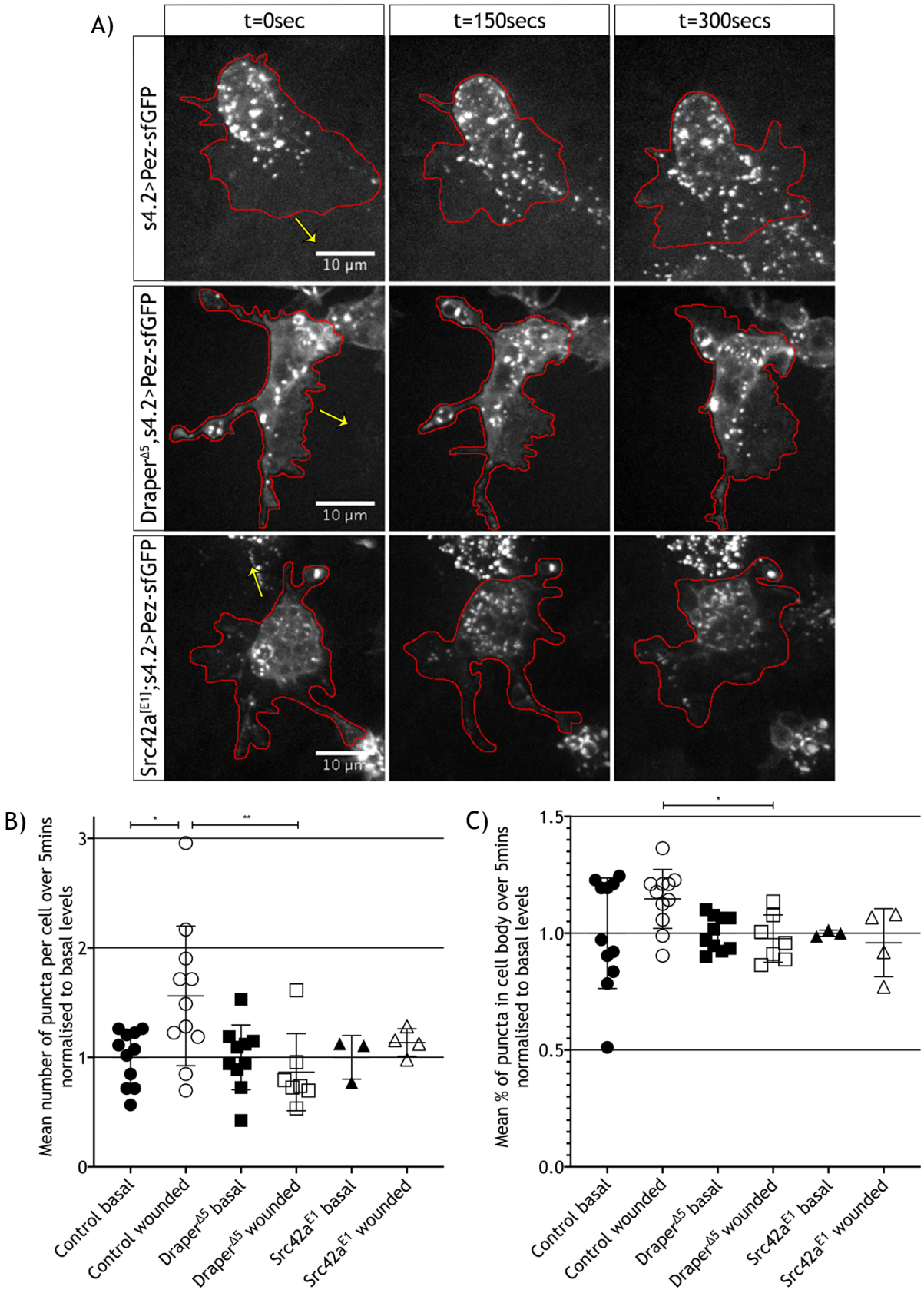
A)
t=0sec
t=150secs
t=300secs
s4.2>Pez-sfGFP
Draper$^{\Delta 5}$,s4.2>Pez-sfGFP
Src42a$^{[E1]}$;s4.2>Pez-sfGFP
10 µm
B)
Mean number of puncta per cell over 5mins normalised to basal levels
Control basal
Control wounded
Draper$^{\Delta 5}$ basal
Draper$^{\Delta 5}$ wounded
Src42a^{E1} basal
Src42a^{E1} wounded
C)
Mean % of puncta in cell body over 5mins normalised to basal levels

Figure 4.7.1: Pez-sfGFP puncta localisation following wounding.

A) Representative images of UAS-Pez-sfGFP expressing hemocytes in control, Draper$^{\Delta 5}$ and Src42a$^{[E1]}$ animals. Cell of interest in each panel outlined in red, with the location of the wound relative to the cell marked by the yellow arrows. Scale bar at 10 μm. B) The mean number of puncta per cell under both basal (data from Figure 4.6.1) and wounded conditions normalised to basal levels of each genotype. Individual data points plotted with mean and SD. Statistical significance determined by One-Way ANOVA. C) Individual percentages of puncta residing in the cell body plotted, along with the mean and SD, normalised to basal levels of each genotype. The percentage of puncta in the cell body of Draper$^{\Delta 5}$ mutant hemocytes remains significantly more than in control following epithelial wounding as tested by Brown Forsthye One-Way Anova due to unequal SD between groups.

Following an increase in the variability of puncta in control animals in the first 5minutes following wounding, Pez-sfGFP puncta were also visualised at the wound site. This revealed that, as under basal conditions, puncta track back from the leading edge of the cell at the wound site into the cell body (Supplementary movie 6).

4.8 There is evidence for Draper-eGFP lamellipodial puncta following wounding within hemocytes

To investigate whether there are any similarities between the localisation of Draper-eGFP and Pez-sfGFP following laser ablation of the epithelium, Draper-eGFP embryos were imaged immediately following tissue injury as described previously. As with Pez-sfGFP, we have identified Draper-eGFP puncta in the lamellipod of cells in the vicinity of the wound site immediately following laser ablation (Figure 4.8.1, white arrow heads). Similarly, these Draper puncta flow back from the leading edge of the cell (wound direction denoted by the yellow arrow) into the cell body (Supplementary movie 7). The Draper-eGFP puncta are more infrequent and less distinct than Pez-sfGFP, therefore quantification of puncta number and localisation could not be completed. Lamellipodial Draper puncta are not seen under basal conditions (Figure 4.5.3), therefore we infer that these are a direct result of H_2O_2/Src42a inflammatory signalling and perhaps represent the internalisation of activated Draper receptor.

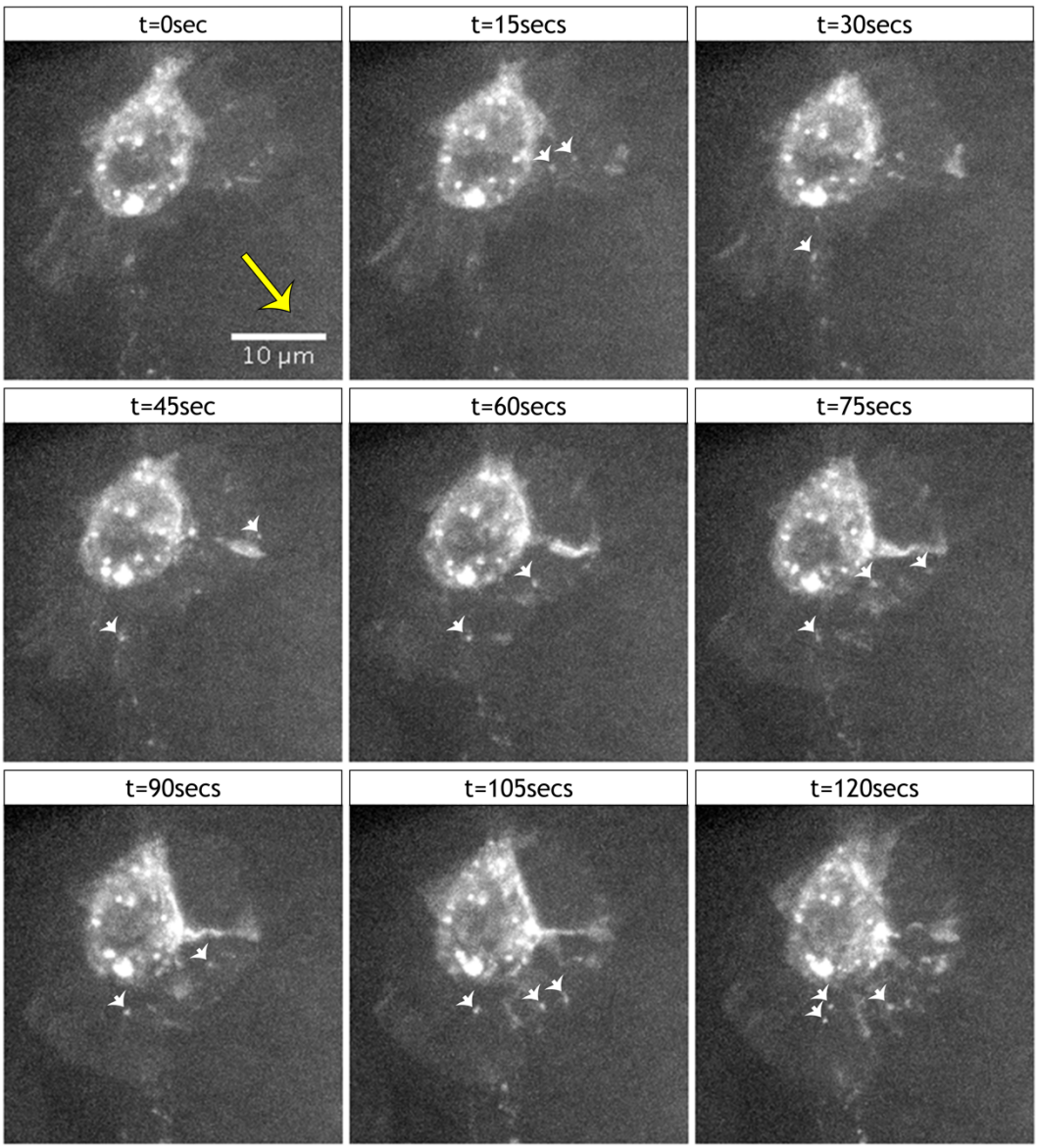

Figure 4.8.1: Evidence for dynamic lamellipodial Draper-eGFP puncta following wounding.

Representative images taken at 15second intervals of Draper-eGFP expressing hemocyte immediately following laser ablation. Wound direction is denoted by the yellow arrow. Scale bar at 10µm. Evidence of Draper-eGFP puncta (denoted by white arrowheads) can be seen 15seconds following the start of imaging – done as close to ablation point as possible.

4.9 Simultaneous imaging of Pez-mCherry and Draper-eGFP following wounding

As both Pez and Draper lamellipodial puncta were observed following wounding, the double transgenic for both Pez-mCherry and Draper-eGFP was used to investigate potential colocalization of Pez and Draper wound-induced puncta. Following wounding by laser ablation, hemocytes were imaged for both Draper-eGFP and Pez-mCh sequentially at 15 second intervals. This approach revealed limited evidence of lamellipodial puncta colocalization (Figure 4.9.1, white arrowheads) using a 63x objective lens with a 1.4 numerical aperture.

Generally, Draper-eGFP puncta were seen in the vicinity of Pez-mCherry puncta but were distinct (Figure 4.9.1, white box). It may be that the temporal resolution achieved by sequential imaging of GFP followed by mCherry is insufficient to colocalise puncta over a 15 μm Z-stack.

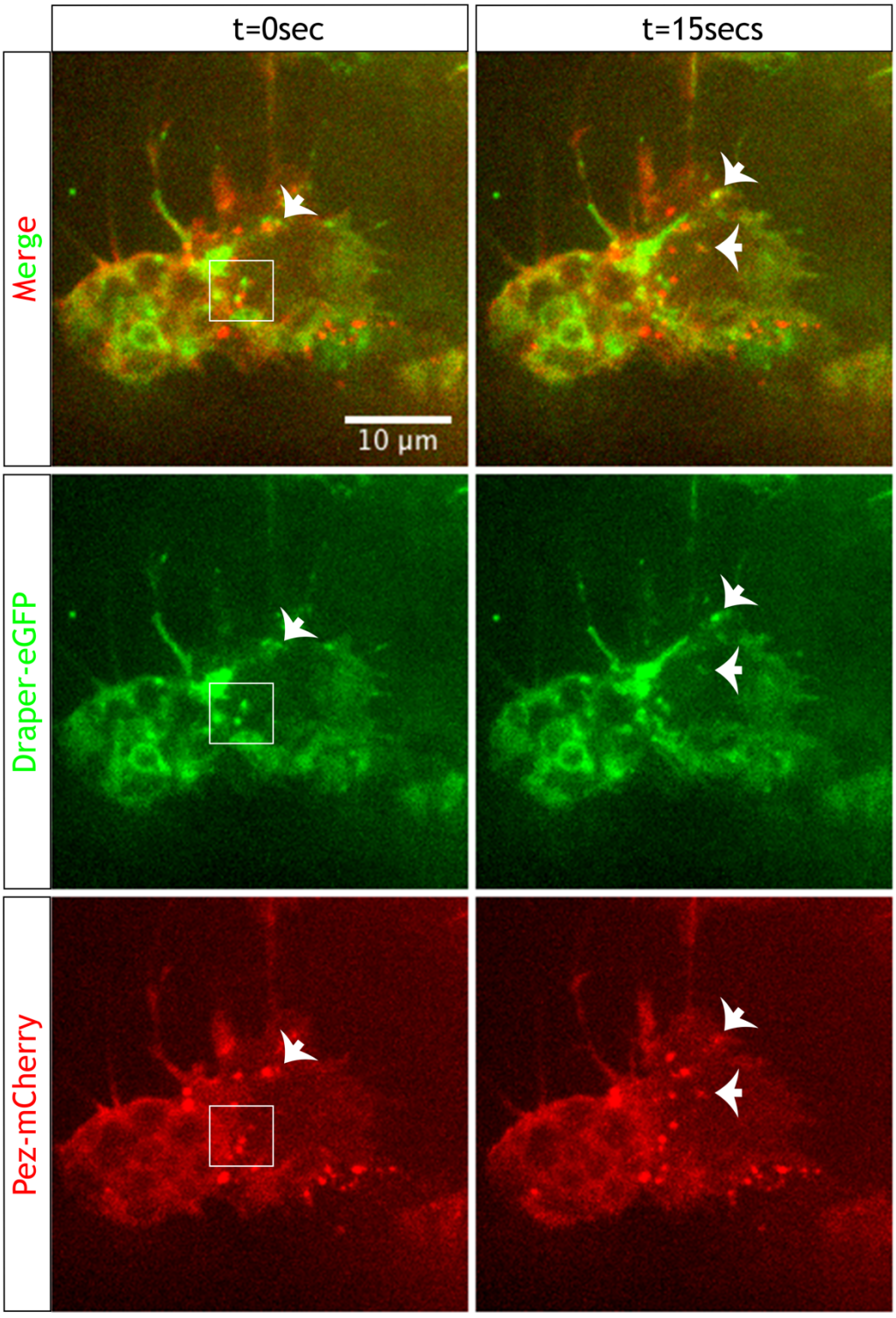

Figure 4.9.1: Draper-eGFP and Pez-mCherry colocalise puncta interact infrequently following wounding.

Representative images of Draper-eGFP and Pez-mCherry puncta following epithelial wounding by laser ablation. Scale bar 10 µm.

4.10 Discussion

4.10.1 Rationale

The inflammatory response of *Drosophila* embryonic hemocytes towards epithelial wounds is centred around H_2O_2 signalling[100] and Src42a kinase activation[73]. A phosphoproteomic approach was therefore utilised to identify novel phosphoproteins following H_2O_2 release (outlined and followed up in Chapter 3). We identified a robust wound recruitment defect in Pez mutant embryos which we sought to further characterise.

4.10.2 Pez mutant hemocytes are unable to efficiently integrate the damage signals released upon wounding

In 2002, *Drosophila* embryos were shown to be a powerful in vivo model for epithelial wounding[238]. Since then, a variety of studies have investigated how cells of the *Drosophila* innate immune system are able to sense and respond to damage signals. Initial work demonstrated hemocytes actively polarise and migrate towards wounds, with a peak in cell numbers at 1 hour post ablation[89]. The generation of dynamic lamellipodial structures, mediated by the small GTPases Rho and Rac were shown to be crucial in the recruitment of hemocytes to wounds. Under basal conditions, hemocytes in Rac and Rho mutants show defects in cell morphology – with the latter's trailing edge morphology directly impeding its recruitment to epithelial wounds. Further, Rac cells fail to undergo normal developmental dispersal. The wound recruitment phenotypes displayed by these small GTPase mutants are distinct from Pez mutant hemocytes - which display normal morphology and complete hemocyte dispersal by stage 15 of development.

Having uncovered the importance of the regulation of cell morphology in hemocyte wound recruitment, later work established the developing embryo as a model to dissect the complex signalling involved in epithelial damage and inflammation. Following the discovery of H_2O_2 mediated leukocyte recruitment to zebrafish tailfin wounds[131], analogous signalling was found to occur in hemocyte wound recruitment[100]. This was shown to be downstream of an intracellular calcium wave that is emitted immediately following wounding[91] which activates the enzyme DUOX via its EF hands. By blocking

H_2O_2 production or calcium signalling within the epithelium, the number of hemocytes recruited to epithelial wounds was dramatically reduced by more than 50% and was evident as early as 15 minutes post injury in the case of H_2O_2 abolition. This defect is far more dramatic than that which we have identified in Pez mutants, thus we conclude Pez mutant hemocytes are still activated by the early damage signal H_2O_2.

The target for inflammatory H_2O_2 in *Drosophila* was identified as the kinase Src42a in 2015[73], again following insight from the zebrafish wounding field[102]. Both Src42a and the vertebrate orthologue Lyn share a redox sensitive cysteine residue, which is oxidised in the presence of H_2O_2 and promotes leukocyte recruitment to wounds. As such, in the absence of Src42a there is a robust decrease in the number of hemocytes recruited to epithelial wounds at both the 20 and 60 minute timepoints. Cell tracking and time-lapse imaging was used to uncover the manner in which Src42a mutant hemocytes migrate following wounding and can be compared to the data gathered in this study for Pez mutants. As we identify here for Pez mutants, the loss of Src42a does not affect the speed in which hemocytes migrate in the presence of a wound but does affect the cell's directionality. Whilst the methods for quantifying directionality differ, here we have conclusively shown that responding Pez hemocytes migrate in less directional manner towards wounds – as calculated by meandering index, where a value of 1 indicates migrating in a true straight line. Analogously, Src42a mutant hemocytes have a true lack of directionality towards the wound centre. This is due to a lack of Src42a-mediated phosphorylation of the intracellular ITAM motif on the cell death receptor Draper, which further transduces the signal to Shark to permit chemotaxis.

As the mammalian orthologue of Pez has been shown to bind to and participate in Src family kinase signalling[206–208], we hypothesised that Pez may also physically interact with the Src42a pathway in hemocytes. To investigate this, we used transheterozygotes to determine whether Pez genetically interacts with Draper or Src42a. This experiment conclusively showed a wound recruitment defect in both transheterozygotes tested. As a

reduction in directionality in both Pez and Src42a mutant hemocytes is apparent, and Pez has been shown to robustly interact with both Draper and Src in wound recruitment, we believe Pez mutants are unable to effectively relay the H_2O_2 inflammatory signal via Src42a to Draper. As a wound recruitment defect is seen earlier in Src42a mutants (20 minutes, in comparison to 40 minutes in Pez mutants) it may be that this signalling is not properly controlled or sustained over time in Pez mutants.

4.10.3 The FERM domain of Pez is required in hemocyte wound recruitment

As well as a C terminal PTP phosphatase domain with disputed activity[205], Pez also contains an N terminal FERM domain – a structure shared by various cytoskeletal/plasma membrane linker proteins[223]. Literature on *Drosophila* Pez is limited, and it is currently described as an upstream regulator of Hippo signalling where it participates in the control of intestinal stem cell proliferation and body size[5] – a function which requires the N terminal FERM domain. However, there is evidence for the mammalian orthologue – PTPN21 – participating in active Src family kinase signalling[206–208].

To investigate which domain of Pez is functional in hemocyte wound recruitment, rescue experiments were performed using truncated UAS-Pez constructs obtained as a kind gift from the Stocker lab[175]. Using full-length UAS-Pez, researchers were able to rescue both the whole animal size and abrogated intestinal stem cell proliferative defects seen in Pez mutants - indicating the functionality of the construct generated[239].

Work in this thesis initially made use of the commercially available Pez^{CB} mutation of Pez in which a large 6.046 kb P element (*P{RS3}*) has been inserted into the Pez locus. This mutant has not been used in previous studies, and its effect on translation of functional Pez protein is unknown. We also validated the functionality of the UAS-Pez construct, as it was able to rescue the wound recruitment defect seen at 1 hour post ablation in this background. For truncated rescue experiments, both Pez lacking the FERM domain and Pez lacking catalytic activity ($Pez^{\Delta PD}$) were able to rescue the

wound recruitment defect. The catalytically related mutant, with removal of the entire PTP domain, could not rescue the defect; however, this dataset was skewed by a low data value that was not removed by ROUT 1% outlier testing. Thus, from this experiment alone we were unable to conclude whether the N-terminal FERM domain or C-terminal PTP domain with phosphatase activity were required in wound recruitment. We attribute this result to genetic ambiguity of the *Pez^{CB}* background.

As well as functional and truncated UAS-Pez constructs, the Stocker lab also generated two genetically validated Pez mutants – *Pez^{1}*, which contains an early stop codon, and *Pez^{2}*, in which a large portion of coding sequence is removed - resulting in a downstream frameshift of the coding region. Both of these mutants were reported to be homozygous viable[175], unlike the *Pez^{CB}* mutant which was lethal in our lab conditions.

We obtained both mutations and repeated the rescue experiments in the *Pez^{2}* excision background. This experiment conclusively demonstrated a requirement for the FERM domain in hemocyte wound recruitment. This perhaps adds further evidence for the complete lack of catalytic activity of *Drosophila* Pez[205], as we and others[175] have shown it is dispensable in two distinct cellular processes. Excitingly, it is the FERM domain of the human orthologue PTPN21 which has been demonstrated to directly bind to Src family kinases[207]. This, along with our genetic interaction result, adds further support for the hypothesis that Pez may bind directly to Src42a during its function in wound recruitment. Having generated fluorophore tagged Pez constructs in this study, future experiments could investigate this by performing GFP pull-down of Pez-sfGFP and probing for interaction with *Drosophila* Src42a.

Other physical interactions between the FERM domain of PTPN21 have been elucidated. This includes actin, which was identified in the same study as Src[207]. More recently, work by Siddiqui et al[240] followed up on a 1998 screen which identified a novel kinesin-like protein - KIF1C - as an interacting partner of PTPN21[241]. The *Drosophila* orthologue of this protein, unc-104,

shares 62% sequence identity. Whilst kinesins are known to 'walk' along microtubules towards the plus end, which is generally oriented away from the cell body, KIF1C transport was shown to be bidirectional[242]. This is particularly interesting as we have visualised Pez dynamics *in vivo* by fluorophore tagging and have identified dynamic puncta which, due to their linearity in movement, we believe are sites of active trafficking.

Unfortunately, sequential imaging of Pez-sfGFP and mCherry-CLIP170 was unable to provide compelling evidence of colocalization of our puncta with microtubules. Due to the dynamic nature of both the microtubule network[60], and the Pez puncta we have identified it may be that imaging the fluorophores sequentially is too slow to capture their interaction. By reducing the Z-stack size, and thus the acquisition time, it may be possible to investigate this further in future.

Previous work focussing on the PTPN21 and KIF1C interaction was able to resolve their binding sites to the amino acid level[240]. Two short peptide sequences in the FERM domain were shown to physically bind to lysines in the stalk region of KIF1C. Aligning Pez and PTPN21 sequences revealed that the first KIF1C binding site is fully conserved (HK*FYR; where * denotes binding to the preceding amino acids), and the second is more loosely related (PTPN21: WHD* compared to Pez: WHE), with the change from aspartic acid in human PTPN21 to glutamic acid in Pez retaining similar structural properties. To see if the KIF1C interacting peptides are also conserved in unc-104, these sequences were also aligned. This revealed that both lysine residues mediating the PTPN21 interaction were conserved, with only a slight deviation in the neighbouring amino acid of the second sequence (KIF1C: EMEK*RL compared to unc-104: EMKK*RL; first sequence GK*NHVFRF). We therefore hypothesise that *Drosophila* Pez and unc-104 may also directly interact, which could be investigated in future by protein pull-down. To determine whether Pez puncta are a result of active KIF1C transport, the localisation of Pez-sfGFP puncta could be investigated in unc-104 mutants and compared to control data presented in this study.

4.10.4 Pez shows dynamic localisation within hemocytes, which is increased following epithelial wounding

As we determined Pez may be playing a localisation-specific role during wound recruitment via its FERM domain, we wanted to investigate Pez dynamics *in vivo*. Previous work looking at Pez localisation made use of genomic tagged Pez-GFP which was visualised following fixation and immunostaining[175,243]. This approach, which may well lose information following protein crosslinking, revealed even expression throughout the adult midgut, with accumulation at the apical surface of midgut enterocytes. GFP-tagged Pez expression was also seen in imaginal discs, where it again localised to the apex of cells. Live imaging of the Pez-GFP genomic construct was attempted, but the fluorescence was far too low for any meaningful interpretation thus the data is not presented here. We therefore generated fluorophore tagged UAS-Pez constructs for expression in the hemocyte lineage. We were able to visualise dynamic Pez puncta under basal conditions, which mis-localised in the absence of Draper and Src42a. More data for the Src42a mutant group would increase the robustness of this experiment - which further suggests a physical interaction between Pez and Src42a in hemocytes.

Using our fluorescent Pez constructs we were also able to investigate Pez dynamics following wounding. We were able to show an increase in the number of Pez puncta following laser ablation that is Draper dependent, with more data required to draw conclusions in the case of the loss of Src42a. We have also demonstrated dynamic Draper-eGFP puncta following wounding, which we were unable to conclusively colocalise to sites of Pez trafficking by sequential imaging. There is currently no evidence for interaction between Pez and Draper and their respective orthologues. As part of this work, Draper pull-down from Pez-sfGFP was attempted from whole adult flies but was unsuccessful. It may be beneficial to repeat this experiment in the minimal system of transformed S2 cells, which are 'hemocyte derived'[79], to achieve a cell-type specific interaction.

Here we present increasing evidence for interaction between Pez and Src42a in *Drosophila* – which we draw rationale from the known binding of the mammalian orthologues of both proteins[206–208]. Having visualised Pez and Draper dynamics in hemocytes via fluorophore tagging, it may be beneficial to investigate Src42a localisation by similar means. As shown here for Pez, this would provide novel information on the localisation of Src42a in motile, living cells.

4.10.5 Alternative proposed models for the involvement of Pez in hemocyte inflammatory signalling

Taking together evidence presented here for the requirement of the FERM domain of Pez in wound recruitment, the genetic interaction between Pez and Src42a/Draper and the mislocalisation of Pez in the absence of the signalling axis we conclude that Pez is playing a physical role in inflammatory signalling within hemocytes. We specifically attribute the mislocalisation of Pez in the absence of Src42a and Draper to Pez being rendered non-functional in these hypoinflammatory cells. As the FERM domain of the Pez orthologue has been shown to bind to Src[207] as well as KIF1C[240,241] and actin[207] we propose two distinct models for the mechanism of Pez involvement in the Draper inflammatory signalling axis.

Our first hypothesis assumes Pez is binding to cortical actin via its FERM domain (Figure 4.10.1). We suggest this explains the diffuse localisation throughout the cell body and lamellipodium – which is actin rich[51] – and reason that the dynamic Pez-sfGFP puncta we observe may be Pez flowing back to the cell body mediated by retrograde actin flow[244]. In this model, Pez is bound at the cortex under resting state. Following activation by H_2O_2, the conformation of Src42a is altered (reviewed in[245]) and we speculate that this, along with phosphorylation of Pez promotes Pez-Src42a complex formation at the cortex. This brings activated Src42a into the vicinity of Draper's ITAM domain to allow for phosphorylation. Thus, when Pez is absent Src42a can still phosphorylate Draper, but this is less efficient - leading to a lack of directionality in responding hemocytes and a subsequent reduction in numbers recruited to sites of damage.

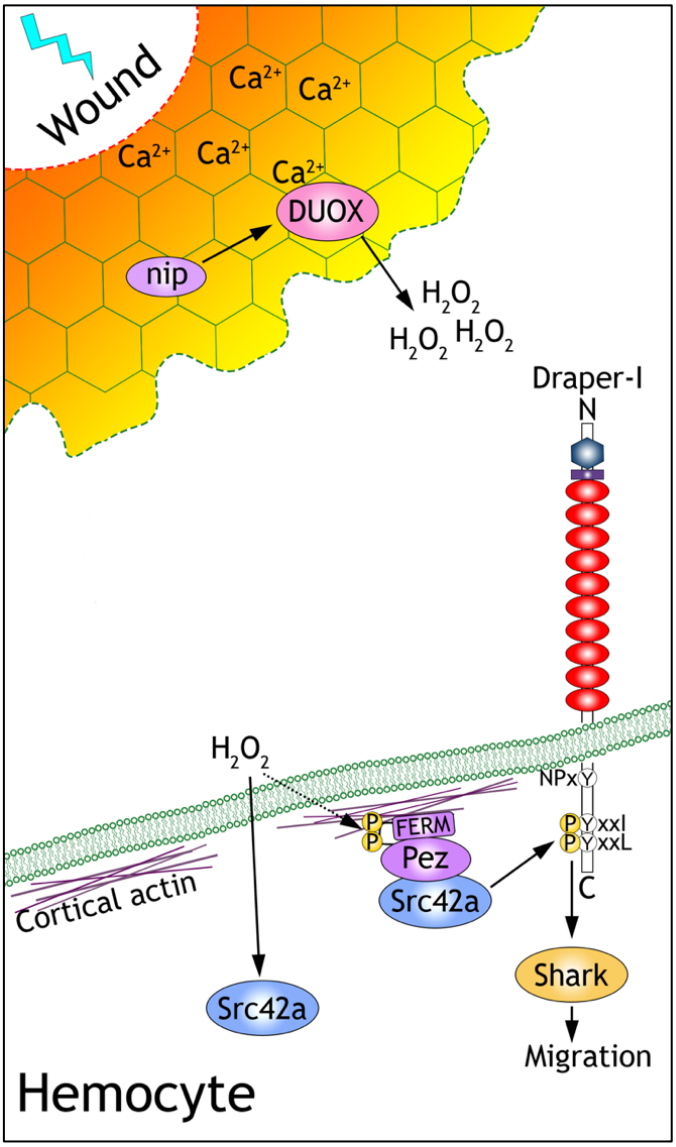

Figure 4.10.5 A: Actin binding model of Pez involvement in Src42a signalling.

Following activation of Src42a downstream of H_2O_2 and the indirect downstream phosphorylation of Pez, Pez captures Src42a at the plasma membrane via its N-terminal FERM domain. This brings Src42a into the vicinity of Draper's ITAM domain to increase phosphorylation efficiency.

For our second model we propose Pez is removing active Src42a from the leading edge via unc-104 (KIF1C), to allow for temporal control over Draper signalling. Here we assume the Pez-sfGFP puncta seen under basal conditions are active Pez transport by KIF1C, and that this transport is increased following wounding – perhaps wound-induced phosphorylated Pez is a better activator of KIF1C transport[240]. In this model, Pez and Src42a associate following wounding, thus Pez transports Src42a away from the leading-edge following phosphorylation of Draper. As Draper puncta have also been observed following wounding, it is possible that activated Draper could also be removed by an unc-104/Pez/Src42a trafficking complex. By doing this, Pez may help control the spatiotemporal activation of downstream Draper signalling.

We suggest that sustained and uncontrolled peripheral activation of Draper would render a cell hyperactivated and unable to transduce further signals or integrate the initial H_2O_2 signal into a meaningful directional output in migration. We believe this can explain why there is no wound recruitment defect seen at the earlier 20 minute timepoint in *Pez* mutants – as cells closest to the wound chemotax before becoming confused. We suggest the phenotype seen at the 40 and 60 minute timepoints and directionality defect in Pez mutants is therefore reflective of cells activated for a wound, but unable to correctly integrate the information following hyperactivation. The generation of a phosphomimetic Draper construct that could be expressed into the *Draper*$^{\Delta 5}$ mutant background would allow for this hypothesis to be tested.

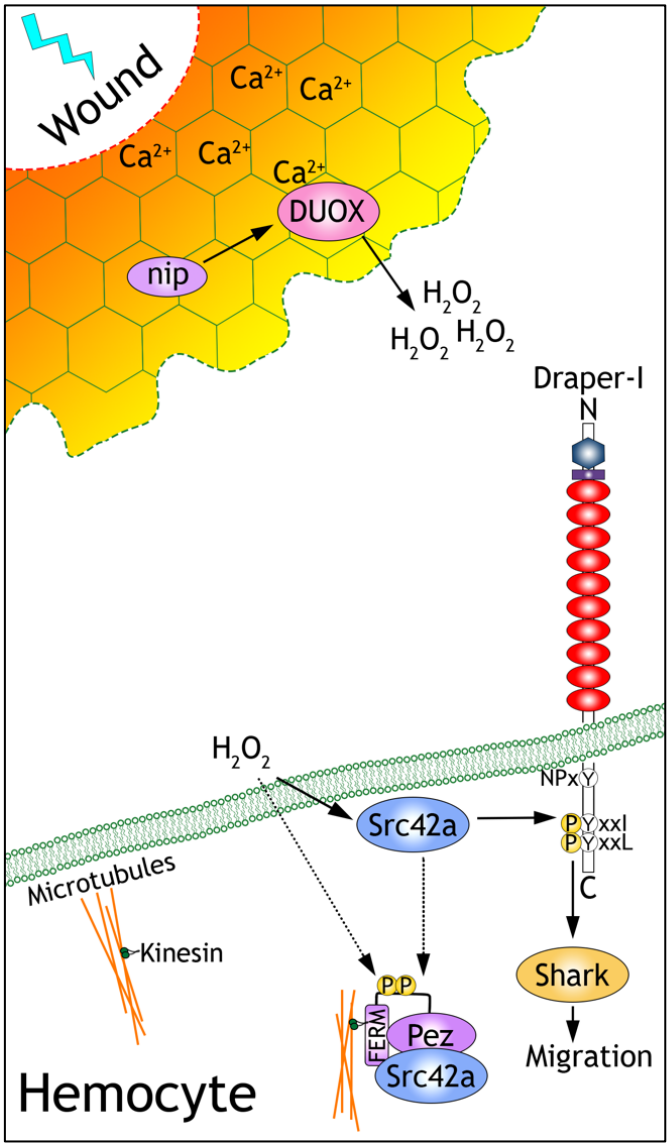

Figure 4.10.5 B: unc-104 (kinesin) binding model of Pez involvement in Src42a signalling.

Following indirect phosphorylation of Pez downstream of H_2O_2 and Src42a, Pez associates with both unc-104 and activated Src42a to remove activated kinase to control signal propagation.

4.10.6 Conclusion

We have identified a novel role for the protein Pez in hemocyte wound recruitment. Pez appears to contribute to polarised cell migration following wounding and participates in the H_2O_2/Src42a signalling axis. Further work is needed to elucidate mechanism, in particular the notion that Pez directly binds to Src42a must be confirmed.

Chapter 5: Investigating Draper and Pez orthologues in neutrophil and macrophage recruitment to tail fin wounds in *Danio rerio*

5.1 Introduction

The freshwater fish *Danio rerio* (zebrafish) is an excellent vertebrate model organism for the study of dynamic processes *in vivo*. Unlike mammalian systems, zebrafish have the distinct advantages of being small in size and easy to maintain – with a rapid generation time. Furthermore, the transparent larval stage of the zebrafish lifecycle also makes it amenable to imaging.

In the context of visualising inflammation, functional granulocytes were first identified at the site of tissue damage in 2001[121]. Following the expansion of the zebrafish genetic toolkit, it became possible to live image leukocyte wound responses[128]. Since then, zebrafish have proved a powerful model for dissecting the complex signalling surrounding involved in damage sensing[102,129,131,134,246,247] - with major work directly showing conserved mechanisms to *Drosophila* hemocyte wound recruitment[102,131]. We therefore sought to demonstrate further parallels in inflammation between these two distinct model organisms.

5.1.1 The zebrafish immune system

During the rapid development of the zebrafish embryo, hematopoiesis begins at 12 hours post fertilisation (hpf) where myeloid progenitors arise from the anterior lateral plate mesoderm[117]. Following this, functional macrophage and neutrophils have been identified at 48 hpf[118,121]. As a vertebrate, zebrafish also possess an adaptive immune system – with fish B cells expressing immunoglobulin (Ig) proteins and T cells harbouring T cell receptor equivalents[123]. However, functional adaptive lymphocytes are not fully developed until at least 3 weeks post fertilisation[124,125,127]. Therefore,

like *Drosophila*, the early zebrafish larva provides an innate immune specific model for the study of inflammation.

5.1.2 Tail fin transection elicits an inflammatory wound response

Advances in innate immune responses to tissue damage in both the fly and fish have been intricately linked – with discoveries in either model informing and corroborating findings both between these organisms and throughout evolution. Early work in the zebrafish wounding field established larval tail fin transection as a model for wound-induced inflammation[121,128]. This method causes the robust recruitment of both neutrophils and macrophages to the site of damage – with neutrophil numbers peaking at 6 hours post injury (hpi), and macrophage numbers continuing to remain high until at least 48 hpi[138].

As seen in *Drosophila*[91], an initial wave of calcium emanates out from the site of damage in clipped 2 dpf zebrafish embryos[129]. Following this, hydrogen peroxide (H_2O_2) is rapidly produced by DUOX enzymes, and is the earliest signal known to mediate innate immune cell recruitment in both organisms[100,131]. In zebrafish neutrophils, H_2O_2 oxidises and activates the Src family kinase member Lyn which permits chemotaxis to the damage site[102]. DUOX induced H_2O_2 also mediates macrophage recruitment to tail fin wounds[133], however in this cell type the H_2O_2 signal is transduced by a second SFK named Yes-related kinase (Yrk)[133] despite Lyn also being expressed in zebrafish macrophages[102].

The function of Lyn in zebrafish neutrophils is directly conserved by the *Drosophila* orthologue Src42a. In hemocytes, Src42a phosphorylates the cell death receptor Draper which ultimately results in the activation of the immune cell and its migration to the wound site[73] (discussed in Chapter 3). An analogous role has not been identified for the Draper orthologue MEGF10 in zebrafish wound recruitment.

5.1.3 The Draper orthologue - MEGF10

Like Draper[177], vertebrate MEGF10 is a direct orthologue of the CED-1 phagocytic receptor - the only engulfment receptor gene described in the nematode *C. elegans*[190,248]. All 3 receptors share several features including multiple extracellular EGF repeats, which vary in number, and an intracellular NPxY motif (Figure 5.1.3A) which is known to facilitate the internalisation of transmembrane receptors[249].

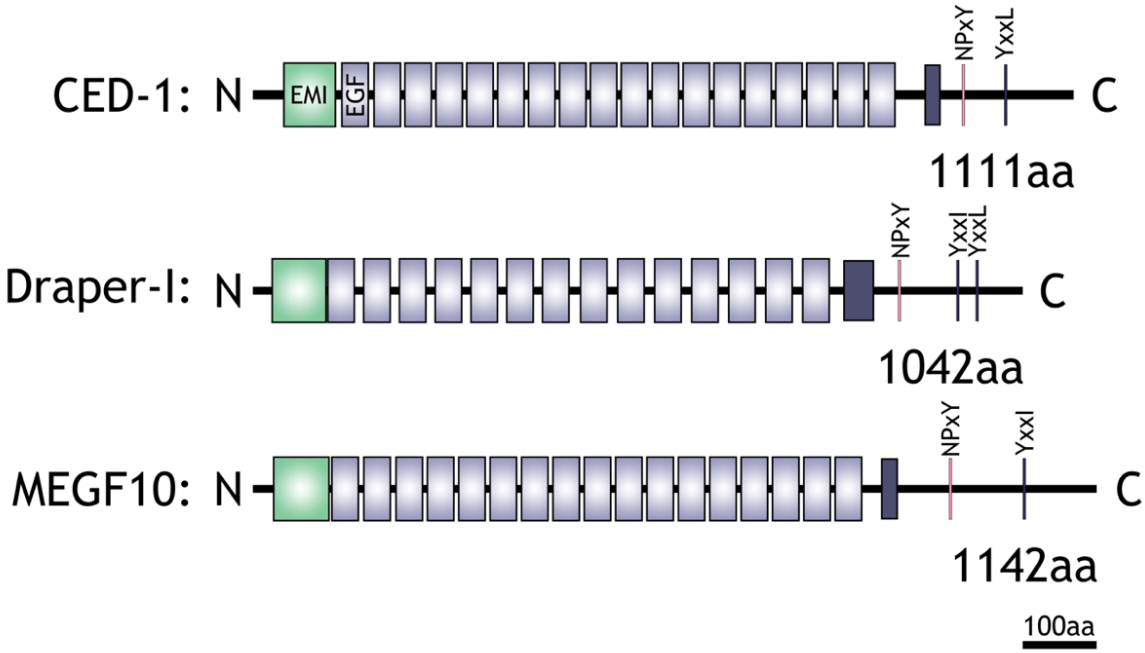

Figure 5.1.3A: Domain organisation of C. elegans CED-1, Drosophila melanogaster Draper-I and Danio rerio MEGF10.

All proteins contain an N terminal EMI domain (green rectangle), followed by a number of EGF-like repeats (light purple rectangles). Following the transmembrane domain (dark purple rectangle), all proteins have a conserved NPxY sequence. There is then loose conservation of YxxI/L motifs at the C terminus of the receptor family.

Crucial to Draper's role in mediating hemocyte inflammation in the fly is the presence of an intracellular immunoreceptor tyrosine-based activation motif (ITAM) domain[73], which, when phosphorylated by Src42a[80,82], transduces the inflammatory signal via the Syk family member Shark kinase. This sequence - YxxI followed shortly by YxxL - is only partially conserved between both Draper and CED-1 and Draper and MEGF10. However, the conserved YxxI found in zebrafish MEGF10 is shortly followed by YxxM (Figure 5.1.3B). Together, these short sequences conform to a non-canonical ITAM domain sequence ($YxxIx_{14}YxxM$)[250]. This module is fully conserved between zebrafish

and human MEGF10 - which retains the ability to bind to human Syk[251]. It is therefore possible that MEGF10 can function to relay the H_2O_2 inflammatory signal in an SFK-ITAM-Syk dependent manner.

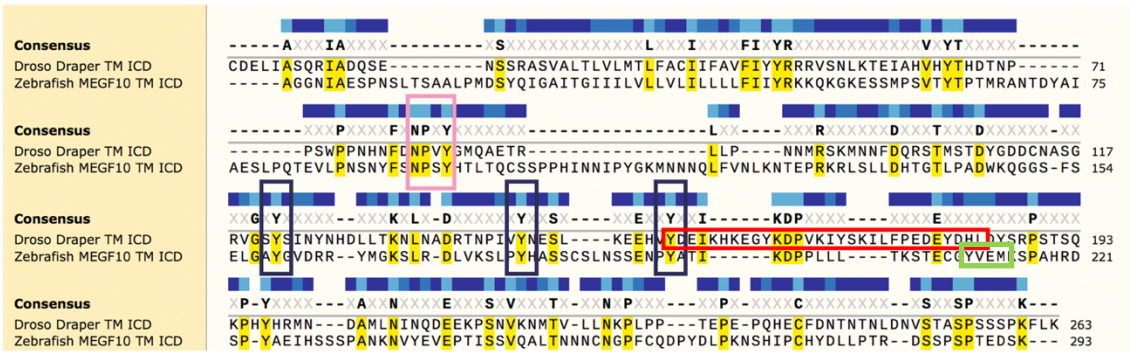

Figure 5.1.3B: Sequence alignment of the intracellular domain of *Drosophila melanogaster* Draper and zebrafish MEGF10.

Sequences were aligned using Clustal Omega as part of Snapgene to visualise the transmembrane and intracellular domains (TM ICD) of Draper and MEGF10. This indicated the conservation of the NPxY motif (pink box), as well as several key tyrosine phosphosites (dark boxes) described for Draper[80] – including the initial Y of the ITAM domain (denoted by the red box). The YxxM of the non-canonical ITAM found in MEGF10 is outlined in green. The consensus sequence is displayed, as well as coloured blocks denoting complete conservation (light blue), amino acid structural similarity (medium blue) and divergence (dark blue).

Zebrafish MEGF10 was first investigated in 2012[190], following the identification of myopathy, areflexia, respiratory distress and dysphagia (EMARDD) causative mutations in the extracellular EGF-like domains in humans. MEGF10 morphant fish were shown to have defects in muscle tissue, along with decreased motility and a reduced lifespan. This was recently corroborated by the generation of a germline mutant colony[252]. A role for Draper in the control of motor function and muscle morphology has also been described in the fly[253], with Draper homozygous mutants also dying earlier than heterozygous animals. In both the fly and the fish, the drug sertraline was able to ameliorate muscle defects and improve lifespan of mutant animals[252]. These studies indicate a conserved role for Draper/MEGF10 in myopathy, with the drug screen results indicating a conserved mechanism of action. Thus far, myopathy is the only confirmed phenotype of MEGF10 disruption in zebrafish.

Further literature on MEGF10 functions exists outside of the fish. MEGF10 transformed HeLa cells display novel phagocytic ability, and, analogous to *Draper* transformed S2 cells, are able to engulf apoptotic cell corpses[80,248]. In the developing mouse brain, MEGF10 expression has been visualised in both glial cell precursors and immature Schwann cells[254]; with more recent work demonstrating expression in astrocytes in postnatal mice[255]. In the brain, MEGF10 removes neuronal cell corpses and prunes synapses by directly mediating efferocytosis. Like MEGF10, Draper is also found expressed in the CNS at several stages in the fly lifecycle where it plays a critical role in apoptotic neuron uptake[177] and synapse pruning[256,257], as well as debris uptake following neuronal injury[81]. The phagocytic function of these CED-1 orthologues is therefore robustly conserved between species of increasing complexity.

5.1.4 Chapter aims

Due to the wealth of literature demonstrating conservation of function between Draper and MEGF10, and the presence of a non-canonical ITAM domain in zebrafish MEGF10 we reason that the function of immune cell recruitment to damage sites may also be conserved. The aims of this chapter are:

1. To establish a model of tail-fin transection inflammation.
2. To investigate whether MEGF10 plays a role in neutrophil and macrophage recruitment to tail-fin wounds.
3. To investigate whether the novel role of Pez in hemocyte wound recruitment (Chapter 4) is conserved by the orthologue PTPN21.

Results

5.2 A model to study tail-fin inflammation in zebrafish

As this zebrafish model is new to the Wood lab, we first sought to characterise wound recruitment in control animals – both to validate the model in comparison to previous work, and to outline quantification parameters. The recruitment of both neutrophils and macrophage to zebrafish tailfin wounds has been previously characterised over a period of 2 days post injury (dpi)[138]. We sought to recapitulate this data up to 22 hpi for our use.

To investigate wound inflammation, *Tg(Lysc:DsRed)*[189] fish – in which DsRed is expressed in neutrophils - were bred according to Home Office guidelines (outlined in Materials and Methods 2.5.2). Embryos were reared to 72 hpf, when all animals had hatched and are considered larva following mouth protrusion[108]. Tailfin transection was performed using a scalpel following the addition of anaesthetic to the embryo medium. A transection site between the end of the caudal vasculature and the trunk mass was selected for consistency in amputation length (Figure 5.2.1 dotted lines). Prior to transection, most leukocytes exist within the CHT – with a limited number found outside of the trunk in the tail fin.

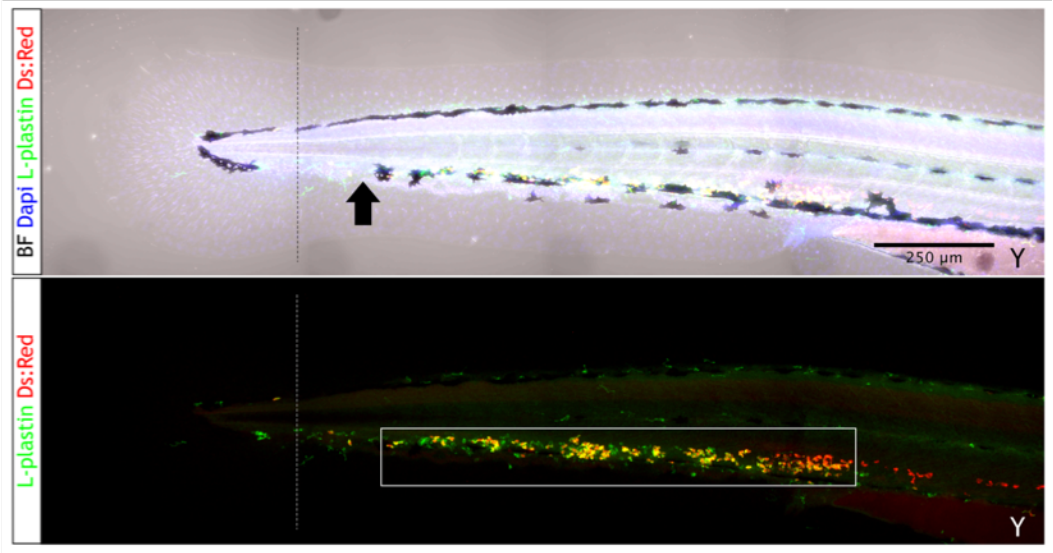

Figure 5.2.1: Representative image of zebrafish tail at 3 dpf.

Images show Tg(Lysc:DsRed) fish stained with L-plastin (488) and Dapi (upper panel only). The end of the caudal vasculature is approximately marked by the arrow. Transection site denoted by dashed lines in both images. L-plastin positive macrophage. Lysc:DsRed/L-plastin double positive neutrophils. CHT marked by white box, Y denotes the end of the yolk extension. Scale bar 250µm.

This transection site removed the entire distal portion of caudal fin and a small amount of trunk tip. Fish were then fixed and stained at a range of timepoints to investigate accumulation of macrophages and neutrophils at the wound site. The DsRed transgenic fluorophore allowed for visualisation of larval neutrophils[258], and fish were co-stained with the pan-leukocyte marker lymphocyte cytosolic protein 1 (L-plastin – antibody generated by Yi Feng)[118,187]. Thus, in these transgenic stained fish double positive cells represent neutrophils, and single positive cells are macrophages for quantification.

An area of approximately 350 μm proximal to the transection site was imaged by confocal microscopy, and the arbitrary distance of 150 μm from the wound margin was selected for quantification of neutrophilic inflammation via the distinct DsRed fluorophore. In this region, we saw a peak in neutrophil recruitment at 6hpi as described previously[138]. There were also significantly more neutrophils at the wound site at 22 hpi in comparison to 2 hpi (Figure 5.2.1). The amount of pan-leukocyte staining with L-plastin in overlapping cells at the wound margin, along with the less-distinct morphology of macrophages made it difficult to accurately count macrophage numbers in the *Tg(Lysc:DsRed)* animals. Therefore, a second transgenic was employed to investigate macrophage responses to tailfin wounds.

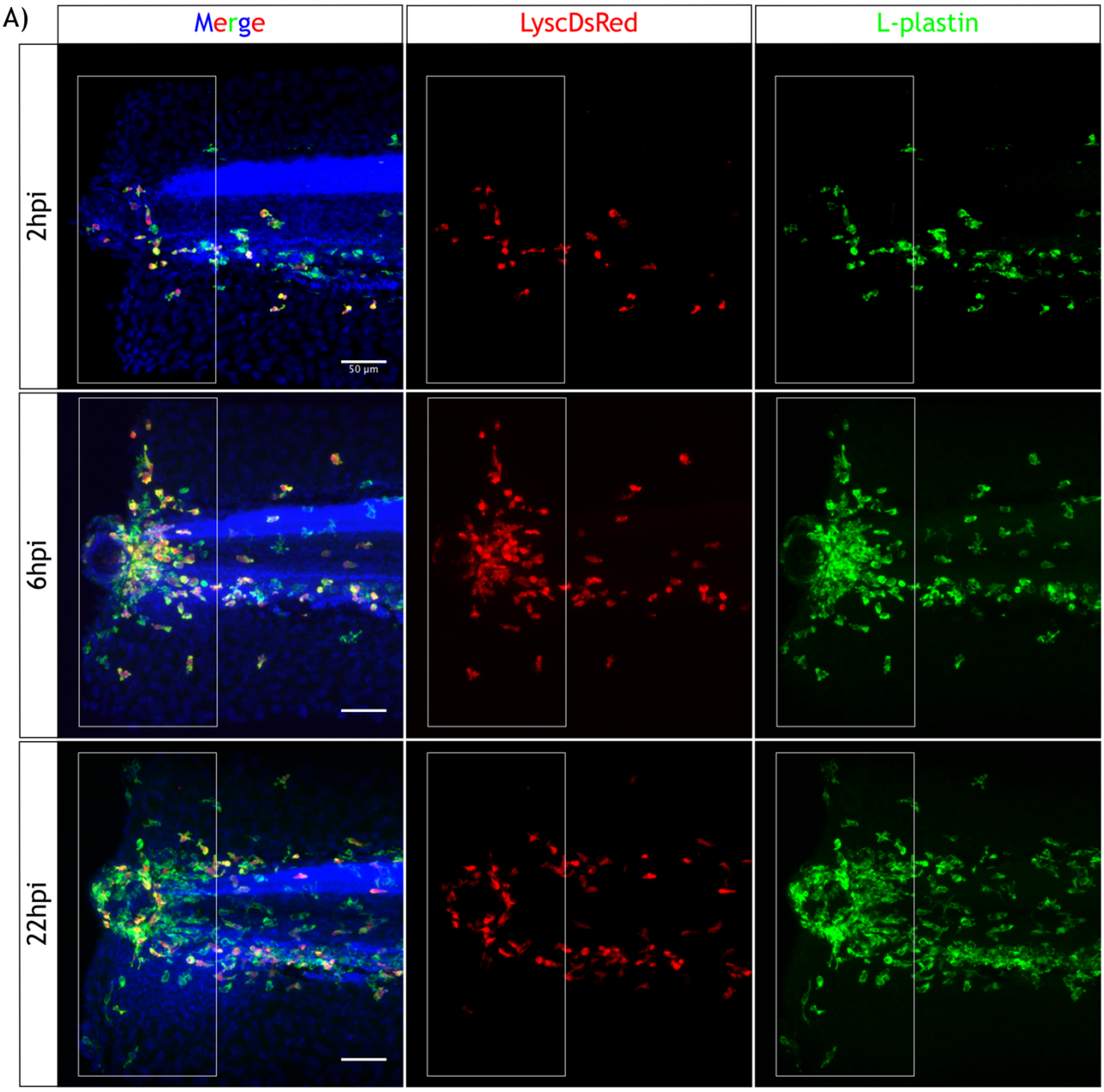
A)
Merge
LyscDsRed
L-plastin
2hpi
6hpi
22hpi
50 µm

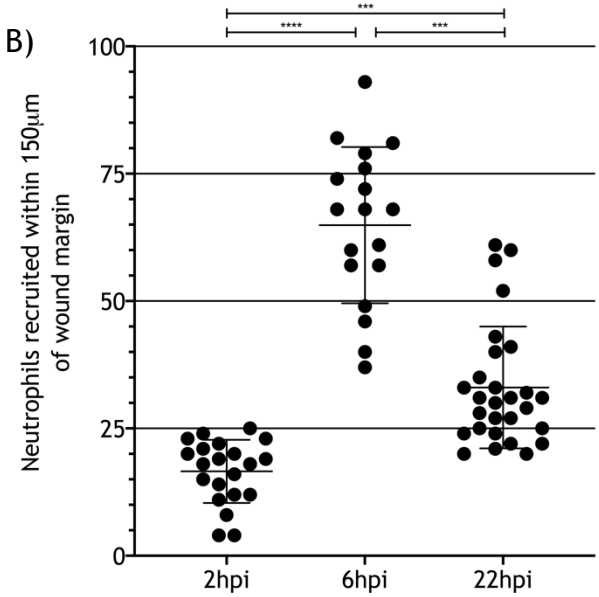
B)
Neutrophils recruited within 150µm of wound margin
100
75
50
25
0
2hpi
6hpi
22hpi
***
****
***

Figure 5.2.2: Neutrophil numbers at tail fin wounds peak at 6 hours post injury.

A) Representative images taken at 2hrs post injury (hpi), 6hpi and 22hpi of wounded *Lysc:DsRed* larvae stained with Dapi and L-plastin (secondary: AF488). Scale bar at 50μm. Quantification zone of 150μm proximal to the wound margin marked by the white box. B) Quantification of neutrophil numbers recruited within 150μm of the wound margin using DsRed. There is a significant increase in the number of neutrophils recruited at 6hpi in comparison to 2hpi. Neutrophil numbers also remain significantly higher at 22hpi compared to 2hpi; however, numbers have significantly reduced from the 6hr timepoint indicating a 6hpi peak. Individual data points plotted along with mean and standard deviation. 2hpi: n=21 larvae, 6hpi n=18, 22hpi n=28, significance tested by ANOVA Kruskal-Wallis test with multiple comparisons due to 22hpi data not being normally distributed.

The Feng lab recently generated the transgenic line *Tg(Mpeg-NLS-mScarlet)* (Dr Nik Ogrykzo, unpublished, map in Appendix 9). As the colony size of this line was small, both in-crossed fish as well as males outcrossed to wild-type *Wt(Tue)* females were used to generate sufficient n numbers. Following tail fin transection, these fish were stained for L-plastin to allow for quantification of recruited L-plastin positive macrophages via the presence of mScarlet positive nuclei. In-crossed and out-crossed fish showed no difference in recruitment and are thus grouped together. This approach revealed an increase in macrophage numbers over the entire time course investigated (Figure 5.2.3).

As the *Tg(Lysc:DsRed)* and *Tg(Mpeg-NLS-mScarlet)* lines are able to faithfully recapitulate previously published data on tailfin inflammation[138] we have therefore validated them for use in our experimental setting to investigate MEGF10 (Draper) and PTPN21 (Pez).

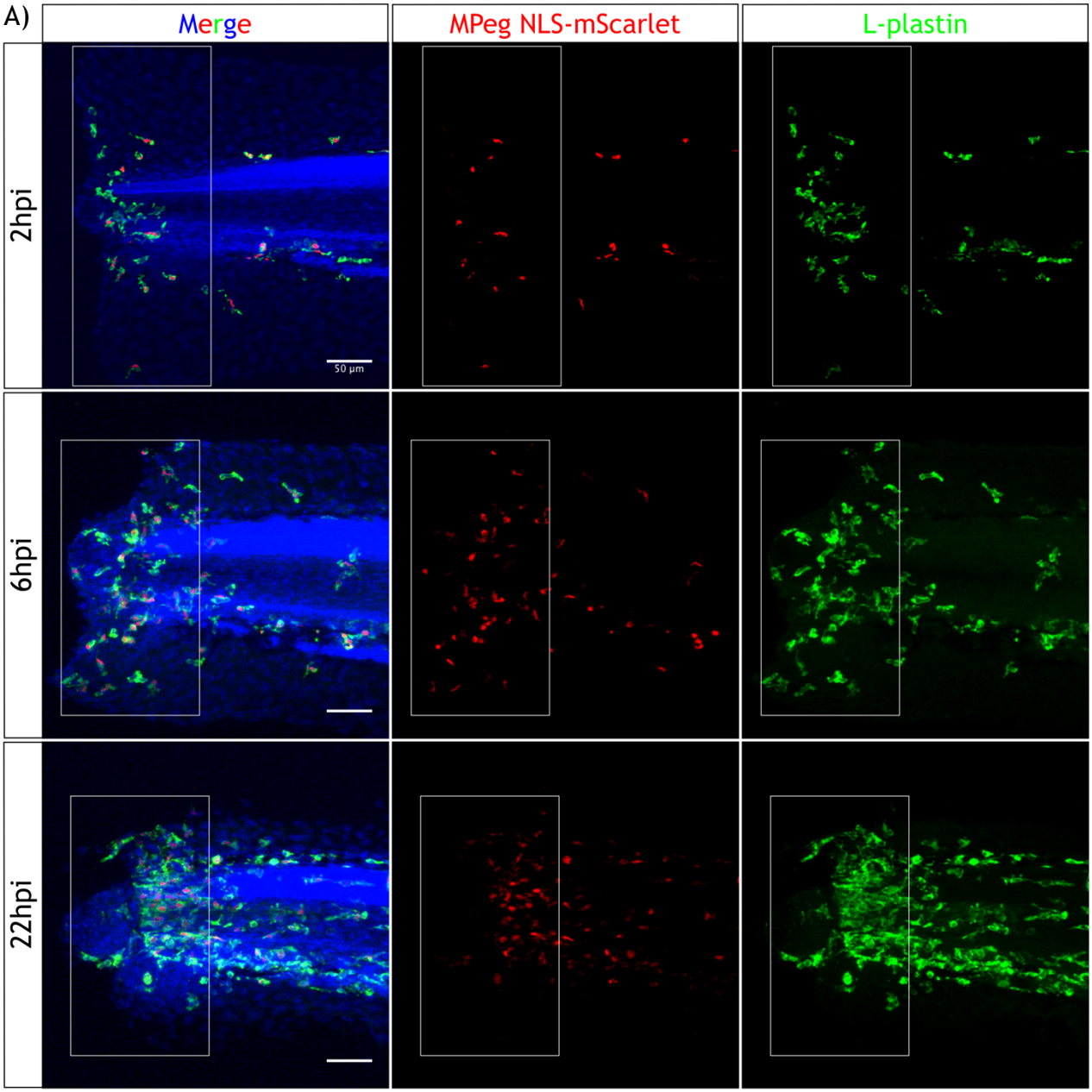
A)
Merge
MPeg NLS-mScarlet
L-plastin
2hpi
6hpi
22hpi
50 µm
B)
Macrophage recruited within 150µm of wound margin
75
50
25
0
****
****
**
2hpi
6hpi
22hpi

Figure 5.2.3: Macrophage numbers at tail fin wounds increase over 22 hours post injury.

A) Representative images taken at 2hrs post injury (hpi), 6 hpi and 22 hpi of wounded *Mpeg-NLS-mScarlet* larvae stained with Dapi and L-plastin (secondary: AF488). Scale bar at 50 μm. Quantification zone of 150 μm proximal to the wound margin marked by the white box. B) Quantification of macrophage numbers recruited within 150μm of the wound margin using nuclear mScarlet. There is a significant increase in the number of macrophages recruited at both 6 hpi and 22 hpi in comparison to 2hpi. Individual data points plotted along with mean and standard deviation. 2 hpi: n=13 larvae, 6 hpi n=20, 22 hpi n=29, significance tested by Brown-Forsythe and Welch ANOVA test with multiple comparisons due to differing SD.

5.3 MEGF10 morphant fish show a reduced inflammatory response following tailfin transection

Previous work on MEGF10 function in zebrafish generated 4 custom morpholinos for disruption of the MEGF10 transcript[190]. Although the use of morpholinos to draw solid conclusions is controversial[259], it provides a rapid, previously validated method for splice disruption of MEGF10 with which an initial screen may be conducted.

Of the morpholinos generated by Boyden et al, morpholinos MO1 and MO3 were chosen due to the high percentage of abnormal phenotype reported relative to toxicity. Synthesised morpholinos were injected into the yolk sac of embryos up to the 4 cell stage at a concentration of 6 ng and 12 ng respectively. Although previous use of MO3 at this higher concentration was shown to have little effect on survival of morphant fish, in our transgenics this proved almost totally lethal. Upon reduction of MO3 dose to 6 ng per injection, survival rates were still exceptionally low. Thus, the use of MO3 for MEGF10 disruption was omitted in this work. To validate splice disruption of MEGF10 occurred following injection, RNA was extracted from 50 3 dpf larva from control (COMO) and MO1 injection groups. Following the generation of cDNA by reverse transcription, PCR of the intron-exon boundary was performed. This positively revealed splice disruption of MEGF10 as described previously (Appendix 10).

MO1 morphant fish were raised to 3 dpf and underwent tail fin transection and antibody staining. For experimentally-matched comparison, clutchmates were also injected with a control morpholino (COMO – commercially available). A significance decrease in neutrophil numbers at wounds at all timepoints was observed in morphant fish in comparison to control. There was also a significant reduction in macrophage numbers at 22 hpi (Figure 5.3.1). Together, these data suggest a role for the Draper orthologue MEGF10 in inflammation in zebrafish.

Neutrophils:

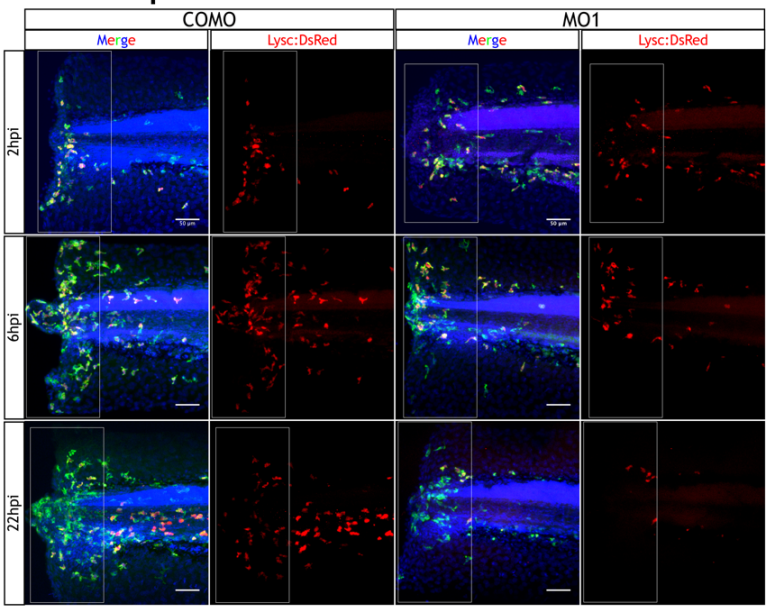

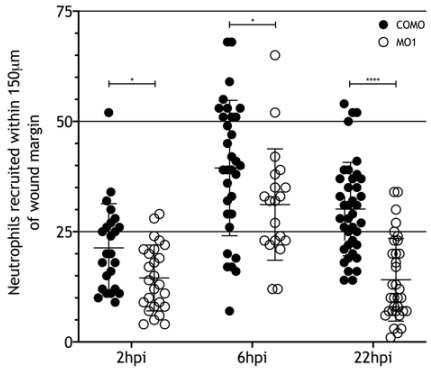

Macrophages:

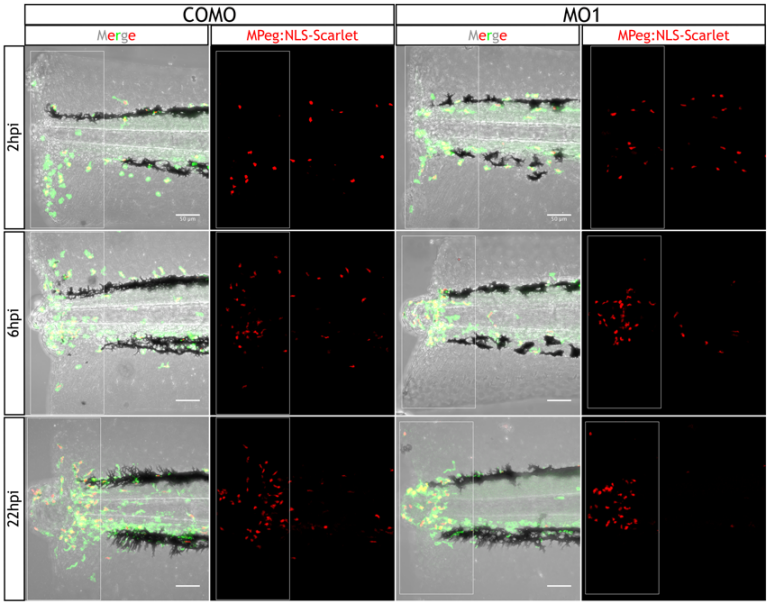

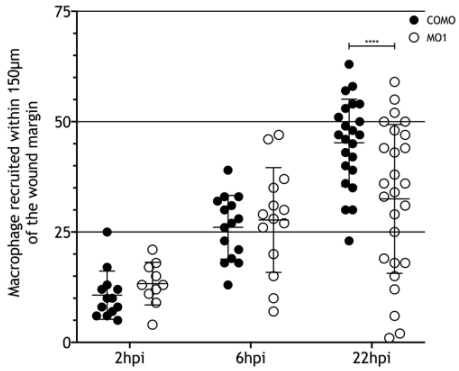

Figure 5.3.1: Disruption of MEGF10 by morpholino injection causes a decrease in the number of neutrophils and macrophage recruited to tail fin wounds.

A) Representative images of control (COMO) and morpholino (MO1) wounded Lysc:DsRed larvae taken at 2 hrs post injury (hpi), 6 hpi and 2 2hpi. Stained with Dapi and L-plastin (secondary: AF488). Scale bar at 50 μm. Quantification zone of 150 μm proximal to the wound margin marked by the white box. There is a significant reduction in the number of neutrophils recruited at all timepoints in MO1 injected fish in comparison to COMO. Individual data points plotted along with mean and standard deviation. COMO: 2 hpi: n=18 larvae, 6 hpi n=32, 22 hpi n=39. MO1: 2 hpi: 26, 6 hpi: n=20, 22 hpi n=33. Significance tested by multiple t-test. B) Representative images of COMO and MO1 wounded Mpeg-NLS-mScarlet larvae stained with L-plastin (secondary: AF488). Brightfield (BF) channel used due to absence of Dapi staining in this experiment. Scale bar at 50 μm. Quantification zone of 150μm proximal to the wound margin marked by the white box. Quantification of macrophage numbers recruited within 150 μm of the wound margin using nuclear mScarlet. There is a significant reduction in the number of macrophage recruited at 22hpi in MO1 morphants in comparison to COMO. Individual data points plotted along with mean and standard deviation. COMO: 2 hpi: n=13 larvae, 6 hpi n=15, 22 hpi n=23. MO1: 2 hpi: 10, 6 hpi: n=14, 22 hpi n=26. Significance tested by multiple t-test.

5.4 Generation of MEGF10 CRISPant zebrafish larvae

We sought to confirm our findings in morphant fish by generating transient mutants using CRISPR-Cas9 gene editing technology. Since its identification in *Streptococcus pyogenes* immunity[169], the CRISPR-Cas9 system has been developed to allow for gene editing[260–263]. Following target sequence recognition and DNA cleavage upstream of the Cas9 cut site (known as the PAM site), DNA repair is carried out by non-homologous end joining. This generates an indel mutation upstream of the PAM site which disrupts the gene. Mutant generation by CRISPR-Cas9 was first used in the fish in 2013[264,265] and its efficiency has been reported to be as high as 86%. Crucially, unlike morpholino disruption, CRISPR gene editing shows little off-target effects[266].

We identified target sequences within the MEGF10 sequence which also conformed to BsiYI restriction enzyme digestion sites - which contain the PAM sequence NGG (Figure 5.4.1). In doing so, we identified indel sites which could be validated by enzyme restriction following PCR of the target locus. If indel at the restriction site was successful, the products of successfully gene-edited fish would be resistant to digestion. We synthesised two distinct CRISPR guide sequences (gRNA) as far upstream of the MEGF10 gene as possible to allow for maximal disruption of the protein. These were injected together into zebrafish embryos at the one-cell stage. Unlike morpholino injections, the single cell was the injection target as opposed to the yolk sac. DNA from ten 3 dpf larvae was extracted and PCR on the CRISPR loci was performed. This indicated the successful generation of mutant fish using this method (Figure 5.4.2).

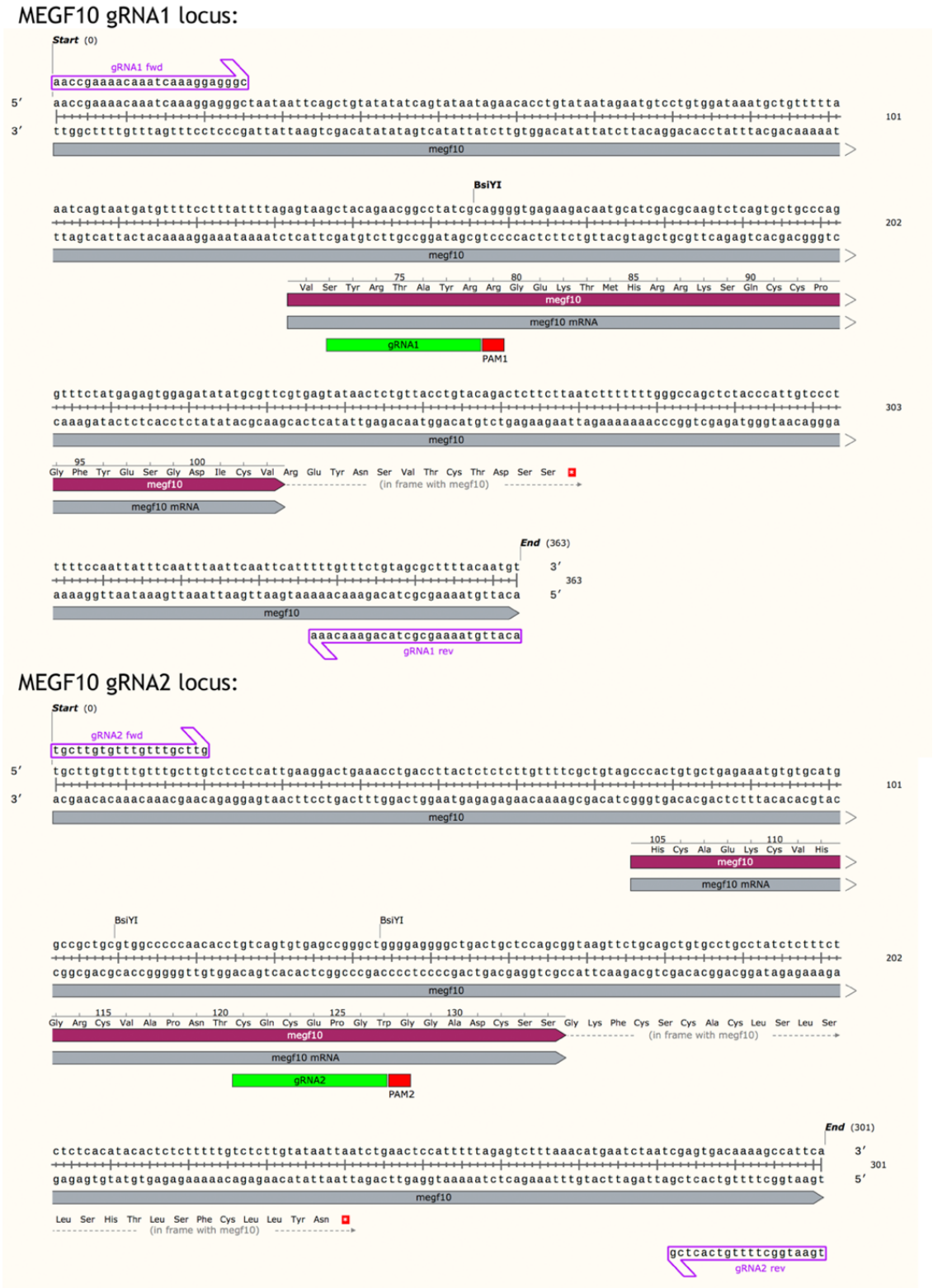

Figure 5.4.1: Schematic to show CRISPR-Cas9 target sites in MEGF10 locus.

CRISPR Guide RNAs (gRNA) shown in green, with PAM site in red. Restriction sites noted, one exists in the gRNA1 locus, and two at the gRNA2 locus. In the absence of digestion, gRNA1 primers will generate a fragment at 363bp; gRNA2 primers will generate 108bp and 193bp fragments if the second BSiYI site is disrupted by indel.

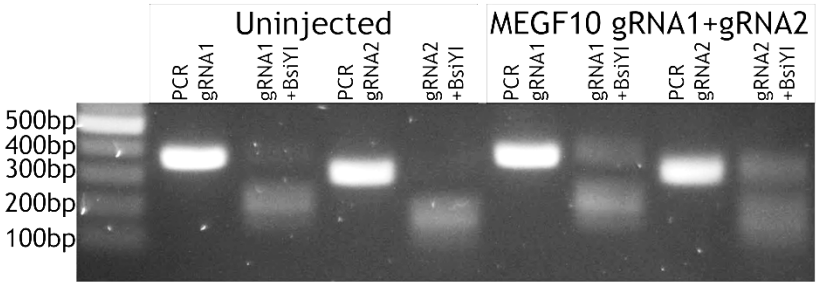

Figure 5.4.2: PCR and restriction digestion of MEGF10 target loci.

DNA was extracted from uninjected fish as well as CRISPR fish and PCR was performed on the locus to show uncut fragment length. PCR products were then digested with BSiYI enzyme. The presence of a band at the same size as the PCR uncut products indicates the disruption of the restriction site following CRISPR-Cas9 targeting.

5.5 MEGF10 CRISPant larvae show a reduction in neutrophil and macrophage numbers at tailfin wounds

Having validated the use of two separate CRISPR guide RNAs for MEGF10 gene disruption, we conducted the tailfin transection assay and investigated wound inflammation. For matched controls, embryos were injected at the single cell stage using the injection mixture without Cas9 enzyme. This approach corroborated our finding in morphant fish, as all timepoints showed less neutrophilic influx in CRISPant fish in comparison to guide injected control animals. (Figure 5.5.1).

Due to the small colony size and time limitations CRISPR data for macrophage numbers were compared to uninjected fish. Without an injection-matched control, this experiment represents preliminary data. However, we are able to justify the use of uninjected control fish as, in the absence of Cas9, guide-only injected fish show no difference in neutrophilic inflammation (Appendix 11). In comparing CRISPant fish to uninjected controls, a reduction in macrophage numbers is seen at 22 hpi which validates our morphant finding (Figure 5.3.2). A decrease in macrophage numbers at 6 hpi was also seen in CRISPant fish, indicating a more severe phenotype than in morpholino knockdown of MEGF10 (Figure 5.5.1). To confirm this data, n numbers must be increased, and data must be compared to injection-matched controls.

Neutrophils:

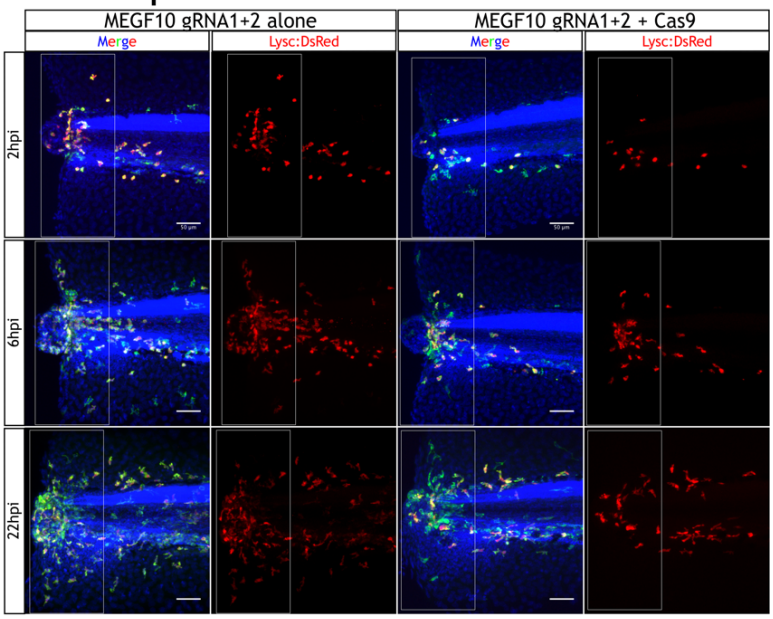

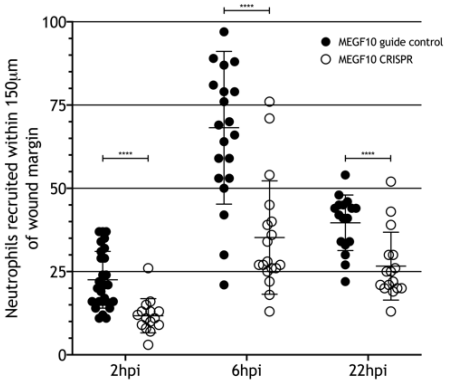

Macrophages:

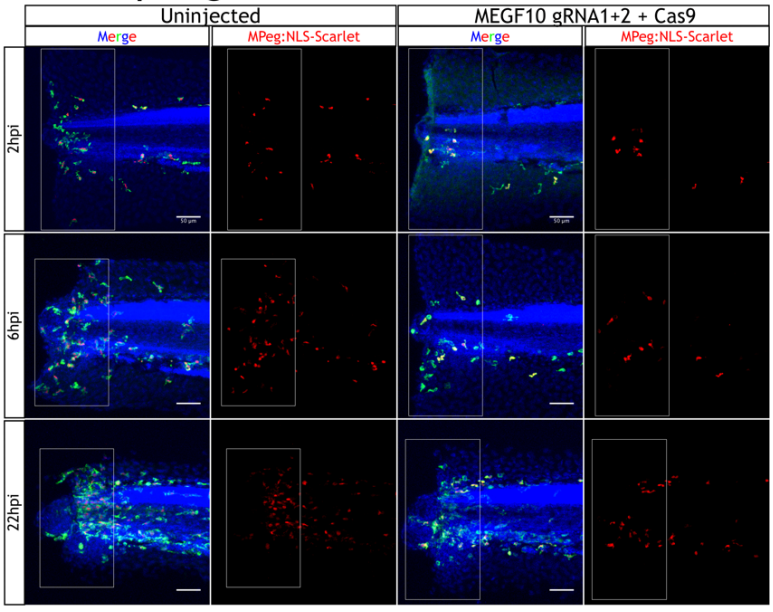

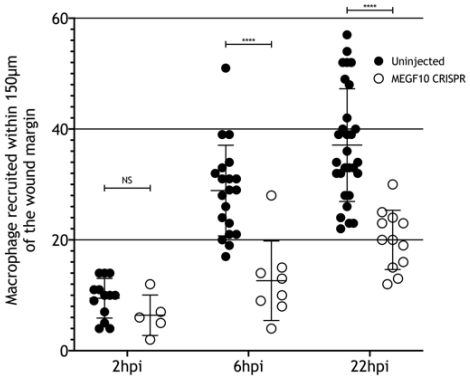

Figure 5.5.1: MEGF10 CRISPant larvae show a reduction of neutrophils and macrophage recruited to tailfin wounds.

A) Representative images of control guide RNA only injected and guides injected alongside Cas9 (MEGF10 + gRNA1+2 + Cas9) wounded Lysc:DsRed larvae taken at 2 hrs post injury (hpi), 6 hpi and 22 hpi. Stained with Dapi and L-plastin (secondary: AF488). Scale bar at 50μm. Quantification zone of 150 μm proximal to the wound margin marked by the white box. There is a significant reduction in the number of neutrophils recruited at all timepoints in CRISPant fish in comparison to control. Individual data points plotted along with mean and standard deviation. MEGF10 guide control: 2 hpi: n=28 larvae, 6 hpi n=21, 22 hpi n=17. MEGF10 CRISPR: 2 hpi: n=15, 6 hpi: n=18, 22 hpi n=16. Significance tested by multiple t-test. B) Representative images of uninjected and MEGF10 CRISPR (MEGF10 + gRNA1+2 + Cas9) wounded *Tg(Mpeg-NLS-Scarlet)* larvae taken at 2 hrs post injury (hpi), 6 hpi and 22 hpi. Stained with Dapi and L-plastin (secondary: AF488). Scale bar at 50 μm. Quantification zone of 150 μm proximal to the wound margin marked by the white box. There is a significant reduction in the number of macrophages recruited at 6 hpi and 22 hpi in CRISPant fish in comparison to uninjected. Individual data points plotted along with mean and standard deviation. Uninjected control: 2 hpi: n=28 larvae, 6 hpi n=21, 22 hpi n=17. MEGF10 CRISPR: 2 hpi: n=13, 6 hpi: n=20, 22 hpi n=29. Significance tested by multiple t-test.

5.6 Generation of PTPN21 CRISPant larvae

Previous work in this thesis has investigated the role of novel players in damage-induced inflammation. Having identified a role for Pez in hemocyte recruitment to epithelial wounds in the fly embryo (Chapter 4), we wanted to investigate whether this role was conserved by the fish orthologue PTPN21 (previously named pez/ptpn14).

PTPN21 was first investigated in the fish in 2007[267] where it was shown to regulate TGFβ expression and epithelial-mesenchymal transition; with PTPN21 morphant fish displaying defects in organogenesis. In this work, PTPN21 was not investigated after 48 hpf, however an expression profile exists up to 72 hpf in a separate study[268] where images are insufficient to conclude expression in leukocytes within the CHT. There is no further published work on PTPN21 in the fish. Due to time limitation and cost, we chose to generate CRISPR larvae for a preliminary screen into a possible role of PTPN21 in zebrafish inflammation.

As described for MEGF10, we chose CRISPR targets within restriction enzyme sites. As BSiYI sites were limited early in the *PTPN21* locus we made use of a second restriction enzyme – MwoI – which also cuts at PAM sites (Figure 5.6.1).

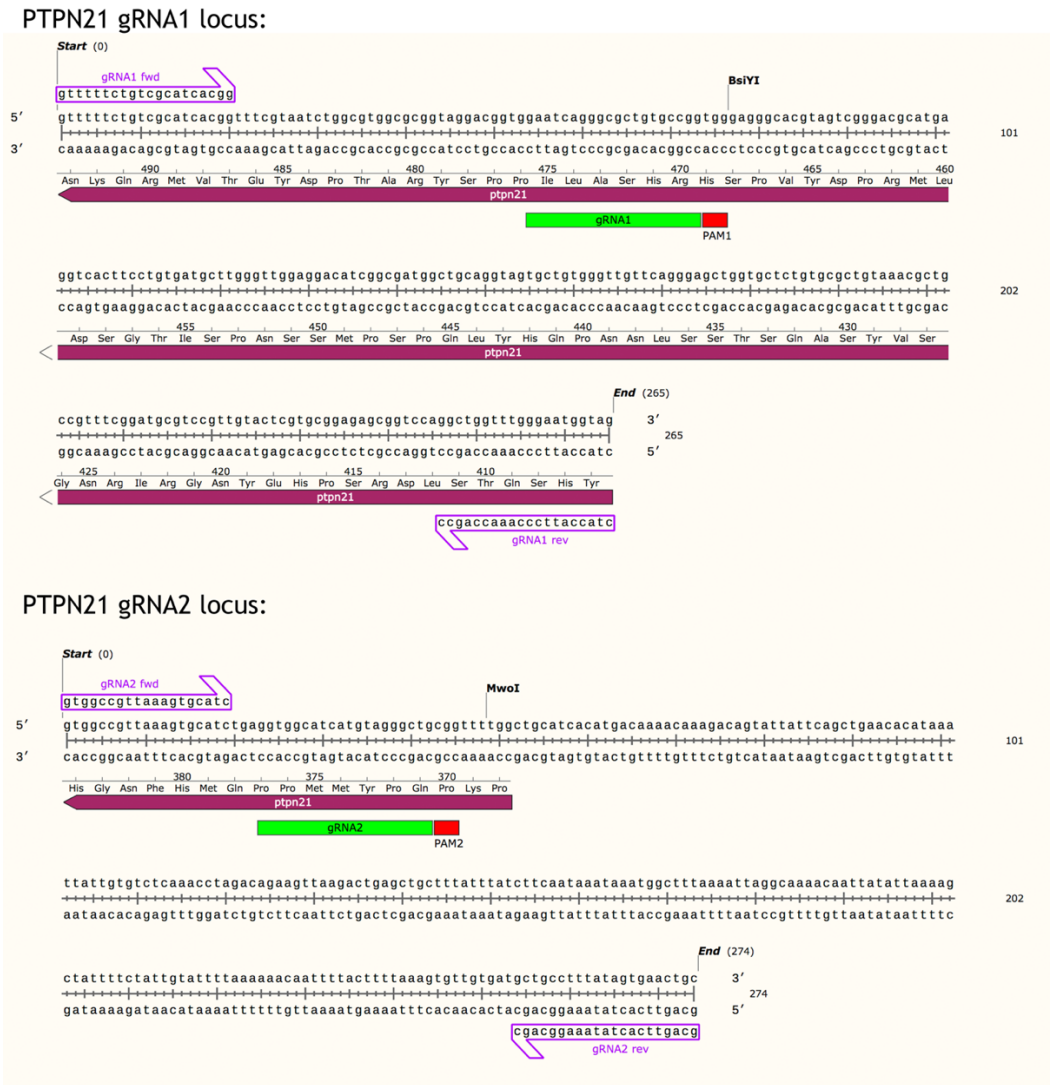

Figure 5.6.1: Schematic to show CRISPR-Cas9 target sites in PTPN21 locus.

CRISPR Guide RNAs (gRNA) shown in green, with PAM site in red. Restriction sites noted, BSiYI in the gRNA1 locus, and MwoI in the gRNA2 locus. In the absence of digestion, gRNA1 primers will generate a fragment at 265 bp; gRNA2 primers will generate 274 bp fragments if the MwoI site is disrupted by indel.

Indels were confirmed in 3 dpf larvae following the injection of the guide target RNAs, tracrRNA and Cas9 into embryos by restriction site disruption (Figure 5.6.2).

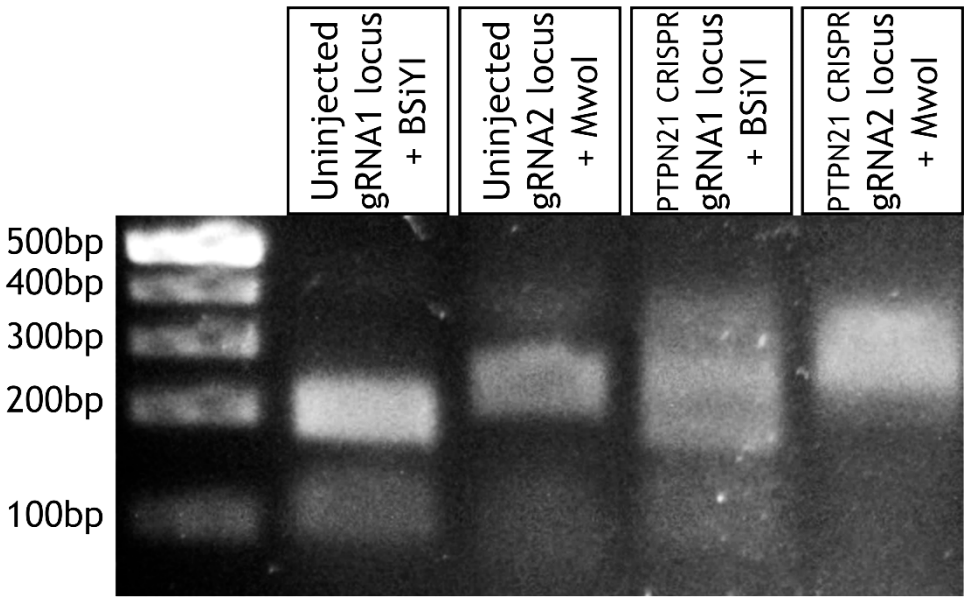

Figure 5.6.2: PCR and restriction digestion of PTPN21 target loci.
The upward shift of the banding in the PTPN21 CRISPR lanes is indicative of disruption of the restriction sites.

5.7 PTPN21 CRISPant larvae show reduced inflammation at tailfin wounds

Inflammation was investigated in *Tg(Lysc:DsRed)* and *Tg(Mpeg-NLS-mScarlet)* PTPN21 CRISPant fish as outlined previously. In comparison to injection-matched controls, there is a significant reduction in the number of neutrophils recruited to tailfin wounds at the 6 hour timepoint (Figure 5.7.1). This suggests that although a neutrophil response is mounted, it is less robust in these CRISPant fish. We also observed a reduction in macrophage numbers at the wound margin at 6 hpi and 22 hpi in comparison to control uninjected fish. This provides solid evidence for a conserved role of PTPN21 in zebrafish inflammation that warrants further investigation.

Neutrophils:

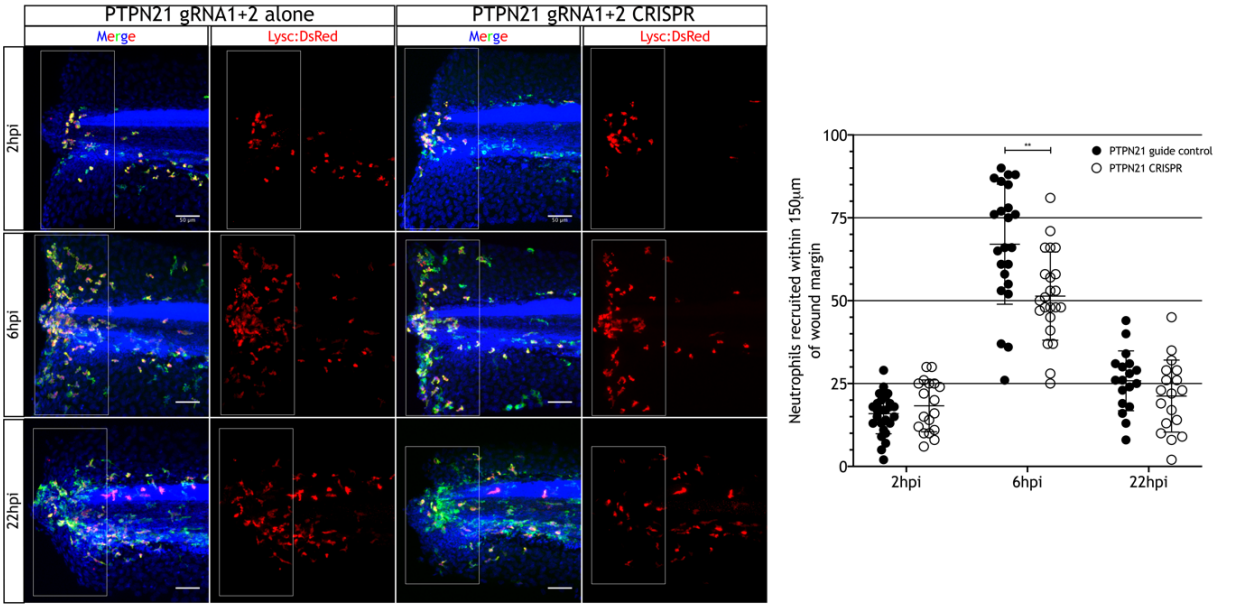

Macrophages:

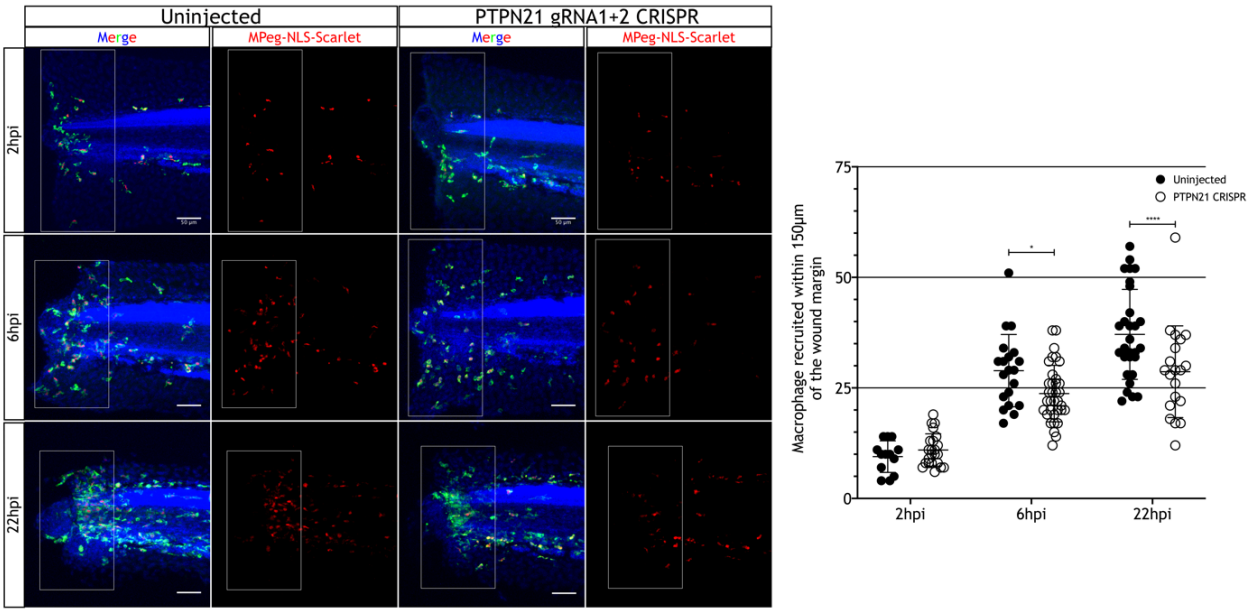

Figure 5.7.1: Peak neutrophilic influx to tailfin wounds is reduced in PTPN21 CRISPant fish.

A) Representative images of control guide RNA only injected and guides injected alongside Cas9 (PTPN21 + gRNA1+2 + Cas9) wounded Lysc:DsRed larvae taken at 2 hrs post injury (hpi), 6 hpi and 22 hpi. Stained with Dapi and L-plastin (secondary: AF488). Scale bar at 50 μm. Quantification zone of 150 μm proximal to the wound margin marked by the white box. There is a significant reduction in the number of neutrophils recruited at 6 hpi in CRISPant fish in comparison to control. Individual data points plotted along with mean and standard deviation. PTPN21 guide control: 2 hpi: n=27 larvae, 6 hpi n=23, 22 hpi n=18. PTPN21 CRISPR: 2 hpi: n=18, 6 hpi: n=23, 22 hpi n=18. Significance tested by multiple t-test. B) Representative images of uninjected and PTPN21 CRISPR (PTPN21 + gRNA1+2 + Cas9) wounded *Tg(Mpeg-NLS-Scarlet)* larvae taken at 2 hrs post injury (hpi), 6 hpi and 22 hpi. Stained with Dapi and L-plastin (secondary: AF488). Scale bar at 50 μm. Quantification zone of 150 μm proximal to the wound margin marked by the white box. There is a significant reduction in the number of macrophages recruited at 6 hpi and 22 hpi in CRISPant fish in comparison to uninjected. Individual data points plotted along with mean and standard deviation. Uninjected control: 2 hpi: n=28 larvae, 6 hpi n=21, 22 hpi n=17. PTPN21 CRISPR: 2 hpi: n=23, 6 hpi: n=35, 22 hpi n=20. Significance tested by multiple t-test.

5.8 Discussion

5.8.1 Rationale

The roles of damage induced H_2O_2 production and subsequent Src family kinase (SFK) activation are crucial to the recruitment of immune cells to sites of tissue damage in both the fly[73,91,100] and the fish[102,129,187]. In *Drosophila* hemocytes, the activated SFK Src42a phosphorylates the damage receptor Draper on its intracellular immunoreceptor tyrosine-based activation motif (ITAM) which permits chemotaxis to epithelial wounds. This occurs via the recruitment of a second kinase Shark – a member of the spleen tyrosine kinase (Syk) family. Whilst a role for the direct orthologue of Src42a – named Lyn – has been characterised in the fish[102], it is not known how the inflammatory H_2O_2 signal is subsequently relayed. Draper and its vertebrate orthologue MEGF10[190,252,254,255] share approximately 42% sequence identity. The ITAM domain found in MEGF10 is non-canonical but has been shown to be a phosphotarget of c-Src[269] and retains the ability to bind to Syk (data from human MEGF10[251]). We therefore hypothesised that MEGF10 may transmit the H_2O_2 signal to recruit immune cells in an SFK-ITAM-Syk dependent manner.

5.8.2 The use of two distinct transgenic zebrafish lines to quantify inflammation

Through collaboration with Dr Yi Feng (University of Edinburgh) we sought to establish zebrafish tailfin transection as a model for wound-induced inflammation to investigate the potential conserved role of MEGF10. Initially, inflammation was characterised in the transgenic *Tg(Lysc:DsRed)*. Although first described as labelling a subset of macrophage as well as granulocytes[189], later work conclusively demonstrated that transgenics under the control of the *Lysc* promoter exclusively mark neutrophils from 48 hpf onwards[258]. Using this line, we hoped to characterise both neutrophil and macrophage accumulation at the wound margin by combining the expression of DsRed with staining for the pan-leukocyte marker L-plastin. Whilst it was possible to accurately quantify neutrophil numbers using this method, macrophage quantification through identification of L-plastin$^+$ *Lysc:DsRed*$^-$

cells proved difficult due to the extent of L-plastin expressing leukocytes in the vicinity of the wound. A second transgenic was therefore employed to improve the reliability of macrophage quantification at tailfin wounds.

The *Tg(Mpeg-NLS-mScarlet)* line was generated previously by the Feng lab and is as yet unpublished. The promoter of Macrophage expressed gene 1 (*mpeg1*) was first used to drive transgene expression in the macrophage lineage in zebrafish in 2011[139]. This new transgenic places a short nuclear localisation sequence (NLS) downstream of the *Mpeg* promoter, followed subsequently by a codon optimised mScarlet-I sequence[270]. The distinct red fluorescent nuclei in this line allowed for accurate counting of macrophages within 150 μm of the transection site. Combined use of this new transgenic line with *Tg(Lysc:DsRed)* following tailfin transection recapitulated published work demonstrating neutrophilic influx peaks at 6 hours post injury (hpi)[138]. For experimental convenience a maximum time period post injury of 22 hpi was chosen. Between 2 hpi, 6 hpi and 22 hpi we showed an increase in macrophages recruited in control animals as described previously[138], thus we have validated the use of this unpublished transgenic to investigate macrophage function. Therefore using both the *Tg(Lysc:DsRed)* and *Tg(Mpeg-NLS-mScarlet)* in tailfin transection assays we have established a zebrafish inflammation model for subsequent use in the Wood lab.

5.8.3 MEGF10 morphant and transient CRISPR mutant fish show reduced inflammation at tailfin transection sites

Similar to the loss of calcium-induced DUOX in the *Drosophila* epithelium[100], global morpholino disruption of zebrafish DUOX dramatically reduces leukocyte recruitment to injury sites[131]. In the fish this inflammatory signal is transduced by the Src family kinases named Yrk in macrophage and Lyn in neutrophils[133]. Following pharmacological SFK inhibition the recruitment of both macrophages and neutrophils to tail fin wounds is reduced by over 50%[131]. This mechanism is entirely conserved by the H_2O_2 activated form of Lyn in *Drosophila* – Src42a[73], with the expression of dominant negative Src42a in the hemocyte lineage reducing wound influx to approximately 50% of control numbers.

Using previously generated morpholinos[190] and novel CRISPR targets we have generated fish in which MEGF10 is disrupted. In morphant animals, neutrophil numbers were reduced by 50-70% at the wound margin across the time course investigated. These results were corroborated by the generation of transient CRISPR mutant larvae – in which the phenotype was more severe across all timepoints. Thus, the loss of MEGF10 in zebrafish affects neutrophilic inflammation to same extent as Draper loss in the fly[73]. As peak recruitment numbers are severely impacted, and not merely delayed, we speculate that MEGF10 promotes the activation of neutrophils downstream of Lyn in an analogous axis to Draper (Figure 5.7).

As transgenic generation in *Drosophila* can be rapidly achieved, the exciting question of whether zebrafish MEGF10 can rescue the Draper mutant phenotype may be investigated. A similar approach utilising mouse MEGF10 has revealed a similar rate of Aβ-42 plaque removal by either UAS-Draper or UAS-MEGF10 expressing glia in a *Drosophila* model of Alzheimer's disease[271].

Here we also present data to demonstrate the involvement of MEGF10 in macrophage wound recruitment up to 22 hpi. It has previously been shown that although macrophages also respond to ROS[133] over this time period their recruitment is delayed in comparison to neutrophils due to decreased migration speed[138]. By disrupting MEGF10, we have affected macrophage recruitment at the later timepoints of 22 hpi in morphants and both 6 hpi and 22 hpi in CRISPants. However, as macrophage numbers continue to increase past 48 hpi[138] we cannot conclude whether we have decreased or delayed peak recruitment. To conclusively demonstrate a role for MEGF10 in macrophage activation following tissue damage, macrophage recruitment must be investigated over an extended time course. Time-lapse imaging of macrophage recruitment from 6 hpi through to 22 hpi of MEGF10 deficient fish will also reveal whether migration speed or directionality are affected.

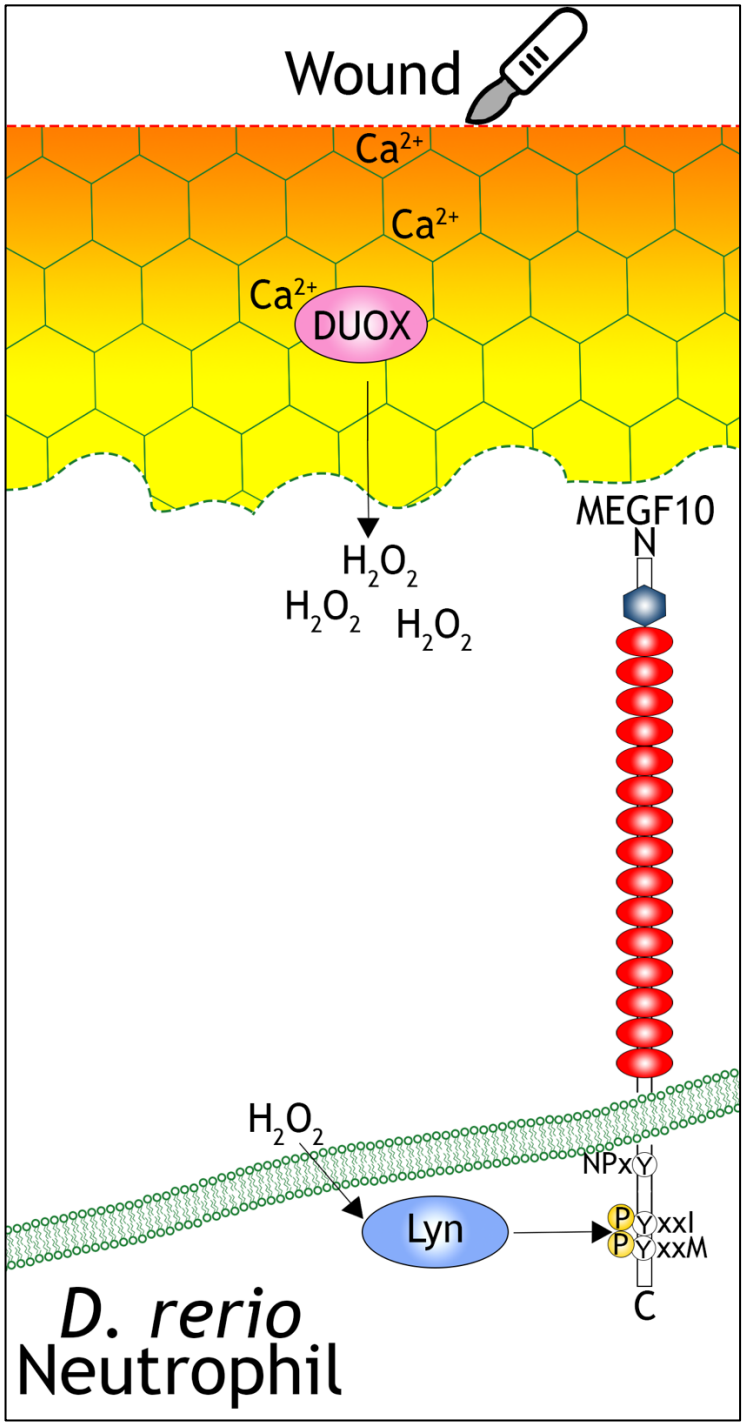

Figure 5.8.3: Proposed model for the mechanism of action of MEGF10 in neutrophil wound recruitment.

Scalpel generated wounds in zebrafish caudal fins leads to an intracellular wave of calcium. DUOX enzymes generated the inflammatory signal H_2O_2, which oxidises and activates the SFK Lyn in neutrophils. We speculate that MEGF10 is a phosphotarget of active Lyn which participates in the transmission of the inflammatory signal. MEGF10 structure shown with extracellular EMI (hexagon) and EGF repeat domains (red ovals). The NPxY sequence and intracellular non-canonical ITAM domain are marked.

5.8.4 Evidence for a conserved role of PTPN21 (Pez) in zebrafish H_2O_2 mediated inflammation

The over-arching aim of this thesis has been to identify novel players in wound-induced inflammation. Following the identification of a hemocyte wound recruitment defect in Pez mutant *Drosophila* embryos (Chapters 3 & 4), we sought to determine whether this function was conserved by the zebrafish orthologue PTPN21.

Previous work on the role of PTPN21 in the developing zebrafish embryo demonstrated a requirement during organogenesis - where PTPN21 directly influences the expression of TGF-β[267]. In this work, researchers generated and validated morpholinos to knockdown PTPN21. Due to cost and off-target effects of morpholino injection[259] we instead chose to generate novel transient CRISPR mutants of PTPN21. Using this approach, we have shown a reduction in peak neutrophil numbers recruited to tailfin wounds in PTPN21 CRISPants. This is reminiscent of the phenotype we observed in *Pez* mutant hemocytes – where numbers are reduced at the wound at the peak time of 60 minutes post ablation, but not at the earlier timepoint of 20 minutes (Chapter 4). PTPN21 gene editing using CRISPR-Cas9 also results in a reduction of macrophages recruited to tailfin wounds at 6 hpi and 22 hpi.

The PTPN21 disruption phenotype identified here is less severe than that observed for MEGF10 in both peak neutrophil recruitment and macrophage influx up to 22 hpi. We have also previously concluded that the loss of Pez in *Drosophila* hemocytes results in a milder phenotype than that observed in Draper and Src42a mutants (Chapter 4 and published[73]). Therefore, these data demonstrate a conserved role for PTPN21 in zebrafish inflammation that warrants further investigation.

5.8.5 The complexity of zebrafish inflammation – where might MEGF10 and PTPN21 fit in?

While further chemotactic signals alongside H_2O_2 mediating hemocyte recruitment in the fly remain enigmatic[104], more is known about the complex nature of neutrophil and macrophage recruitment in zebrafish. Within 1 hour of wounding several cytokines are produced, including IL-1β[134,246]. The expression of *IL-1β* was later shown to be independent from Duox-produced ROS at the damage site, and mediates neutrophil recruitment via a distinct signalling axis[272]. Like the loss of H_2O_2/Lyn signalling, the effect of IL-1β is exerted early following injury – with a hypoinflammatory neutrophil phenotype evident at 2 hpi. In *il-1β* morphants, this phenotype is not sustained from 6 hpi onwards. Further, IL-1β is not involved in macrophage inflammation. Here we have presented evidence for two proteins – MEGF10 and PTPN21 – which affect both macrophage and neutrophil recruitment, and we suggest they play a more overarching role in the ROS-mediated aspect of inflammation.

The first cytokine discovered - IL-8[273] (also known as Cxcl8) - has also been investigated in the context of wound inflammation in the developing fish. Like IL-1β, the expression of two members of the cxcl8 family – *cxcl8-l1* and *cxcl8-l2* – were shown to peak at 1 hpi[246]. Both Cxcl8 morphants show reduced neutrophil recruitment to tailfin wounds in the first 6 hours post injury. Interestingly, the loss of IL-8 family cytokines did not affect the directionality of chemotaxing neutrophils, and their speed was, in fact, significantly increased. This is in direct contrast to H_2O_2[131] and Lyn[102] which both promote more linear migration of neutrophils towards the wound site. It is therefore possible that whilst H_2O_2 signalling activates all neutrophils and macrophages to promote chemotaxis, a distinct subset of neutrophils retain the ability to efficiently respond in the absence of IL-8 cytokines. It would be intriguing to investigate the manner in which neutrophils and macrophages migrate in the absence of MEGF10 and PTPN21 by live imaging and cell tracking. This would reveal whether a subset of cells are affected, or if all leukocytes are not adequately activated following wounding. We

hypothesise that the latter is true as existing literature from *Drosophila*[73] suggests that Draper activates hemocytes to promote efficient chemotaxis following H_2O_2 detection.

5.8.6 The roles of neutrophils and macrophage in repair and regeneration

In the developing *Drosophila* embryo, hemocytes are, in fact, dispensable for reepithelialisation despite their rapid recruitment[89]. Instead, wound repair is dependent upon actin dynamics within the border cells and is accelerated by the presence of an actomyosin 'purse string'[238]. Epithelial cells further back from the wound edge also contribute to wound closure by constricting in their apicobasal axis and thus expanding their lateral area in a non-muscle myosin dependent manner[274]. This promotes the intercalation of cells at the wound edge which are also required for efficient wound closure[275]. Thus, the functional role of hemocytes following wounding is restricted to the phagocytosis of cellular debris and pathogen clearance[89].

Similarly to *Drosophila* epithelial wounds, the cells surrounding tailfin transection sites in zebrafish are seen to contract – a process also thought to involve an actin-purse string[130]. However, unlike hemocytes, zebrafish leukocytes have been shown to actively contribute to repair and regeneration. Neutrophils function as the major clearers of cellular debris following tissue damage[134]. Following this, they undergo apoptosis and are cleared by inflammatory macrophages. This process is important in reducing cytokine production at the wound edge, allowing the resolution stage to begin. In the absence of macrophages, larval neutrophils respond normally to tailfin wounds, but fin regeneration is dramatically slowed. In contrast, the loss of neutrophils improves the growth rate of the regenerating tail. Similarly, in adult fish, the loss of macrophages but not neutrophils impairs caudal fin regeneration[276]. This shows distinct roles for both leukocyte populations in mediating the repair of tissue damage. As we have generated fish with defective inflammatory responses to tailfin wounds, it is likely that the regenerative capacity of these animals is also affected. Since MEGF10 has previously been shown to be amenable to pharmacological manipulation

in the context of myopathy[252] we have perhaps identified a novel target for therapeutic augmentation during tissue healing.

5.8.7 Conclusion

Having generated exciting data which demonstrates conservation of function between of MEGF10 and PTPN21 in zebrafish inflammation several key follow up questions include:

1. Does the loss of MEGF10 delay or attenuate peak macrophage influx to tail fin wounds?
2. Is zebrafish MEGF10 a phospho-target of Lyn/Yrk?
3. Is there a role for Syk kinases in macrophage and neutrophil recruitment to tail fin wounds?
4. Does the loss of MEGF10/PTPN21 impact on fin regeneration?

Further, the expression of both MEGF10 and PTPN21 in zebrafish leukocytes must be confirmed.

Chapter 6: Final discussion

The activation of innate immune cells is crucial for the correct coordinated response to tissue damage. The ability to genetically manipulate and live image both *Drosophila melanogaster* and *Danio rerio* has directly informed our understanding of damage signalling, as well as provided insight into the involvement of innate immune cells in repair. Through developing our knowledge of inflammation in these organisms through the identification of novel regulators, we can outline conserved mechanisms that may offer therapeutic targets in pathologies characterised by chronic or aberrant inflammation.

6.1 The relevance of hemocytes to vertebrate innate immune cells

Whilst the use of mammalian, vertebrate model organisms is important for translational medical research, their use is constrained and subject to the concept of 'reduce, refine and replace' to regulate both procedures and experimental numbers. Therefore, invertebrates represent valuable *in vivo* model systems that can be exploited for fundamental biological research in order to directly inform the viability and importance of mammalian experiments. *Drosophila* hemocytes offer an attractive innate immune cell model for the study of damage responses which show conservation with vertebrate signalling pathways in zebrafish[73,91,100,102,129,131].

Hemocytes share core similarities to mammalian macrophages. Following their differentiation from the head mesoderm, the majority of embryonic hemocytes in *Drosophila* develop into functional plasmatocytes[50]. Like mammalian embryonic macrophage which also derive early in embryogenesis, these cells go on to colonise the entirety of the developing organism. Throughout development hemocytes play important macrophage-like roles - including the removal of apoptotic debris and deposition of extracellular matix[51,277]. In order to carry out their phagocytic function, hemocytes express a plethora of scavenger receptors like their mammalian counterparts. This includes the CD36 orthologue Croquemort (Crq) which

plays a critical role in apoptotic cell clearance[87]. Similarly, mammalian macrophage also utilise CD36 in corpse clearance[278,279]. The rapid, H_2O_2 mediated response of hemocytes to epithelial wounds is perhaps more reminiscent of neutrophils[131,133] which are some of the first inflammatory cells recruited to tissue damage. Although macrophages have also been shown to respond to this damage signal in zebrafish[133].

Ultimately, *Drosophila* hemocytes provide a model for the rapid screening of inflammatory genes *in vivo* in an innate immune cell type which is comparable to mammalian counterparts. In this work, we have demonstrated that the identification of a novel mediator of inflammation using a phosphoproteomics approach – Pez - can subsequently be tested and validated in the zebrafish to identify conservation of function. We have also demonstrated that Draper, the key mediator of hemocyte inflammation[72,73], plays a role in both neutrophil and macrophage wound recruitment in the fish. By strengthening the parallels in these systems, we identify a signalling axis centred around SFK activation and ITAM phosphorylation which warrants further investigation.

6.2 Using laser ablation in the generation of tissue damage

In the developing *Drosophila* embryo, laser ablation by UV light has been extensively used in the generation of epithelial wounds[73,89,91,274] and is the main method of tissue damage used in this thesis. Initial work using this technique demonstrated that low-level UV laser power is sufficient and accurate in the instantaneous ablation of a small number of target cells[90]. However, the destruction of further neighbouring cells was identified through a possible combination of thermal and mechanical forces, as well as weaker exposure to the UV pulse. In order to generate sufficiently sized wounds to induce quantifiable inflammation significantly higher laser power was used in this thesis, which undoubtedly causes excessive further damage to the organism other than the ablation of the ventral epithelium.

Previously, our understanding of the damage at laser wounds was restricted to the lack of cleaved-caspase staining – indicating the generation of necrotic, rather than apoptotic, debris[72]. Recently, work in the lab (by Dr Andrew Davidson) has shown the presence of an immediate necrotic wound core, followed by secondary apoptosis at the wound periphery. This was achieved following the injection of SYTOX Blue DNA dye – which can only intercalate into nucleic acids following plasma membrane permeation in necrotic cells[280] –, and annexin-V - which binds to PS exposed on the surface of apoptotic cells[281,282] (Figure 6.2.1). Thus, the combination of these two dyes is able to differentiate between types of cell death and indicates the complexity of the debris that hemocytes must clear following laser ablation. This type of damage is physiologically relevant to dermal burns which also show large amounts of necrosis[283]. Furthermore, necrotic debris was found to predominate in murine liver injury following ischemia, with lower, transient levels of apoptosis detected[284].

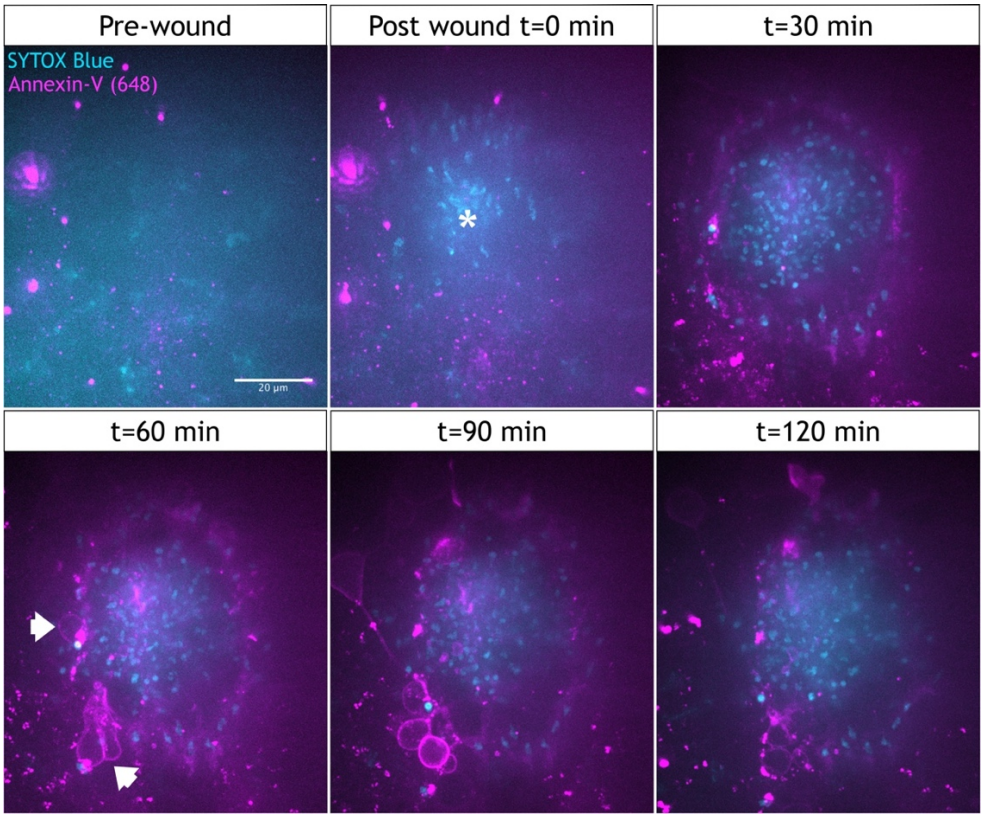

Figure 6.2.1: Injection of SYTOX Blue and Annexin-V (648) into *Drosophila* embryos. Experiment conducted by Dr Andrew Davidson. Prior to ablation there is little SYTOX staining (background fluorescence), and Annexin-V (dense puncta represent debris generated by injection). Immediately following ablation (t=0 min) a dense necrotic core is seen following the intercalation of SYTOX into the DNA. Apoptotic debris does not arise until later (white arrows in 60 min panel). Scale bar at 20 µm.

6.3 What are the consequences further downstream of wounding?

Apoptotic corpses have been shown to prime hemocytes via the upregulation of croquemort[88], as well as Draper[72] - which directly permits subsequent inflammatory responses. This raises the interesting question of whether the necrotic debris generated by ablation is able to perform a similar or parallel function to shape hemocyte identity. Furthermore, although wounds close in the absence of hemocytes[89] consequences of wounding on development and further insult responses are not known. As hemocytes require a refractory period of 90 minutes to respond to a further wound or pathogens[104] and increased levels of cell corpses render hemocytes hypoinflammatory[85] it is likely that the organism is more susceptible to subsequent infections post-ablation.

6.4 The conserved role of MEGF10 in zebrafish wound recruitment

In this work we have implicated a role for the Draper orthologue receptor MEGF10 in zebrafish inflammation following tissue damage. As additional functions between MEGF10 and Draper seem remarkably well conserved[80,177,190,248,252–254,256,257], further interesting parallel questions arise in the context of inflammation. Like Draper, is MEGF10 similarly upregulated by signalling downstream of apoptotic corpse ingestion[72]? Is MEGF10 upregulation also required for pathogen clearance[72]? Does the loss of MEGF10 also lead to defects in vacuole processing[73]? Does a Shark kinase orthologue (Syk/Zap70) lie downstream of MEGF10? These questions undoubtedly warrant investigation through further collaborative research.

In this work, we have generated CRISPR target gRNAs that are capable of inducing indel mutation the MEGF10 gene which may be used to generate a stable germline mutant colony. Alternatively, an established mutant colony has recently been published[252] and may provide a further resource for future projects investigating MEGF10 function in inflammation in zebrafish.

6.5 H_2O_2 signalling and innate immune cell recruitment to cancer

Cancer is the result of hyperproliferative cells with genetic mutations that both dysregulate apoptosis and subvert their normal functions to result in tumour formation that progresses to malignancy and metastasis[285].In the 19th Century tumour associated inflammation was discovered by the abundant presence of leukocytes in surgically removed tumours[286]. Since then, inflammation has been identified as both a risk factor in cancer development[287–289] as well as a driver in cancer by aiding angiogenesis[290] and growth[291,292]. More evidence for the role of inflammation in cancer comes directly from the observation that the repeated use of Aspirin – a non-steroidal anti-inflammatory drug – dramatically reduced gastrointestinal cancer incidence, and further resulted in a significant reduction in other cancer types[293]. Tumour promoting inflammation is thus a hallmark of cancer, and a promising area of intense research for cancer therapies[285].

Studies in the early zebrafish larva have demonstrated the recruitment of innate leukocytes to oncogenic *RAS* transformed pre-neoplastic cell clones[187]. Following time lapse imaging, this was shown to be similar to the manner in which neutrophils and macrophages are recruited to fin wounds, and leukocytes were shown to extensively interact with the transformed cells. Crucially, in the absence of innate immune cells proliferation of cells expressing oncogenic *RAS* was reduced. This indicates a role for leukocytes in the promotion of cancer *in vivo* at the early stage, prior to becoming a mature tumour. Of relevance to this work, H_2O_2 was found to be produced both by the pre-neoplastic cells and their immediate neighbours downstream of DUOX, and was shown to drive leukocyte recruitment analogous to its role in wounding[131]. Thus, modulation of a H_2O_2 mediated signalling axis may provide an attractive target for an early anti-inflammatory cancer therapy.

As seen with zebrafish leukocytes, hemocytes are also recruited to *RAS* transformed pre-neoplastic cells in the antennal imaginal disc - where they are seen to adhere to the tumour mass following the detection of basement membrane breach[294]. A similar is result is also seen in tumorigenic salivary

glands, which show dramatic hemocyte infiltration[295]. At the tumour site hemocytes are seen to perform a similar function to tumour associated neutrophils and macrophages in zebrafish where they directly aid tumour growth[294]. It is an attractive hypothesis that this may also be mediated by H_2O_2 analogous to leukocyte tumours responses in the fish[100]. If true, tumour generation and inflammation in *Drosophila* would thus provide an additional, rapidly screenable model which is not subject to animal licencing for the investigation of cancer-induced inflammation. Of direct relevance to the work presented in this thesis would be the subsequent investigation into the involvement of Src42a/Lyn and Draper/MEGF10 in tumour-associated inflammation.

6.6 Concluding statements

In this thesis I have investigated novel regulators of hemocyte biology and uncovered a cell-autonomous role for the protein Pez in hemocyte wound recruitment. I speculate that Pez is physically involved in the Src42a/Draper signalling axis following the identification of a reduction in wound recruitment in transheterozygotes and a mislocalisation of Pez in the absence of Src42a and Draper. Through collaboration with Dr Yi Feng at the University of Edinburgh, I have identified exciting conserved roles for the orthologues of Draper and Pez (MEGF10 and PTPN21) in leukocyte wound recruitment in zebrafish. Together this work strengthens the parallels in inflammatory signalling between the fly and fish. In conclusion I have identified further conserved members of the H_2O_2/SFK signalling pathway which warrant further investigation.

Appendices

Appendix 1: Fly food recipes

All dispensed into Drosophila Tube PS 25x95mm (Pk500) (SLS, 789008/FLY1310) or bottles: Drosophila polypropylene Flasks 237mL Round Bottom (SLS, 789021/FLY1012). FlyStuff flugs (49-102) and (49-100) respectively (SLS)

Bristol ingredients:

Ingredient	Supplier/code	Amount (per single batch)
Maizeflour	BuyWholeFoodsOnline (SKU90560)	60g
Soyaflour	BuyWholeFoodsOnline (SKU47645)	9g
Yeast, dry	Sigma (51457-2.5kg)	17g
Malt extract	Muntons (80616)	39g
Plant Agar	Oxoid LP0011 (Fisher Scientific, 10351303)	6g
Sugar	Granulated	64g
Nipagin	Nipagin (Sigma Aldrich, H3647-1kg)	1.5g
100% Ethanol	Fischer Scientific (10437341-2.5L)	15mL
Propionic acid	Sigma Aldrich, (81910-1L)	5.3mL in 7.7mL distilled water
Distilled water		1200mL
	Yield = 100 vials	

Food made by hand on benchtop heat plate following standard recipe and dispensed using a Drosofiller (FlyStuff, SLS).

6 months prior to lab relocation to the University of Edinburgh and subsequently onwards, the Iberian food recipe (Cambridge) was adopted due to improved batch consistency.

Edinburgh ingredients – Iberian Food:

Ingredient	Supplier/code	Amount (per 12L batch)
Flour	Bacheldre Watermill Organic Flour unbleached (Amazon)	420g
Yeast, dry	Sigma (51457-2.5kg)	600g
Agar	Oxoid LP0011 (Fisher Scientific, 10351303)	90g
Glucose	D-Glucose (Fischer, G/0500/61)	660g
Nipagin 10%	Nipagin (Sigma Aldrich, H3647-1kg)	30g nipagin in 300mL ethanol
100% Ethanol	Fischer Scientific (10437341-2.5L)	300mL
Propionic acid	Sigma Aldrich, (81910-1L)	48mL
Distilled water		12L

Food made using a JONI 60L (Skanos) kettle and dispensed using a Drosofiller (FlyStuff SLS).

Appendix 2: Apple juice agar recipe

Ingredient	Supplier/code	Amount (1L)
Agar	BD Difco, Appleton Woods (MO386)	20g
Sucrose	Sigma Aldrich (S7903-1kg)	12g
Apple juice	Commercial purchase	250mL
Nipagen	Sigma Aldrich (H3647-1kg)	2g
100% ethanol	Sigma Aldrich (32221-2.5L)	10mL
Distilled water		750L
	Yield = 120 dishes	

Apple juice agar plates were made by dissolving agar in 500mL of distilled water by microwaving prior to the addition of other ingredients. Plates were poured by hand.

Appendix 3: Zebrafish embryo medium

The following ingredients were obtained from Sigma-Aldrich and prepared in the QMRI (University of Edinburgh) zebrafish facility by technician staff.

0.5μM NaCl

0.17μM KCl

0.33μM CaCl

0.33μM $MgSO_4$

0.1% Methylene Blue

In distilled water.

Appendix 4: Visualisation of the wound perimeter by bright-field microscopy.

In order to detect the wound perimeter at 1 hour following laser ablation, images were obtained by brightfield microscopy. Below is representative images of the epithelium both prior to ablation, and at the 1 hour timepoint.

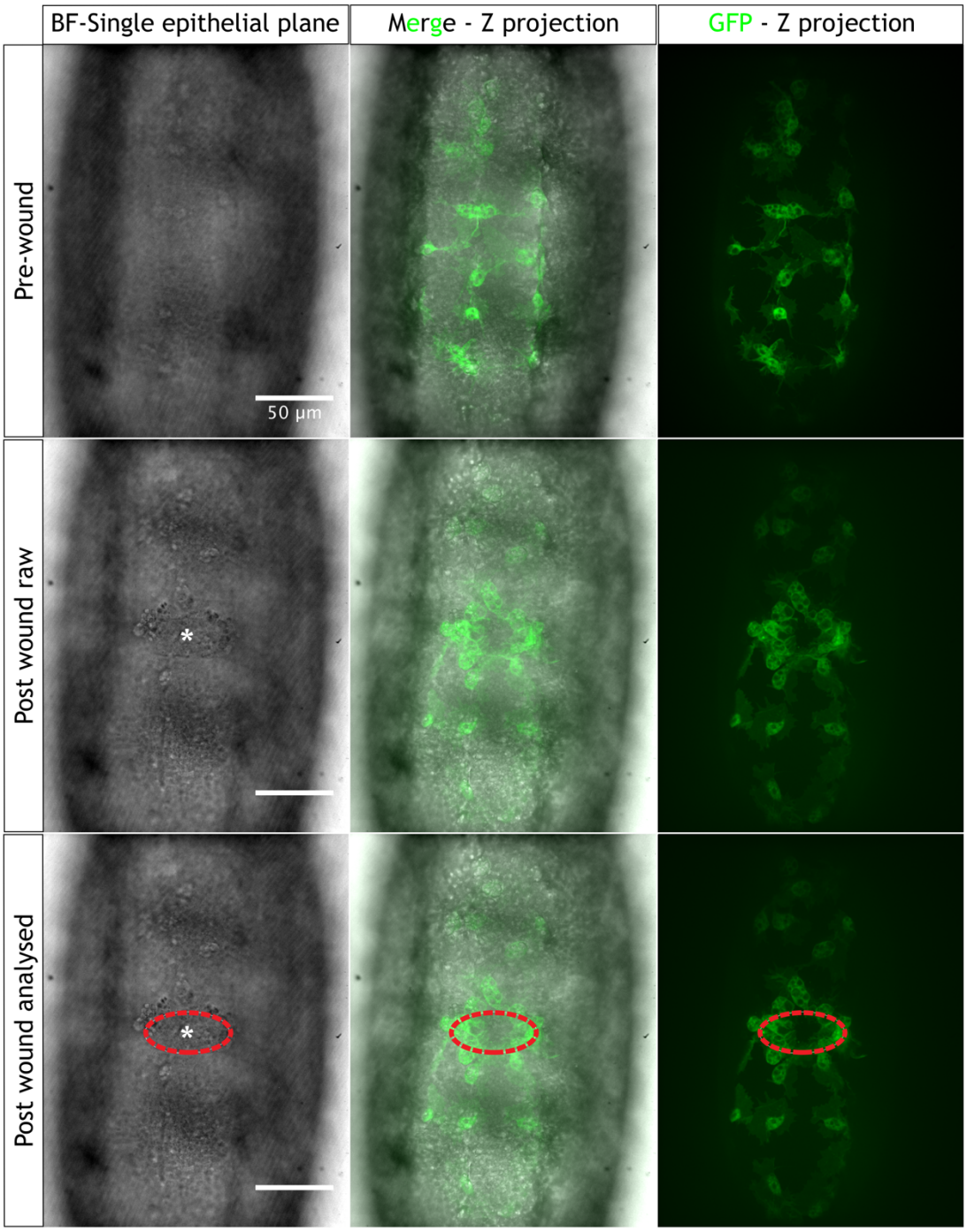

Appendix Figure 3.4.1: Pre and 1hr post ablation images. The plane of epithelium is shown in the brightfield channel is shown, as well as Z projections of the merge images and GFP channel containing hemocytes (*srp-gal4,UAS-GFP)*. The ablation site is denoted by the Asterix and outlined in the analysed images with the red dotted line. Scale bars at 50µm.

Appendix 5: Engagement of the RNAi machinery does not affect hemocyte recruitment to epithelial wounds

To validate that the engagement of the RNAi machinery does not affect hemocyte wound recruitment, controls for the GD and KK RNAi library (which do not contain a UAS-RNAi construct) were compared to the TRiP RNAi control directed against luciferase.

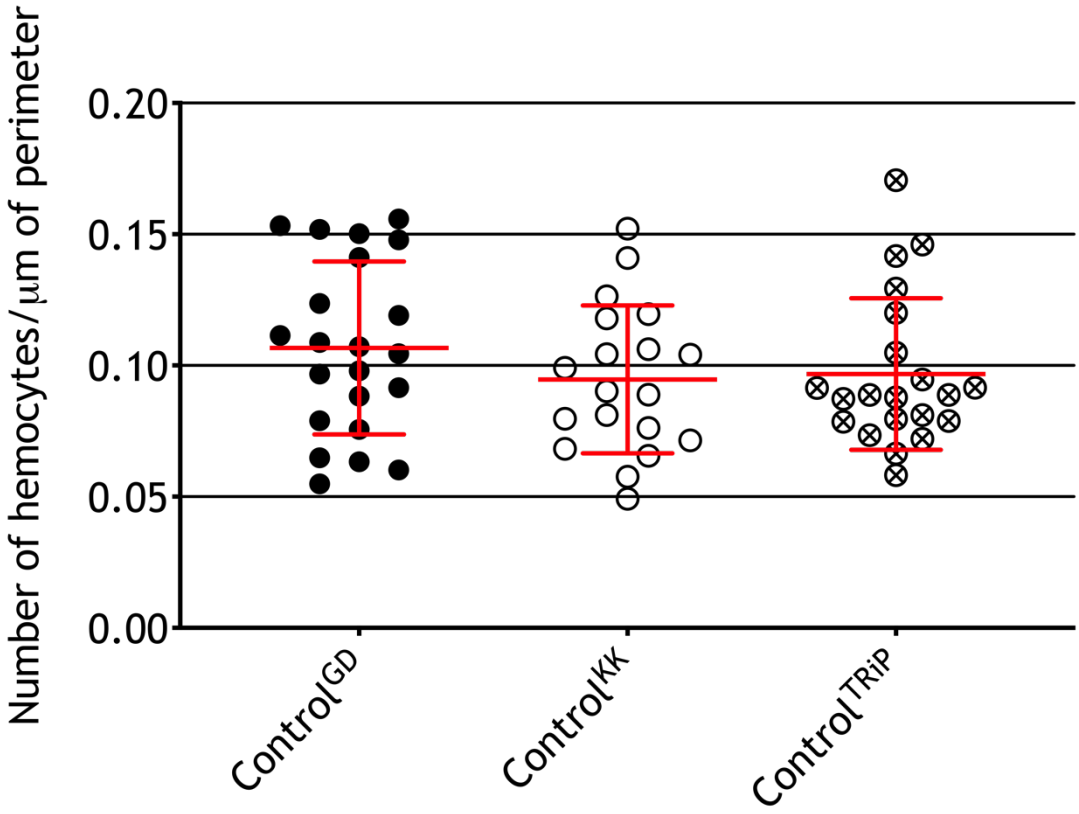

Appendix 3.4.2: The engagement of the RNAi machinery does not affect hemocyte wound recruitment.

Individual data points plotted as well as mean and standard deviation. GD control n=22; KK control n=19; TRiP control (UAS-RNAi directed against luciferase for machinery engagement) n=21.

Appendix 6: Extended wound recruitment profile in *Pez* mutants

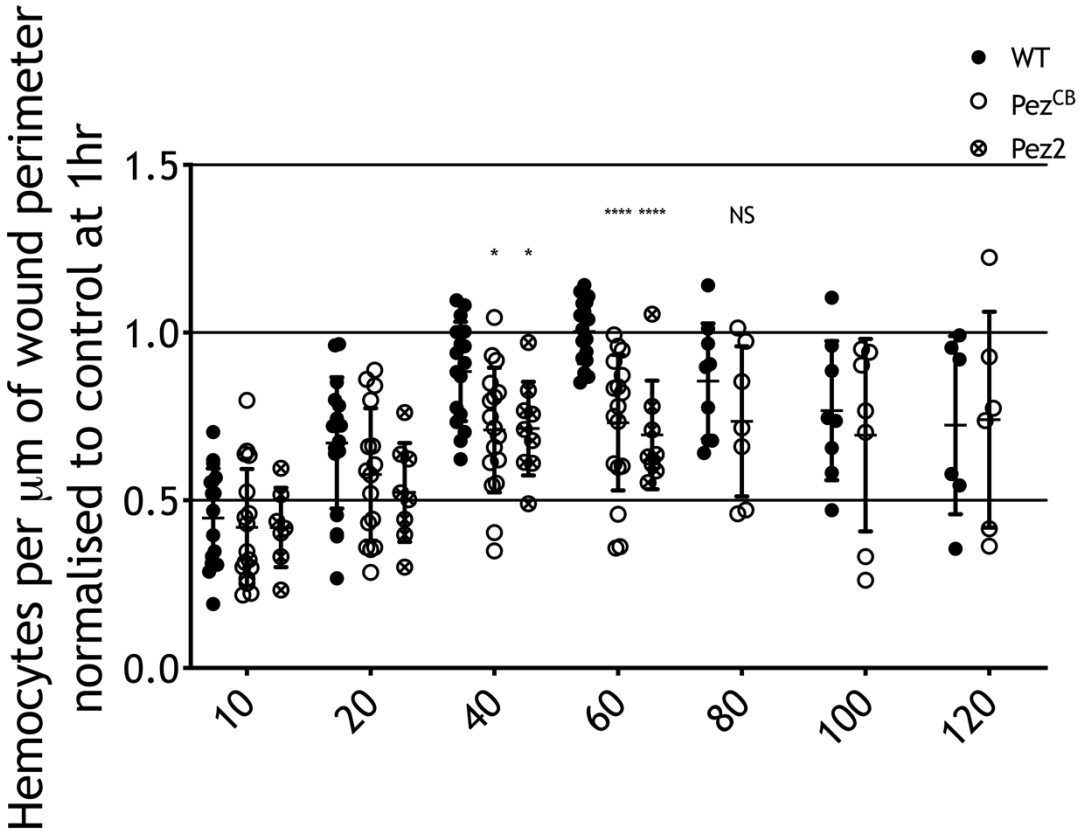

Appendix 4.2.1: The wound recruitment phenotype in *Pez^{CB}* mutants does not persist post 1 hour.

Early recruitment data identical to that presented in main figure. No data for Pez^{2} was collected past 60 minutes. Mean and SD plotted as well as individual data points. WT 80 minutes n=9; 100 minutes n=8 and 120 minutes n=6. Pez^{CB} 80 minutes n=7; 100 minutes n=7 and 120 minutes n=6. Multiple T tests uses to determine significance.

Appendix 7: Pez-sfGFP and Pez-mCherry constructs

Construct maps of synthesised fluorescent UAS constructs cloned into pAttB vectors for targeted integration into the *Drosophila* genome. The pAttB vector harbours a mini-white selection marker (for red eye progeny). The fluorescent tagged peptide sequences are cloned downstream of 5xUAS, an hsp70 promoter and a KOZAK sequence. Fluorescent peptide sequences were codon optimised for expression in *Drosophila*.

Appendix 4.5.1A: Pez-sfGFP in pAttB vector.

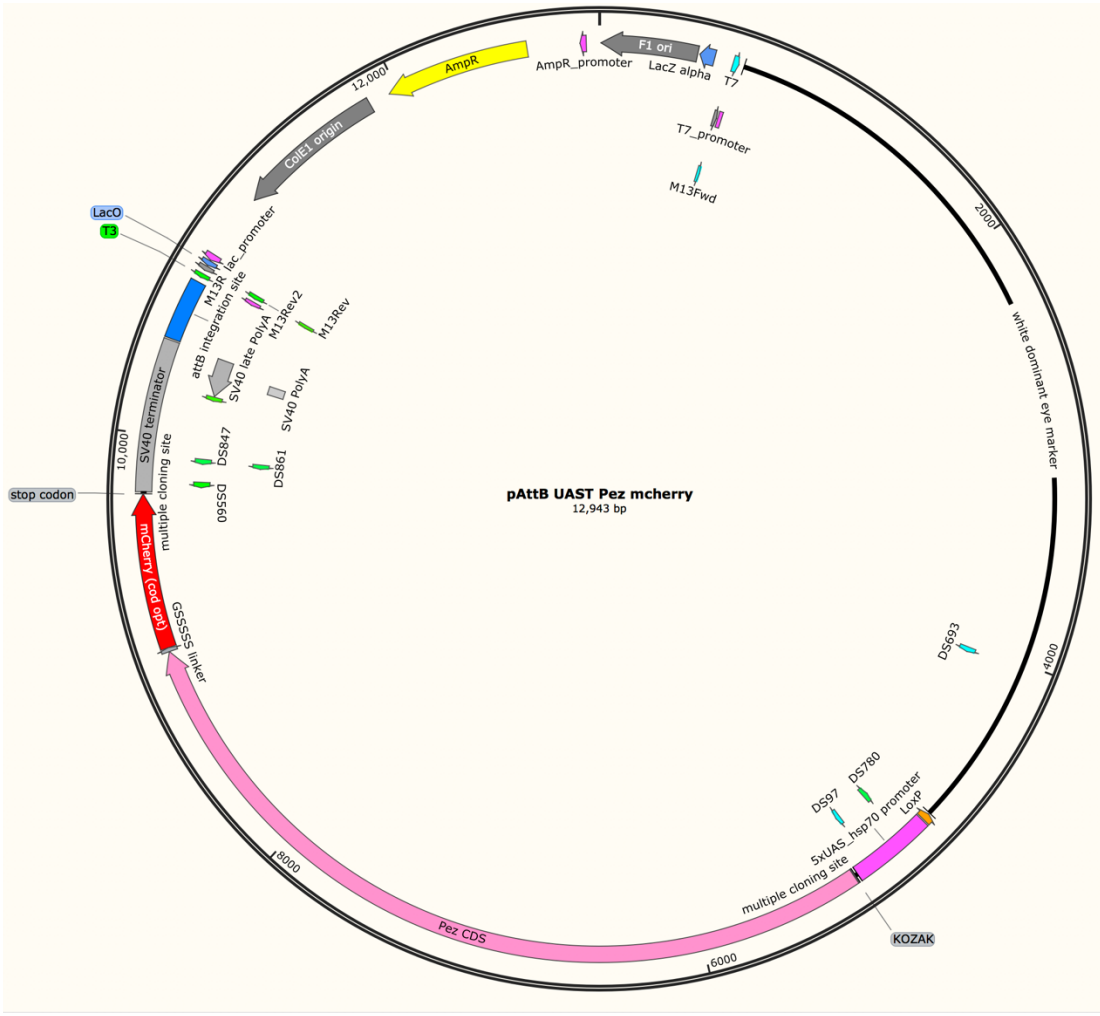

Appendix 4.5.1B: Pez-mCherry in pAttB vector.

Appendix 8: Draper-GFP pAttB construct

Appendix 4.5.2: Draper-eGFP in pAttB vector - generated by Dr Fred Rodrigues.

Appendix 9: Mpeg NLS-Scarlet construct for transgenic zebrafish

The following construct was generated by Dr Nik Ogryzko in the lab of Dr Yi Feng at the University of Edinburgh. By gateway reaction the Mpeg1 promoter, a nuclear localisation sequence and mSarlet-I sequence were cloned into a pDest2PA2 destination vector. A woodchuck hepatitits post-transcriptional regulatory element (WPRE) was added after the mScarlet stop codon to stabilise the mRNA. The sequences were codon optimised for zebrafish.

The vector was injected into zebrafish to generate a stable transgenic line.

Appendix 5.2.1: Mpeg NLS-Scarlet vector for zebrafish transgenesis.
Generated by Dr Nik Ogryzko.

Appendix 10: Splice disruption of MEGF10 following MO1 injection

The injection of MEGF10 MO1 induces exon skipping following splice disruption. Therefore RT-PCR of the target site will result in a band of shorter length.

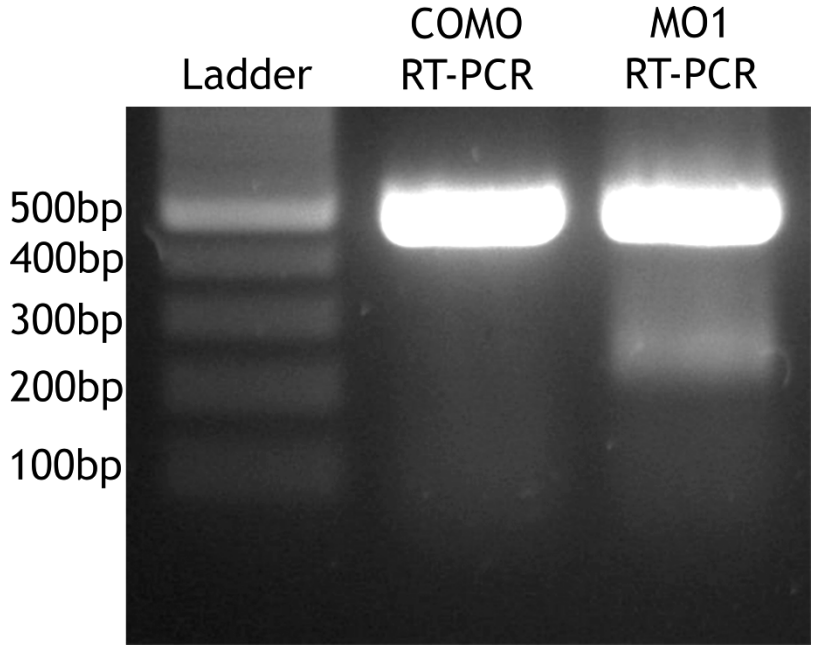

Appendix 5.3.1: Validation of exon skipping following MO1 injection into zebrafish embryos.

RNA collected from 50 injected embryos from each condition. Exon skipping is confirmed by the presence of a shorter DNA fragment following RT-PCR from MO1 injected fish.

Appendix 11: The injection of guide RNAs in the absence of Cas9 does not affect neutrophil recruitment to tailfin wounds

To determine whether the injection of gRNAs alone affected neutrophil recruitment to tailfin wounds, injected and injused *Tg(Lysc:DsRed)* fish were compared to uninjected fish. This revealed the presence of exogenous RNA alone is insufficient to reduce inflammation in the absence of Cas9.

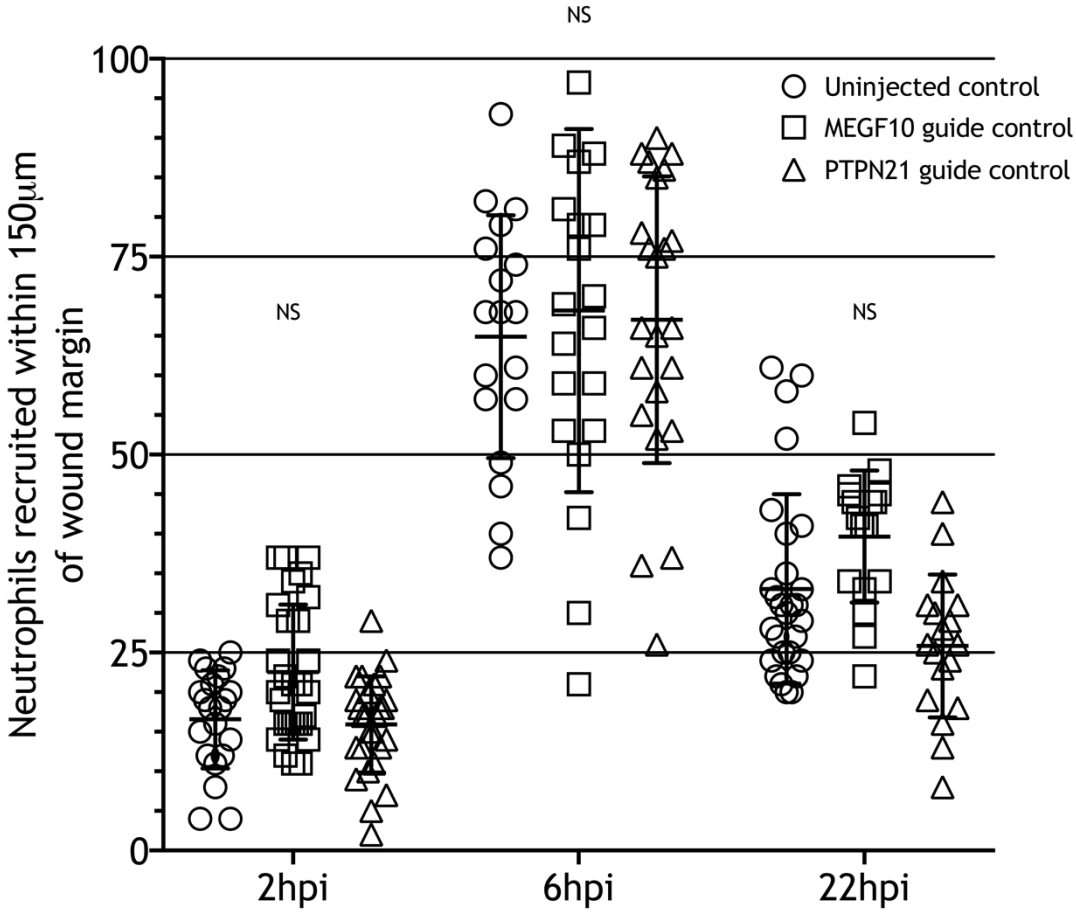

Appendix 5.5.1: Injection of gRNAs alone does not affect neutrophil numbers at wounds. Determined by fixation and immunostaining and counting of Lysc:DsRed positive cells at the wound site. Individual data points plotted along with mean and SD. Uninjected 2 hpi n=21; 6 hpi n=18; 22 hpi n=28. MEGF10 guide control (i.e. guide RNA injected alone) 2 hpi n =28; 6 hpi n=21; 22 hpi n=17. PTPN21 guide control 2 hpi n=27; 6 hpi n=23 and 22 hpi n=18. Significance determined by multiple T tests.

Supplementary movies

All movies supplied on accompanying USB drive in TIFF, MOV and AVI formats for maximum compatibility. All were acquired on a spinning disc confocal microscope (Ultraview; PerkinElmer) as outlined in methods 2.4.2.

Supplementary movie 1: Basal migration of embryonic hemocytes.
Stage 15 embryo expressing *serpent-gal4, UAS-GFP* – ventral view, Z-projection of 10µm Z-stack, acquired at 0.5µm intervals. Embryo was imaged for 1 hour at 30 second intervals using a 40x objective lens (NA 1.3). Scale bar 20 µm. As exemplified by this movie, hemocytes are highly dynamic and extend lamellipodia out from their main cell body. They patrol the developing organism.

Supplementary movie 2: Disruption of hemocyte morphology in *msn^{172}* mutants
Stage 15 *msn^{172}; srp-Gal4.2, UAS-2xeGFP, srp-3xH2AmCherry* ventral view, Z-projection of 10µm Z-stack, acquired at 0.5µm intervals. Embryo was imaged for 1 hour at 30 second intervalsusing a 40x objective lens (NA 1.3). Scale bar 20 µm. *Misshapen* mutant hemocytes display stringy, stellate morphology with long and thin projections that often link an area of cell body without a nucleus (red, H2AmCherry) back to the main cell body.

Supplementary movie 3: Dynamic nature of Pez-sfGFP puncta in hemocytes
Stage 15 *srp-gal4.2, UAS-Pez-sfGFP* embryo mounted ventrally and an area of hemocytes highlighted. Z-projection of 7µm Z-stack, acquired at 0.5µm intervals. Embryo was imaged for 20 minutes at 15 second intervals using a 63x objective lens (NA 1.4). Scale bar 20 µm. Pez-sfGFP puncta flow back into the cell body through the lamellipod. Pez-sfGFP puncta are also seen within the cell body.

Supplementary movie 4: Limited evidence for Pez-sfGFP puncta tracking along microtubules within hemocytes

Stage 15 *srp-gal4.2, UAS-Pez-sfGFP,UAS-mCherry-CLIP170* embryo mounted ventrally and a single hemocyte highlighted. Z-projection of 7µm Z-stack, acquired at 0.5µm intervals. Embryo was imaged for 20 minutes at 15 second intervals using a 63x objective lens (NA 1.4). Scale bar 20 µm. Image includes overly, and separate Pez-sfGFP (green) and mCherryCLIP170 (magenta) channels. Both the puncta and microtubules are highly dynamic; thus it is difficult to determine whether Pez puncta are tracking along these structures at this resolution.

Supplementary movie 5: Pez-sfGFP mislocalises in *Draper* mutant hemocytes

Stage 15 *Draper$^{\Delta 5}$,srp-gal4.2, UAS-Pez-sfGFP* embryo mounted ventrally and an area of hemocytes highlighted. Z-projection of 7µm Z-stack, acquired at 0.5µm intervals. Embryo was imaged for 20 minutes at 15 second intervals using a 63x objective lens (NA 1.4). Scale bar 20 µm. Can be viewed in conjunction with supplementary movie 3 for clarity. There is a predominance of Pez-sfGFP within the hemocyte cell body in *Draper* mutants. There is evidence of 'flashing' around vacuoles as exemplified at 05:45 sec – cell on the right-hand side.

Supplementary movie 6: Pez-sfGFP puncta flow back into the cell body at the wound site

Stage 15 *srp-gal4.2, UAS-Pez-sfGFP,UAS-mCherry-CLIP170* embryo mounted ventrally and a single hemocyte highlighted. Z-projection of 7µm Z-stack, acquired at 0.5µm intervals. Embryo was imaged for 30 minutes (time-lapse is shortened in movie) at 10 second intervals using a 63x objective lens (NA 1.4). Scale bar 20 µm. Wound site denoted by Asterix (*). There is an increase in Pez-sfGFP puncta following wounding. At the wound site, puncta are seen to flow back towards the cell body.

Supplementary movie 7: Evidence for Draper-GFP puncta following wounding

Stage 15 *srp-gal4.2, UAS-Pez-sfGFP,UAS-mCherry-CLIP170* embryo mounted ventrally and a single hemocyte highlighted. Z-projection of 7µm Z-stack, acquired at 0.5µm intervals. Embryo was imaged for 20 minutes (time-lapse is shortened in movie) at 15 second intervals using a 63x objective lens (NA 1.4). Scale bar 20 µm. Wound site denoted by Asterix (*). The top cell left hand side shows evidence for Draper puncta following wounding.

Reference list

1. Palis, J. *et al*. Spatial and temporal emergence of high proliferative potential hematopoietic precursors during murine embryogenesis. *Proc. Natl. Acad. Sci.* **98**, 4528 LP – 4533 (2001).
2. Palis, J., Robertson, S., Kennedy, M., Wall, C. & Keller, G. Development of erythroid and myeloid progenitors in the yolk sac and embryo proper of the mouse. *Development* **126**, 5073 LP – 5084 (1999).
3. Ovchinnikov, D. A. *et al*. Expression of Gal4-dependent transgenes in cells of the mononuclear phagocyte system labeled with enhanced cyan fluorescent protein using Csf1r-Gal4VP16/UAS-ECFP double-transgenic mice. *J. Leukoc. Biol.* **83**, 430–433 (2008).
4. Lang, R. A. & Bishop, J. M. Macrophages are required for cell death and tissue remodeling in the developing mouse eye. *Cell* **74**, 453–462 (1993).
5. Stevens, B. *et al*. The Classical Complement Cascade Mediates CNS Synapse Elimination. *Cell* **131**, 1164–1178 (2007).
6. Fantin, A. *et al*. Tissue macrophages act as cellular chaperones for vascular anastomosis downstream of VEGF-mediated endothelial tip cell induction. *Blood* **116**, 829 LP – 840 (2010).
7. Hopkinson-Woolley, J., Hughes, D., Gordon, S. & Martin, P. Macrophage recruitment during limb development and wound healing in the embryonic and foetal mouse. *J. Cell Sci.* **107 (Pt 5**, 1159–1167 (1994).
8. De Kleer, I., Willems, F., Lambrecht, B. & Goriely, S. Ontogeny of Myeloid Cells. *Front. Immunol.* **5**, 423 (2014).
9. Kumaravelu, P. *et al*. Quantitative developmental anatomy of definitive haematopoietic stem cells/long-term repopulating units (HSC/RUs): role of the aorta-gonad-mesonephros (AGM) region and the yolk sac in colonisation of the mouse embryonic liver. *Development* **129**, 4891–4899 (2002).
10. Medvinsky, A. L., Gan, O. I., Semenova, M. L. & Samoylina, N. L. Development of day-8 colony-forming unit-spleen hematopoietic progenitors during early murine embryogenesis: spatial and temporal mapping. *Blood* **87**, 557–566 (1996).
11. McKercher, S. R. *et al*. Targeted disruption of the PU.1 gene results in multiple hematopoietic abnormalities. *EMBO J.* **15**, 5647–5658 (1996).
12. Dai, X.-M. *et al*. Targeted disruption of the mouse colony-stimulating factor 1 receptor gene results in osteopetrosis, mononuclear phagocyte deficiency, increased primitive progenitor cell frequencies, and reproductive defects. *Blood* **99**, 111 LP – 120 (2002).
13. Ginhoux, F. *et al*. Fate Mapping Analysis Reveals That Adult Microglia Derive from Primitive Macrophages. *Science (80-.).* **330**, 841–845 (2010).
14. Chorro, L. *et al*. Langerhans cell (LC) proliferation mediates neonatal development, homeostasis, and inflammation-associated expansion of the epidermal LC network. *J. Exp. Med.* **206**, 3089–3100 (2009).
15. Hoeffel, G. *et al*. Adult Langerhans cells derive predominantly from embryonic fetal liver monocytes with a minor contribution of yolk

sac–derived macrophages. *J. Exp. Med.* **209**, 1167–1181 (2012).
16. Guilliams, M. *et al.* Alveolar macrophages develop from fetal monocytes that differentiate into long-lived cells in the first week of life via GM-CSF. *J. Exp. Med.* **210**, 1977–1992 (2013).
17. Ginhoux, F., Schultze, J. L., Murray, P. J., Ochando, J. & Biswas, S. K. New insights into the multidimensional concept of macrophage ontogeny, activation and function. *Nat. Immunol.* **17**, 34 (2015).
18. Lavin, Y. *et al.* Tissue-resident macrophage enhancer landscapes are shaped by the local microenvironment. *Cell* **159**, 1312–1326 (2014).
19. Xue, J. *et al.* Transcriptome-based network analysis reveals a spectrum model of human macrophage activation. *Immunity* **40**, 274–288 (2014).
20. Slayton, W. B. *et al.* The first-appearance of neutrophils in the human fetal bone marrow cavity. *Early Hum. Dev.* **53**, 129–144 (1998).
21. Laver, J. *et al.* High levels of granulocyte and granulocyte-macrophage colony-stimulating factors in cord blood of normal full-term neonates. *J. Pediatr.* **116**, 627–632 (1990).
22. Manroe, B. L., Weinberg, A. G., Rosenfeld, C. R. & Browne, R. The neonatal blood count in health and disease.I. Reference values for neutrophilic cells. *J. Pediatr.* **95**, 89–98 (1979).
23. Lawrence, S. M., Corriden, R. & Nizet, V. The Ontogeny of a Neutrophil: Mechanisms of Granulopoiesis and Homeostasis. *Microbiol. Mol. Biol. Rev.* **82**, e00057-17 (2018).
24. Campbell, M. S., Lovell, M. A. & Gorbsky, G. J. Stability of nuclear segments in human neutrophils and evidence against a role for microfilaments or microtubules in their genesis during differentiation of HL60 myelocytes. *J. Leukoc. Biol.* **58**, 659–666 (1995).
25. Sanchez, J. A., Karni, R. J. & Wangh, L. J. Fluorescent in situ hybridization (FISH) analysis of the relationship between chromosome location and nuclear morphology in human neutrophils. *Chromosoma* **106**, 168–177 (1997).
26. Spicer, S. S. & Hardin, J. H. Ultrastructure, cytochemistry, and function of neutrophil leukocyte granules. A review. *Lab. Invest.* **20**, 488–497 (1969).
27. Klebanoff, S. J. Myeloperoxidase: friend and foe. *J. Leukoc. Biol.* **77**, 598–625 (2005).
28. Rice, W. G. *et al.* Defensin-rich dense granules of human neutrophils. *Blood* **70**, 757 LP – 765 (1987).
29. Masson, P. L., Heremans, J. F. & Schonne, E. Lactoferrin, an iron-binding protein in neutrophilic leukocytes. *J. Exp. Med.* **130**, 643–58 (1969).
30. Fleming, A. & Allison, V. D. Further Observations on a Bacteriolytic Element Found in Tissues and Secretions. *Proc. R. Soc. B Biol. Sci.* **94**, 142–151 (1922).
31. Faurschou, M. & Borregaard, N. Neutrophil granules and secretory vesicles in inflammation. *Microbes Infect.* **5**, 1317–1327 (2003).
32. Carvalho, L. O., Aquino, E. N., Neves, A. C. D. & Fontes, W. The Neutrophil Nucleus and Its Role in Neutrophilic Function. *J. Cell. Biochem.* **116**, 1831–1836 (2015).
33. Fuchs, T. A. *et al.* Novel cell death program leads to neutrophil extracellular traps. *J. Cell Biol.* **176**, 231 LP – 241 (2007).

34. Amulic, B. *et al*. Cell-Cycle Proteins Control Production of Neutrophil Extracellular Traps. *Dev. Cell* **43**, 449–462.e5 (2017).
35. Csepregi, J., Kása, O., Szikszai, D., He, Y. & Mócsai, A. A1.18 Characterisation of a novel neutrophil-deficient mouse strain. *Ann. Rheum. Dis.* **74**, A8.1-A8 (2015).
36. Klein, C. Genetic Defects in Severe Congenital Neutropenia: Emerging Insights into Life and Death of Human Neutrophil Granulocytes. *Annu. Rev. Immunol.* **29**, 399–413 (2011).
37. Moore, K. L. *et al*. P-selectin glycoprotein ligand-1 mediates rolling of human neutrophils on P-selectin. *J. Cell Biol.* **128**, 661–71 (1995).
38. Lawrence, M. B. & Springer, T. A. Neutrophils roll on E-selectin. *J. Immunol.* **151**, 6338–6346 (1993).
39. Hammond, M. E. *et al*. IL-8 induces neutrophil chemotaxis predominantly via type I IL-8 receptors. *J. Immunol.* **155**, 1428–33 (1995).
40. Dovi, J. V., He, L.-K. & DiPietro, L. A. Accelerated wound closure in neutrophil-depleted mice. *J. Leukoc. Biol.* **73**, 448–455 (2003).
41. Simpson, D. M. & Ross, R. The neutrophilic leukocyte in wound repair a study with antineutrophil serum. *J. Clin. Invest.* **51**, 2009–23 (1972).
42. Daley, J. M., Brancato, S. K., Thomay, A. A., Reichner, J. S. & Albina, J. E. The phenotype of murine wound macrophages. *J. Leukoc. Biol.* **87**, 59–67 (2010).
43. Goren, I. *et al*. A transgenic mouse model of inducible macrophage depletion: effects of diphtheria toxin-driven lysozyme M-specific cell lineage ablation on wound inflammatory, angiogenic, and contractive processes. *Am. J. Pathol.* **175**, 132–147 (2009).
44. Zhao, R., Liang, H., Clarke, E., Jackson, C. & Xue, M. Inflammation in Chronic Wounds. *Int. J. Mol. Sci.* **17**, (2016).
45. Leibovich, S. J. & Ross, R. The role of the macrophage in wound repair. A study with hydrocortisone and antimacrophage serum. *Am. J. Pathol.* **78**, 71–100 (1975).
46. Diegelmann, R. F. Excessive neutrophils characterize chronic pressure ulcers. *Wound Repair Regen.* **11**, 490–495 (2003).
47. Loots, M. A. M. *et al*. Differences in Cellular Infiltrate and Extracellular Matrix of Chronic Diabetic and Venous Ulcers Versus Acute Wounds. *J. Invest. Dermatol.* **111**, 850–857 (1998).
48. Okizaki, S. *et al*. Suppressed recruitment of alternatively activated macrophages reduces TGF-beta1 and impairs wound healing in streptozotocin-induced diabetic mice. *Biomed. Pharmacother.* **70**, 317–325 (2015).
49. Adams, M. D. *et al*. The Genome Sequence of Drosophila melanogaster *Science (80-.).* **287**, 2185 LP – 2195 (2000).
50. Tepass, U., Fessler, L. I., Aziz, A. & Hartenstein, V. Embryonic origin of hemocytes and their relationship to cell death in Drosophila. *Development* **120**, 1829–37 (1994).
51. Wood, W. & Jacinto, A. Drosophila melanogaster embryonic haemocytes: masters of multitasking. *Nat. Rev. Mol. Cell Biol.* **8**, 542–51 (2007).
52. Rehorn, K. P., Thelen, H., Michelson, A. M. & Reuter, R. A molecular aspect of hematopoiesis and endoderm development common to vertebrates and Drosophila. *Development* **122**, 4023 LP – 4031 (1996).

53. Fujiwara, Y., Browne, C. P., Cunniff, K., Goff, S. C. & Orkin, S. H. Arrested development of embryonic red cell precursors in mouse embryos lacking transcription factor GATA-1. *Proc. Natl. Acad. Sci. U. S. A.* **93**, 12355–12358 (1996).
54. Pevny, L. *et al.* Erythroid differentiation in chimaeric mice blocked by a targeted mutation in the gene for transcription factor GATA-1. *Nature* **349**, 257–260 (1991).
55. Persons, D. A. *et al.* Enforced expression of the GATA-2 transcription factor blocks normal hematopoiesis. *Blood* **93**, 488–499 (1999).
56. Holz, A., Bossinger, B., Strasser, T., Janning, W. & Klapper, R. The two origins of hemocytes in Drosophila *Development* **130**, 4955 LP – 4962 (2003).
57. Wood, W., Faria, C. & Jacinto, A. Distinct mechanisms regulate hemocyte chemotaxis during development and wound healing in Drosophila melanogaster. *J. Cell Biol.* **173**, 405–416 (2006).
58. Cho, N. K. *et al.* Developmental Control of Blood Cell Migration by the Drosophila VEGF Pathway. *Cell* **108**, 865–876 (2002).
59. Parsons, B. & Foley, E. The Drosophila platelet-derived growth factor and vascular endothelial growth factor-receptor related (Pvr) protein ligands Pvf2 and Pvf3 control hemocyte viability and invasive migration. *J. Biol. Chem.* **288**, 20173–20183 (2013).
60. Stramer, B. *et al.* Clasp-mediated microtubule bundling regulates persistent motility and contact repulsion in Drosophila macrophages in vivo. *J. Cell Biol.* **189**, 681 LP – 689 (2010).
61. Comber, K. *et al.* A dual role for the βPS integrin myospheroid in mediating Drosophila embryonic macrophage migration. *J. Cell Sci.* **126**, 3475–3484 (2013).
62. Paladi, M. & Tepass, U. Function of Rho GTPases in embryonic blood cell migration in Drosophila *J. Cell Sci.* **117**, 6313 LP – 6326 (2004).
63. Svitkina, T. M. & Borisy, G. G. Arp2/3 Complex and Actin Depolymerizing Factor/Cofilin in Dendritic Organization and Treadmilling of Actin Filament Array in Lamellipodia. *J. Cell Biol.* **145**, 1009 LP – 1026 (1999).
64. Davidson, A. J., Millard, T. H., Evans, I. R. & Wood, W. Ena orchestrates remodelling within the actin cytoskeleton to drive robust Drosophila macrophage chemotaxis. *J. Cell Sci.* **132**, jcs224618 (2019).
65. Insall, R. H. & Machesky, L. M. Actin Dynamics at the Leading Edge: From Simple Machinery to Complex Networks. *Dev. Cell* **17**, 310–322 (2009).
66. Evans, I. R., Ghai, P. A., Urbancic, V., Tan, K.-L. & Wood, W. SCAR/WAVE-mediated processing of engulfed apoptotic corpses is essential for effective macrophage migration in Drosophila. *Cell Death Differ.* **20**, 709–720 (2013).
67. Zanet, J. *et al.* Fascin is required for blood cell migration during Drosophila embryogenesis. *Development* **136**, 2557 LP – 2565 (2009).
68. Ono, S. *et al.* Identification of an actin binding region and a protein kinase C phosphorylation site on human fascin. *J. Biol. Chem.* **272**, 2527–2533 (1997).

69. Tucker, P. K., Evans, I. R. & Wood, W. Ena drives invasive macrophage migration in Drosophila embryos. *Dis. Model. Mech.* **4**, 126–134 (2011).
70. Bilancia, C. G. *et al.* Enabled Negatively Regulates Diaphanous-Driven Actin Dynamics In Vitro and In Vivo. *Dev. Cell* **28**, 394–408 (2014).
71. Lee, H. *et al.* The Microtubule Plus End Tracking Protein Orbit/MAST/CLASP Acts Downstream of the Tyrosine Kinase Abl in Mediating Axon Guidance. *Neuron* **42**, 913–926 (2004).
72. Weavers, H., Evans, I. R., Martin, P. & Wood, W. Corpse Engulfment Generates a Molecular Memory that Primes the Macrophage Inflammatory Response. *Cell* **165**, 1658–1671 (2016).
73. Evans, I. R., Rodrigues, F. S. L. M., Armitage, E. L. & Wood, W. *Draper/CED-1 Mediates an Ancient Damage Response to Control Inflammatory Blood Cell Migration In Vivo. Current Biology* **25**, (2015).
74. White, K. *et al.* Genetic control of programmed cell death in Drosophila. *Science (80-.).* **264**, 677–683 (1994).
75. Fadok, V. A., Bratton, D. L., Frasch, S. C., Warner, M. L. & Henson, P. M. The role of phosphatidylserine in recognition of apoptotic cells by phagocytes. *Cell Death Differ.* **5**, 551–562 (1998).
76. Tung, T. T. *et al.* Phosphatidylserine recognition and induction of apoptotic cell clearance by Drosophila engulfment receptor Draper. *J. Biochem.* **153**, 483–491 (2013).
77. Venegas, V. & Zhou, Z. Two alternative mechanisms that regulate the presentation of apoptotic cell engulfment signal in Caenorhabditis elegans. *Mol. Biol. Cell* **18**, 3180–3192 (2007).
78. Manaka, J. *et al.* Draper-mediated and phosphatidylserine-independent phagocytosis of apoptotic cells by Drosophila hemocytes/macrophages. *J. Biol. Chem.* **279**, 48466–48476 (2004).
79. Schneider, I. Cell lines derived from late embryonic stages of Drosophila melanogaster *J. Embryol. Exp. Morphol.* **27**, 353 LP – 365 (1972).
80. Williamson, A. P. & Vale, R. D. Spatial control of Draper receptor signaling initiates apoptotic cell engulfment. *J. Cell Biol.* **217**, 3977 LP – 3992 (2018).
81. MacDonald, J. M. *et al.* The Drosophila Cell Corpse Engulfment Receptor Draper Mediates Glial Clearance of Severed Axons. *Neuron* **50**, 869–881 (2006).
82. Ziegenfuss, J. S. *et al.* Draper-dependent glial phagocytic activity is mediated by Src and Syk family kinase signalling. **453**, 935–939 (2008).
83. Kurant, E., Axelrod, S., Leaman, D. & Gaul, U. Six-Microns-Under Acts Upstream of Draper in the Glial Phagocytosis of Apoptotic Neurons. *Cell* **133**, 498–509 (2008).
84. Yu, X., Odera, S., Chuang, C.-H., Lu, N. & Zhou, Z. C. elegans Dynamin Mediates the Signaling of Phagocytic Receptor CED-1 for the Engulfment and Degradation of Apoptotic Cells. *Dev. Cell* **10**, 743–757 (2006).
85. Roddie, H. G., Armitage, E. L., Coates, J. A., Johnston, S. A. & Evans, I. R. Simu-dependent clearance of dying cells regulates macrophage function and inflammation resolution. *PLOS Biol.* **17**, e2006741 (2019).

86. Navazo, M. D. *et al*. Identification of a domain (155-183) on CD36 implicated in the phagocytosis of apoptotic neutrophils. *J. Biol. Chem.* **271**, 15381–15385 (1996).
87. Franc, N. C., Heitzler, P., Alan B., R., Ezekowitz & White, K. Requirement for Croquemort in Phagocytosis of Apoptotic Cells in Drosophila *Science (80-.).* **284**, 1991 LP – 1994 (1999).
88. Franc, N. C., Dimarcq, J.-L., Lagueux, M., Hoffmann, J. & Ezekowitz, R. A. B. Croquemort, A Novel Drosophila Hemocyte/Macrophage Receptor that Recognizes Apoptotic Cells. *Immunity* **4**, 431–443 (1996).
89. Stramer, B. *et al*. Live imaging of wound inflammation in Drosophila embryos reveals key roles for small GTPases during in vivo cell migration. *J. Cell Biol.* **168**, 567–573 (2005).
90. Kiehart, D. P., Galbraith, C. G., Edwards, K. A., Rickoll, W. L. & Montague, R. A. Multiple forces contribute to cell sheet morphogenesis for dorsal closure in Drosophila. *J. Cell Biol.* **149**, 471–90 (2000).
91. Razzell, W., Evans, I. R., Martin, P. & Wood, W. Calcium Flashes Orchestrate the Wound Inflammatory Response through DUOX Activation and Hydrogen Peroxide Release. *Curr. Biol.* **23**, 424–429 (2013).
92. Xu, S. & Chisholm, A. D. A Gα$_q$-Ca^{2+} Signaling Pathway Promotes Actin-Mediated Epidermal Wound Closure in C. elegans. *Curr. Biol.* **21**, 1960–1967 (2011).
93. Hinman, L. E., Beilman, G. J., Groehler, K. E. & Sammak, P. J. Wound-induced calcium waves in alveolar type II cells. *Am. J. Physiol.* **273**, L1242-8 (1997).
94. Leiper, L. J. *et al*. The roles of calcium signaling and ERK1/2 phosphorylation in a Pax6+/- mouse model of epithelial wound-healing delay. *BMC Biol.* **4**, 27 (2006).
95. Shabir, S. & Southgate, J. Calcium signalling in wound-responsive normal human urothelial cell monolayers. *Cell Calcium* **44**, 453–464 (2008).
96. Bauer, R., Lehmann, C., Martini, J., Eckardt, F. & Hoch, M. Gap junction channel protein innexin 2 is essential for epithelial morphogenesis in the Drosophila embryo. *Mol. Biol. Cell* **15**, 2992–3004 (2004).
97. Rigutto, S. *et al*. Activation of dual oxidases Duox1 and Duox2: differential regulation mediated by camp-dependent protein kinase and protein kinase C-dependent phosphorylation. *J. Biol. Chem.* **284**, 6725–6734 (2009).
98. Bedard, K. & Krause, K.-H. The NOX family of ROS-generating NADPH oxidases: physiology and pathophysiology. *Physiol. Rev.* **87**, 245–313 (2007).
99. Grasberger, H. & Refetoff, S. Identification of the maturation factor for dual oxidase. Evolution of an eukaryotic operon equivalent. *J. Biol. Chem.* **281**, 18269–18272 (2006).
100. Moreira, S., Stramer, B., Evans, I., Wood, W. & Martin, P. *Prioritization of Competing Damage and Developmental Signals by Migrating Macrophages in the Drosophila Embryo. Current Biology* **20**, (2010).

101. Enyedi, B., Zana, M., Donkó, Á. & Geiszt, M. Spatial and Temporal Analysis of NADPH Oxidase-Generated Hydrogen Peroxide Signals by Novel Fluorescent Reporter Proteins. *Antioxid. Redox Signal.* **19**, 523–534 (2012).
102. Yoo, S. K., Starnes, T. W., Deng, Q. & Huttenlocher, A. Lyn is a redox sensor that mediates leukocyte wound attraction in vivo. *Nature* **480**, 109–112 (2011).
103. Gronski, M. A., Kinchen, J. M., Juncadella, I. J., Franc, N. C. & Ravichandran, K. S. An essential role for calcium flux in phagocytes for apoptotic cell engulfment and the anti-inflammatory response. *Cell Death Differ.* **16**, 1323 (2009).
104. Weavers, H. *et al.* Systems Analysis of the Dynamic Inflammatory Response to Tissue Damage Reveals Spatiotemporal Properties of the Wound Attractant Gradient. *Curr. Biol.* **26**, 1975–1989 (2016).
105. la Sala, A. *et al.* Alerting and tuning the immune response by extracellular nucleotides. *J. Leukoc. Biol.* **73**, 339–343 (2003).
106. Di Virgilio, F. *et al.* Nucleotide receptors: an emerging family of regulatory molecules in blood cells. *Blood* **97**, 587 LP – 600 (2001).
107. Spence, R., Gerlach, G., Lawrence, C. & Smith, C. The behaviour and ecology of the zebrafish, Danio rerio. *Biol. Rev.* **83**, 13–34 (2008).
108. Kimmel, C. B., Ballard, W. W., Kimmel, S. R., Ullmann, B. & Schilling, T. F. Stages of embryonic development of the zebrafish. *Dev. Dyn.* **203**, 253–310 (1995).
109. Creaser, C. W. The Technic of Handling the Zebra Fish (Brachydanio rerio) for the Production of Eggs Which Are Favorable for Embryological Research and Are Available at Any Specified Time Throughout the Year. *Copeia* **1934**, 159–161 (1934).
110. Streisinger, G., Walker, C., Dower, N., Knauber, D. & Singer, F. Production of clones of homozygous diploid zebra fish (Brachydanio rerio). *Nature* **291**, 293–296 (1981).
111. White, R., Rose, K. & Zon, L. Zebrafish cancer: the state of the art and the path forward. *Nat. Rev. Cancer* **13**, 624 (2013).
112. Fontana, B. D., Mezzomo, N. J., Kalueff, A. V & Rosemberg, D. B. The developing utility of zebrafish models of neurological and neuropsychiatric disorders: A critical review. *Exp. Neurol.* **299**, 157–171 (2018).
113. Prince, V. E., Anderson, R. M. & Dalgin, G. Chapter Seven - Zebrafish Pancreas Development and Regeneration: Fishing for Diabetes Therapies. in *Zebrafish at the Interface of Development and Disease Research* (ed. Sadler, K. C. B. T.-C. T. in D. B.) **124**, 235–276 (Academic Press, 2017).
114. Zang, L., Shimada, Y. & Nishimura, N. Development of a Novel Zebrafish Model for Type 2 Diabetes Mellitus. *Sci. Rep.* **7**, 1461 (2017).
115. Heckler, K. & Kroll, J. Zebrafish as a Model for the Study of Microvascular Complications of Diabetes and Their Mechanisms. *International Journal of Molecular Sciences* **18**, (2017).
116. Goessling, W. & Sadler, K. C. Zebrafish: An Important Tool for Liver Disease Research. *Gastroenterology* **149**, 1361–1377 (2015).
117. Ellett, F. & Lieschke, G. J. Zebrafish as a model for vertebrate hematopoiesis. *Curr. Opin. Pharmacol.* **10**, 563–570 (2010).
118. Herbomel, P., Thisse, B. & Thisse, C. Ontogeny and behaviour of

early macrophages in the zebrafish embryo. *Development* **126**, 3735 LP – 3745 (1999).
119. Murayama, E. *et al*. Tracing Hematopoietic Precursor Migration to Successive Hematopoietic Organs during Zebrafish Development. *Immunity* **25**, 963–975 (2006).
120. Bennett, C. M. *et al*. Myelopoiesis in the zebrafish, Danio rerio. *Blood* **98**, 643–651 (2001).
121. Lieschke, G. J., Oates, A. C., Crowhurst, M. O., Ward, A. C. & Layton, J. E. Morphologic and functional characterization of granulocytes and macrophages in embryonic and adult zebrafish. *Blood* **98**, 3087 LP – 3096 (2001).
122. Willett, C. E., Cortes, A., Zuasti, A. & Zapata, A. G. Early hematopoiesis and developing lymphoid organs in the zebrafish. *Dev. Dyn.* **214**, 323–336 (1999).
123. Haire, R. N., Rast, J. P., Litman, R. T. & Litman, G. W. Characterization of three isotypes of immunoglobulin light chains and T-cell antigen receptor alpha in zebrafish. *Immunogenetics* **51**, 915–923 (2000).
124. Lam, S. H., Chua, H. L., Gong, Z., Lam, T. J. & Sin, Y. M. Development and maturation of the immune system in zebrafish, Danio rerio: a gene expression profiling, in situ hybridization and immunological study. *Dev. Comp. Immunol.* **28**, 9–28 (2004).
125. Langenau, D. M. *et al*. In vivo tracking of T cell development, ablation, and engraftment in transgenic zebrafish. *Proc. Natl. Acad. Sci. U. S. A.* **101**, 7369 LP – 7374 (2004).
126. Danilova, N. & Steiner, L. A. B cells develop in the zebrafish pancreas. *Proc. Natl. Acad. Sci.* **99**, 13711 LP – 13716 (2002).
127. Page, D. M. *et al*. An evolutionarily conserved program of B-cell development and activation in zebrafish. *Blood* **122**, e1 LP-e11 (2013).
128. Renshaw, S. A. *et al*. A transgenic zebrafish model of neutrophilic inflammation. *Blood* **108**, 3976 LP – 3978 (2006).
129. Yoo, S. K., Freisinger, C. M., LeBert, D. C. & Huttenlocher, A. Early redox, Src family kinase, and calcium signaling integrate wound responses and tissue regeneration in zebrafish. *J. Cell Biol.* **199**, 225 LP – 234 (2012).
130. Kawakami, A., Fukazawa, T. & Takeda, H. Early fin primordia of zebrafish larvae regenerate by a similar growth control mechanism with adult regeneration. *Dev. Dyn.* **231**, 693–699 (2004).
131. Niethammer, P., Grabher, C., Look, A. T. & Mitchison, T. J. A tissue-scale gradient of hydrogen peroxide mediates rapid wound detection in zebrafish. *Nature* **459**, 996–999 (2009).
132. de Oliveira, S. *et al*. ATP Modulates Acute Inflammation In Vivo through Dual Oxidase 1–Derived H₂O₂ Production and NF-κB Activation. *J. Immunol.* **192**, 5710 LP – 5719 (2014).
133. Tauzin, S., Starnes, T. W., Becker, F. B., Lam, P. & Huttenlocher, A. Redox and Src family kinase signaling control leukocyte wound attraction and neutrophil reverse migration. *J. Cell Biol.* **207**, 589 LP – 598 (2014).
134. Li, L., Yan, B., Shi, Y.-Q., Zhang, W.-Q. & Wen, Z.-L. Live Imaging Reveals Differing Roles of Macrophages and Neutrophils during

Zebrafish Tail Fin Regeneration. *J. Biol. Chem.* **287**, 25353–25360 (2012).
135. Wang, J. *et al.* Visualizing the function and fate of neutrophils in sterile injury and repair. *Science (80-.).* **358**, 111 LP – 116 (2017).
136. Hind, L. E. & Huttenlocher, A. Neutrophil Reverse Migration and a Chemokinetic Resolution. *Dev. Cell* **47**, 404–405 (2018).
137. Powell, D. *et al.* Chemokine Signaling and the Regulation of Bidirectional Leukocyte Migration in Interstitial Tissues. *Cell Rep.* **19**, 1572–1585 (2017).
138. Gray, C. *et al.* Simultaneous intravital imaging of macrophage and neutrophil behaviour during inflammation using a novel transgenic zebrafish. *Thromb. Haemost.* **105**, 811–819 (2011).
139. Ellett, F., Pase, L., Hayman, J. W., Andrianopoulos, A. & Lieschke, G. J. mpeg1 promoter transgenes direct macrophage-lineage expression in zebrafish. *Blood* **117**, e49-56 (2011).
140. Romero, M. M. G., McCathie, G., Jankun, P. & Roehl, H. H. Damage-induced reactive oxygen species enable zebrafish tail regeneration by repositioning of Hedgehog expressing cells. *Nat. Commun.* **9**, 4010 (2018).
141. Klyubin, I. V, Kirpichnikova, K. M. & Gamaley, I. A. Hydrogen peroxide-induced chemotaxis of mouse peritoneal neutrophils. *Eur. J. Cell Biol.* **70**, 347–351 (1996).
142. Ogura, M. & Kitamura, M. Oxidant Stress Incites Spreading of Macrophages via Extracellular Signal-Regulated Kinases and p38 Mitogen-Activated Protein Kinase. *J. Immunol.* **161**, 3569 LP – 3574 (1998).
143. Roy, S., Khanna, S., Nallu, K., Hunt, T. K. & Sen, C. K. Dermal wound healing is subject to redox control. *Mol. Ther.* **13**, 211–220 (2006).
144. Fitzer-Attas, C. J. *et al.* Fcγ Receptor–Mediated Phagocytosis in Macrophages Lacking the Src Family Tyrosine Kinases Hck, Fgr, and Lyn. *J. Exp. Med.* **191**, 669 LP – 682 (2000).
145. Lowell, C. A., Soriano, P. & Varmus, H. E. Functional overlap in the src gene family: inactivation of hck and fgr impairs natural immunity. *Genes Dev.* **8**, 387–398 (1994).
146. Ernst, M. *et al.* Constitutive Activation of the Src Family Kinase Hck Results in Spontaneous Pulmonary Inflammation and an Enhanced Innate Immune Response. *J. Exp. Med.* **196**, 589 LP – 604 (2002).
147. Mócsai, A., Zhou, M., Meng, F., Tybulewicz, V. L. & Lowell, C. A. Syk Is Required for Integrin Signaling in Neutrophils. *Immunity* **16**, 547–558 (2002).
148. Lowell, C. A. & Berton, G. Resistance to endotoxic shock and reduced neutrophil migration in mice deficient for the Src-family kinases Hck and Fgr. *Proc. Natl. Acad. Sci.* **95**, 7580 LP – 7584 (1998).
149. Dal Porto, J. M. *et al.* B cell antigen receptor signaling 101. *Mol. Immunol.* **41**, 599–613 (2004).
150. Letourneur, F. & Klausner, R. D. Activation of T cells by a tyrosine kinase activation domain in the cytoplasmic tail of CD3 epsilon. *Science* **255**, 79–82 (1992).
151. Lanier, L. L., Corliss, B. C., Wu, J., Leong, C. & Phillips, J. H. Immunoreceptor DAP12 bearing a tyrosine-based activation motif is involved in activating NK cells. *Nature* **391**, 703–707 (1998).
152. Humphrey, M. B., Lanier, L. L. & Nakamura, M. C. Role of ITAM-

containing adapter proteins and their receptors in the immune system and bone. *Immunol. Rev.* **208**, 50–65 (2005).
153. Mkaddem, S. Ben *et al.* Lyn and Fyn function as molecular switches that control immunoreceptors to direct homeostasis or inflammation. *Nat. Commun.* **8**, 246 (2017).
154. Klar, A. J. S. & Halvorson, H. O. Studies on the positive regulatory gene, GAL4, in regulation of galactose catabolic enzymes in Saccharomyces cerevisiae. *Mol. Gen. Genet. MGG* **135**, 203–212 (1974).
155. Fischer, J. A., Giniger, E., Maniatis, T. & Ptashne, M. GAL4 activates transcription in Drosophila. *Nature* **332**, 853–856 (1988).
156. Scheer, N. & Campos-Ortega, J. A. Use of the Gal4-UAS technique for targeted gene expression in the zebrafish. *Mech. Dev.* **80**, 153–158 (1999).
157. Carthew, R. W. & Sontheimer, E. J. Origins and Mechanisms of miRNAs and siRNAs. *Cell* **136**, 642–655 (2009).
158. Fire, A. *et al.* Potent and specific genetic interference by double-stranded RNA in Caenorhabditis elegans. *Nature* **391**, 806–811 (1998).
159. Heigwer, F., Port, F. & Boutros, M. RNA Interference (RNAi) Screening in Drosophila *Genetics* **208**, 853 LP – 874 (2018).
160. Dietzl, G. *et al.* A genome-wide transgenic RNAi library for conditional gene inactivation in Drosophila. *Nature* **448**, 151–156 (2007).
161. Perkins, L. A. *et al.* The Transgenic RNAi Project at Harvard Medical School: Resources and Validation. *Genetics* **201**, 843 LP – 852 (2015).
162. Summerton, J. Morpholino antisense oligomers: the case for an RNase H-independent structural type. *Biochim. Biophys. Acta - Gene Struct. Expr.* **1489**, 141–158 (1999).
163. SUMMERTON, J. & WELLER, D. Morpholino Antisense Oligomers: Design, Preparation, and Properties. *Antisense Nucleic Acid Drug Dev.* **7**, 187–195 (1997).
164. Nasevicius, A. & Ekker, S. C. Effective targeted gene 'knockdown' in zebrafish. *Nat. Genet.* **26**, 216–220 (2000).
165. Stainier, D. Y. R. *et al.* Guidelines for morpholino use in zebrafish. *PLOS Genet.* **13**, e1007000 (2017).
166. Eisen, J. S. & Smith, J. C. Controlling morpholino experiments: don't stop making antisense. *Development* **135**, 1735 LP – 1743 (2008).
167. Barrangou, R. The roles of CRISPR–Cas systems in adaptive immunity and beyond. *Curr. Opin. Immunol.* **32**, 36–41 (2015).
168. Makarova, K. S. *et al.* Evolution and classification of the CRISPR–Cas systems. *Nat. Rev. Microbiol.* **9**, 467 (2011).
169. Deltcheva, E. *et al.* CRISPR RNA maturation by trans-encoded small RNA and host factor RNase III. *Nature* **471**, 602 (2011).
170. Brückner, K. *et al.* The PDGF/VEGF Receptor Controls Blood Cell Survival in Drosophila. *Dev. Cell* **7**, 73–84 (2004).
171. Gyoergy, A. *et al.* Tools Allowing Independent Visualization and Genetic Manipulation of Drosophila melanogaster Macrophages and Surrounding Tissues. *G3 Genes|Genomes|Genetics* **8**, 845 LP – 857 (2018).
172. Yeh, E., Gustafson, K. & Boulianne, G. L. Green fluorescent protein

as a vital marker and reporter of gene expression in Drosophila. *Proc. Natl. Acad. Sci. U. S. A.* **92**, 7036–40 (1995).
173. Halfon, M. S. *et al.* New fluorescent protein reporters for use with the drosophila gal4 expression system and for vital detection of balancer chromosomes. *genesis* **34**, 135–138 (2002).
174. Carrera, I., Zavadil, J. & Treisman, J. E. Two Subunits Specific to the PBAP Chromatin Remodeling Complex Have Distinct and Redundant Functions during Drosophila Development. *Mol. Cell. Biol.* **28**, 5238 LP – 5250 (2008).
175. Poernbacher, I., Baumgartner, R., Marada, S. K., Edwards, K. & Stocker, H. *Drosophila Pez Acts in Hippo Signaling to Restrict Intestinal Stem Cell Proliferation*. *Current Biology* **22**, (2012).
176. Treisman, J. E., Ito, N. & Rubin, G. M. misshapen encodes a protein kinase involved in cell shape control in Drosophila. *Gene* **186**, 119–125 (1997).
177. Freeman, M. R., Delrow, J., Kim, J., Johnson, E. & Doe, C. Q. Unwrapping Glial Biology: Gcm Target Genes Regulating Glial Development, Diversification, and Function. *Neuron* **38**, 567–580 (2003).
178. Tateno, M., Nishida, Y. & Adachi-Yamada, T. Regulation of JNK by Src During Drosophila Development. *Science (80-.).* **287**, 324 LP – 327 (2000).
179. McPhee, C. K., Logan, M. A., Freeman, M. R. & Baehrecke, E. H. Activation of autophagy during cell death requires the engulfment receptor Draper. *Nature* **465**, 1093 (2010).
180. Su, Y.-C., Treisman, J. E. & Skolnik, E. Y. The Drosophila Ste20-related kinase misshapen is required for embryonic dorsal closure and acts through a JNK MAPK module on an evolutionarily conserved signaling pathway. *Genes Dev.* **12**, 2371–2380 (1998).
181. Perkins, L. A., Holderbaum, L. & Perrimon, N. Luciferase RNAi construct P{TRiP.JF01355}. (2010).
182. Dickson, B., Dietzl, G., Keleman, K. & VDRC project members, ?. RNAi construct and insertion data submitted by the Vienna Drosophila RNAi Center. (2007).
183. Keleman, K., Micheler, T. & VDRC project members. RNAi-phiC31 construct and insertion data submitted by the Vienna Drosophila RNAi Center. (2009).
184. Ni, J.-Q. *et al.* A genome-scale shRNA resource for transgenic RNAi in Drosophila. (2010).
185. Riggleman, B., Schedl, P. & Wieschaus, E. Spatial expression of the Drosophila segment polarity gene armadillo is posttranscriptionally regulated by wingless. *Cell* **63**, 549–560 (1990).
186. Cant, K., Knowles, B. A., Mooseker, M. S. & Cooley, L. Drosophila singed, a fascin homolog, is required for actin bundle formation during oogenesis and bristle extension. *J. Cell Biol.* **125**, 369 LP – 380 (1994).
187. Feng, Y., Santoriello, C., Mione, M., Hurlstone, A. & Martin, P. Live imaging of innate immune cell sensing of transformed cells in zebrafish larvae: parallels between tumor initiation and wound inflammation. *PLoS Biol.* **8**, e1000562–e1000562 (2010).
188. Hartenstein, V. *Atlas of Drosophila Development*. (Cold Spring Harbor Laboratory Press, 1993).

189. Hall, C., Flores, M. V., Storm, T., Crosier, K. & Crosier, P. The zebrafish lysozyme C promoter drives myeloid-specific expression in transgenic fish. *BMC Dev. Biol.* **7**, 42 (2007).
190. Boyden, S. E. *et al.* Mutations in the satellite cell gene MEGF10 cause a recessive congenital myopathy with minicores. *Neurogenetics* **13**, 115–124 (2012).
191. Peterson, S. M. & Freeman, J. L. RNA isolation from embryonic zebrafish and cDNA synthesis for gene expression analysis. *J. Vis. Exp.* 1470 (2009). doi:10.3791/1470
192. Underhill, D. M. & Goodridge, H. S. The many faces of ITAMs. *Trends Immunol.* **28**, 66–73 (2007).
193. Mi, H. *et al.* Protocol Update for large-scale genome and gene function analysis with the PANTHER classification system (v.14.0). *Nat. Protoc.* **14**, 703–721 (2019).
194. Bahri, S. M., Yang, X. & Chia, W. The Drosophila bifocal gene encodes a novel protein which colocalizes with actin and is necessary for photoreceptor morphogenesis. *Mol. Cell. Biol.* **17**, 5521–5529 (1997).
195. Ruan, W., Long, H., Vuong, D. H. & Rao, Y. Bifocal Is a Downstream Target of the Ste20-like Serine/Threonine Kinase Misshapen in Regulating Photoreceptor Growth Cone Targeting in Drosophila. *Neuron* **36**, 831–842 (2002).
196. Babu, K., Bahri, S., Alphey, L. & Chia, W. Bifocal and PP1 interaction regulates targeting of the R-cell growth cone in Drosophila. *Dev. Biol.* **288**, 372–386 (2005).
197. Viola, A., Munari, F., Sánchez-Rodríguez, R., Scolaro, T. & Castegna, A. The Metabolic Signature of Macrophage Responses . *Frontiers in Immunology* **10**, 1462 (2019).
198. Mohrmann, L. *et al.* Differential targeting of two distinct SWI/SNF-related Drosophila chromatin-remodeling complexes. *Mol. Cell. Biol.* **24**, 3077–88 (2004).
199. Bonnay, F. *et al.* Akirin specifies NF-κB selectivity of Drosophila innate immune response via chromatin remodeling. *EMBO J.* **33**, 2349–2362 (2014).
200. He, X. *et al.* Bap180/Baf180 is required to maintain homeostasis of intestinal innate immune response in Drosophila and mice. *Nat. Microbiol.* **2**, 17056 (2017).
201. Izumi, Y., Yanagihashi, Y. & Furuse, M. A novel protein complex, Mesh-Ssk, is required for septate junction formation in the Drosophila midgut. *J. Cell Sci.* **125**, 4923–33 (2012).
202. Xiao, X. *et al.* A Mesh–Duox pathway regulates homeostasis in the insect gut. *Nat. Microbiol.* **2**, 17020 (2017).
203. Rämet, M. *et al.* Drosophila Scavenger Receptor CI Is a Pattern Recognition Receptor for Bacteria. *Immunity* **15**, 1027–1038 (2001).
204. Kline, A., Curry, T. & Lewellyn, L. The Misshapen kinase regulates the size and stability of the germline ring canals in the Drosophila egg chamber. *Dev. Biol.* **440**, 99–112 (2018).
205. Chen, D.-Y. *et al.* The Bro1-domain-containing protein Myopic/HDPTP coordinates with Rab4 to regulate cell adhesion and migration. *J. Cell Sci.* **125**, 4841 LP – 4852 (2012).
206. Møller, N. P. *et al.* Src kinase associates with a member of a distinct subfamily of protein-tyrosine phosphatases containing an ezrin-like domain. *Proc. Natl. Acad. Sci. U. S. A.* **91**, 7477–81 (1994).

207. Carlucci, A. *et al*. Protein-tyrosine Phosphatase PTPD1 Regulates Focal Adhesion Kinase Autophosphorylation and Cell Migration. *J. Biol. Chem.* **283**, 10919–10929 (2008).
208. Cardone, L. *et al*. Mitochondrial AKAP121 binds and targets protein tyrosine phosphatase D1, a novel positive regulator of src signaling. *Mol. Cell. Biol.* **24**, 4613–26 (2004).
209. Evans, I. R., Hu, N., Skaer, H. & Wood, W. Interdependence of macrophage migration and ventral nerve cord development in Drosophila embryos. *Development* **137**, 1625 LP – 1633 (2010).
210. Castillejo-López, C. & Häcker, U. The serine protease Sp7 is expressed in blood cells and regulates the melanization reaction in Drosophila. *Biochem. Biophys. Res. Commun.* **338**, 1075–1082 (2005).
211. Venken, K. J. T. *et al*. MiMIC: a highly versatile transposon insertion resource for engineering Drosophila melanogaster genes. *Nat. Methods* **8**, 737–743 (2011).
212. Nagarkar-Jaiswal, S. *et al*. A genetic toolkit for tagging intronic MiMIC containing genes. *Elife* **4**, e08469 (2015).
213. Plutoni, C. *et al*. Misshapen coordinates protrusion restriction and actomyosin contractility during collective cell migration. *Nat. Commun.* **10**, 3940 (2019).
214. Houalla, T., Hien Vuong, D., Ruan, W., Suter, B. & Rao, Y. The Ste20-like kinase misshapen functions together with Bicaudal-D and dynein in driving nuclear migration in the developing drosophila eye. *Mech. Dev.* **122**, 97–108 (2005).
215. Su, Y.-C., Maurel-Zaffran, C., Treisman, J. E. & Skolnik, E. Y. The Ste20 Kinase Misshapen Regulates Both Photoreceptor Axon Targeting and Dorsal Closure, Acting Downstream of Distinct Signals. *Mol. Cell. Biol.* **20**, 4736 LP – 4744 (2000).
216. Lewellyn, L., Cetera, M. & Horne-Badovinac, S. Misshapen decreases integrin levels to promote epithelial motility and planar polarity in Drosophila *J. Cell Biol.* **200**, 721 LP – 729 (2013).
217. Cobreros-Reguera, L. *et al*. The Ste20 kinase misshapen is essential for the invasive behaviour of ovarian epithelial cells in Drosophila *EMBO Rep.* **11**, 943 LP – 949 (2010).
218. Babu, K., Cai, Y., Bahri, S., Yang, X. & Chia, W. Roles of Bifocal, Homer, and F-actin in anchoring Oskar to the posterior cortex of Drosophila oocytes. *Genes Dev.* **18**, 138–143 (2004).
219. Speck, O., Hughes, S. C., Noren, N. K., Kulikauskas, R. M. & Fehon, R. G. Moesin functions antagonistically to the Rho pathway to maintain epithelial integrity. *Nature* **421**, 83–87 (2003).
220. Linardopoulou, E. V *et al*. Human subtelomeric WASH genes encode a new subclass of the WASP family. *PLoS Genet* **3**, e237 (2007).
221. Sit, S.-T. & Manser, E. Rho GTPases and their role in organizing the actin cytoskeleton. *J. Cell Sci.* **124**, 679 LP – 683 (2011).
222. Fukata, M., Nakagawa, M. & Kaibuchi, K. Roles of Rho-family GTPases in cell polarisation and directional migration. *Curr. Opin. Cell Biol.* **15**, 590–597 (2003).
223. Chishti, A. H. *et al*. The FERM domain: a unique module involved in

the linkage of cytoplasmic proteins to the membrane. *Trends Biochem. Sci.* **23**, 281–282 (1998).
224. Turunen, O., Wahlström, T. & Vaheri, A. Ezrin has a COOH-terminal actin-binding site that is conserved in the ezrin protein family. *J. Cell Biol.* **126**, 1445 LP – 1453 (1994).
225. Polesello, C., Delon, I., Valenti, P., Ferrer, P. & Payre, F. Dmoesin controls actin-based cell shape and polarity during Drosophila melanogaster oogenesis. *Nat. Cell Biol.* **4**, 782–789 (2002).
226. Estecha, A. *et al.* Moesin orchestrates cortical polarity of melanoma tumour cells to initiate 3D invasion. *J. Cell Sci.* **122**, 3492–3501 (2009).
227. Vogt, W. Oxidation of methionyl residues in proteins: Tools, targets, and reversal. *Free Radic. Biol. Med.* **18**, 93–105 (1995).
228. Edwards, K., Davis, T., Marcey, D., Kurihara, J. & Yamamoto, D. Comparative analysis of the Band 4.1/ezrin-related protein tyrosine phosphatase Pez from two Drosophila species: implications for structure and function. *Gene* **275**, 195–205 (2001).
229. Huttlin, E. L. *et al.* A Tissue-Specific Atlas of Mouse Protein Phosphorylation and Expression. *Cell* **143**, 1174–1189 (2010).
230. Pinna, L. A. & Ruzzene, M. How do protein kinases recognize their substrates? *Biochim. Biophys. Acta - Mol. Cell Res.* **1314**, 191–225 (1996).
231. Wang, W. *et al.* PTPN14 is required for the density-dependent control of YAP1. *Genes Dev.* **26**, 1959–1971 (2012).
232. Liu, X. *et al.* PTPN14 interacts with and negatively regulates the oncogenic function of YAP. *Oncogene* **32**, 1266–1273 (2013).
233. Huang, J.-M. *et al.* YAP modifies cancer cell sensitivity to EGFR and survivin inhibitors and is negatively regulated by the non-receptor type protein tyrosine phosphatase 14. *Oncogene* **32**, 2220–2229 (2013).
234. Michaloglou, C. *et al.* The Tyrosine Phosphatase PTPN14 Is a Negative Regulator of YAP Activity. *PLoS One* **8**, e61916 (2013).
235. Wadham, C., Gamble, J. R., Vadas, M. A. & Khew-Goodall, Y. The Protein Tyrosine Phosphatase Pez Is a Major Phosphatase of Adherens Junctions and Dephosphorylates ß-Catenin. *Mol. Biol. Cell* **14**, 2520–2529 (2003).
236. Sears, H. C., Kennedy, C. J. & Garrity, P. A. Macrophage-mediated corpse engulfment is required for normal Drosophila CNS morphogenesis. *Development* **130**, 3557 LP – 3565 (2003).
237. Meehan, T. L. *et al.* Components of the Engulfment Machinery Have Distinct Roles in Corpse Processing. *PLoS One* **11**, e0158217 (2016).
238. Wood, W. *et al.* Wound healing recapitulates morphogenesis in Drosophila embryos. *Nat. Cell Biol.* **4**, 907–912 (2002).
239. Ryder, E. *et al.* The DrosDel Collection. *Genetics* **167**, 797 LP – 813 (2004).
240. Siddiqui, N. *et al.* PTPN21 and Hook3 relieve KIF1C autoinhibition and activate intracellular transport. *Nat. Commun.* **10**, 2693 (2019).
241. Dorner, C. *et al.* Characterization of KIF1C, a New Kinesin-like Protein Involved in Vesicle Transport from the Golgi Apparatus to the Endoplasmic Reticulum. *J. Biol. Chem.* **273**, 20267–20275 (1998).
242. Theisen, U., Straube, E. & Straube, A. Directional persistence of

migrating cells requires Kif1C-mediated stabilization of trailing adhesions. *Dev. Cell* **23**, 1153–1166 (2012).
243. Wang, C. *et al.* Suppressor of Deltex mediates Pez degradation and modulates Drosophila midgut homeostasis. *Nat. Commun.* **6**, 6607 (2015).
244. Davis, J. R. *et al.* Inter-cellular forces orchestrate contact inhibition of locomotion. *Cell* **161**, 361–373 (2015).
245. Huse, M. & Kuriyan, J. The Conformational Plasticity of Protein Kinases. *Cell* **109**, 275–282 (2002).
246. de Oliveira, S. *et al.* Cxcl8 (IL-8) Mediates Neutrophil Recruitment and Behavior in the Zebrafish Inflammatory Response. *J. Immunol.* **190**, 4349 LP – 4359 (2013).
247. Loynes, C. A. *et al.* Pivotal Advance: Pharmacological manipulation of inflammation resolution during spontaneously resolving tissue neutrophilia in the zebrafish. *J. Leukoc. Biol.* **87**, 203–212 (2010).
248. Hamon, Y. *et al.* Cooperation between Engulfment Receptors: The Case of ABCA1 and MEGF10. *PLoS One* **1**, e120 (2006).
249. Pandey, K. N. Functional roles of short sequence motifs in the endocytosis of membrane receptors. *Front. Biosci. (Landmark Ed.* **14**, 5339–5360 (2009).
250. Ohtsuka, M. *et al.* NFAM1, an immunoreceptor tyrosine-based activation motif-bearing molecule that regulates B cell development and signaling. *Proc. Natl. Acad. Sci. U. S. A.* **101**, 8126–8131 (2004).
251. Scheib, J. L., Sullivan, C. S. & Carter, B. D. Jedi-1 and MEGF10 Signal Engulfment of Apoptotic Neurons through the Tyrosine Kinase Syk. *J. Neurosci.* **32**, 13022 LP – 13031 (2012).
252. Saha, M. *et al.* Selective serotonin reuptake inhibitors ameliorate MEGF10 myopathy. *Hum. Mol. Genet.* **28**, 2365–2377 (2019).
253. Draper, I. *et al.* Silencing of drpr Leads to Muscle and Brain Degeneration in Adult Drosophila. *Am. J. Pathol.* **184**, 2653–2661 (2014).
254. Wu, H.-H. *et al.* Glial precursors clear sensory neuron corpses during development via Jedi-1, an engulfment receptor. *Nat. Neurosci.* **12**, 1534 (2009).
255. Chung, W.-S. *et al.* Astrocytes mediate synapse elimination through MEGF10 and MERTK pathways. *Nature* **504**, 394 (2013).
256. Awasaki, T. *et al.* Essential Role of the Apoptotic Cell Engulfment Genes draper and ced-6 in Programmed Axon Pruning during Drosophila Metamorphosis. *Neuron* **50**, 855–867 (2006).
257. Fuentes-Medel, Y. *et al.* Glia and Muscle Sculpt Neuromuscular Arbors by Engulfing Destabilized Synaptic Boutons and Shed Presynaptic Debris. *PLOS Biol.* **7**, e1000184 (2009).
258. Yang, C.-T. *et al.* Neutrophils Exert Protection in the Early Tuberculous Granuloma by Oxidative Killing of Mycobacteria Phagocytosed from Infected Macrophages. *Cell Host Microbe* **12**, 301–312 (2012).
259. Kok, F. O. *et al.* Reverse Genetic Screening Reveals Poor Correlation between Morpholino-Induced and Mutant Phenotypes in Zebrafish. *Dev. Cell* **32**, 97–108 (2015).
260. Jinek, M. *et al.* A Programmable Dual-RNA–Guided DNA Endonuclease in Adaptive Bacterial Immunity. *Science (80-.).* **337**, 816 LP – 821 (2012).

261. Larson, M. H. *et al*. CRISPR interference (CRISPRi) for sequence-specific control of gene expression. *Nat. Protoc.* **8**, 2180 (2013).
262. Qi, L. S. *et al*. Repurposing CRISPR as an RNA-Guided Platform for Sequence-Specific Control of Gene Expression. *Cell* **152**, 1173–1183 (2013).
263. Maeder, M. L. *et al*. CRISPR RNA–guided activation of endogenous human genes. *Nat. Methods* **10**, 977 (2013).
264. Hwang, W. Y. *et al*. Efficient genome editing in zebrafish using a CRISPR-Cas system. *Nat. Biotechnol.* **31**, 227 (2013).
265. Chang, N. *et al*. Genome editing with RNA-guided Cas9 nuclease in Zebrafish embryos. *Cell Res.* **23**, 465 (2013).
266. Hruscha, A. *et al*. Efficient CRISPR/Cas9 genome editing with low off-target effects in zebrafish. *Development* **140**, 4982 LP – 4987 (2013).
267. Wyatt, L., Wadham, C., Crocker, L. A., Lardelli, M. & Khew-Goodall, Y. The protein tyrosine phosphatase Pez regulates TGFß, epithelial-mesenchymal transition, and organ development. *J. Cell Biol.* **178**, 1223 LP – 1235 (2007).
268. van Eekelen, M., Overvoorde, J., van Rooijen, C. & den Hertog, J. Identification and Expression of the Family of Classical Protein-Tyrosine Phosphatases in Zebrafish. *PLoS One* **5**, e12573 (2010).
269. Mitsuhashi, S., Mitsuhashi, H., Alexander, M. S., Sugimoto, H. & Kang, P. B. Cysteine mutations cause defective tyrosine phosphorylation in MEGF10 myopathy. *FEBS Lett.* **587**, 2952–2957 (2013).
270. Bindels, D. S. *et al*. mScarlet: a bright monomeric red fluorescent protein for cellular imaging. *Nat. Methods* **14**, 53 (2016).
271. Ray, A., Speese, S. D. & Logan, M. A. Glial Draper Rescues Aß Toxicity in a Drosophila Model of Alzheimer's Disease. *J. Neurosci.* **37**, 11881 LP – 11893 (2017).
272. Yan, B. *et al*. Il-1ß and Reactive Oxygen Species Differentially Regulate Neutrophil Directional Migration and Basal Random Motility in a Zebrafish Injury–Induced Inflammation Model. *J. Immunol.* **192**, 5998 LP – 6008 (2014).
273. Lindley, I. *et al*. Synthesis and expression in Escherichia coli of the gene encoding monocyte-derived neutrophil-activating factor: biological equivalence between natural and recombinant neutrophil-activating factor. *Proc. Natl. Acad. Sci.* **85**, 9199 LP – 9203 (1988).
274. Razzell, W., Wood, W. & Martin, P. Recapitulation of morphogenetic cell shape changes enables wound re-epithelialisation. *Development* **141**, 1814 LP – 1820 (2014).
275. Tetley, R. J. *et al*. Tissue fluidity promotes epithelial wound healing. *Nat. Phys.* (2019). doi:10.1038/s41567-019-0618-1
276. Petrie, T. A., Strand, N. S., Tsung-Yang, C., Rabinowitz, J. S. & Moon, R. T. Macrophages modulate adult zebrafish tail fin regeneration. *Development* **141**, 2581 LP – 2591 (2014).
277. Martinek, N., Shahab, J., Saathoff, M. & Ringuette, M. Haemocyte-derived SPARC is required for collagen-IV-dependent stability of basal laminae in Drosophila embryos. *J. Cell Sci.* **121**, 1671 LP – 1680 (2008).
278. Savill, J., Hogg, N., Ren, Y. & Haslett, C. Thrombospondin cooperates with CD36 and the vitronectin receptor in macrophage recognition of neutrophils undergoing apoptosis. *J. Clin. Invest.* **90**, 1513–22 (1992).
279. Savill, J., Dransfield, I., Hogg, N. & Haslett, C. Vitronectin receptor-

mediated phagocytosis of cells undergoing apoptosis. *Nature* **343**, 170–173 (1990).
280. Roth, B. L., Poot, M., Yue, S. T. & Millard, P. J. Bacterial viability and antibiotic susceptibility testing with SYTOX green nucleic acid stain. *Appl. Environ. Microbiol.* **63**, 2421 LP – 2431 (1997).
281. van Genderen, H. *et al.* In vitro measurement of cell death with the annexin A5 affinity assay. *Nat. Protoc.* **1**, 363–367 (2006).
282. Poot, M., Gibson, L. L. & Singer, V. L. Detection of apoptosis in live cells by MitoTracker red CMXRos and SYTO dye flow cytometry. *Cytometry* **27**, 358–364 (1997).
283. Singer, A. J., McClain, S. A., Taira, B. R., Guerriero, J. L. & Zong, W. Apoptosis and Necrosis in the Ischemic Zone Adjacent to Third Degree Burns. *Acad. Emerg. Med.* **15**, 549–554 (2008).
284. Yang, M. *et al.* Biomarkers distinguish apoptotic and necrotic cell death during hepatic ischemia/reperfusion injury in mice. *Liver Transplant.* **20**, 1372–1382 (2014).
285. Hanahan, D. & Weinberg, R. A. Hallmarks of Cancer: The Next Generation. *Cell* **144**, 646–674 (2011).
286. Del Prete, A. *et al.* Molecular pathways in cancer-related inflammation. *Biochem. Medica* **21**, 264–275 (2011).
287. Gillen, C. D., Walmsley, R. S., Prior, P., Andrews, H. A. & Allan, R. N. Ulcerative colitis and Crohn's disease: a comparison of the colorectal cancer risk in extensive colitis. *Gut* **35**, 1590–2 (1994).
288. Sfanos, K. S., Yegnasubramanian, S., Nelson, W. G. & De Marzo, A. M. The inflammatory microenvironment and microbiome in prostate cancer development. *Nat. Rev. Urol.* **15**, 11–24 (2018).
289. Elinav, E. *et al.* Inflammation-induced cancer: crosstalk between tumours, immune cells and microorganisms. *Nat. Rev. Cancer* **13**, 759 (2013).
290. Du, R. *et al.* HIF1alpha induces the recruitment of bone marrow-derived vascular modulatory cells to regulate tumor angiogenesis and invasion. *Cancer Cell* **13**, 206–220 (2008).
291. Caux, C., Ramos, R. N., Prendergast, G. C., Bendriss-Vermare, N. & Ménétrier-Caux, C. A Milestone Review on How Macrophages Affect Tumor Growth. *Cancer Res.* **76**, 6439 LP – 6442 (2016).
292. Ocana, A., Nieto-Jiménez, C., Pandiella, A. & Templeton, A. J. Neutrophils in cancer: prognostic role and therapeutic strategies. *Mol. Cancer* **16**, 137 (2017).
293. Rothwell, P. M. *et al.* Effect of daily aspirin on long-term risk of death due to cancer: analysis of individual patient data from randomised trials. *Lancet (London, England)* **377**, 31–41 (2011).
294. Pastor-Pareja, J. C., Wu, M. & Xu, T. An innate immune response of blood cells to tumors and tissue damage in Drosophila. *Dis. Model. & Mech.* **1**, 144 LP – 154 (2008).
295. Hauling, T. *et al.* A Drosophila immune response against Ras-induced overgrowth. *Biol. Open* **3**, 250 LP – 260 (2014).